

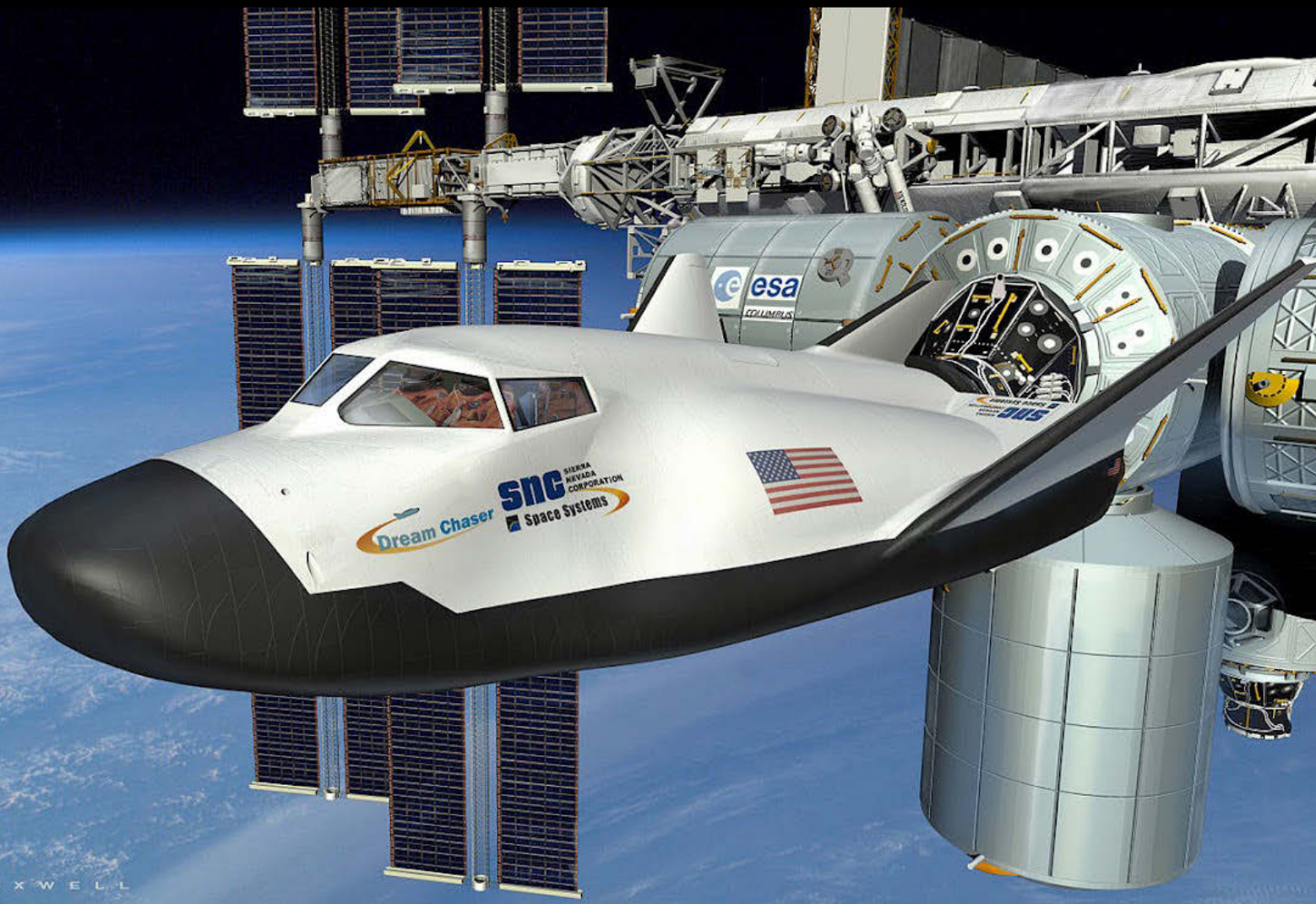
WISCONSIN SPACE GRANT CONSORTIUM

Proceedings of the 24th Annual
Wisconsin Space Conference

COMMERCIAL SPACE

August 15, 2014

Biopharmaceutical Technology Center Institute
Fitchburg, Wisconsin



Commercial Space

24th Annual Wisconsin Space Conference

August 15, 2014

Host: Biopharmaceutical Technology Center Institute
Fitchburg, Wisconsin

Edited by: Kevin M. Crosby, Director, Wisconsin Space Grant Consortium
Chris Thompson, Program Manager, Wisconsin Space Grant Consortium

Eric Barnes, University of Wisconsin – La Crosse
Bill Dirienzo, University of Wisconsin – Sheboygan
Duane Foust, University of Wisconsin – Platteville
Rex Hanger, University of Wisconsin – Whitewater
John Heasley, Kickapoo Valley Reserve
Coggin Heeringa, Crossroads at Big Creek
Beth Johnson, University of Wisconsin – Fox Valley
Nadedjda Kaltcheva, University of Wisconsin – Oshkosh
Vera Kolb, University of Wisconsin – Parkside
Leah Simon, Ripon College
Paul Smith, Alverno College
Glenn Spiczak, University of Wisconsin – River Falls
Sebastian Zamfir, University of Wisconsin – Stevens Point
Todd Zimmerman, University of Wisconsin – Stout

Cover Art: Sierra Nevada Corporation Dream Chaser. Courtesy: ORBITEC, Inc.

Published by: Wisconsin Space Grant Consortium
Carthage College
2001 Alford Park Drive
Kenosha, WI 53140-1994

Publication Data: ISSN: 2374-8877 (print) / 2374-8885 (electronic)
Frequency: annual publication
Year established: 1994

For more information on the Proceedings of the Wisconsin Space Conference:

| | | |
|---|--|---|
|  | <p>Wisconsin Space Grant Consortium Carthage College 2001 Alford Park Drive Kenosha, WI 53140-1994 (262) 551-6054 spacegrant@carthage.edu https://spacegrant.carthage.edu</p> |  <p>CARTHAGE COLLEGE</p> |
|---|--|---|

Commercial Space

24th Annual Wisconsin Space Conference

August 15, 2014

**Host: Biopharmaceutical Technology Center Institute
Fitchburg, Wisconsin**



Copyright © 2014 Wisconsin Space Grant Consortium
Wisconsin Space Grant Consortium
Carthage College
2001 Alford Park Drive
Kenosha, WI 53140

January, 2015

Preface to the Proceedings of the 24th Annual Wisconsin Space Conference

New Beginnings

The challenge and excitement of starting something new is still with me as I write this, my first introduction to these Proceedings. As new Director of the Wisconsin Space Grant Consortium, I am honored to serve this vibrant and powerful organization, and *very* grateful for the leadership of my predecessors, Dr. Yingst and the outgoing staff of the WSGC. Aileen leaves us having built the second largest Space Grant Consortium in the country and yet one that remains agile and responsive to the evolving needs of our affiliates.

Reading the papers and reports in this year's Proceedings reminds me again of the vital role Wisconsin plays in the engines of innovation and discovery that power our national space efforts. I am also reminded of the privilege we each share of using the WSGC to help our students launch careers. The efforts and successes we read about in these pages are the seeds for future lives in STEM fields and in aerospace, particularly. It is our core mission to support the kinds of educational and professional activities that provide pathways to careers, and ultimately, to the economic vitality of the aerospace industry in Wisconsin.

In that bright light, the theme of this year's Wisconsin Space Conference is timely and appropriate. Commercial Space has never before been such a source of both hope and anxiety. From the successes of SpaceX and Boeing in NASA's Commercial Crew Program contract announcements to the very bad week in late October that saw the loss of the Antares rocket and the tragic loss of human life resulting from the breakup of Virgin Galactic's SpaceShipTwo, 2014 has truly been a defining year for Commercial Space.

For their role in shrewdly picking the perfect conference theme, I am grateful to Dr. Aileen Yingst and Tori Nelson, and to our conference host, Dr. Karin Borgh. I am equally grateful to Dr. Borgh for once again allowing us to use the beautiful facilities at the Biopharmaceutical Technology Center Institute for our annual conference. A better place to contemplate the future, I cannot imagine. Jeff Johnson, ORBITEC's Environmental Control & Life Support System (ECLSS) Program Manager for Sierra Nevada Corporation's Dream Chaser program, served as the keynote speaker. His presentation was widely regarded as one of the more engaging and instructive talks we've enjoyed. Student feedback on Jeff's talk suggested that his overview of commercial space efforts was eye opening and inspiring.

It is from this unique position of strength and hope that I invite you to peruse the articles and reports in these Proceedings. I think you will agree that the future of Wisconsin STEM/aerospace education and research is bright and worthy of your continued support.

Kevin M. Crosby, Director

Wisconsin Space Grant Consortium

Programs for 2014

Student Programs

- Undergraduate Scholarship
- Undergraduate Research
- Graduate Fellowship
- Dr. Laurel Salton Clark Memorial Graduate Fellowship
- University Sounding Rocket Team Competition
- Student High-Altitude Balloon Launch
- Student High-Altitude Balloon Payload
- Industry Member Internships
- NASA Academy Leadership Internships
- NASA Centers/JPL Internships
- NASA Reduced Gravity Team Programs
- Relevant Student Travel

(see detailed descriptions on next page)

Research

The Research Infrastructure Program provides Research Seed Grant Awards to faculty and staff from WSGC Member and Affiliate Member colleges and universities to support individuals interested in starting or enhancing space- or aerospace-related research program(s).

Higher Education

The Higher Education Incentives Program is a seed-grant program inviting proposals for innovative, value-added, higher education teaching/training projects related to space science, space engineering, and other space- or aerospace-related disciplines. The Student Satellite Program including Balloon and Rocket programs is also administered under this program.

Industry Program

The WSGC Industry Program is designed to meet the needs of Wisconsin Industry member institutions in multiple ways including:

- 1) the Industry Member Internships (listed under students above),
- 2) the Industry/Academic Research Seed Program designed to provide funding and open an avenue for member academia and industry researchers to work together on a space-related project, and
- 3) the Industrial Education and Training Program designed to provide funding for industry staff members to keep up-to-date in NASA-relevant fields.

Aerospace Outreach Program

The Aerospace Outreach Program provides grant monies to promote outreach programs and projects that disseminate aerospace and space-related information to the general public, and support the development and implementation of aerospace and space-related curricula in Wisconsin classrooms. In addition, this program supports NASA-trained educators in teacher training programs.

Special Initiatives

The Special Initiatives Program is designed to provide planning grants and program supplement grants for ongoing or new programs which have space or aerospace content and are intended to encourage, attract, and retain under-represented groups, especially women, minorities and the developmentally challenged, in careers in space- or aerospace-related fields.

Wisconsin Space Conference

The Wisconsin Space Conference is an annual conference featuring presentations of students, faculty, K-12 educators and others who have received grants from WSGC over the past year. The Conference allows all to share their work with others interested in Space. It also includes keynote addresses, and the announcement of award recipients for the next year.

Regional Consortia

WSGC is a founding member of the Great Midwest Regional Space Grant Consortia. The Consortia consists of eight members, all Space Grants from Midwest and Great Lakes States.

Communications

WSGC web site www.uwgb.edu/wsgc provides information about WSGC, its members and programs, and links to NASA and other sites.

Contact Us

Wisconsin Space Grant Consortium
Carthage College
2001 Alford Park Drive
Kenosha, Wisconsin 53140-1994
Phone: (262) 551-6054
E-mail: spacegrant@carthage.edu
Website: spacegrant.carthage.edu



Wisconsin Space Grant Consortium

Student Programs for 2014

Undergraduate Scholarship Program

Supports outstanding undergraduate students pursuing aerospace, space science, or other space-related studies or research.

Undergraduate Research Awards

Supports qualified students to create and implement a small research study of their own design during the summer or academic year that is directly related to their interests and career objectives in space science, aerospace, or space-related studies.

Graduate Fellowships

Support outstanding graduate students pursuing aerospace, space science, or other interdisciplinary space-related graduate research.

Dr. Laurel Salton Clark Memorial Graduate Fellowship

In honor of Dr. Clark, Columbia Space Shuttle astronaut and resident of Wisconsin, this award supports a graduate student pursuing studies in the fields of environmental or life sciences, whose research has an aerospace component.

University Sounding Rocket Team Competition

Provides an opportunity and funding for student teams to design and fly a rocket that excels at a specific goal that is changed annually.

High School Sounding Rocket Team Competition

For high school students. This program is in its initial stages. It mimics the university competition.

Student High-Altitude Balloon Instrument Development

Students participate in this instrument development program through engineering or science teams. Working models created by the students will be flown on high-altitude balloons.

Student High-Altitude Balloon Payload/Launch Program

The Elijah Project is a high-altitude balloon program in which science and engineering students work in integrated science and engineering teams, to design, construct, launch, recover and analyze data from a high-altitude balloon payload. These balloons travel up to 100,000 ft., considered “the edge of space.” Selected students will join either a launch team or a payload design team.

Industry Member Internships

Supports student internships in space science or engineering for the summer or academic year at WSGC Industry members co-sponsored by WSGC and Industry partners.

NASA ESMD Internships

Supports student internships at NASA centers or WSGC industry members that tie into NASA’s Exploration Systems Mission Directorates.

NASA Academy Leadership Internships

This summer internship program at NASA Centers promotes leadership internships for college juniors, seniors and first-year graduate students and is co-sponsored by participating state Space Grant Consortia.

NASA Centers/JPL Internships

Supports WSGC students for research internships at NASA Centers or JPL.

NASA Reduced Gravity Program

Operated by the NASA Johnson Space Center, this program provides the unique “weightless” environment of space flight for test and training purposes. WSGC student teams submit reduced gravity experiments to NASA and, if selected, get to perform their experiments during a weightless environment flight with the support of WSGC.

Relevant Student Travel

Supports student travel to present their WSGC-funded research.

2014 Wisconsin Space Conference

Commercial Space

TABLE OF CONTENTS

| | |
|---------------------------|-----|
| General Information | i |
| Issue Credits..... | ii |
| Director’s Welcome | iii |
| WSGC Programs | iv |

Part One: Astronomy and Cosmology

| | |
|--|----|
| <i>Black Holes, Lasers and Data Analysis: Contributions to Gravitational Wave Searches with the Excess Power Pipeline</i> , Sydney J. Chamberlin | 2 |
| <i>Clarifying the Role of Thermodynamics in Self-gravitating Dark Matter Systems</i> , Colin P. Egerer, Eric I. Barnes | 5 |
| <i>Expanding Our Knowledge of Interstellar Neutral Hydrogen Shells</i> , Tyler Laszczkowski, Shauna Sallmen..... | 15 |
| <i>Searching for Gravitational Waves from Sub-Solar Mass Black Holes</i> , Madeline Wade, Jolien Creighton | 25 |

Part Two: Physics and Engineering

| | |
|--|----|
| <i>Fire in Orbit: Equipping the Commercial Spaceflight Industry for Fighting Fire in Micro-Gravity</i> , Trent Cybela | 31 |
| <i>Simulations with Granular Material Motion for Extraterrestrial Applications</i> , David S. Helminiak | 40 |
| <i>Experiments with Granular Material Motion for Extraterrestrial Applications</i> , Nathaniel S. Helminiak | 50 |
| <i>A study on Select Solar Cell’s Voltage Output at High Altitudes Using a Weather Balloon</i> , Jalal M. Nawash, Rebecca Holzer, Rebekah Taylor, Jacob Bogeuschuetz | 60 |
| <i>Design of a Lunar Solar Wind Volatiles Extraction System</i> , Aaron D.S. Olson, John F. Santarius, Gerald L. Kulcinski | 69 |
| <i>Human Factor Analysis of Light Emitting Diode Technologies for Cabin Lighting in Manned Space Flight Applications</i> , Todd H. Treichel | 79 |

Part Three: Biosciences and Geosciences

| | |
|---|----|
| <i>“Hands-on” Remote Sensing of Physical Models in Exploration of Surficial Processes</i> , Jeffrey J. Clark | 88 |
| <i>Assessment of Ecosystem Photosynthetic Parameters along Two California Climate Gradients</i> , Sean DuBois | 97 |

| | |
|--|-----|
| <i>Testing for Wildfire Feedbacks in Forests of the US Northern Rockies Initial Report</i> , Brian J. Harvey | 106 |
| <i>Size differences of the Post-anoxia, Biotic Recovery Brachiopod, Dyoros sp., in Hughes Creek Shale (Carboniferous), Richardson County, Nebraska</i> , Daryl Johnson, Rex Hanger | 114 |
| Part Four: Team Projects | |
| <i>2014 WSGC Elijah High-Altitude Balloon Payload Project Final Report</i> , Jadee Kellogg, Madeline Lambert, Danny Ochoa, Evan Schilling, Michael Stefik | 122 |
| <i>The Onset of Normal Field Instability in a Ferrofluid in a Reduced Gravity Environment</i> , Brendan Krull, Tessa Rundle, Kevin LeCaptain, Justin Barhite, Amelia Gear | 132 |
| <i>Team Whoosh Generator 2014 WSGC Collegiate Rocket Competition</i> , Kirsti Pajunen, Eric Johnson, James Ihrcke, Stephan Skibinski, Kathryn Baisley | 140 |
| <i>Pioneer Rocketry 2014 WSGC Collegiate Rocket Competition</i> , Maria Smiles, Trent Cybela, Jacob Ellenberger, Luke Sackash | 150 |
| <i>2014 HUNCH SPIDER</i> , Jonathon Woods | 160 |
| <i>Wombat 1 Team Night Skies 2014 WSGC Collegiate Rocket Competition</i> , Grace Zeit, Christine Sutherland, Aaron Jarosh, Randy Lutz | 163 |
| Part Five: Education and Public Outreach | |
| <i>Science Outreach at the BTC Institute - Aerospace Outreach Program & Special Initiatives Program</i> , Barbara Bielec | 179 |
| <i>Teaching Teachers from Standards to Lessons</i> , Coggin Heeringa | 189 |
| <i>Driftless Dark Skies Initiative: Training Astronomy Educators</i> , Jonel Kiesau, John Heasley | 192 |
| <i>Simpson Street Free Press: Using Science to Bridge Achievement Gaps</i> , James Kramer | 197 |
| <i>Promoting Women in Physics and Astronomy Through a Public Lecture Series at UW-La Crosse</i> , S. R. Leshner | 203 |
| <i>Rocket Science for Educators Workshop for Science Technology Engineering and Mathematics</i> , Todd H. Treichel, Daniel W. Bateman | 207 |
| Part Six: Conference Program | |
| <i>2014 Wisconsin Space Conference Program</i> | 218 |

24th Annual Wisconsin Space Conference

PART ONE

Astronomy and Cosmology

Black Holes, Lasers and Data Analysis: Contributions to Gravitational Wave Searches with the ExcessPower Pipeline

Sydney J. Chamberlin¹

Department of Physics
University of Wisconsin-Milwaukee
Milwaukee, WI

Introduction

Gravitational waves (GWs) are tiny perturbations to the spacetime structure of the universe that propagate freely as wavelike solutions to the Einstein equations. The direct detection of GWs is currently a major goal in experimental physics, and a number of large scale efforts to detect them are currently underway.

Designed to detect GWs in the 10 Hz – 10³ Hz frequency band, the Advanced Laser Interferometer Gravitational-wave Observatory (aLIGO) is network of kilometer scale ground-based laser interferometers that will recover signals generated by astrophysical sources such as supernovae, rotating neutron stars and the coalescence and eventual inspiral of compact binary objects [1].

Gravitational wave *bursts* are transient GW signals and differ from other types of GW signals in the sense that they 1) have durations much shorter than the observational timescale, and 2) they are identifiable by a distinct arrival time. One of the most important sources of GW bursts is compact binary coalescence (CBC).

If the anticipated waveform from a CBC event can be well-modeled with post-Newtonian techniques or numerical relativity, matched filtering techniques can be employed to search for GW bursts in detector data: a template bank containing some large number of possible waveforms is constructed, and the GW signal is extracted from the data by correlating the template to the data. For some astrophysical systems, however, the dynamics underlying the gravitational field are complex enough that exact forms of the GW signal cannot be obtained. Additionally, unknown signals from unanticipated sources could exist. In this case, a technique other than matched filtering is necessary to extract the signal of unknown shape from the data. One method that has been proposed and employed for this type of *unmodeled* search is the excess power method, which involves studying time-frequency decompositions of detector data [2–5].

¹ The author gratefully acknowledges the Wisconsin Space Grant Consortium for financially supporting this work. Thanks are also extended to Chris Pankow and Jolien Creighton for several informative discussions.

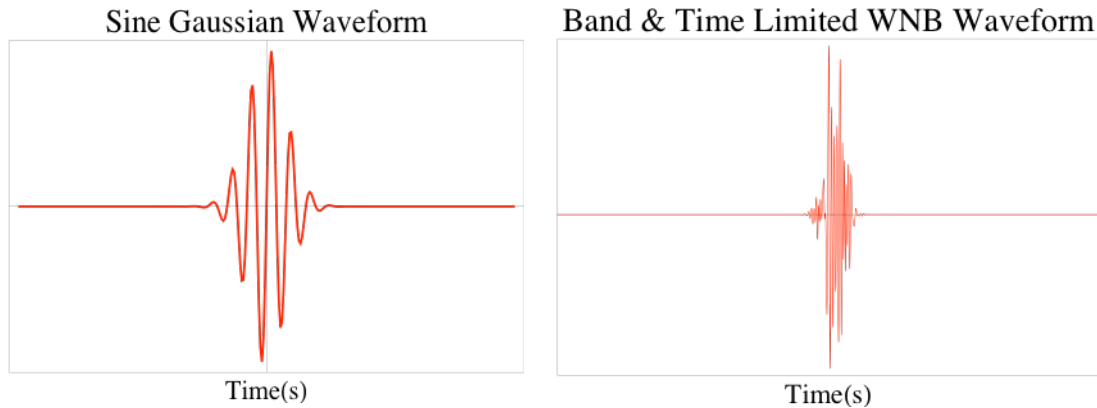


Figure 1. Sine Gaussian (left) and band and time limited white noise burst (right) waveforms serve as the basis for injections in the ExcessPower injection study.

The excess power method effectively scans detectors' outputs for transients that are statistically significant relative to back- ground noise: blocks of time and frequency (or time-frequency tiles) are constructed based on knowledge of the signal's duration and frequency, and the total power within each tile is calculated: the energy in each tile is determined, and added in quadrature. If a signal exists in the data, more power should be present than would exist from detector noise alone. The *ExcessPower pipeline* is a data analysis pipeline (or set of software tools) that employs the excess power method in unmodeled GW searches using LIGO data.

ExcessPower Pipeline Efficiency Test

Pipeline efficiency tests aim to identify how well a given pipeline can recover signals with known parameters. To do this, signals with known (desired) parameters are injected into appropriate background noise and analyzed by the pipeline. An efficient pipeline is one that recovers the injected signals within some specified level of accuracy.

The work described in this document aims to quantitatively assess the efficiency of ExcessPower for burst searches of GWs. Because the objective is to simulate any sort of signal that ExcessPower may come across in real data, two types of signal waveforms are being used in the study: Sine Gaussians, which are sine signals modulated by Gaussian envelopes, and band-and-time limited white noise bursts (BTLWNBs) (see Figure 1). These two families of signals have the advantage that they can be used as templates for nearly any practical signal.

Signals were injected into simulated aLIGO data and analyzed with ExcessPower, resulting in *triggers* (or candidate GW signals).

Preliminary Results

Out 40274 injections, 33974 were recovered by ExcessPower. This is about 85% of the injections (see Figure 2). Initial results indicate that while some bulk parameters (time and frequency) are recovered well by ExcessPower, additional work needs to be done to correctly estimate the signal-to-noise ratio and amplitude of injected signals. This work is ongoing.

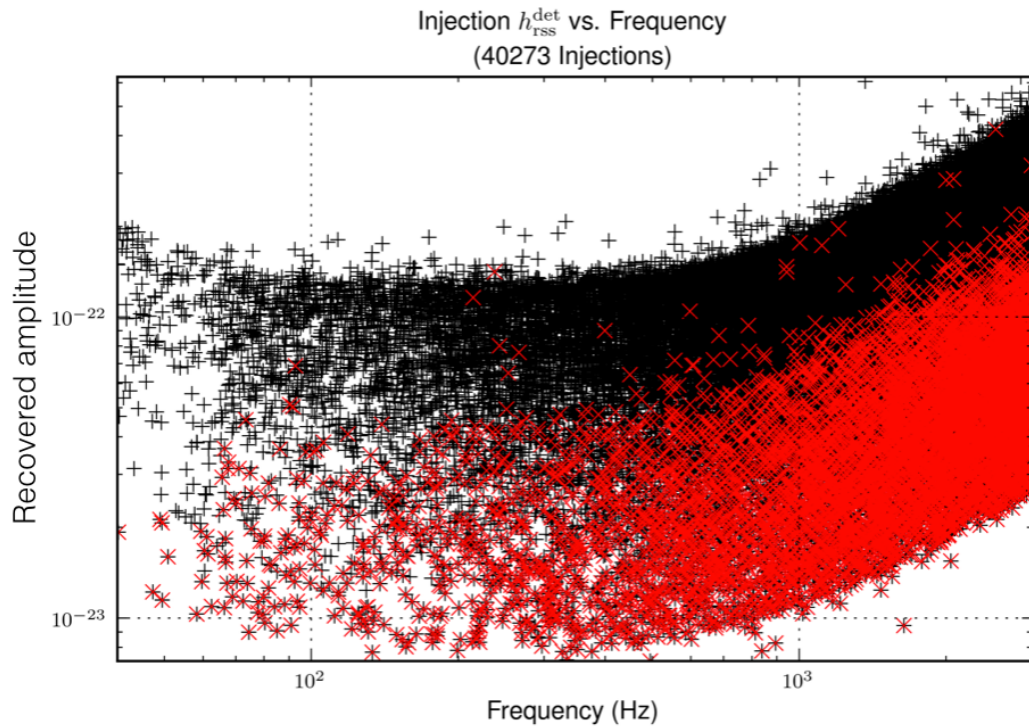


Figure 2. Recovered injections (black cross-hairs) are shown along with missed injections (black cross-hairs superimposed with red xs). Note that many recovered injections are covered by the missed injections. The total number of injections recovered was near 85%.

References

- [1] A. Abramovici, W. E. Althouse, R. W. Drever, Y. Gursel, S. Kawamura, et al., *Science* 256, 325 (1992).
- [2] W. G. Anderson, P. R. Brady, J. D. Creighton, and E. E. Flanagan, *Phys. Rev. D* 63, 042003 (2001), arXiv:gr-qc/0008066.
- [3] P. Brady, D. Brown, K. Cannon, and S. Ray-Majumder, *Excess Power*, <https://dcc.ligo.org/LIGO-T1200125> (2007), LIGO Document T1200125.
- [4] J. D. E. Creighton and W. G. Anderson, *Gravitational-wave Physics and Astronomy* (Wiley-VCH, 2011).
- [5] C. Pankow, *Excess Power: A Status Report*, <https://dcc.ligo.org/cgi-bin/private/DocDB/ShowDocument?docid=97802> (2012), LIGO Document G1201140-v1.

Clarifying the Role of Thermodynamics in Self-gravitating Dark Matter Systems¹

Colin P. Egerer
Eric I. Barnes - Faculty Advisor

Department of Physics, University of Wisconsin --- La Crosse, La Crosse, WI 54601

ABSTRACT

Astrophysicists currently favor the idea that the vast majority of mass in the universe exists in a collisionless form that interacts only through gravity. This paradigm has been successful in allowing computer simulations of cosmological volumes to reproduce structures similar to those observed. Our work aims to better understand the physics at work in collisionless systems, in general. Specifically, we investigate how well thermodynamics-based approaches to understanding equilibrium structures agree with results of computer simulations. Using a suite of N -body simulations with differing initial conditions, we examine the density and velocity profiles of self-gravitating collisionless systems. Statistical comparisons between simulated equilibrium structures and two thermodynamics-based models indicate the relative appropriateness of the models. We find that no single model can describe systems resulting from the entire range of initial conditions investigated here. Our major result is that these thermodynamics-based models can successfully reproduce equilibria that arise in gently evolving systems. However, the failure of thermodynamics-based models to describe the equilibria of more violent evolutions suggests that they must retain some memory of their initial conditions.

1 Introduction

In recent decades, groups have created models of dark matter halos with varying levels of sophistication (Navarro, Frenk, & White 1996; Moore et al. 1999). Following increased computing power, simulations with greater resolutions (particles per halo) are constantly being performed. We utilize modest simulations to investigate some basic questions, rather than replicate these state-of-the-art simulations. The systems we simulate evolve under collisionless self-gravitation - physical conditions of dark matter halos. Our simulations are similar to those that have shown evidence of "universal" halo behaviors such as radial density profiles (Navarro, Frenk, & White 1997; Navarro et al. 2004). Power-law radial distributions of $\rho(r)/\sigma(r)^3$ (which has dimensions of a phase-space density, Taylor & Navarro 2001), have also led some to suggest that a more basic physical mechanism may underlie the formation of these self-gravitating equilibria.

The simulations we have performed create data sets of particle positions and velocities at equally spaced times during an evolution of a system. Each simulated system has been prescribed by a set of

¹Funding provided by the Wisconsin Space Grant Consortium and the UW-La Crosse Foundation's Gubbi R. Sudhakaran Fund for Physics Research.

initial particle positions and velocities which have then been allowed to evolve. These initial conditions provide discrimination between the models. The industry-standard GADGET code (Springel 2005) has been used to advance particles in time according to calculated self-gravitating forces between the particles. GADGET utilizes softened particle-particle interaction forces to approximate collisionless behavior. Although the GADGET code is capable of including gas dynamics and Hubble expansion, we have elected not to include these features in our simulations. Our simulations are therefore not putative dark matter halos. Although cosmological simulations involving these processes often yield interesting results (Governato et al. 2010), they do not necessarily provide direct insight to the physical processes governing dark matter systems.

To focus more on the physics involved in our N -body simulations, we have investigated how well models based on thermodynamic considerations describe the results of simulations. We also compare simulations to several common empirical fitting functions. Both the empirical and physically motivated models have been fit to the simulated density and velocity distributions, after they have attained virial equilibrium. The suitability of each model is judged using the reduced χ^2 statistic for quantifying differences between models and data. We extend the model/data comparison to include density and velocity dispersion profiles, a step often neglected in these kinds of studies (Lithwick & Dalal 2011).

2 Model Descriptions

2.1 Empirical models. The models we have investigated reflect a range of possible self-gravitating collisionless systems. We consider the Plummer, de Vaucouleurs, and Generalized NFW (Navarro, Frenk, and White) empirical models. Plummer models (Plummer 1911) were initially motivated by the stellar distributions in globular clusters, and have a density distribution given by

$$\rho = \frac{\rho_0}{\left(1 + \frac{1}{3} \left(\frac{r}{r_0}\right)^2\right)^{5/2}}, \quad (1)$$

where ρ_0 is a scaling density and r_0 is a scaling radius. Plummer models are a specific example of a polytropic system (Binney & Tremaine 1987), where the equation of state relating pressure P and density ρ is $P = K\rho^\Gamma$. In a collisionless situation, the exponent is often written in terms of the polytropic index n , where $\Gamma = 1 + \frac{1}{n}$. The density profiles of polytropic systems (with $n \gtrsim 1$) are relatively constant near the core of the system and rapidly decline near the outer edge. Plummer models have $n = 5$ ($\Gamma = \frac{6}{5}$).

The de Vaucouleurs profile (de Vaucouleurs 1948) has been used to fit the light profiles of elliptical galaxies. The density profile of the de Vaucouleurs profile is given by

$$\rho = \rho_0 \left(\frac{r}{r_0}\right)^{-\delta} \left(1 + \frac{r}{r_0}\right)^{\delta-4}, \quad (2)$$

where $\delta = \frac{1}{2}$, and ρ_0 and r_0 are again a scaling density and radius, respectively. A de Vaucouleurs density profile has a central cusp, in contrast to the central density core behavior of the Plummer model.

Navarro, Frenk, and White (NFW) (Navarro, Frenk, & White 1996, 1997) have developed a density profile that describes the results of simulated dark matter halos resulting from cosmological initial conditions. The specific form of an NFW profile has density rising towards the center, $\rho \propto \frac{1}{r}$, with a rapid drop-off near the outer edge, $\rho \propto \frac{1}{r^3}$. Specifically, the NFW profile is,

$$\rho = \rho_0 \left(\frac{r}{r_0} \right)^{-n_1} \left(1 + \frac{r}{r_0} \right)^{-n_2}, \quad (3)$$

where $n_1 = 1$ and $n_2 = 2$. In our work, however, we consider a generalized NFW profile. This form maintains the broken power-law nature of the de Vaucouleurs and NFW profiles, but allows us to estimate variations to the inner and outer behaviors.

2.2 Thermodynamic models. In this work, we examine two physically motivated models of self-gravitating collisionless systems. Non-extensive and Lynden-Bell models are based on thermodynamic approaches to understanding the equilibrium attained by our simulations. These thermodynamic models are appealing because they ignore complicated microscopic (particle-by-particle) dynamics of the situation and instead focus on collective quantities, like entropy.

The density profiles investigated here derive from a distribution function $f(\mathbf{x}, \mathbf{v})$ that defines how many particles occupy small volumes $d^3x d^3v$ of phase space. The standard statistical approach is to divide the phase space of a dynamical system into macrocells and microcells. Macrocells are assumed to be small compared to the full phase-space extent of the system, each containing a large number of smaller microcells. Maxwell-Boltzmann statistics asserts that any microcell of a system can be multiply occupied by distinguishable particles as would occur in a collisional system. Lynden-Bell statistics declares that only one distinguishable particle may occupy a given microcell. Since a collisionless system has an incompressible distribution function, $df/dt = 0$, the Lynden-Bell exclusion condition seems to correspond to such a system. This condition can be re-cast as the collisionless Boltzmann (or Vlasov) equation in three dimensions,

$$\frac{\partial f}{\partial t} + \mathbf{v} \cdot \nabla f + \mathbf{a} \cdot \nabla_{\mathbf{v}} f = 0. \quad (4)$$

Note that the specific energy (energy per unit mass) of a particle at any given (\mathbf{x}, \mathbf{v}) is

$$e = \frac{E}{m} = \frac{v^2}{2} + \Phi(\mathbf{x}), \quad (5)$$

where v is the particle speed and Φ is the gravitational potential. This connection allows one to treat a distribution function as $f(\mathbf{x}, \mathbf{v})$ or as $f(e)$ (assuming the velocity distribution is isotropic).

Non-extensive thermodynamics posits that the total entropy S of two interacting systems is not simply the sum of their individual entropies (Tsallis 1988). This alteration creates the opportunity for self-gravitating systems to have density distributions comparable to the results of cosmological N -body simulations (Plastino & Plastino 1993; Kronberger, Leubner, & van Kampen 2006). Here, we investigate the ability of the non-extensive approach to describe non-cosmological systems.

As detailed in Plastino & Plastino 1993, a non-extensive entropy leads to a polytropic distribution function with the form,

$$f(e) = B \left[1 - \frac{e}{\kappa \epsilon} \right]^{-\kappa}, \quad (6)$$

where B , ϵ , and κ are constants; ϵ is an energy scale, and κ determines the polytropic index n . This form of distribution function provides a simple link between the spherically symmetric density profile and the underlying potential (Barnes et al. 2007). To actually determine $\rho(r)$, we numerically solve the Poisson equation,

$$\nabla^2 \Phi = 4\pi G \rho. \quad (7)$$

For a system with isotropic velocities, the non-extensive distribution function also provides a simple way to calculate the velocity dispersion distribution (Barnes et al. 2007).

Lynden-Bell models are derived from a statistical approach to entropy in collisionless systems (Lynden-Bell 1967). These models use the standard, extensive, definition of entropy,

$$S = k \ln \Omega, \quad (8)$$

where k is Boltzmann's constant and Ω is the number of available energy states, which is related to f . The impact of Lynden-Bell statistics lies in how the number of available energy states is calculated. The equilibrium distribution function $f(e)$ is found by assuming S is maximized for a constant mass and energy system.

The equilibrium Lynden-Bell distribution function is not analytical (in the absence of the Stirling approximation), and numerical methods are required to determine the corresponding density. Our technique relies on an iterative solution to the Poisson equation. The distribution function is defined by a parameter ν that describes the number of microcells inhabiting a macrocell. For a given ν , $f(e)$ is determined numerically by finding f values that satisfy,

$$\ln \left(\frac{f+1}{\nu-f+1} \right) + \frac{(f-\nu/2)}{(f+1)(\nu-f+1)} - \frac{2f^2 - 2f\nu - (1 + 600/576)\nu - 600/288}{f^2 - f\nu - (600/576)\nu + (600/576)^2} + \mu + \beta e = 0. \quad (9)$$

In this context μ and β are Lagrange multipliers associated with the mass and energy of the system. After isolating the distribution function, density is determined using,

$$\rho(\mathbf{x}) = \int f(\mathbf{x}, \mathbf{v}) d^3v, \quad (10)$$

where the integration is over all accessible velocity space. Assuming velocity space is isotropic gives it spherical symmetry, and allows a spherically-symmetric density to be written (using Equation 5) as,

$$\rho(r) = 4\pi \int_{v_{lo}}^{v_{hi}} f(\mathbf{x}, \mathbf{v}) v^2 dv = 8\pi \int_{E_{lo}}^{E_{hi}} f(e) [e - \Phi(\mathbf{x})] de. \quad (11)$$

Substituting this expression into the Poisson equation (Equation 7), produces an integro-differential equation for Φ . To solve this, we begin with a trial potential function. Using this trial Φ and $f(e)$, the right-hand side of the Poisson equation is determined as a function of radius. An updated potential is then determined by numerical solution of the Poisson equation. The next trial potential is created from averaging the previous and updated versions. The process is repeated until the variation in successive trial potentials falls below a threshold (10^{-4} in our code). At this point, Equation 11 produces a density distribution that is ready to be compared to simulation results. Corresponding

velocity dispersion distributions are found by using the model density in the spherically symmetric Jeans equation (which defines mechanical equilibrium),

$$\frac{1}{\rho(r)} \frac{d}{dr} \rho(r) \sigma_r^2(r) + 2 \frac{\beta(r) \sigma_r^2(r)}{r} = - \frac{GM(r)}{r^2}, \quad (12)$$

where $\sigma_r^2(r)$ is the variance of the radial velocity, $\beta(r)$ is the velocity anisotropy function, $M(r)$ is the mass enclosed at radius r , and G is Newton's gravitational constant. Mass at a particular radius is said to be isotropic if $-1.0 < \beta < 0.5$, radially anisotropic if $\beta > 0.5$, or tangentially anisotropic if $\beta < -1.0$. To create an isotropic model, one sets $\beta(r) = 0$.

3 Simulations

3.1 Initial conditions. When utilizing N -body simulations the initial position, initial kinetic and potential energy, and the initial orientations of the velocity vectors of all particles must be defined. Moreover, the overall density distribution and the number of particles within the simulated halo must also be accounted for. Following the lead of van Albada (1982), we define two distinct initial particle position prescriptions for all simulated systems - single and clumpy setups. In a single setup, all particles are distributed throughout a single spherical boundary of a simulated system. Consequently, all particles in a single setup orbit about the center of mass of the system. Particles in a clumpy system exist in a large number of smaller, overlapping spherical sub-systems. Clump sizes (radii and masses) are randomly chosen from power-law distribution functions. In each case, the specific particle locations are determined based on an assumed initial density profile. Our simulations assume initial density profiles that are either cuspy, $\rho \propto 1/r$, or Gaussian, $\rho \propto \exp(-r^2)$. Given an initial profile choice, particle locations are selected to reproduce the profile using a simple rejection method. For single systems, each particle position is specified. For clumpy setups, clump centers-of-mass are distributed according to the chosen profile, and each clump has a uniform distribution of particles within it.

The gravitational potential energy is then calculated after positions are assigned. This energy scale provides the basis for assigning particle velocities. The virial theorem provides a relation between a system's kinetic energy T , potential energy W , and second time derivative of its moment of inertia. For a steady-state system, $2T - |W| = 0$. We define the initial virial ratio as,

$$Q_0 = \frac{2T}{|W|}, \quad (13)$$

so that $Q_0 = 1$ indicates a system in virial equilibrium initially. Our investigations are limited to systems with $Q_0 \leq 1$, as $Q_0 > 1$ corresponds to an unbound system. In general, systems with lower virial ratios tend to undergo early, violent collapses due to the dominance of potential energy, while systems with higher virial ratios tend to experience only mild density variations as they approach mechanical equilibrium.

All particles are given the same initial speed necessary to produce the kinetic energy. Particle velocities are assigned with random orientations, producing initially isotropic systems. In single systems, the velocity assignment is straightforward. However, assigning only one set of velocity vectors to a clumpy system is insufficient, as the particles can move relative to the system center-of-mass as well as the clump center-of-mass. As such, we define a temperature fraction T_f to

distinguish the possible velocity arrangements. Systems in which particles initially move with the center-of-mass of their parent clump are designated $T_f = 1$, or "cold" systems. Conversely, systems with particles that move entirely randomly with respect to the halo center of mass are designated $T_f = 0$, or "hot" systems. Systems where particles move with respect to both centers-of-mass are designated $T_f = 0.5$, or "cool" systems.

3.2 Evolutions. For the simulations discussed here, $N = 10^5$ particles have been used to define systems. Additional simulations with different numbers of particles have also been performed, but have yielded little difference with regards to the quantities relevant to this project. The major differences lie in the spatial resolution scale and estimated uncertainties. Simulations discussed here include only Newtonian gravitational interaction between particles, thus maintaining classical dynamics and collisionless evolution. We do not consider self-annihilation or other interaction terms.

Once a simulated halo has been prescribed with a set of initial conditions, it is evolved using the publicly-available GADGET code (Springel 2005). GADGET produces snapshots of the system at specified intervals, providing access to particle positions and velocities. For each snapshot, we calculate radial profiles of density, velocity dispersion, and velocity anisotropy. To accomplish this, we first assign particles to concentric spherical shells. Each shell contains the 10^3 particles (1% of total) closest to the system center-of-mass that have not already been assigned to an interior shell. Using the shell boundaries, the average density is then calculated. Splitting each shell into three sub-shells and determining their densities allows us to estimate uncertainties as the range of sub-shell densities. Radial, polar, and azimuthal velocity statistics (averages and root-mean-square values) are also calculated per shell; uncertainties are estimated similarly to those for density.

3.3 Fitting models. We fit the empirical and thermodynamic models to density and velocity dispersion profiles derived from simulations after the simulations have settled to mechanical equilibrium. Mechanical equilibrium is verified by guaranteeing that the virial ratio of the system has reached a value of one and that the average radial velocity is zero throughout the system. We use the reduced χ^2 statistic as the figure of merit for our fits,

$$\chi^2 = \frac{1}{N_{data}} \sum_{i=1}^{N_{data}} \frac{(M_i - D_i)^2}{\Delta_i^2}. \quad (14)$$

where a data point value is denoted D_i , the corresponding model value is M_i , and Δ_i is the data uncertainty.

Since the generalized NFW and non-extensive models are not constrained to have well-defined total masses, we do not use the half-mass radius as the normalizing position. Instead, we force our model profiles to match data profiles at the location where the data logarithmic density slope γ is 2. However we use a smoothed version of the γ profile, as the data density gamma profile is noisy. We are therefore unable to interpret our χ^2 in an absolute sense. Notwithstanding, Lynden-Bell model fits produce substantially lower χ^2 values when the half-mass radius is used for linking to the data.

Due to their fixed shapes, Plummer and de Vaucouleurs density profiles are fit to the data density profiles by aligning their $\gamma = 2$ locations to that of the data. In order to isolate the best-fit parameters

for the generalized NFW and thermodynamic models, a nonlinear "amoeba" minimization scheme was implemented; a multi-dimensional minimization for non-analytical models. For a given initial parameter guess, a value of χ^2 is calculated and then several other parameter- χ^2 pairs are generated. The amoeba then "oozes" in the direction of the lowest χ^2 value.

For several simulations, amoeba minimization generated widely disparate minimum ν values for the Lynden-Bell model depending on the initial step size in the search. To clarify the amoeba behavior, we have implemented a Markov Chain Monte Carlo (MCMC) minimization to locate the region in parameter space wherein the minimum parameter value is located. Performing the MCMC minimization prior to the amoeba minimization of Lynden-Bell models ensures that an appropriate initial step size is chosen, resulting in the best-fit parameters for each evolved system.

4 Results

The results of this work explore the applicability of both empirical and thermodynamic models to simple self-gravitating collisionless equilibria. We have not found any one model that is capable of accurately describing all of our simulated systems. We highlight the successes and failures of the thermodynamic models as functions of the simulation initial conditions. Very few of our fits result in $\chi^2 \approx 1$, and it is unclear if this is a result of misestimation of uncertainties or simple inadequacy of the models (or some combination of the two). Since all model fits utilize the same uncertainties with the same $\gamma = 2$ position, we attempt to minimize their impacts on the fits by taking ratios of χ^2 values. The plots associated with this section normalize χ^2 values to the Lynden-Bell model χ^2 . To facilitate the range of ratios found, we plot the logarithm of the relative χ^2 -- negative (positive) values indicate models that outperform (underperform) the Lynden-Bell model.

4.1 Density fits.

4.1.1 Single and hot clumpy halos. The random initial orientation of velocity vectors within a hot ($T_f = 0.0$) clumpy system creates a close resemblance to a single system as it evolves, with each reaching mechanical equilibria that are extremely similar for a given Q_0 . We find that Lynden-Bell models generally provide density fits with lower χ^2 for single systems than for clumpy systems. The extent of these high quality density fits is limited to $Q_0 \gtrsim 0.7$ for single systems with Gaussian initial densities, and $Q_0 \gtrsim 0.4$ for single systems with cuspy initial densities. In line with their close resemblance, Lynden-Bell models have also shown success at modeling hot clumpy systems; high quality fits exist for $Q_0 \gtrsim 0.5$. With that being said, the non-extensive model provides the best fits for single systems with a Gaussian initial density when $Q_0 \gtrsim 0.2$. For single systems with cuspy initial densities, the non-extensive models provide the best fits for systems with low virial ratios. For hot clumpy systems, non-extensive models provide the best fits for systems with $Q_0 \gtrsim 0.3$ and Gaussian initial densities. When compared to the empirically derived models, the Lynden-Bell and non-extensive models together yield the best fits for hot clumpy systems with $Q_0 \gtrsim 0.2$ and cuspy initial densities. Figures 1 and 2 show how the relative χ^2 values compare for model fits to single and hot clumpy systems, respectively.

4.1.2 Cool and cold clumpy halos. We find that systems with minimal initial kinetic energy (small virial ratio Q_0) and cold ($T_f = 1.0$) clumpy systems evolve to have cuspy density profiles. The cuspy natures of de Vaucouleurs and generalized NFW profiles allow them to more accurately

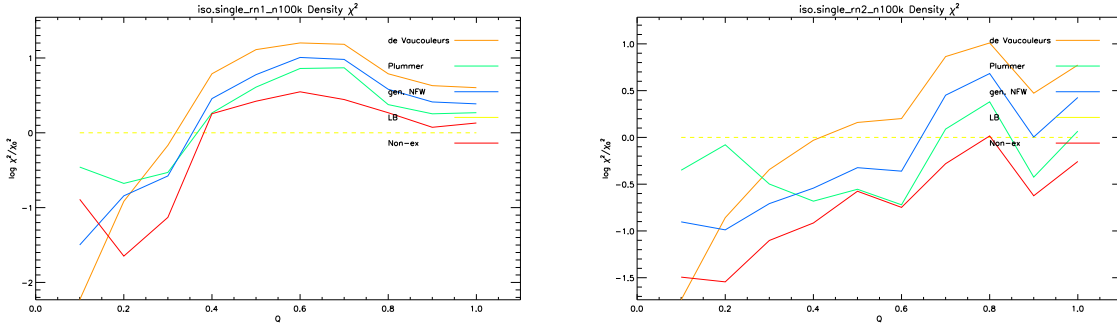


Fig. 1.--- The behavior of relative density χ^2 values for single systems with cuspy (left) and Gaussian initial densities (right) as a function of initial virial ratio. The curves plotted represent the logarithm of the individual model χ^2 values divided by the Lynden-Bell χ^2 values. Lynden-Bell models provide the best fits to high- Q_0 , cuspy systems. Non-extensive models outperform all other models for nearly all Gaussian systems.

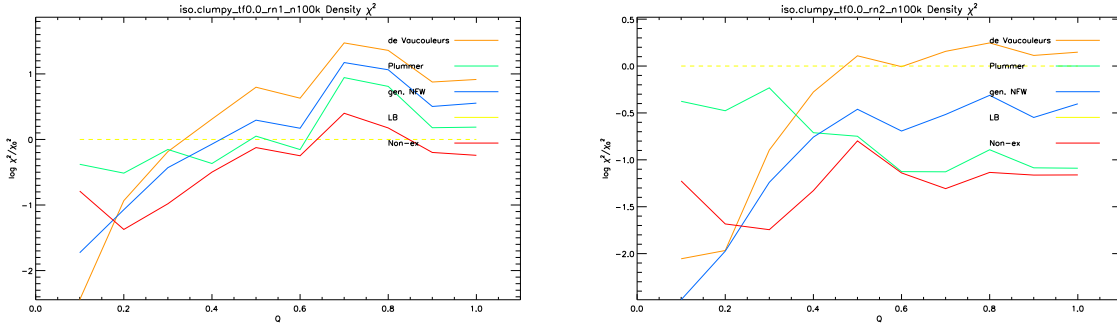


Fig. 2.--- For comparison with Figure 1, the behavior of relative density χ^2 values for hot clumpy systems with cuspy (left) and Gaussian initial densities (right) as a function of initial virial ratio. The curves represent the same quantities as in Figure 1. Lynden-Bell models provide good fits to high- Q_0 , cuspy systems, but they are now comparable to non-extensive model fits in several cases. Non-extensive models continue to outperform all other models for essentially all Gaussian systems.

model systems with these initial conditions. Moreover, as the initial virial ratio of a system increases, de Vaucouleurs and generalized NFW model fits decrease in quality.

We find that Lynden-Bell models provide very poor quality density fits for clumpy systems with $T_f = 1.0$ or $T_f = 0.5$. Since Lynden-Bell models derive from a distribution function that maximizes entropy, we infer that cool and cold clumpy systems do not achieve a state of maximum entropy once mechanical equilibrium is reached. Non-extensive models also have a particular difficulty matching density distributions for cold clumpy systems. However, non-extensive models are able to successfully describe clumpy systems with $T_f = 0.5$ for $Q_0 \gtrsim 0.3$.

4.2 Velocity fits. Non-extensive models predict velocity dispersion profiles for systems with isotropic velocity dispersions. In principle, one could likewise predict an isotropic velocity dispersion profile for Lynden-Bell models. In practice, it is simpler to find these profiles (and those for the empirical models) by solving the Jeans equation (Equation 12) with $\beta(r) = 0$. In general, there is little agreement between model isotropic velocity distributions and the simulations, independent

of initial conditions. Both thermodynamic models' root-mean-square speeds tend to be larger than simulation results at small radii, and the distribution shapes are rarely similar. Non-extensive models, however, describe velocity distributions of cuspy, single simulations with $Q_0 \gtrsim 0.4$ better than any other model.

Many of our simulations result in anisotropic systems. We also explore the impact of a non-zero $\beta(r)$. We assume the corresponding change in density is small, as the impact of the anisotropy on the amount of mass with a given energy is small (Binney & Tremaine 1987). The isotropic system density is then a good approximation for the anisotropic system density. We choose the $\beta(r)$ to be used in the Jeans equation to be a fourth-order polynomial fit to the data anisotropy. When the data velocity anisotropy is taken into account, Lynden-Bell model velocity distributions nearly always do a better job of describing the data than do non-extensive models. In line with the behavior of their density fits, anisotropic Lynden-Bell velocity fits fare worse than de Vaucouleurs and/or generalized NFW models for simulations with $Q_0 \lesssim 0.5$. We interpret this to mean that Lynden-Bell models can accurately represent the equilibria of collisionless self-gravitating systems that do not undergo violent collapses.

5 Summary & Conclusions

In an attempt to develop a better understanding of some key physical processes governing dark matter halos, we have created a suite of simulated self-gravitating collisionless systems. The initial conditions of the systems vary in density distributions and kinetic energy content. After evolution to mechanical equilibrium, density and velocity profiles have been created. We have systematically compared two physically motivated and three empirically-derived models of dark matter systems by their relative χ^2 values, based on fits to density and velocity profiles.

Independent of initial density profile, single and hot clumpy systems with virial ratios $Q_0 \lesssim 0.3$, cool clumpy systems with $Q_0 \lesssim 0.5$, and cold clumpy systems with $Q_0 \lesssim 0.9$ evolve to cuspy density distributions. Plummer and Lynden-Bell models do not accurately model the resulting density and velocity profiles of these systems, as they involve constant density cores. In agreement with previous studies, we find that non-extensive models can match the density profiles in many of these cases, but the velocity distributions of most simulations are not well-described. de Vaucouleurs and generalized NFW models match many density profiles produced by these kinds of systems. In some cases, these good density matches are accompanied by equally high-quality velocity fits. No systems are best-fit by a Plummer model.

We see a surprisingly strong influence of the initial density profile on a particular model's ability to match data. Lynden-Bell models generally provide high-quality density and velocity fits for single cuspy systems with modest to large virial ratios. Non-extensive models show similar behavior for simulations with Gaussian initial densities. While each of the thermodynamics-based models is suited to describe at least some simulated systems, Lynden-Bell and non-extensive models are not universally useful for describing the equilibria of self-gravitating collisionless systems. Apparently, in all but the most gentle relaxations, the dynamics present in the systems cannot erase the imprint of initial conditions. Any set of self-gravitating, collisionless equilibria that share common characteristics (radial density profiles, radial pseudo-phase-space ρ/σ^3 profiles, etc.) must result from some shared, common initial conditions.

We gratefully acknowledge support from the Wisconsin Space Grant Consortium and the University of Wisconsin-La Crosse Foundation's Gubbi R. Sudhakaran Fund for Physics Research. We also thank Amanda Alexander, Chintan Modi, and Melissa Wheeler for helpful discussions regarding model fitting procedures.

REFERENCES

- [1] Barnes, E. I., Williams, L. L. R., Babul, A., Dalcanton, J. J., 2007, *The Astrophysical Journal*, 655, 847
- [2] Binney, J., Tremaine, S. 1987, *Galactic Dynamics*, Princeton University Press, Princeton, N.J.
- [3] de Vaucouleurs, G. 1948, *Ann. d'Astrophys.*, 11, 247
- [4] Governato, F., Brook, C., Mayer, L., Brooks, A., Rhee, G., Wadsley, J., Jonsson, P., Willman, B., Stinson, G., Quinn, T., Madau, P. 2010, *Nature*, 463, 203
- [5] Kronberger, T., Leubner, M. P., van Kampen, E. 2006, *Astronomy & Astrophysics*, 453, 21
- [6] Lithwick, Y., Dalal, N. 2011, *The Astrophysical Journal*, 734, 100
- [7] Lynden-Bell, D., 1967, *Monthly Notices of the Royal Astronomical Society*, 136, 101
- [8] Moore, B., Quinn, T., Governato, F., Stadel, J., Lake, G., 1999, *Monthly Notices of the Royal Astronomical Society*, 310, 1147
- [9] Navarro, J. F., Frenk, C. S., White, S. D. M. 1996, *The Astrophysical Journal*, 462, 563
- [10] Navarro, J. F., Frenk, C. S., White, S. D. M. 1997, *The Astrophysical Journal*, 490, 493
- [11] Navarro, J. F., Hayashi, E., Power, C., Jenkins, A. R., Frenk, C. S., White, S. D. M., Springel, V., Stadel, J., Quinn, T. R. 2004, *Monthly Notices of the Royal Astronomical Society*, 349, 1039
- [12] Plastino, A. R., Plastino, A. 1993, *Physics Letters A*, 174, 384
- [13] Plummer, H. C. 1911, *Monthly Notices of the Royal Astronomical Society*, 72, 460
- [14] Springel, V. 2005, *Monthly Notices of the Royal Astronomical Society*, 364, 1105
- [15] Taylor, J. E., Navarro, J. F. 2001, *The Astrophysical Journal*, 563, 483
- [16] Tsallis, C. 1988, *Journal of Statistical Physics*, 52, 479
- [17] van Albada, T. S. 1982, *Monthly Notices of the Royal Astronomical Society*, 201, 939

Expanding Our Knowledge of Interstellar Neutral Hydrogen Shells

Tyler Laszczkowski¹

Shauna Sallmen

University of Wisconsin – La Crosse

Abstract

The purpose of this research is to increase the number of Galactic neutral hydrogen (HI) shells available for study. By identifying and studying more HI shells at various stages of their evolution, we can start to fill the gap in our understanding of the interactions of structures in the interstellar medium. This project consisted of visually identifying new HI Shells using 21-cm data downloaded from the GALFA-HI online database. This survey has higher angular resolution than the data used in previous searches, allowing us to discover smaller features. The results include a new list of previously undiscovered shell-like HI features along with measurements of their basic properties: location, mean angular diameter, shape, signs of expansion. Upon completing the search of 1/7th of the data cubes containing complete GALFA data, 141 potential shells were discovered. Additionally, one pattern appeared several times while identifying potential shells. This pattern can be described as a “figure-eight” feature composed of two features that are likely related. The completion of this project has expanded the current database of potential HI Shells in our galaxy, which can be used to provide important data in regards to the study of shell evolution and the role of shells within the ISM.

¹ I would like to acknowledge the WSGC for granting me this award and allowing me this opportunity to further my education and involvement in Astronomy research. Further acknowledgments are included at the end of the paper.

Background

The matter which makes up the interstellar medium (ISM) is full of complex, interacting features. In terms of mass, this matter is 99% gas and 1% dust with only 2% of the atoms being elements heavier than helium. In general, the ISM has a very low density, but it is far from uniform. Through winds and supernova explosions, stars send out material that is enriched with the heavy elements made in stars during their lives and deaths. Eventually, this enriched material mixes into and is distributed throughout the turbulent ISM. This allows for the formation of new stars as well as star systems. Thus the heavy elements found within our own solar system were created and distributed by these processes.

As a result of these stellar winds and supernovae, expanding bubbles of hot gas will commonly form in the ISM. As such a bubble expands; it pushes the surrounding cool neutral hydrogen into a shell around the bubble. We can observe and study these shells using the 21cm radiation from neutral hydrogen atoms using radio telescopes. Over time, the shell expansion will begin to slow as it interacts with the ISM and eventually the bubble cools as it loses energy and mixes with the surrounding ISM.

While we have a general understanding of the evolution of the ISM, much is still uncertain. Various models have attempted to identify the processes and structures that contribute to the evolution of the ISM in our Galaxy, and it is clear that shell evolution plays a key role (e.g. models of McKee & Ostriker 1977, Shapiro & Field 1976, Slavin & Cox 1993). As described by the galactic fountain model, superbubbles (the result of multiple supernovae) can cause hot gas to rise out of the Galactic plane where it will then cool, and fall back onto the Galaxy's disk.

However there still exist gaps in our understanding so we lack a complete picture of the details involved; for example the role of magnetic fields and exactly how energy of supernova explosions disrupts the medium (e.g. see review by Cox 2005). By identifying and studying more HI shells at various stages of their evolution, we can start to fill this gap in our understanding of the interactions of structures in the ISM. We need to study as many shells as possible in order to understand the complete picture.

Our research group works to increase our knowledge of HI Shells by discovering new shells and measuring their properties. For suitable shells, detailed follow-up study at various wavelengths increases the number of well-observed shells that can be used to study the processes of shell evolution. Using the 21-cm neutral hydrogen maps available in the SETHI (Search for Extraterrestrial HI) database (Korpela 2002, 2004), my advisor and her research students have created a list of 71 shells at various reference velocities, none of which had been previously identified (Sallmen et al., in preparation). This search resulted in shells missed by previous searches for several reasons. (1) The SETHI database had improved angular resolution compared with other 21-cm surveys away from the Galactic plane (e.g. Leiden-Dwingeloo survey, Hartmann & Burton 1997), so smaller shells could be found. (2) Many searches identify shells by signs of expansion, so older shells expanding more slowly are absent from these catalogs (e.g. Ehlerová & Palouš 2005). (3) The visual identification techniques that were utilized allowed for the discovery of shells that could have been missed by an automated search (fragmented, incomplete, or small shells).

The Galactic Arecibo L-band Feed Array HI (GALFA-HI) survey (Peek et al. 2011) is producing neutral-hydrogen maps of Galactic gas with better angular resolution, sensitivity, and calibration than SETHI. This made it an ideal dataset for further shell identification activities.

Procedure

This summer, our project consisted of visually identifying new HI Shells using data downloaded from the GALFA-HI online database. For each data cube, we visually searched for new shells, compared my discovered shells with catalogs of known shells, and generated a new catalog of previously unknown shells including measurements of their basic properties.

We began by creating custom cubes in which to search for shells. The data used in this project are publicly available online via the GALFA-HI website (<https://sites.google.com/site/galfahi/Home>). This survey covers the region of the sky visible from the Arecibo Telescope. HI maps are available for regions with celestial coordinates 0^{h} to 24^{h} in Right Ascension and -2° to $+38^{\circ}$ in Declination, although data are complete for only about 1/3 of the sky, and is not contiguous in all regions. Note that Right Ascension & Declination are the sky equivalents of longitude and latitude here on Earth.

Each custom data cube covered a portion of the Arecibo sky approximately $20^{\circ} \times 20^{\circ}$ in size. At every location in the sky, the amount of 21-cm emission has been measured for all radial velocities corresponding to motions of Galactic gas. Because of its orbits around the Galactic center, gas at different distances from us will be detected at different radial velocities. In addition, shell expansion, as well as turbulent and streaming motions affects the observed velocities. The data cubes that were created contain 512 HI maps at radial velocities spaced by 0.74 km/s. These cubes overlapped in position in order to detect shells which could potentially lie on the edge of the cube.

Each cube was then methodically searched for potentially undiscovered shells. Visual identification was the preferred method due to other search methods excluding shells that are oddly shaped or extreme in size, and excluding older non-expanding shells. A majority of the work being done for this project utilized the <kvis> software of the Karma Toolkit (Gooch 1996) in order to satisfy the project goals. This general purpose image and movie viewer is capable of loading multiple data sets and displaying multiple windows. These features allow one to step through the various velocity slices and to adjust histogram and pseudo color settings in order to highlight features in both faint & bright gas regions. Each cube was searched using multiple display settings in order to conduct a complete analysis of the data.

Although the online GALFA database is currently incomplete, the existing data proved to be more than sufficient for a significant number of new potential shells to be identified and measured.

Upon discovering a potential shell, we recorded its center coordinates, the reference velocity at which it is most shell-like, its right ascension, and its declination. After recording the findings for a particular cube, we compared the shell candidates with catalogs of previously known shells. This allowed for the determination of which of the shells were previously unknown.

Each of the newly discovered shells was further analyzed using <kvis>. This included measuring quantitative values such as the minimum and maximum values for Right Ascension, Declination and velocities at which it appeared shell-like. We also recorded qualitative data regarding the behavior of the potential shell while stepping through the velocity slices. These data were used to create a GSH ID (an identifier for a specific shell using the Galactic coordinate system) and to tabulate a mean angular diameter and shape parameter for each shell. The mean angular diameter ($\Delta\theta_{\text{avg}}$) is a basic size description based on the lengths of the short and long axes, assuming the shell is elliptical in shape. By determining four points within the shell walls at the end of each axis, we computed the axis lengths, $\Delta\theta_1$, $\Delta\theta_2$ (the distance between each set of points), and the mean angular diameter (the average of the two distances). Using the same four boundary points, we also calculated the shape parameter, a value that specifies the eccentricity of a given shell. For our purposes, we've defined the shape parameter to be a value ranging from 0 to 1 where 0 represents a straight line and 1 represents a perfect circle [$S = 1 - (\Delta\theta_1 - \Delta\theta_2) / 2\Delta\theta_{\text{avg}}$]. We also determined the range of velocities at which the feature is shell-like, and made an image of the shell at its reference velocity. An example of such an image can be seen in Figure 1. This process was repeated over and over in order to create a large catalog of previously unknown potential shells.

GSH 167-13-042

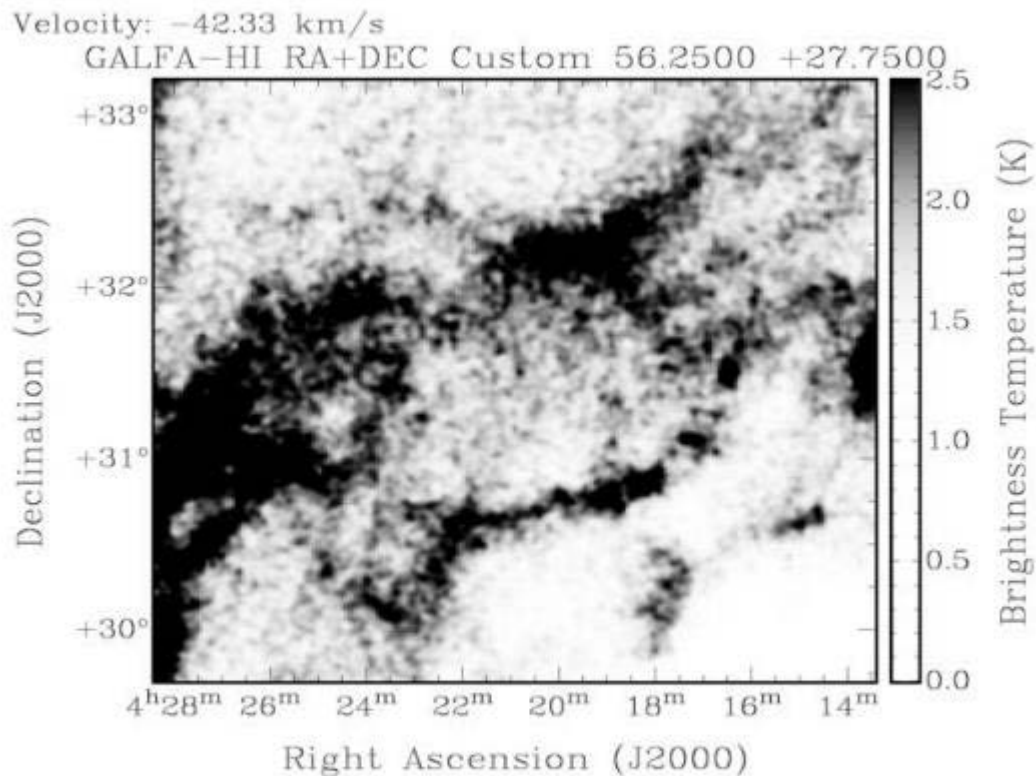


Figure 1: Image produced in <kvis> of a Neutral Hydrogen (HI) Shell discovered in the 21cm GALFA-HI database. We can see that it is centered at 04h 21m in Right Ascension and 31.3° in Declination. It's reference velocity is -42.33 km/s and it has a Mean Angular Diameter of 1.79°.

Results

The results of this project include a new list of previously undiscovered shell-like HI features along with measurements of their basic properties, and images of each feature. The search process utilized six data cubes and resulted in the identification of 141 potential shells. While the total number of shells discovered was 151, ten of these shells were not included in the final list. Of these ten, seven were already listed in online catalogs and were confirmed as previously identified, while the remaining three features were considered to be insufficiently shell-like for inclusion.

Table 1 displays sample data regarding 7 of the shells. The first column contains the GSH identifier based on the shell's Galactic coordinates. For each shell, the table includes celestial coordinates for the center of the shell (RA, Dec, columns 2-3), and the Mean Angular Diameter and Shape values (columns 4-5), which are a direct result of four measured boundary points, as described in the Procedure.

The Quality Parameter in the final column is a summary of overall shell quality based on five shell parameters, each represented with a value between 0 and 1. These factors, shown in columns 5-9, include the shape parameter (column 5), the completeness of the shell walls at the reference velocity (column 6), the extent to which the shell's shape and location remain constant over its velocity range (column 7), whether or not its front & rear expanding walls are visible (column 8), and the fraction of the velocity range at which the shell appears relatively complete, as opposed to merely shell-like (column 9). For columns 7 & 8, the parameter will have a value of 1 if the feature behaves exactly as expected for an expanding shell, and 0 if it does not behave at all like an expanding shell. The final Quality value weights all 5 parameters equally, so is represented by a number between 0 and 5, where 5 is a perfect shell, exhibiting all the features of an interstellar shell. Note that a shell with little expansion will not have obvious front and rear walls, so will be limited in quality. The quality of the potential shells ranged from values of 2.53 to 4.55 with an average value at 3.46.

Table 1 – Measured Parameters for Selected Shells

| Official ID | Center RA (hh mm) | Center Dec (Deg) | MAD (Deg) | Shape Parameter | Fraction Closed | Same Shape/Location at Multiple Vels? | Front/Rear Caps Visible? | Fraction of Range over which completeness is at Maximum | Summary (Quality Parameter) |
|----------------|-------------------|------------------|-----------|-----------------|-----------------|---------------------------------------|--------------------------|---|-----------------------------|
| GSH 171-11+017 | 04 42 | 29.8 | 7.8 | 0.86 | 0.9 | 1 | 0.5 | 0.45 | 3.71 |
| GSH 147-28-068 | 02 31 | 30.4 | 0.56 | 1 | 1 | 1 | 0 | 0.5 | 3.5 |
| GSH 169-28-016 | 03 40 | 19.6 | 0.96 | 0.97 | 1 | 1 | 1 | 0.58 | 4.55 |
| GSH 156-17+001 | 03 31 | 35.7 | 3.4 | 0.55 | 0.8 | 0.8 | 0 | 0.38 | 2.53 |
| GSH 162-13-027 | 04 06 | 35.2 | 1.17 | 0.57 | 1 | 1 | 0.5 | 0.38 | 3.45 |
| GSH 165-21-004 | 03 49 | 27 | 2.33 | 0.66 | 1 | 0.8 | 0 | 0.36 | 2.82 |
| GSH 173-19+017 | 04 20 | 22.9 | 1.6 | 0.59 | 1 | 1 | 0.5 | 0.33 | 3.42 |

The shells discovered during this project vary greatly in size and shape. Included in this table are the largest shell (GSH171-11+017), the smallest shell (GSH147-28-068), the highest quality shell (GSH169-28-016), and the lowest quality shell (GSH156-17+001). The remaining shells in the table are typical examples of the majority of potential shells discovered.

While many shells exhibited complete walls and a uniform circular shape, many also displayed odd or elongated shapes as well as incomplete walls or varying wall thickness. The mean angular diameter for the shells discovered in this search ranged from 0.56 to 7.80 degrees with a

mean value of 1.85° . The shape parameter ranged from values of 0.42 to 1.00 with 0.79 representing the mean value. The distributions of mean angular diameters and shape parameters are shown in Figure 2. The left figure highlights the fact that a majority of the potential shells were small in size. It is likely that these shells were missed in previous searches due to the limited resolution of those data. The right figure tells us that most shells were relatively circular in shape. This is what we expect due to the fact that shape parameters near zero look increasingly less shell-like and hence aren't included in the final results.

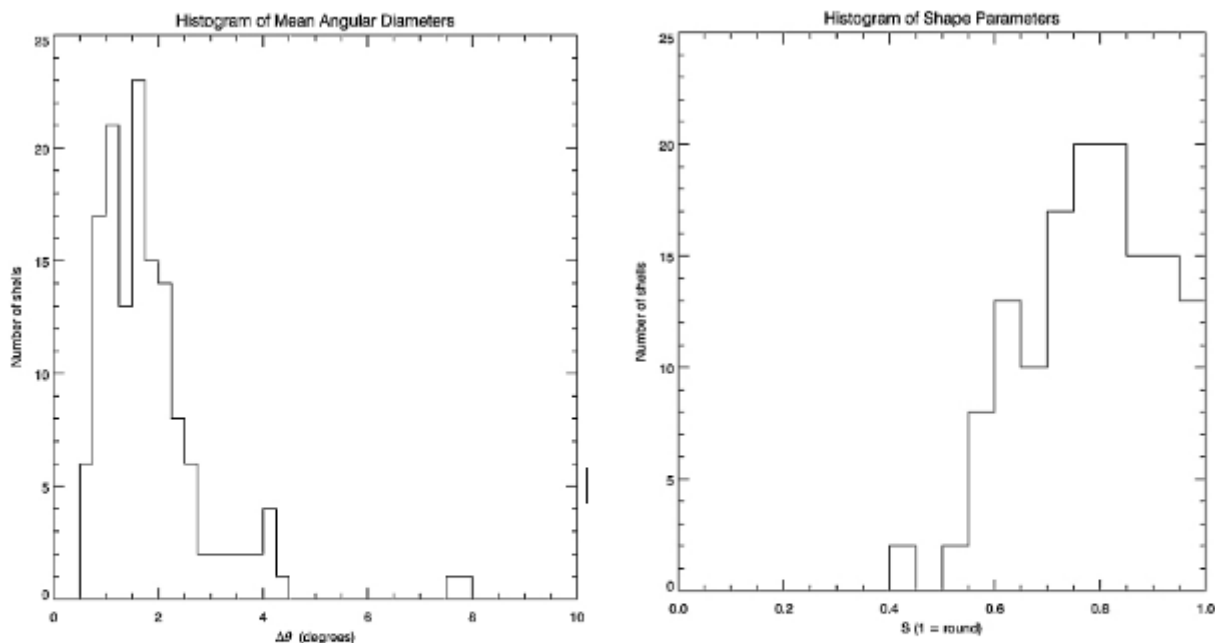


Figure 2: Histograms of Mean Angular Diameters (left) and Shape parameters (right) of neutral Hydrogen (HI) Shells discovered in the 21cm GALFA-HI database. Mean angular diameters range from 0.56° to 7.8° , with a majority of the potential shells $0.5^\circ < \theta < 3^\circ$ in size. The average shape parameter was 0.79. The lack of low shape parameters is due to line-like features not being considered sufficiently shell-like for inclusion in the catalog.

Many shells also displayed evidence for expansive behavior. When stepping through the velocity slices, a clearly expanding shell will contain both a front and rear wall at the maximum and minimum velocity values respectively. Shells which are considered to show signs of expansion will display at least one of these two walls. Shells without such features may be older shells whose expansion has slowed over time and are in the process of cooling and mixing with their surroundings. However, it is also possible that these features are absent in various shells because they contain low density walls that are only visible along the edges.

Of the total number of shells discovered (141), 100 displayed possible signs of expansion by appearing to exhibit at least one front or rear wall. If this were accurate (see below), we could conclude that roughly 71% of the shells observed were still in the expansion process while the remaining 29% are older shells whose expansion has slowed or halted over time. However this is likely an overestimate. Upon viewing the GALFA data, it becomes apparent that the vast number of random interstellar features could have been mistaken for a shell wall in many cases.

When we examine the 100 potential shells which showed possible signs of expansion, only three shells contained both a front and rear wall. It is very likely however, that these are indeed expanding shells. It is evident that shells which are obviously expanding do not represent the majority of features observed. Roughly 2% of the total 141 shells were found to contain both a front and rear wall. This supports the idea that visual identification is not biased towards expanding features.

It is clear that the observed “single-wall” potential shells will require re-examination in order to accurately determine if they qualify as shells displaying signs of expansion or were simply mistaken as such. Such future work will entail the study of changes in shell size on either side of the reference velocity, and examination of the data in position-velocity space to search for further evidence of expansion.

We created a sky map displaying locations and relative sizes of the newly identified potential shells. Figure 3 plots the shells using the equatorial coordinate system and ranges from 0 to 6 hours in Right Ascension and 16 to 40 degrees in Declination. Although the shells are represented as perfect circles on the figure, we must note that they are in fact irregular. The relative sizes are based on the mean angular diameter of the respective shells. Upon viewing the figure, we can clearly see a higher number of potential shells being identified proximate to the Galactic plane. Near the left side of the diagram, we see a vertical dashed line located at 5.25 hours in Right Ascension. This line represents the edge of the data searched, hence there were no potential new shells discovered beyond this boundary (Right Ascension > 5.25 hours).

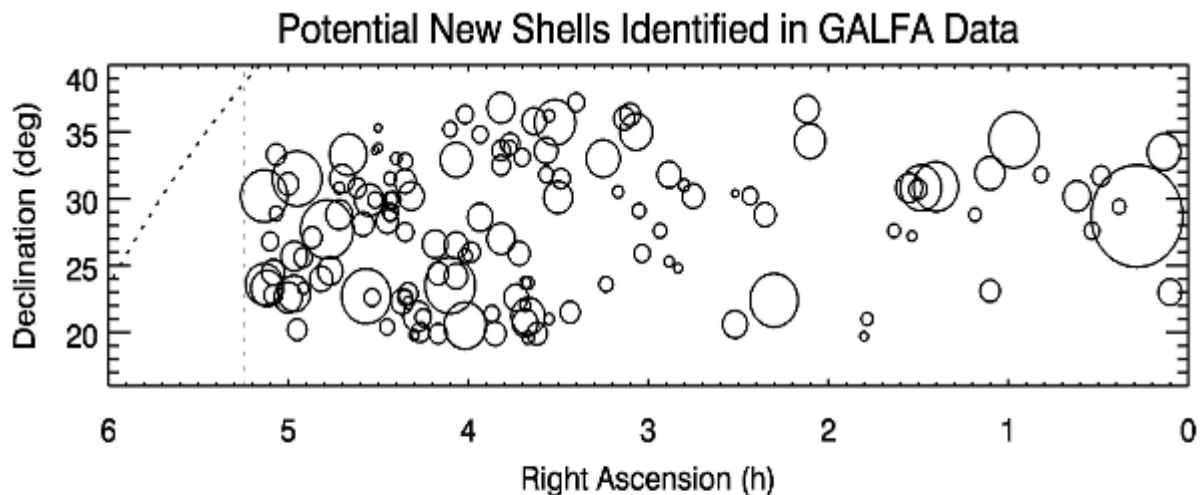


Figure 3: Sky map of neutral Hydrogen (HI) Shells discovered in the 21cm GALFA-HI database. We can see that it ranges from 0h to 6h in Right Ascension and 16° to 40° in Declination. Each circle charts the location and relative size of the respective potential shell. The diagonal dashed line on the far left of the figure represents the location of the Galactic plane while the vertical dashed line at 5.25 hours Right Ascension represents the “edge” of the data searched.

In addition, a common object resembling a “figure-eight” design was observed multiple times in various data cubes. A total of seven of these objects were discovered (seven figure-eights, fourteen potential shells). Each figure eight showed a consistent trend of being composed of small, complete, circular shells which were clearly related to one another upon stepping through their velocity range. An example of such an object can be observed in Figure 3.

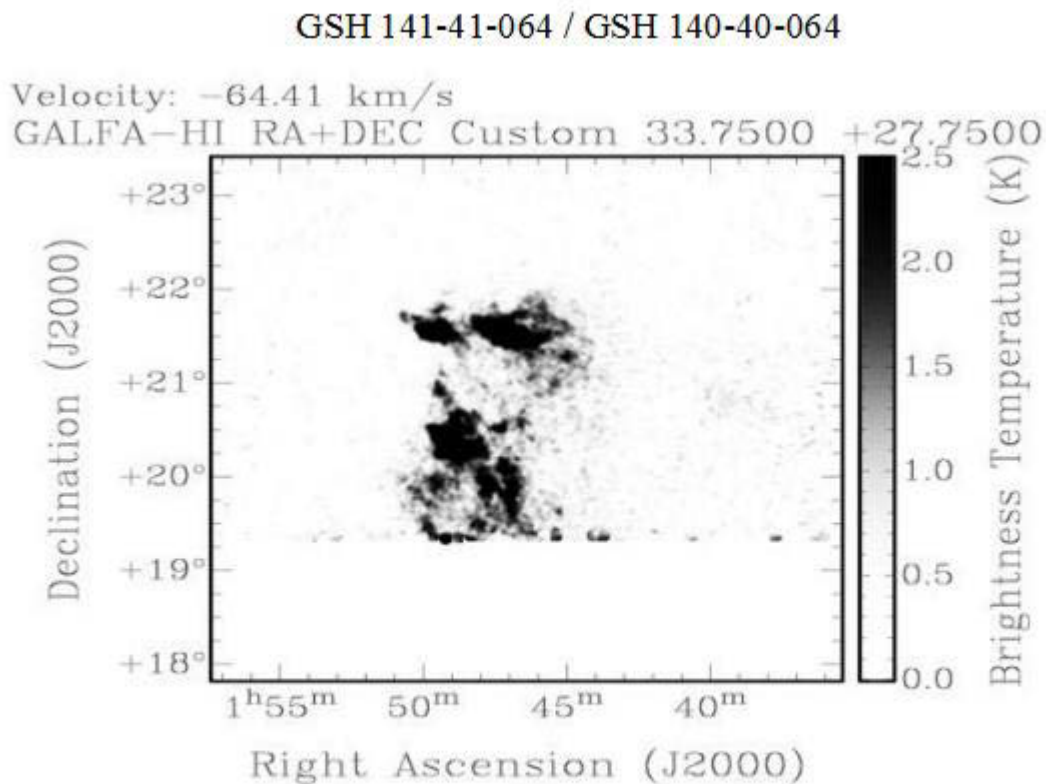


Figure 4: Image produced in `<kvis>` of a “Figure-eight” pair of shells discovered in the 21cm GALFA-HI database. We can see that the object is composed of two distinct shells; one centered at 01h 48m in Right Ascension and 19.6 degrees in Declination, while the other is centered at 1h 47m in Right Ascension and 21 degrees in Declination.

Conclusions

This project has expanded the current database of potential HI Shells in our Galaxy. A more complete list of HI shells will provide important data in regards to the study of shell evolution and the role of shells within the ISM. The visual identification methods that were used allowed for the identification of many shells which undoubtedly would have been missed by a computer search.

The mean angular diameter data for the newly discovered shells reveals that a majority of the shells are small in angular size. Many large shells have been previously discovered by visual searches, making the identification of small shells a priority with regards to completing the

overall picture of shell evolution. While a primary advantage of visual searches is the ability to identify odd-shaped shells, such features must also be “sufficiently shell-like” in order to qualify as a shell at all. The shape parameter data reveals that a typical potential shell included in our catalog is slightly elliptical, however some shells were measured to be extremely analogous to a perfect circle. By definition, features with a low shape parameter would appear line-like and therefore would not qualify as a potential shell for our catalog.

The high number of small shells discovered can be attributed to the improved angular resolution of the GALFA-HI survey as compared to previous surveys. Many of the shells were in fact too small to resolve prior to the release and examination of these data. We identified a very large number of new features per data cube, which then limited the overall number of cubes that could be searched within the time frame. The study of these small, previously unknown shells will be key to completing the overall picture of shell evolution.

The completion of this project also gives one a good perspective regarding the time required to complete the search of a given data cube. Even as the search procedure was optimized with repetition, the search process in general required more time than originally anticipated and as a result, fewer cube searches were completed. Approximately 1/7th of the total amount of data cubes containing GALFA data were searched, revealing the vast amount of potential future work yet to be completed. Additionally, as the project progressed, the cubes being searched were increasingly closer to the Galactic plane, yielding more shells per cube as opposed to those cubes farther from the Galactic plane. The sky map (See figure 3) that was generated displays this result as well as the relative sizes of the shells.

It is also likely that a large number of small potential shells were missed by the initial search, solely due to the overwhelming number of features now visible with the improved angular resolution. Later study of these data will not only include the search of the remaining data cubes, but also the reinvestigation of each cube by another set of eyes. This will likely add features to our catalog which were initially missed, resulting in a more complete search by eliminating bias. It will be interesting to compare the results of two visual searches of the same data by different observers.

It will also be crucial to calculate the kinematic distances to the potential shells. Because the data provides an angular view of the sky, it is impossible to determine whether a shell that is measured to be small is actually small in size or simply appears small due to its distance from Earth. Following the computation of kinematic distances, it will be possible to estimate the actual shell sizes, the energy required for the shells to form, and the approximate age of any expanding shells.

We also need to re-examine the signs of expansion properties for each potential shell. The initial search revealed an unusually high number of potential shells with at least some possible signs of front or rear walls. Expanding shells should appear to have different sizes at different velocities, and their expansion should also be visible in position-velocity space. By determining whether these features are actually shell walls or just random interstellar features, we can more accurately classify these potential shells as expanding or not expanding. Complete data on shell sizes, ages, energy required to form, and expansion properties is necessary to understanding their role in Galactic evolution.

Acknowledgments

I would like to acknowledge the WSGC for granting me this award and allowing me this opportunity to further my education and involvement in Astronomy research.

We acknowledge the use of the GALFA-HI database (<https://sites.google.com/site/galfahi/>), which uses data acquired at Arecibo Observatory. The Arecibo Observatory is operated by SRI International under a cooperative agreement with the National Science Foundation (AST-1100968), and in alliance with Ana G. Méndez-Universidad Metropolitana, and the Universities Space Research Association.

This research has also made use of the <kvis> software of the Karma Toolkit.

In addition, this research has made use of the SIMBAD database and the VizieR catalogue access tool operated at CDS, Strasbourg, France.

References

Cox, D. P. 2005, ARA&A, 43, 337.

Ehlerová, S. & Palouš, 2005, Astron. & Astrophys., 437, 101.

Gooch, R. 1996, Astronomical Data Analysis Software and Systems V, 101, 80.

Hartmann, D., & Burton, W. B. 1997, Atlas of Galactic Neutral Hydrogen (Cambridge University Press), ISBN 0521471117.

Korpela, E. J., Demorest, P., Heien, E., Heiles, C., & Werthimer, D. 2002, Seeing Through the Dust: The Detection of HI and the Exploration of the ISM in Galaxies, 276, 100.

Korpela, E. J., Demorest, P., Heien, E., Heiles, C., & Werthimer, D. 2004, How Does the Galaxy Work?, 315, 97.

McKee, C. F., & Ostriker, J. P. 1977, ApJ, 218, 148.

Peek, J. E. G., Heiles, C., Douglas, K. A., et al. 2011, ApJS, 194, 20.

Shapiro, P. R., & Field, G. B. 1976, ApJ, 205, 762.

Slavin, J. D., & Cox, D. P. 1993, ApJ, 417, 187.

Searching for Gravitational Waves from Sub-Solar Mass Black Holes

Madeline Wade and Jolien Creighton

Physics Department, UW – Milwaukee, Milwaukee, WI

Abstract

We are searching for gravitational-wave signals from sub-solar mass black hole binary systems in initial Laser Interferometer Gravitational-wave Observatory (LIGO) data. The most likely candidates for such systems are primordial black holes that have formed from the collapse of quantum fluctuations in the early universe. Primordial black holes have not yet been ruled out by microlensing experiments, but the allowable masses have been restricted. The gravitational-wave strain from such an inspiralling binary system is well modeled with the post-Newtonian formalism. Therefore, a modeled search for gravitational-wave signals is employed. The search technique is known as matched filtering and is implemented using a codebase that is well-suited for fast searches with long signals. One of the biggest challenges in performing this search is dealing with the heavy computational burden. The gravitational-wave signals from such low-mass binary systems are long (about 10 minutes) and require a large number of models, or templates, spread across the parameter space. A large effort has been focused on speeding up the search while using a reasonable amount of computational resources.

Introduction

The field of gravitational-wave physics has become increasingly relevant in the past decade. The first generation of the Laser Interferometer Gravitational-wave Observatory (LIGO) was a ground-based interferometer designed to detect gravitational waves as predicted in Einstein's theory of General Relativity. The instrument performed six science runs over the course of six years. The collected data has been analyzed for the most likely gravitational-wave signals with no detections evident yet. However, the next generation of LIGO, the advanced Laser Interferometer Gravitational-wave Observatory (aLIGO), should be completed in 2015. It will be the best ground-based interferometer designed to detect gravitational waves to date. When completed, aLIGO will provide a dramatic improvement in sensitivity that will virtually guarantee detections, likely in abundance (Abadie *et al.*, 2010). With gravitational-wave detections, we will learn more about astrophysical systems that still remain a large mystery.

Ground based interferometers, such as LIGO and aLIGO, are especially sensitive to gravitational waves from compact binary coalescence events. A compact binary coalescence event comprises the inspiral, merger, and ringdown of two massive, compact, astrophysical objects, such as neutron stars and/or black holes. The data collected during initial LIGO's science runs have been analyzed for compact binary coalescence events only where the two components of the binary have masses larger than one solar mass. We perform a search on data from initial LIGO's fifth and sixth science runs for sub-solar mass compact binary coalescence events. In addition to

The authors acknowledge the support of the Wisconsin Space Grant Consortium Graduate Fellowship. The authors would also like to acknowledge contributions to this work from Kipp Cannon (CITA, University of Toronto) and Chad Hanna (Penn State University) in development of and assistance with the coding infrastructure used.

searching for gravitational waves, the search we perform also serves as a test of aLIGO computational technologies.

Background and Motivation

Gravitational-wave signature from compact binary coalescence events. The existence of sub-solar mass black holes has not been ruled out by microlensing experiments (Alcock *et al.*, 2000; Tisserand *et al.*, 2007; Wyrzykowski *et al.*, 2003), though their existence is thought less likely than super-solar mass black holes. The most popular theory for the formation of sub-solar mass black holes involves primordial black holes (PBHs), which would have evolved through the collapse of quantum fluctuations in the early universe (Hartle, 2003).

No matter the mechanism that produces them, if two sub-solar mass black holes are undergoing compact binary coalescence, the gravitational waves from the inspiral portion of such a system are well modeled with post-Newtonian theory. The gravitational-wave strain $h(t)$ is a measure of the stretching and compressing of spacetime caused by a passing gravitational-wave. The gravitational-wave radiation produced by the inspiral of a compact binary coalescence event is simply modeled in the frequency domain as

$$h(f) = Af^{7/6}e^{i\psi_{SPA}(f)}$$

where A is an amplitude factor, f is the gravitational-wave frequency, and ψ_{SPA} is the phase found using the stationary phase approximation. The parameters of the system, such as the component masses of the binary, the sky location of the binary, and the distance to the binary, are included in the amplitude factor A and the phase $\psi_{SPA}(f)$.

In this way, when LIGO makes its first gravitational-wave detection from the inspiral of a compact binary coalescence event, not only will the detection confirm the existence of gravitational waves, but information about the astrophysical system producing the gravitational waves can also be extracted from the detected signal. The data analysis procedures are broken into two components: detection and parameter estimation. The detection effort tries to state with some level of confidence that a gravitational-wave signal is present in the data. The parameter estimation effort looks more closely at the time period surrounding a detection and tries to pin-point the type of system that sourced the detected gravitational-wave. The search we perform focuses on detection of gravitational-waves in LIGO data and not on parameter estimation.

Initial LIGO network. The search we perform is on the initial LIGO network of interferometers. During initial LIGO's fifth science run, there were three interferometers in operation. There was one interferometer in Livingston, Louisiana, and there were two co-located interferometers in Hanford, Washington. One of the interferometers in Hanford was more sensitive than the other interferometer on site. The more sensitive interferometer in Hanford had about equal sensitivity to the interferometer in Livingston.

Since the two Hanford interferometers were co-located, it is possible to combine the data from the two interferometers into two new types of data streams: a coherent combination and a null combination (Creighton & Anderson, 2011). The coherent combination is a linear combination of the two individual interferometer data streams, and it contains noise along with

any gravitational-wave signals. The coherent combination has the benefit of an improved sensitivity of about 10% over the individual interferometer data streams. The null combination is a simple subtraction of the two data streams obtained from each individual interferometer. Since a gravitational wave will manifest in the same way in co-located interferometers, the null combination will contain no gravitational-wave signal. Therefore, the null combination can be used to veto large transient events that are only noise.

While coherent and null combinations are possible to create for interferometers that are not co-located, the formation of these streams is more complicated and computationally expensive for such systems. For interferometers that are not co-located, the coherent and null combinations are only produced when a sky position for the source of the gravitational waves is known to some degree.

In this search, we only use the coherent and null combination for the two co-located Hanford interferometers. The null combination is used to veto time periods where known glitches (non-gravitational-wave transient events) occurred. The coherent combination is used in the matched filter search, described below.

Methodology

The technique used to pick out a gravitational-wave signal from background detector noise is called matched filtering. This technique involves comparing the detector data with templates of the expected gravitational-wave signal for the inspiral portion of a compact binary coalescence event. To create a template, parameters are chosen (i.e. component masses, sky position, distance) for the source of the gravitational-wave signal and used along with the gravitational waveform to create a time series or frequency series of the expected gravitational-wave signal.

We have created a “template bank” by producing these templates for a selection of parameters where the component masses m_i are chosen such that $0.1 M_{\text{sun}} < m_i < 1.4 M_{\text{sun}}$ with the ratio of component masses restricted to be between 1 and 3. This mass space was chosen so that it covers the most likely value for primordial black holes as obtained from microlensing surveys. However, we have chosen not to search below $0.1 M_{\text{sun}}$ due to computational resources. The number of templates required to properly populate the parameter space scales with the minimum mass in the template bank as $m_{\text{min}}^{-8/3}$ (Owen & Sarhyaprakash, 1999). We have also restricted the mass ratio of the templates so that interesting systems, such as a $0.1 M_{\text{sun}} - 0.3 M_{\text{sun}}$ binary, are included; not all mass ratios are considered, however, in order to improve computational costs. Even though this is a sub-solar mass binary search, we have extended the upper mass cutoff to $1.4 M_{\text{sun}}$. Neutron star-PBH binaries have also never been searched for in initial LIGO data, so extending this upper mass cutoff allows us to search for systems such as a $0.8 M_{\text{sun}} - 1.4 M_{\text{sun}}$ binary. The total number of templates required to appropriately populate the parameter space for these mass ratios is about 140,000. For such small mass systems, these templates are also very long (on the order of 10 minutes). This is a large number of long templates, and, as a result, a major part of this search is reducing the computational time required to perform the search given our limited resources.

For this search, we are using code that can handle long templates and run relatively quickly. The codebase we are using is known as *gstlal* and has been developed for low-latency

gravitational-wave searches. We are using the matched filtering detection pipeline in *gstlal* known as *gstlal_inspiral*. We have fine-tuned how the pipeline is configured to run in order to optimize the computational speed without sacrificing the pipeline's efficiency. We are testing the fine-tuning by injecting a number of fake gravitational-wave signals, known as "injections", into one day of data. We then run the pipeline on this data stretch and determine how long it took and how many computational resources it required. We also see how many injections we were able to recover with the pipeline. Efficiency is measured by the number of found injections divided by the total number of injections.

Results and Future Work

We have been working to reduce computational resources required to a reasonable number of CPUs without hurting our efficiency too much. We have been doing this by tweaking various components of the search process, such as the number of templates in the template bank and the I/O (input/output) efficiency for reading in data and writing out results. In addition, we have been exploring an optimization of the statistic used to determine if a signal in our data is truly a signal or is just a result of noise.

Test runs on one-day stretches of data have proven promising. The search so far has tested to have about 50% efficiency. This means that 50% of the injected signals are found with enough statistical significance by the search pipeline. Injected signals are recovered out to about 11 Mpc, which means we have the ability to probe galaxy halos outside of the Milky Way Galaxy.

This project will continue into the 2014-2015 school year with further support from the Wisconsin Space Grant Consortium Graduate Fellowship. The focus of next year's work will be to run the optimized search on at least one full month of data and practice analyzing the results of the search. Upon the completion of this, a search on the full two years of data will follow. The search will either result in a direct detection of gravitational-waves or will set a halo-model independent upper limit on the existence of sub-solar mass binary systems.

Conclusions

A detection of gravitational waves with LIGO will push our current understanding of cosmology into a new era. Not only will we be able to test for the correct theory of gravity, but we will also have at our fingertips a new type of telescope to probe dramatic astrophysical events. Gravitational-wave detections will be very complementary to our on-going electromagnetic observations with telescopes around the world and neutrino detection efforts, such as with Ice Cube. Together, these different types of telescopes will allow us to test theories and discover astrophysical systems that were previously unavailable to us.

The search we are performing not only contributes to the effort towards the first direct detection of gravitational waves, but it also serves as an excellent test of our detection pipeline for the next generation of gravitational-wave detectors. In the advanced detector era, we expect to have long signals (also about 10 minutes) that will require about 200,000 templates per template bank for our most promising sources. By performing this search on initial LIGO data for sources that will manifest similarly to promising aLIGO sources, we are stress testing our detection pipeline on real data with real templates. This search will lay the foundational work for the aLIGO detection pipelines. In addition to the possibility of direct gravitational-wave detection, the search

we are performing is an excellent stepping stone into the advanced era of gravitational-wave astronomy.

References

J. Abadie, B.P. Abbott, R. Abbott, M. Abernathy *et al.* TOPICAL REVIEW: Predictions for the rates of compact binary coalescences observable by ground-based gravitation-wave detectors. *Classical and Quantum Gravity*, 27(17):173001, September 2010.

C. Alcock, R. A. Allsman, D. R. Alves, T. S. Axelrod *et al.* The MACHO Project: Microlensing Results from 5.7 Years of Large Magellanic Cloud Observations. *Astrophysical Journal*, 542:281-307, October 2000.

J. D.E. Creighton and W. G. Anderson. *Gravitational-Wave Physics and Astronomy: An Introduction to Theory, Experiment and Data Analysis*. Wiley-VCH, first edition, 2011.

J. B. Hartle. *Gravity: An Introduction to Einstein's General Relativity*. Addison Wesley, 2003.

B. J. Owen and B. S. Sarhyaprakash. Matched filtering of gravitational waves from inspiralling compact binaries: Computational cost and template placement. *Physical Review D*, 60(2):022002, July 1999.

P. Tisserand, L. Le Guillou, C. Afonso, J. N. Albert *et al.* Limits on the Macho content of the Galactic Halo from the EROS-2 Survey of the Magellanic Clouds. *Astronomy and Astrophysics*, 469:387-404, July 2007.

L. Wyrzykowski, J. Skowron, S. Kozłowski, A. Udalski *et al.* The OGLE view of microlensing towards the Magellanic Clouds – IV. OGLE-III SMC data and final conclusions on MACHOs. *Monthly Notices of the RAS*, 416:2949-2961, October 2011.

24th Annual Wisconsin Space Conference

PART TWO

Physics and Engineering

Fire in Orbit: Equipping the Commercial Spaceflight Industry for Fighting Fire in Micro-Gravity

Trent Cybela¹

Orbital Technologies Corporation, Madison WI
University of Wisconsin – Platteville, Platteville WI

List of Terms

| | |
|--------|---|
| CCiCap | Commercial Crew Integrated Capability |
| ECLSS | Environmental Control and Life Support System |
| EVA | Extra-Vehicular Activity |
| FWM | Fine Water Mist |
| ISS | International Space Station |
| LEO | Low Earth Orbit |
| PFE | Portable Fire Extinguisher |
| UHPFE | Ultra High Pressure Fire Extinguisher |
| USOS | United States Orbital Segment |

Abstract

For several years, Orbital Technologies (ORBITEC) has had keen interest in the development of a portable fire suppression system intended for use in commercial spaceflight applications. With the aid of recent developments in fine water mist (FWM) atomization technologies, and partnerships with the University of Wisconsin – Platteville, work is commencing to develop a portable fire extinguisher (PFE). The extinguisher will be capable of operation in both gravity and microgravity environments regardless of orientation, and eliminate the use of toxic carbon dioxide as a fluid suppressant. The extinguisher will take advantage of the unique physics of microgravity to better suppress fires compared to previously used equipment. The following report outlines baseline research into the historical precedence of spacecraft fires, and common modes of fire ignition in microgravity. From this information we investigate design considerations necessary for the construction of a prototype PFE, as well as the market value of such a device.

Introduction

In the design of new space habitats and vehicles, considerations for the prevention and suppression of fires must be made. As far back as the Mercury and Gemini missions, astronauts had at their disposal various methods by which to extinguish fires (Friedman, 1999). PFE technology used today onboard the ISS is outdated, expensive, and not conducive for investment by the commercial spaceflight industry. Advances in fire suppression technology can be applied to new PFE systems which are effective at eliminating many common microgravity fire threats while being cost effective, lightweight, and portable. ORBITEC stands at a position currently to leverage industry experience towards creating a new PFE system for microgravity environments. In order to move forward, a strong foundation must be established in the history, causes, and current methods used to extinguish fires in space. This report follows the research phase of the

¹ Special thanks to the Wisconsin Space Grant Consortium (WSGC) who provided the necessary funding for student involvement in this project.

project, with commentary describing our intentions for the design and prototyping of the PFE. A first-level prototype is on schedule for completion before year's end, 2014.

Fire Science Overview

There are three elements required for a combustion reaction to take place: a fuel source, oxidizer, and heat energy. Removal of just one of these three elements will cause a fire to collapse. Most portable fire suppression systems focus on the removal of the oxidizer or heat energy from the combustion system. This is done because removing the fuel source after the advent of a fire is typically not practical. The three components required for combustion are the same both on earth and in space. The behavior of fire in microgravity however, is different compared to earth.

The “teardrop” shape of a candle flame does not occur in orbit. On Earth, the flame's shape is defined by the effects of gravity: the buoyancy of hot gases and movement of convection currents. Without gravity fire takes a much more spherical shape, as shown in Figure 1. There is no natural convection in microgravity. In the absence of an upward direction for a fire to burn, it burns in all directions. Typically microgravity fires burn slower as well; mainly because flames tend to be weaker without the aid of convection currents. New oxygen is not “swept” into the fire but needs to diffuse into the combustion area, which takes more time to accomplish (Friedman, 1999). Fires in space:

1. Burn at slower rates
2. Burn at lower temperatures, requiring less heat energy
3. Burn at lower oxygen levels, using 2-3% less oxygen compared to earth.

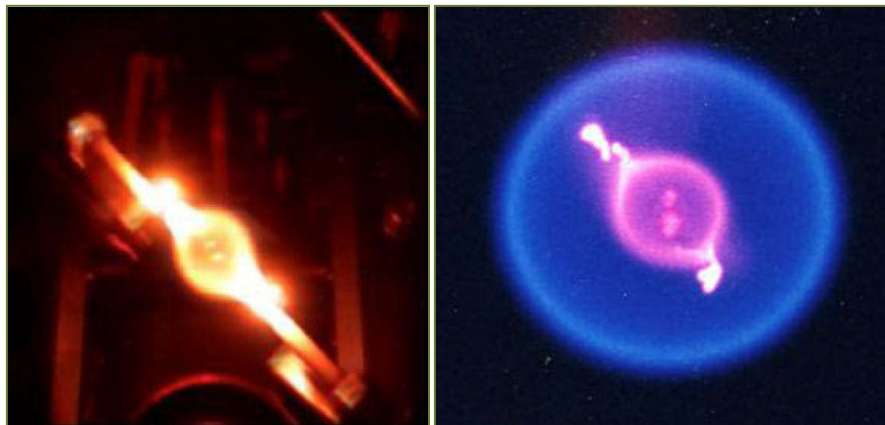


Figure 1: N-Heptane burning in micro-gravity, Credit: NASA.

These factors mentioned, fire in space can be both harder to detect and more persistent. Although we had previously mentioned the absence of natural convection in microgravity, there are other methods of airflow which occur in these environments. Human spaceflight requires ventilation systems to circulate and filter the enclosed atmosphere. These systems can be very effective at moving large volumes of gas and vapors over short periods of time. The ISS — having a pressurized internal volume of 388 cubic meters — could easily circulate smoke and harmful gases through the entire station in less than a half hour period (McKinnie, 1997). Additionally,

airflow from the ventilation system has the ability to stoke potential fires, or give direction and speed to fires that already have started to burn.

Historical Overview

Over the course of 30 years from 1967 to 1997 there have been a least seven recorded incidents of fire onboard spacecraft and space stations (Barr, 2010; Sanchez, 2000). Figure 2 gives a timeline of incidents along with the specific craft involved (red crosses denote loss of life or life threatening situation). Aside from the Apollo 1 fire in 1967 all incidents occurred during actual flight. The frequency of these incidents together with other risk assessment analysis led NASA to predict that over the lifespan of the ISS a minimum of two fires would occur on the station (McKinnie, 1997).

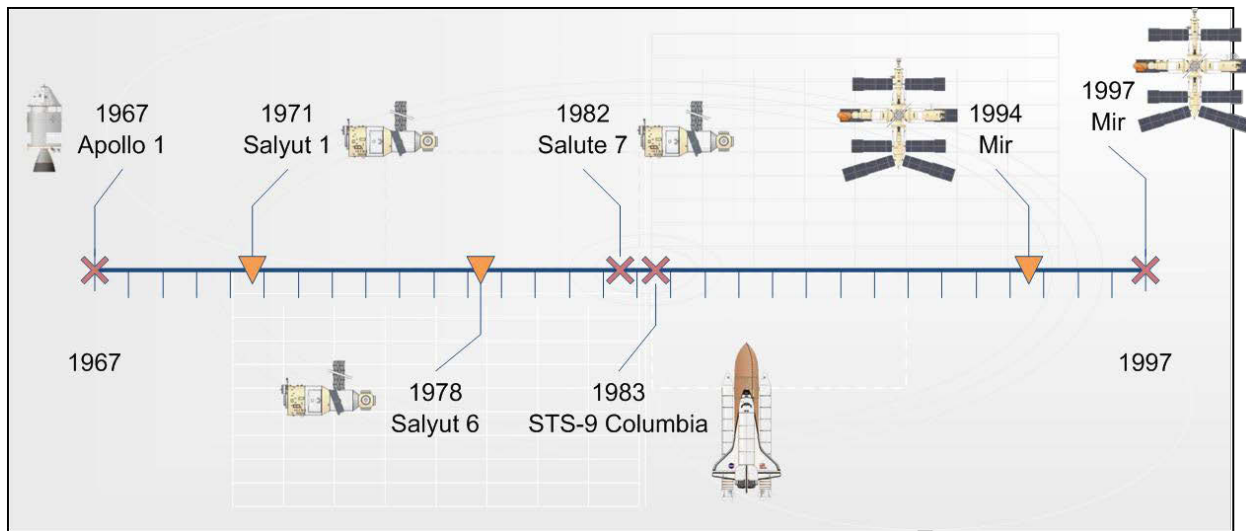


Figure 2: Timeline of fire occurrences. Red crosses denote life threatening situations.

The most serious of the orbital fires occurred on space station Mir. The station caught fire twice both in 1994 and 1997. The '97 event was the most serious, where a failure in one of two oxygen generation systems onboard caused a fire which burned for 15 minutes before finally self-extinguishing (Figure 3). The crew was not able to suppress the reaction because the foaming-agents used in the station's PFEs were designed to blanket and suffocate fire. Because the system which had caught fire was designed to generate oxygen, blanketing the fire to eliminate oxygen was ineffective. The system created oxygen by burning what is commonly called "oxygen candles". Similar candles to those onboard the station are commonly used throughout the commercial airline industry to generate emergency oxygen for passengers.



Figure 3: Fire-damaged panel onboard Mir, Credit: NASA.

Fire Modes in Microgravity

Fire is taken very seriously onboard the ISS. The USOS alone houses 13 fire extinguishers, and many studies have been done to determine the most likely causes of fire. Besides oxygen candles, various spaceflight applications (including astronaut EVAs) require elevated oxygen as part of the ambient atmosphere, which heightens the risk of fire. There is also growing concern regarding the amount of lithium-ion (Li-ion) batteries currently being used on the ISS in laptops and other electronics. Looking forward it is likely that commercial spaceflight will also rely heavily on these batteries. Recall when the Boeing's Dreamliner aircraft were grounded after fires involving Li-ion batteries. These batteries can also burn in the absence of atmospheric oxygen as well. This property eliminates one possible mode of defense against spacecraft fires, which would include depressurizing the cabin to remove the oxygen.

Liquid chemical fires are possible as well, although less likely to occur in habitable segments of a spacecraft. Hydrazine is a common fuel source for both power and propulsion in the space industry. A hydrazine leak from several of space shuttle Columbia's auxiliary power units caused a fire which could have crippled the craft's hydraulic systems needed for re-entry (Barr, 2010).

Historically through to the present, electrical fires have always been the biggest concern in regards to human spaceflight. Due to the size and volume constraints placed on Earth-launched vehicles, electrical wiring is typically packed as tight as possible inside a spacecraft. These wires are many times hidden away behind panels where it would be very difficult to visually identify the source of any smoldering or combustion taking place in the wire bundles. It is important to note that reaching the necessary heats for combustion is much easier in microgravity. Overheated motors, bearings, wires and other components will remain hot longer due to a lack of convective heat transfer in microgravity (Friedman, 1999).

Current Systems

The US orbital segment's PFE represents the most modern system currently available for space (Wieland, 1999). It is a compressed CO₂ extinguisher, designed to be discharged completely in the event of a fire over a 60 second period. A diagram of the PFE can be seen in Figure 4. It carries 6 lbs (2.7 kg) of CO₂ with a net weight of 12 lbs (5.35 kg). The discharge pressure is around 850 psi (8.56 MPa). The design intent behind this device was the elimination of fires which cannot be directly observed, occurring behind electrical panels or inside experiment racks onboard the ISS. In many ways it is a brute force tool, meant to indiscriminately fill a large volume quickly and remove breathable air from the combustion reaction. For this reason it is also required for astronauts to use portable breathing equipment while operating the PFE, else they may be injured by the large concentrations of CO₂. During operation, rapid expansion of the enclosed gas will cause the tank surface temperature to drop as low as -37 degrees C. Once the fire is extinguished the additional carbon dioxide is scrubbed by environmental controls, and excess pressure is vented from the cabin to space.

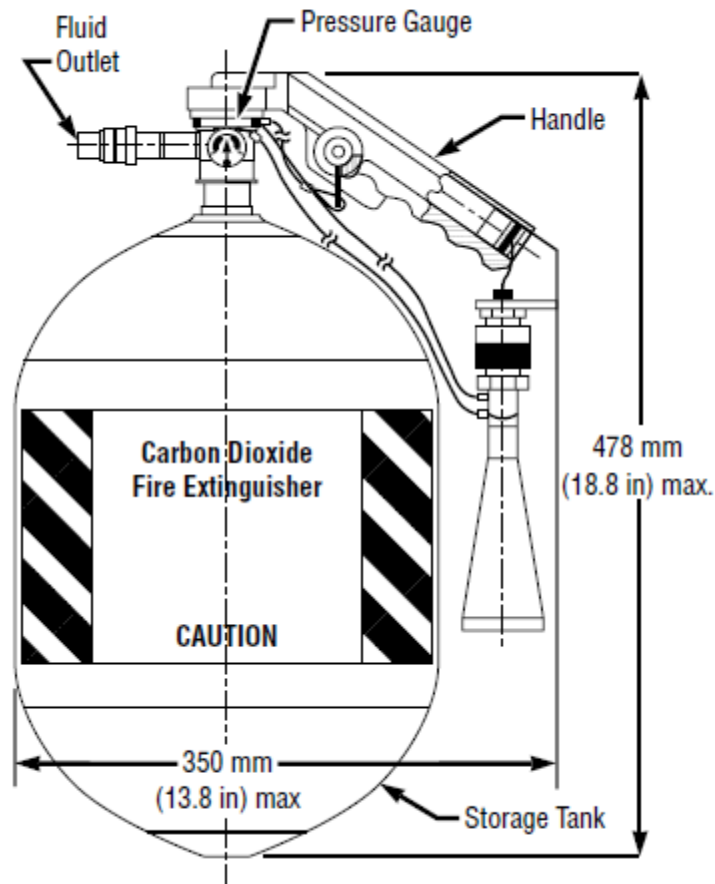


Figure 4: USOS PFE Diagram, Credit: NASA.

Analyses of the present options for space-application fire extinguishers lead us to conclude they are not acceptable for commercial spaceflight. For instance, they are far too expensive. The sales price for just one USOS unit is approximately one million dollars. They are also heavy, cannot be easily operated single-handed, and take up a large volume of usable storage space. A PFE suitable for commercial spaceflight needs to be highly mobile, effective at removing most if not

all of the fire hazards previously discussed, and cost effective. This is why ORBITEC will develop a more acceptable alternative for spaceflight applications. Doing so will require several important decisions to be made regarding the function of the device. Mainly, the type of fluid used as a fire suppressant will need to be determined.

The use of gas as a suppressing fluid is a good choice for microgravity environments because of its ability to fill three-dimensional space. Liquid suppressants travelling through free space tend to “ball up” due to surface tension effects and wander around instead of canvassing the combustion event (Butz, Carriere, Abbud-Madrid, & Easton, 2011) (Butz, Carriere, Abbud-Madrid, & Easton, 2011). Liquids however do have other properties which could apply very well to microgravity applications, provided the delivery mode is effective at concentrating the fluid to where the fire actually occurs.

New Technologies

Over the past decade studies have been conducted on the effectiveness of water-based fire suppression systems in microgravity. Studies led by researchers at the Colorado School of Mines used atomized water droplets to fight microgravity fires (Angel & McKinnon, 2003). The findings from these studies have been subsequently applied to the development of delivery methods for these highly atomized droplets referred to as FWM (fine water mist) systems (Butz & Abbud-Madrid, 2010). FWM allows liquid to behave in open areas like gases, operating three-dimensionally and creating a dense fog rather than a continuous stream of fluid. This gas-like behavior is enhanced by the microgravity environment of a spacecraft.

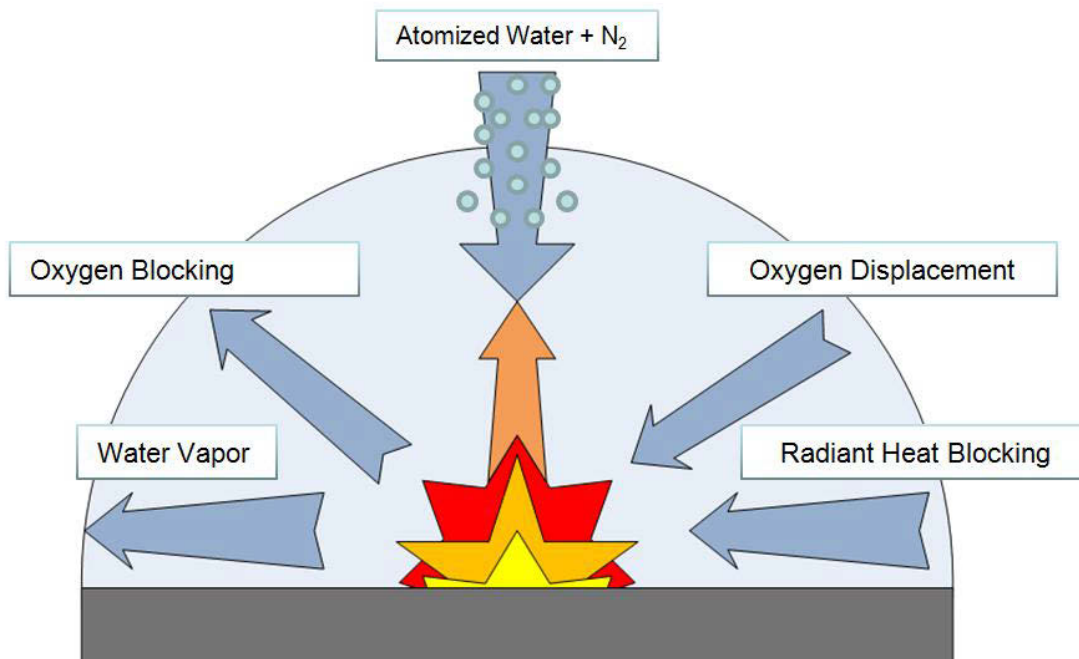


Figure 5: Diagram of PFE spray/combustion interaction.

Water has a very large latent heat capacity; meaning its ability to absorb heat energy is substantial. By delivering water to the fire as micron-sized droplets the liquid can readily absorb conducted and radiated heat, rapidly decreasing the thermal energy in the system below what is

necessary for sustained combustion. As the water droplets begin to vaporize, the resulting steam displaces ambient oxygen to quicken the extinguishing process (Figure 5). The FWM valve assembly works to atomize the water droplets by mixing a continuous water stream with nitrogen (an inert gas) prior to expulsion from the nozzle (Figure 6). Under ultra high pressure (UHP), the nitrogen and water mix effervescently and travel in tandem towards the fire. By using compressed nitrogen as part of the PFE system, the mean diameter of the water droplets is reduced to sizes otherwise unobtainable using only mechanical fluid separation (Butz & Abbud-Madrid, 2010). The use of nitrogen also works to further reduce the amount of available oxygen in the combustion area. Research done onboard space shuttle Columbia in 2003 showed that water droplets between 20 and 50 microns in diameter were most effective at absorbing the heat energy of fire. This level of atomization is possible with the FWM system.

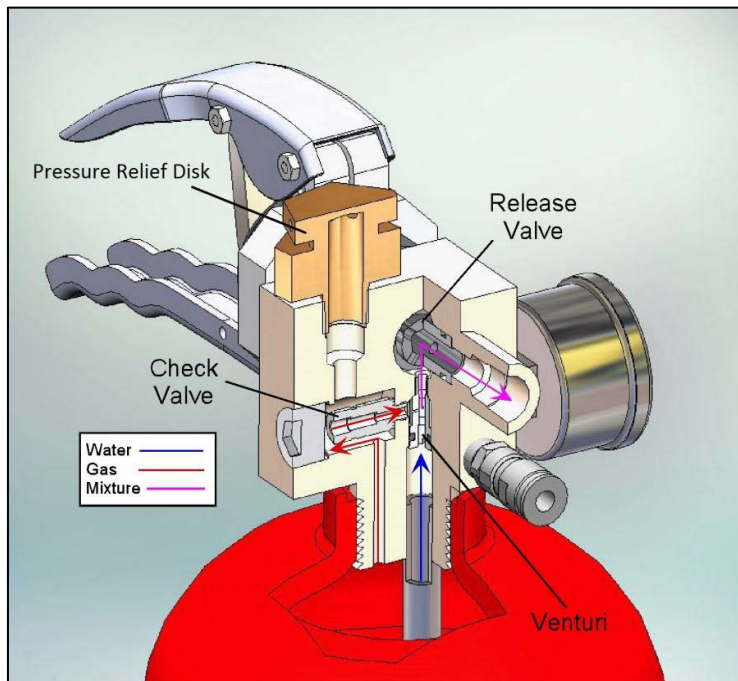


Figure 6: FWM PFE fluid flow path, Credit: ADA Technologies.

Because operation of the PFE will require the storage and pressurization of both nitrogen and water, a unique two-phase fluid management system must be developed for use with the FWM nozzle assembly. Leading design alternatives involve the use of an elastic bladder inserted into the PFE's tank. The water-filled bladder would be kept under pressure by compressed nitrogen which fills the remainder of the tank's volume. The tank and bladder assembly would need to withstand pressures in excess of 1000 psi for nominal atomization to take place.

Other alternatives to using bladders are possible. Another design would include taking advantage of the unique physics of micro-gravity and capillary-actions to deliver the fluids into the FWM assembly. This method would work without needing to physically separate the gas and liquid phases inside the tank, but would also make operation of the PFE under normal gravity much more difficult.

Future Markets

The only other PFE currently under development for space is being championed by NASA as a possible replacement solution for the majority of CO₂ extinguishers already on the ISS. Although the water atomization process for this extinguisher is similar to what has been described previously, this unit is far too massive and expensive for investment consideration by commercial spaceflight. This is why ORBITEC is looking into the development of a lightweight and cost effective prototype, which could be marketed to major aerospace companies. Boeing, SpaceX, and Sierra Nevada Corporation all are developing crew transport vehicles. Countless other companies are trying for the same goals without the aid of CCIcap funding. Any craft carrying humans will require auxiliary fire suppression capabilities in addition to standard ECLSS functions. At the current stage of development it is doubtful that any of these companies have a completely clear solution in regards to PFE integration. Additionally, the markets available to an environmentally friendly PFE with such unique operating features extend beyond the scope of LEO flight operations (perhaps even to ground-based “spin-off” products).

Vehicles which provide the opportunity for space tourism also need to consider fire protection. Virgin Galactic’s space plane, *SpaceShip Two* is the current poster-child for space tourism ventures. Other companies are in the development of suborbital space planes, as well as other creative methods to bring citizens to the edge of space. World View Enterprises, a company from the American Southwest, plans to take passengers aboard a high altitude balloon to experience extremely high altitudes at a fraction of the cost of rockets.

Bigelow Aerospace is also an interesting opportunity. This company has been developing inflatable space habitats for over a decade, and in 2015 plans to attach an inflatable module (titled *BEAM*) to the ISS for further expansion of the station. They also are developing standalone private space stations using the same technology. Because their designs do inflate, venting the craft’s internal atmosphere in an attempt to extinguish a fire becomes more problematic. Having a reliable PFE system to handle fire events would be very beneficial.

Although currently more loosely connected to microgravity fire suppression, companies including Planetary Resources and Deep Space Industries (DSI) would be interested in space PFE technology as well. These companies have long-term ambitions to develop the infrastructure needed for mining, refining, and manufacturing in places off-earth and beyond LEO. It goes without saying that wherever humans dare venture, fire will follow.

Conclusion

For any company looking to invest in commercial spaceflight, there will come a time when the issue of fire suppression needs to be addressed. As it stands, ORBITEC is an aerospace company with many products and systems already used in spaceflight applications. ORBITEC also happens to have significant experience in ultra high pressure fire suppression equipment, being the owner of HMA Fire Apparatus. Over the coming months, ORBITEC will continue to work with both university partners and the Wisconsin Space Grant Consortium (WSGC) to build, test, and validate ultra-high pressure portable fire extinguishers suitable for commercial spaceflight applications — with a first-level prototype ready for testing before the end of 2014. By building this PFE we will be closer to the creation of a great commercial product, which in turn will help protect the lives of astronauts.

References

- Angel, A.-M., & McKinnon, J. T. (2003). *Suppression of Premixed Flames by Water Mist in Microgravity: Findings from the MIST Experiment on STS-107*. Golden: Colorado School of Mines.
- Barr, S. (2010). *Evaluating Failures and Near Misses in Human Spaceflight History for Lessons for Future Human Spaceflight*. Houston: The Aerospace Corporation.
- Butz, J. R., Tuchi, C. S., Kimball, A., McKinnon, T., & Riedel, E. P. (2014). *Patent No. 8746357 B2*. United States of America.
- Butz, J., Carriere, T., Abbud-Madrid, A., & Easton, J. (2011). Zero Gravity Aircraft Testing of a Prototype Portable Fire Extinguisher for use in Spacecraft. *International Association for the Advancement of Space Safety*.
- Friedman, R. (1999). *Fire Safety in the Low-Gravity Spacecraft Environment*. Cleveland: NASA Glenn Research Center.
- Hickman, J. M., Dietrich, D. L., Hicks, M. C., Nayagam, V., & Stocker, D. (2012). FLEX: A Decisive Step Forward in NASA's Combustion Research Program. *1st Annual International Space Station Research and Development* (p. 21). Denver: American Astronautical Society.
- Martin, C. E., & Dalee, R. C. (1993). *Spacecraft Fire Detection and Suppression (FDS) Systems: An Overview and Recommendations for Future Flights*. Warrendale, PA: SAE.
- McKinnie, J. M. (1997). *Fire Response Aboard the International Space Station*. Warrendale, PA: SAE.
- Rodriguez, B., & Young, G. (2013). Development of the International Space Station Fine Water Mist Portable Fire Extinguisher. *American Institute of Aeronautics and Astronautics*, 1-8.
- Sanchez, M. J. (2000). *A Human Factors Evaluations of a Methodology for Pressurized Crew Module Acceptability for Zero-Gravity Ingress of Spacecraft*. Houston: NASA Johnson Space Center.
- Smith, R. L., & Kashiwagi, T. (1989). *Expert Systems Applied to Spacecraft Fire Safety*. Gaithersburg: National Institute of Standards and Technology.
- UCSD Jacobs. (2012, January 31). *How Do You Fight Fire in Space? Experiments Provide Some Answers*. Retrieved June 30, 2014, from UCSD Jacobs School of Engineering: http://www.jacobsschool.ucsd.edu/news/news_releases/release.sfe?id=1156
- Wieland, P. O. (1999). *Living Together in Space: The Design and Operation of the Life Support Systems on the International Space Station*. Huntsville: NASA Marshall Space Flight Center.
- Youngblood, W. W., & Vedha-Nayagam, M. (1989). *Advanced Spacecraft Fire Safety: Proposed Projects and Program Plan*. Huntsville: Wyle Laboratories.

Simulations with Granular Material Motion for Extraterrestrial Applications

David S. Helminiak¹

Department of Computer Engineering
Marquette University, Milwaukee

Abstract

A simulation study utilizing Hooke style particle models was conducted to better understand the characteristic modes, translational/rotational energy distribution, the complete energy cascade and applications of granular interactions occurring within a horizontal drum tumbler. This study was conducted in conjunction with a physical study performed by Nathaniel Helminiak, entitled: “*Experiments with Granular Material Motion for Extraterrestrial Applications.*” These simulations were created through the discrete element modeling software: LIGGGHTS (LAMMPS Improved for General Granular and Granular Heat Transfer Simulations) and the program it is based upon, LAMMPS (Large-scale Atomic/Molecular Massively Parallel Simulator). The resulting flows were visualized within VisIt visualization software and analyzed using the high-level computer language, GNU Octave. Simulations predicted areas of interest to study and extend tests beyond the physical test bed’s material limitations. The study suggests the existing idea of force chains as applied to rotational forces, namely “bro-chains,” and also that the industry mass finishing process may benefit from investigation into a complete energy characterization of granular flow.

Background

A comprehensive and complete understanding of granular motion has continued to evade precise definition or formulation. This is due to its unique material properties, as it does not directly mesh with pre-existing understandings of either liquid or solid matter states, rather exhibiting traits of both. Mathematically defining these flows has been and remains critical to understanding particle interactions, which range from meteor impacts and the creation of galaxies to simply transferring sugar to a cup of coffee.

Previous studies have traditionally consisted of examining overall translational motion using micro-sized particles (Nitin Jain; 2002). This has limited a link from micro to macroscopic research from being established. By bringing these larger particles into greater study, both rotational and translational energy could be mapped and modeled for macroscopic granular flows. To do so, this project sought to mathematically model the interactions between macroscopic particles within a rotary tumbler.

This study used simulations to model and predict behaviors as characterized by an experimental study conducted by Nathaniel Helminiak: “*Experiments with Granular Material Motion for Extraterrestrial Applications.*” The experimental study created a unique granular flow device to achieve more observable granular flows in order to validate resultant simulated data sets. These experiments and simulations were used to gain a greater mathematical understanding of how both kinetic rotational and translational energy becomes distributed within the system. Further, it was theorized that the interactions would yield data relevant to optimizing industrial mass-finishing machines (granular interactions between aggregate compounds to clean manufactured parts of excess material) and to extraterrestrial particle interactions.

¹ Wisconsin Space Grant Consortium, University of Wisconsin-Green Bay
Advisors: Dr. John Borg, P.E., Dr. Vikram Cariapa, P.E

Procedure

In design, there are two main types of modeling: physical and simulated. Physical models are often difficult to fully build and analyze, while mathematically developed models are fully reliant upon quantifiable aspects of reality. The resulting predictions of the simulated models can save both time and money. Starting by simplifying assumptions in this research, mathematical models were used to generate an environment based on the physical laws of nature. From this initial model, findings were then compared with experimental results, in order to refine and improve simulations, until a working computer model independently predicted physical occurrences and outcomes.

Some initial consideration was given to developing an original physics engine utilizing C or C++ coding. However, research revealed suitable software packages known as LAMMPS (Large-scale Atomic/Molecular Massively Parallel Simulator) and LIGGGHTS (LAMMPS Improved for General Granular and Granular Heat Transfer Simulations), which met the requirements for this research. These programs were written for simulating interactions between particles within varying environments, both having been used in the past by researchers for similar studies (Nitin Jain; 2002).

As both software packages had multiple authors, preliminary tests were conducted to determine the comparative reliability of the programs to the physical reality of a newly created granular flow device. Upon acceptable initial findings, additional layers of complexity were added to accurately gauge the reliability of particle positions within the generated flow field.

The LIGGGHTS program assigned several material property values for the Hooke particle model. These included Young's modulus, Poisson's ratio, the coefficient of restitution, the coefficient of friction and a characteristic velocity value. For the granular simulations within this study, the Hooke model was selected as the generalized representation for particle interaction properties. This model uses both an elastic spring constant and dampening system to determine the resulting forces from a particle interaction, through the formula shown within Figure 1:

$$\begin{aligned}k_n &= \text{Normal elastic constant} \\k_t &= \text{Tangential elastic constant} \\\gamma_n &= \text{Normal viscoelastic dampening constant} \\\gamma_t &= \text{Tangential viscoelastic dampening constant} \\m_{eff} &= \text{Effective mass} \\\Delta s_t &= \text{Tangential displacement vector} \\n_{ij} &= \text{Vector between particles' centers} \\v_n &= \text{Normal relative velocity} \\v_t &= \text{Tangential relative velocity} \\F_{hk} &= (k_n \delta n_{ij} - m_{eff} \gamma_n v_n) - k_t \Delta s_t + m_{eff} \gamma_t v_t\end{aligned}$$

Figure 1: Variables and formula governing particle interactions as calculated by the Hooke model

If in a given frame, or time step, the distance between two particles becomes less than the sum of the particles' combined radii, then the formula used provides both forces for normal and tangential contact. In the case of a rotary tumbler, where solids are almost constantly interacting with one another or are in contact with the rotary tumbler's drum wall, the computational time required increases exponentially. It has only recently become possible to perform the complex calculations on a time efficient basis.

Therefore, to make the generation and analysis of data as expeditious as possible, a 64-core Thinkmate computer was utilized to rapidly generate simulations. To perform simulations, pipeline parallel processing was used. This method utilized multiple computer cores collectively working upon a single task at the same time. However, given the varying rates of communication between cores, this occasionally became more time intensive than having a single core perform the simulation. Resultant data was processed through independent parallel processing. This method distributed different parts of each task to a separate core, then reassembled the data into a single package at the end of the relevant calculations.

The most critical value within these particular simulations was the coefficient of friction between the wall boundaries and the particles. It was necessary to determine as precisely as possible this value for accurate modeling. To do this, the actual experimental drum was placed upon a sine bar measuring 5.00 inches and also upon gauge blocks of varying height. Eventually, the height at which a trio of connected marbles (linked to prevent rotation) began to slide down the drum was 1.25 inches. The margin of error for this test was ± 0.05 inches. The height and length of these measuring devices were used to determine the angle at which the marbles slid and the resulted friction value of 0.25 appeared to correctly model the behaviors exhibited in the physical model.

Further physical testing with a set of calipers revealed the radius of the experimental marbles to be 7.9375 ± 0.0001 mm, while the diameter of the drum was 0.1397 m. Given the likelihood of the marbles' composition to be borosilicate glass, the density of the marbles was assumed to be 2.230 g/cc. All other values pertaining to their physical properties, including the Modulus of Elasticity (Young's Modulus), Poisson's Ratio and coefficient of friction were found on three Internet site sources: (1) the Matweb (n.d.); (2) a glassblowing reference guide ("Glass Properties," n.d.); and (3) Engineering Toolbox ("Friction and Coefficients of Friction," n.d.). While a value for the coefficient of restitution between two glass marbles could not be measured or found in common literature, the coefficient of restitution was determined to be 0.97 ± 0.01 as measured between a glass ball and a sheet of Soda-Lime Glass (Gondret, Lance, & Petit, 2002).

According to supplier documentation for the acrylic material used to construct the physical drum, the Modulus of Elasticity (Young's Modulus) for their standard molding grade acrylics is $4.3e5$ psi or 2.96 GPa ("Technical Specifications" n.d.). Poisson's ratio for acrylic was assumed to be 0.430, as this is the maximum value possible for the extruded pieces of acrylic used in the drum's construction ("Web - The Online Materials Information Resource," n.d.).

In order to model the acrylic drum, a computer aided three-dimensional design was created and exported as a text .stl file. One of LIGGGHTS' key features was the capability for the importation of complex geometries in the form of ASCII .stl or ASCII .VTK files. The drum design was generated within CAD software and then converted to having granular walls. The walls acted as idealized frictional boundaries, with which the particles interacted. The .stl geometries were converted into a series of triangular sections, which followed the basic geometric structure of the original shape. Essentially, these areas acted as small two-dimensional planes encompassing a given volume. Similar to how particles interact with one another, if in a single time step a given particle, or the mesh itself, came within half the skin distance of another particle, the program then began to track the particle interactions. The properties of the triangle's materials, including the method by which it interacts upon contact with a particle, were defined by entered values. The converted mesh was translated and rotated to the desired position and angle, including during simulation run-time, which allowed for a high-degree of flexibility and convenience.

Using LIGGGHTS, wall boundaries with the same properties as the cylinder were created to model the viewing port and adjustable piston from the experimental model. Particles were generated directly inside of the drum and allowed to settle for about two seconds and rotate for another two seconds to achieve a steady flow state, matching the experimental model's data collection style.

Outputted data sets come in the form of .lammgs (molecules) and .vtk (mesh) files, which provided all resulting physical data. The mesh included the relevant position data for the drum's walls. The molecules themselves included a wide range of information including their radius, type, species, x-y-z position, rotation and velocities for each time step calculation. These resultant files were imported into visualization software, Pizza.py, Paraview and VisIt. For the purposes of cross-referencing data with particle image velocimetry, VisIt illustrated a better range of particle properties and so was chosen for this study. Further resultant data from the simulations was pulled into Octave; a high level command-line program, designed for numerical computation. Afterwards the gathered information was efficiently organized into a three-dimensional array. This array in combination with scripting techniques then exported multiple plots of data, which were used to visually characterize and understand the granular motion.

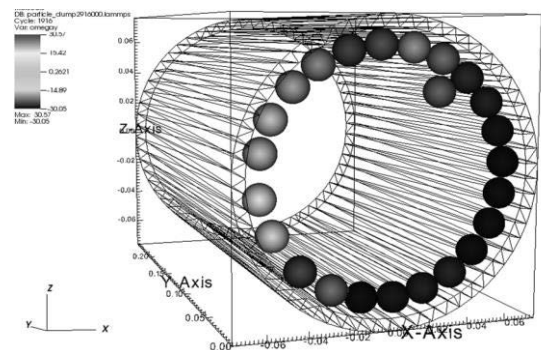


Figure 3: VisIt visualization of 24 particles within a single-layer spinning at 4 revolutions per second (Shading denote rotational speed: darker coloring = clockwise, lighter coloring = counter-clockwise)

Results

While many avenues of research were explored, a basic and clear understanding of the fundamentals was determined to be the most pressing need within this line of research. Within granular motion, there exist six distinctive granular flow characteristic modes: Slipping, Slumping, Rolling, Cascading, Cataracting and Centrifuging. The size of the particles used in the simulations however, prevented the distinction between cascading and cataracting modes. With the constructed physical model, a single layer of particles was generated for validation of the simulations. These were generated through LIGGGHTS simulations and confirmed to achieve identical flow behaviors and characteristics in the experimental model (Figure 4).

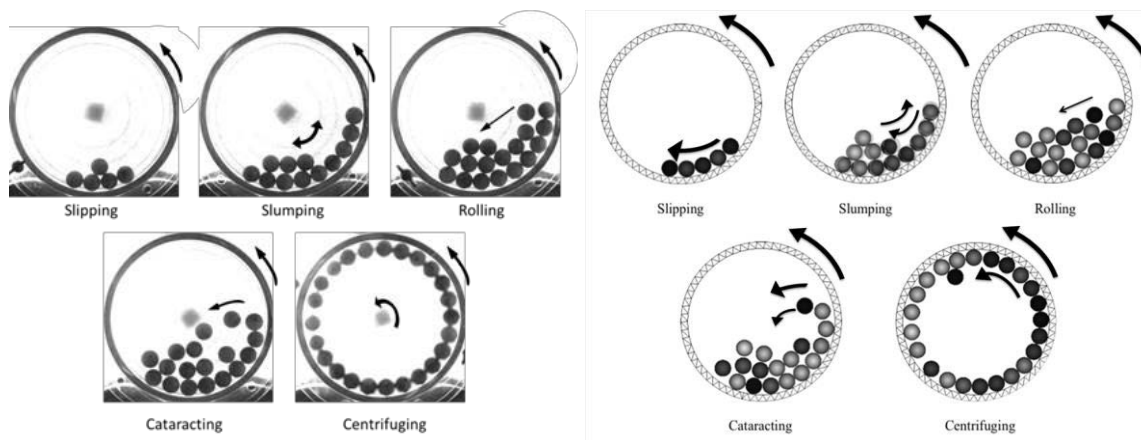


Figure 4: Characteristic granular modes (% Fill, Froude #): Slipping (4%, 0.56), Slumping (10%, 0.09), Rolling (15%, 0.14), Cataracting (15%, 1.44) and Centrifuging (20%, 9).

For each of these data sets, histograms were used to reveal the energy distribution within each particular flow characteristic. As may be inferred from how the particles moved in a single layer, slipping and slumping had more rotational energy relative to other characteristic modes, rolling not being completely dominated by either energy, cataracting, having more translational than rotational and finally centrifuging, which possessed the greatest translational energy and least rotational (Figure 5).

The energy distribution becomes further exemplified when examining the frequency of rotation rates within the characteristic modes, which showed that the drum rotation rate remained paramount to determining the balls rotational rates (as visualized in column 1 of Figure 6). Most of the rotation occurred near the outside layers of the flow, where particles were exposed to the drum itself. As particles interacted with one another, the rotation propagated through the flow, causing the neighbors of a particle to spin in the opposite direction. The various boundary layers can be seen in the third column of Figure 6. Fortran code was used to navigate through all frames of a set of either experimental or simulated data. For all time steps, if a particle entered an interrogation square measuring 2×10^{-4} by 2×10^{-4} m, then that position data was added to a temporary array. After examining each frame and counting how many particles had entered that square, the data was averaged to form a new data set. Similarly conducted, an ensemble average of the rotational speeds was also generated, using interrogation squares measured by a factor of the particle diameter of itself. These plots may be seen in the second column of Figure 6.

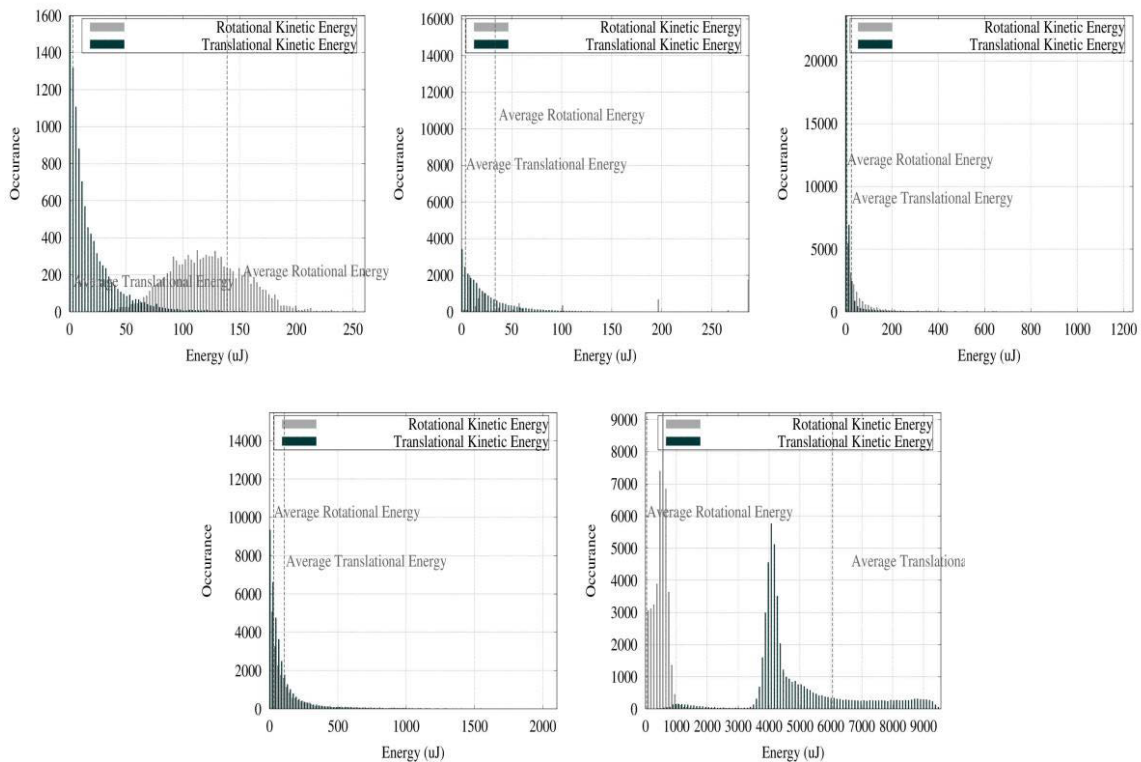


Figure 5: Histograms of translational and rotational energy (uJ) occurrences at simulated characteristic modes noted in Figure 5. Left to Right: Row 1: Slipping, Slumping, Rolling; Row 2: Cataracting, Centrifuging

Chains of rotational forces, or “bro-chains,” are present within the majority of flows. The main exception to this rule was centrifuging, where the tremendous translational forces prevented tangential interactions with the drum wall and other particles. If there was sufficient room between particles and relatively low drum speed, clockwise (deemed positive) rotation rates were seen in a counterclockwise spinning drum as the particles fell down the drum wall. Counterclockwise (deemed negative) rotation tendencies were seen as the particles spun up the drum wall. The resultant non-dimensional streamwise and transverse velocity profiles (Figure 7) demonstrated the changes in flow field velocities as functions of non-dimensionalized positions (streamwise showing horizontal velocity and transverse illustrating velocity as a function of depth) for each of the fundamental modes. Examining these graphs shows the existence of pockets of isolated granular particles, which did not become directly involved with the positional movements of the flow field. However, rotational energy continued to propagate through multiple layers to areas of translational calm, dispensing additional energy to the top exposed boundary layer.

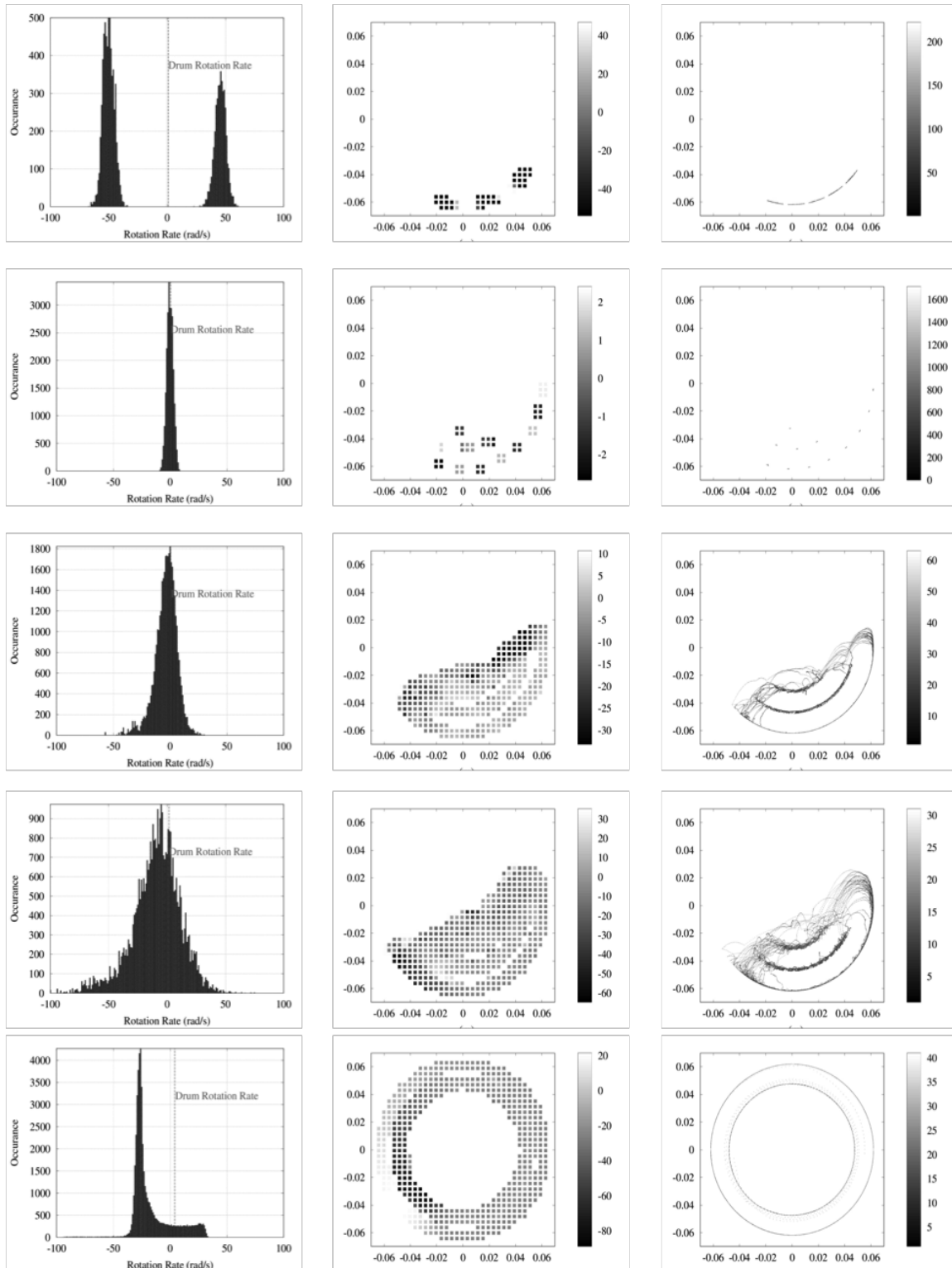


Figure 6: Top to Bottom (characteristic mode): Slipping, Slumping, Rolling, Cataracting, Centrifuging; Column 1: Histograms detailing the distribution of rotation rate occurrence within simulated characteristic modes noted in Figure 5; Column 2: Ensemble average of rotation rates (rad/s) within the drum during each characteristic mode; Column 3: Ensemble average of particle position (m) within the drum during each characteristic mode

The data was non-dimensionalized in order to begin the creation of a mathematical model for characterizing granular flow within any given rotary tumbler system. Primary among existing non-dimensional values is the Froude number (the ratio of a characteristic velocity to a gravitational wave velocity), which showed the overall characteristic nature of that flow. The energy distribution for over 20 particle flows was plotted through multiple characteristic modes and their related Froude numbers. A particle depth of 15% relative to the drum diameter was used and then divided by the known total energy within the system (Figure 8). While this method most certainly comprised a large portion of the flow, it did not entirely manage to describe it. Further characterization will require additional research and experimentation. The method of using non-dimensionalized data was not completely successful within the experimental model, due to the inability to account for every single variable present within the system. Many of the environmental conditions continually changed throughout the flow's development. However, using simulations, experiments were easily repeatable and highly precise, taking into account only the most relevant variables within the system, which were and actually can be controlled by researchers and industrial manufacturers in other settings.

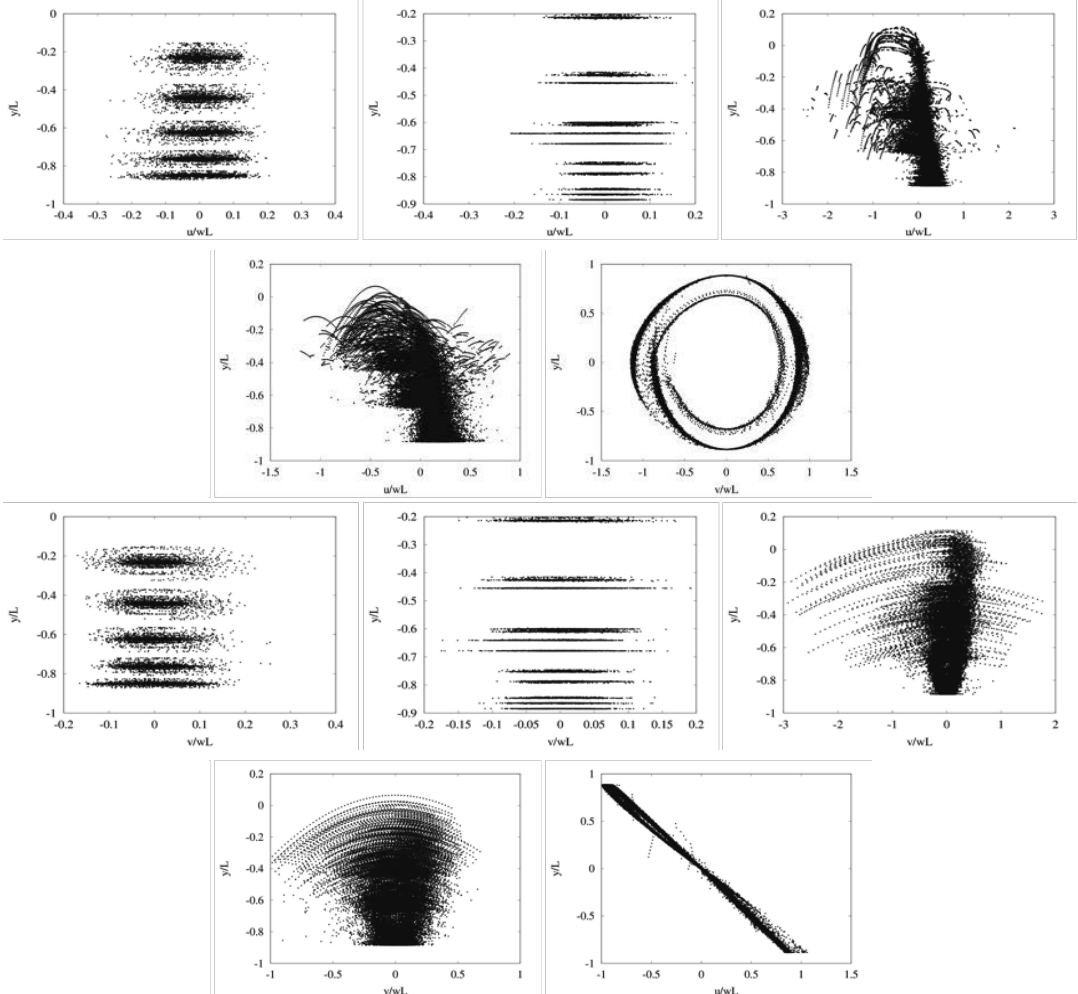


Figure 7: Left to Right: Rows 1 and 3: Slipping, Slumping, Rolling; Rows 2 and 4: Cataracting, Centrifuging; Rows 1 and 2: Streamwise (x-velocity) profiles for characteristic granular flows; Rows 3 and 4: Transverse (y-velocity) profiles for characteristic granular flows

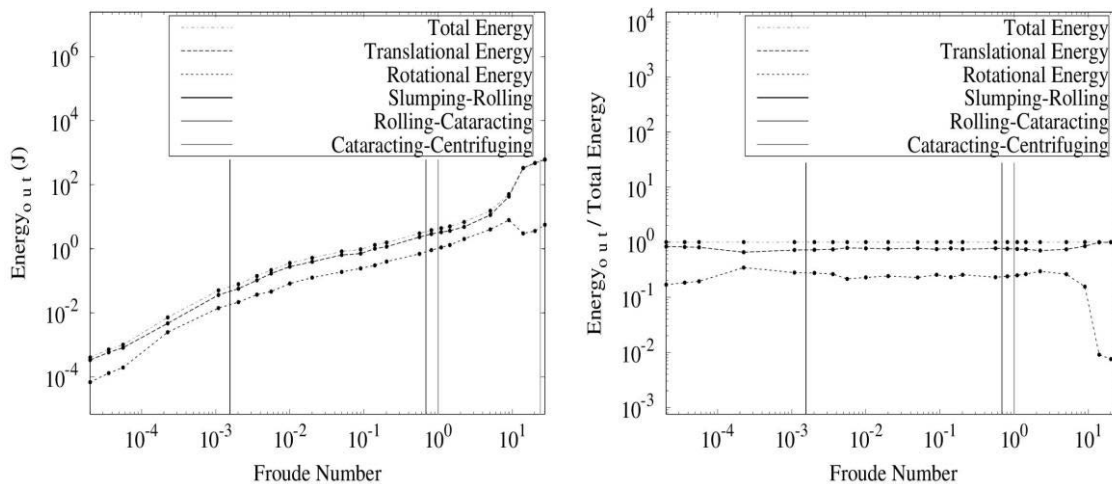


Figure 8: Left: translational, rotational and total system particle energy at a constant 15% fill as a function of Froude number; Right: translational, rotational and total system particle energy divided by total system particle energy at a constant 15% fill as a function of Froude number

Conclusions

Through a comparative analysis of an experimental rotary tumbler and simulations using highly precise physical property values, LIGGGHTS code was successfully able to demonstrate the distribution of translational and rotational energy within a granular flow system. The resulting visualizations matched both the experimental companion study and the intuitive understanding of particle interactions and fluid dynamics. Knowing the simulations to be accurate for modeling granular flows reinforces its potential for assistance in predictions where certain phenomenon or desired states may exist. Through the process of simulated experimenting, both researchers and manufacturers can better streamline their respective efforts, using virtual models to indicate areas of interest

Using ensemble averaging of particle position and rotation, a clearer understanding of fundamental granular flow modes was generated, revealing additional characteristics and trends that may be used to describe a system of motion. Making note of “bro-chains” may help in the process of mass finishing, reducing the amount and time needed to finish parts and provide an opportunity for further research into tangential interactions and their overall importance.

In attempting to non-dimensionalize the flow field’s energy, progress was made in mathematically defining that flow. Examining the streamwise and transverse velocity profiles of the characteristic modes showed how particle movement changed with respect to position within the flow field. In particular, it was observed that pockets of isolated particles existed, possessing little or no translational movement, but which, as visualized in other graphs, continued to propagate rotational energy throughout the system from the outermost boundary layers. The Froude number, while a critical number in helping to understand the characteristics of a granular flow, does not describe it fully. More understanding and characterization of granular flow can be achieved through additional investigation, following from this work.

References

- "Borosilicate Glass." *Borosilicate Glass*. MatWeb, LLC, n.d. Web. 29 May 2014. <<http://www.matweb.com/search/DataSheet.aspx?MatGUID=b0dbbac859444ffe98307f24ffd4c6a2>>.
- "Friction and Coefficients of Friction." *Friction and Coefficients of Friction*. The Engineering ToolBox, n.d. Web. 29 May 2014. <http://www.engineeringtoolbox.com/friction-coefficients-d_778.html>.
- "Glass Properties.", *Technical Data for Borosilicate and Silica Quartz*. Cambridge Glassblowing Ltd, n.d. Web. 29 May 2014. <<http://www.camglassblowing.co.uk/gproperties.htm>>.
- Gondret, P.; M. Lance and L. Petit (2002). "Bouncing Motion of Spherical Particles in Fluids". *Physics of Fluids* 14 (2): 643–652. doi:10.1063/1.1427920.
- "Technical Specifications." *Midland Plastics, Inc.* Midland Plastics, Inc., n.d. Web. 29 May 2014. <[http://www.midlandplastics.com/download.php?p=pdfs/\)/acrylic.pdf&d=2&n=Acrylic](http://www.midlandplastics.com/download.php?p=pdfs/)/acrylic.pdf&d=2&n=Acrylic)>.
- "MatWeb - The Online Materials Information Resource." *MatWeb - The Online Materials Information Resource*. MatWeb, LLC, n.d. Web. 29 May 2014. <<http://www.matweb.com/search/DataSheet.aspx?MatGUID=632572aeef2a4224b5ac8fbd4f1b6f77>>.
- Nitin Jain - J. M.Ottino - R. M.Lueptow. "An Experimental Study of the Flowing Granular Layer in a Rotating Tumbler." *Physics of Fluids* 14.2 (2002)

Experiments with Granular Material Motion for Extraterrestrial Applications

Nathaniel S. Helminiak¹

Department of Mechanical Engineering
Marquette University, Milwaukee

Abstract

In this study, a horizontal drum tumbler, filled at variable depths with spherical media, was rotated at constant speeds. An exposed monoplane layer of aggregate was photographed with a high-speed camera, in order to perform a particle tracking velocimetry (PTV) algorithm followed by image registering. The algorithms extracted both the translational and rotational velocities. To our knowledge, this is the first reported experimental measurement of rotational velocities in a rotary drum tumbler with granular media. The objective of this study, companioned with David Helminiak's "*Simulations with Granular Material Motion for Extraterrestrial Applications*", sought to measure the induced rotational velocity of individual grains and characterize the distribution of energy, both translational and rotational. The study not only proposes an addition to the existing idea of force chains, namely rotational "Bro-chains", but also suggests that within industry, mass finishing can benefit from complete energy characterization.

Background

Granular flow and related mechanics are uniquely fascinating as they combine mechanics of both fluids and solids. While granular materials tend to conform to their surroundings, they fill space in a much less efficient manner than would their liquid counterparts. Similarly, granular materials behave like solids with regard to packing efficiencies and resistance to shear. In any case, granular material interactions are among the most prevalent phenomenon on earth and in our universe. Through the characterization of these flows, we can better model such everyday processes as mass finishing to such extraordinary ideas as describing the makeup of a meteor strike on Mars.

In industry, granular flow fields induced in a rotating tumbler have a variety of applications, including mixing, segregation processes, as well as mass finishing, such as deburring and surface hardening. A common industrial deburring technique involves immersing the part in a drum with an abrasive aggregate. The drum is then agitated to induce an abrasive action. Burr removal is accomplished by relative velocity between the part and aggregate in contact with the part, as well as the relative rotation between individual aggregate and the part (T. Deng; 2004). In the study of granular flow in mass finishing, the most relevant results of the vibratory motion are those that lead to the grinding and polishing of the chosen media.

Within rotary mass finishing, there exist two main modes of material removal: impact and abrasive rotary friction. Impact occurs when outermost particles are flung upwards, free of the surrounding particles before following a projectile motion path back onto the heap of other aggregates. Impact mechanics of the two methods has had much investigative research both experimental and simulated with emphasis on deformation and mechanics (Warr, S; 1994). The second mode by which material is ground is through erosive wear of the aggregate surfaces stemming from individual particle translations and rotations as they move up and around the cylinder. Improvements in deburring processes can be accomplished by better understanding the relationship between the drum and the induced granular flow.

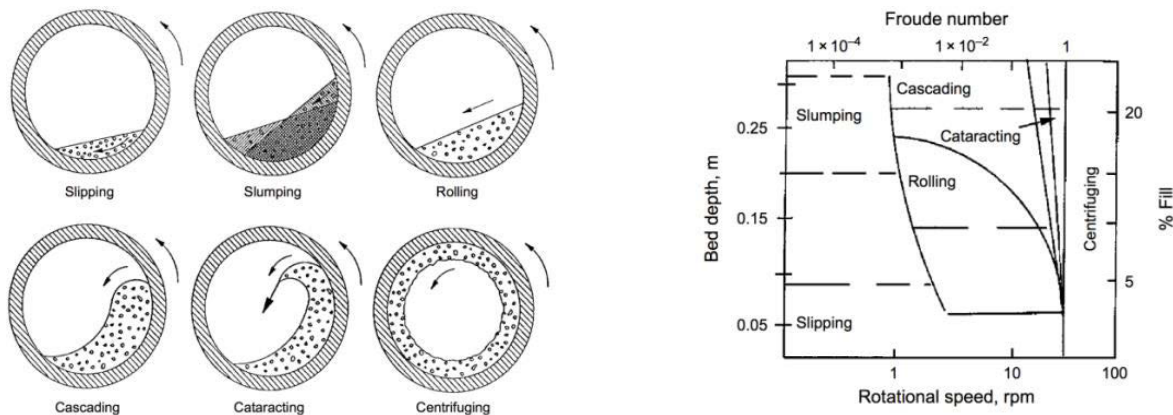
¹ Wisconsin Space Grant Consortium, University of Wisconsin-Green Bay
Advisors: Dr. John Borg, P.E., Dr. Vikram Cariapa, P.E

When working in three-dimensional space, problems, especially in high particle density situations, often occur with particles overlapping and obscuring each other leading to lost identities. While some studies suggest that by using colored, flagged, or tracer particles, more information might be gleaned from a single run of particle within a three-dimensional field (Bendicks C; 2011), it still cannot with high repeatability track all particles. Furthermore, PTV or Particle Tracking Velocimetry developed for three-dimensional tracking requires utilizing multiple cameras (Homeniuk, Darren; 2010). Our study, having one camera, focused on two-dimensional flow.

The 2D flow field can be characterized in a variety of ways. A common non-dimensional characterization is the Froude number, in this case defined as

$$Fo = \frac{\omega^2 D}{g}, \tag{1}$$

where ω is the rotational rate of the drum, D is the drum diameter, and g is gravity ($9.81 \frac{m}{s^2}$). The Froude number represents the ratio of rotational force to gravitational force or rotational energy to potential energy. When characterized in this way, distinct flow regimes describing the translational velocity field emerge (see Figure 1-1). The exact location of transition of modes (highlighted in Figure 1-2) can change as the ratio of the drum diameter and the granular media vary. Thus, Froude number alone is not sufficient to describe mode of operation.



Figures 1-1 and 1-2. Characterization of granular flow in a horizontal rotary tumbler, the results collected by past studies (Valle, Romero; 2012): the figure on the left displays the six characteristic flow fields while the one on the right displays a non-dimensional mode map of the flow fields.

The granular medium is energized by inputting energy via rotation. This rotational energy goes into several mechanisms, including translational, rotational, potential, acoustic, friction, and wear. The translational velocity induced by a rotary tumbler has been well characterized utilizing a variety of techniques such as PIV, MRI (Nitin Jain; 2002) (Florent Pignatel; 2012) and simulation (Pengfei Chen; 2008) (Valle, Romero; 2012). However, the rotation of the medium during the agitation has been characterized to a lesser degree.

The most common mode of operating a mass finishing device is somewhere between rolling and cascading. Rolling flows have been investigated and found to exhibit boundary layer like flow, with the highest translational velocities at the surface and along the internal wall boundary.

Another important phenomenon, when investigating granular flows, is the existence of force chains. Force chains are the mechanisms by which boundary conditions communicate loads through the grain bed. Since not all grains participate in the force chain network, heterogeneous loading exists in the grain bed. This can result in some grains experiencing high loading and wear in specific regions of the flow. The goal was then to both repeat studies done by past researchers, who focused work on the linear motion of granular materials, and augment it with the inclusion of method and insight to measure rotational motion.

Procedure

Experimental Setup. After investigation and literary search, our work focused on the behavior of granular flow within a cylindrical rotary tumbler used in mass finishing applications. A tumbler design was then fabricated creating a clear tumbler with an interior diameter of 13.97 cm and inclusion of clear walls for viewing on all axes, stepper motor for variable speed control, and variable depth piston cylinder for 2D and 3D experimental analysis. The granular media, constrained to a single plane of motion, consisted of speckled glass spheres, each with a density of 2.23 g/cc and a diameter of 1.5 cm. Wheels supporting the tumbler were soft rubber and rotated freely on cylindrical roller bearings for a smooth controlled orbit.

Within experiments, marble number and drum rotation rate were variable with other conditions kept constant to study the various characteristic flows. A Photron camera, shooting at a speed of 500 frames per second and a resolution of 1024x1024p, captured high-resolution data while not losing track of the particles. In order to light the media without glare, the room was kept dark while a diffuse studio light was used in coordination with a back-light to provide controlled lighting. After setting motor speed and waiting for a steady state, the Photron recorded up to four consecutive seconds of data (enough for most particles to travel at least once around the outer surface of the tumbler), which were collected in the form of raw images to be processed.

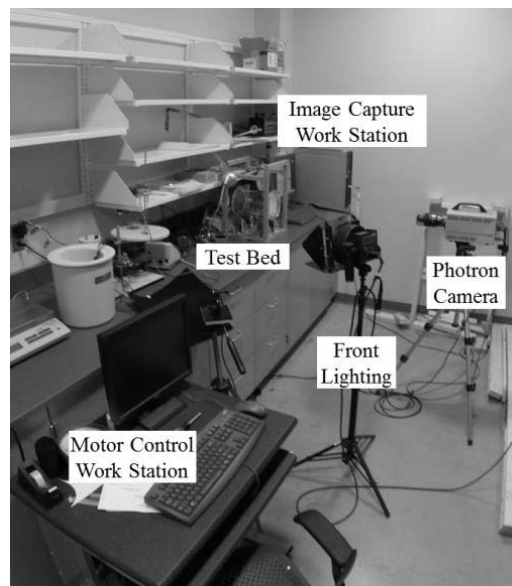
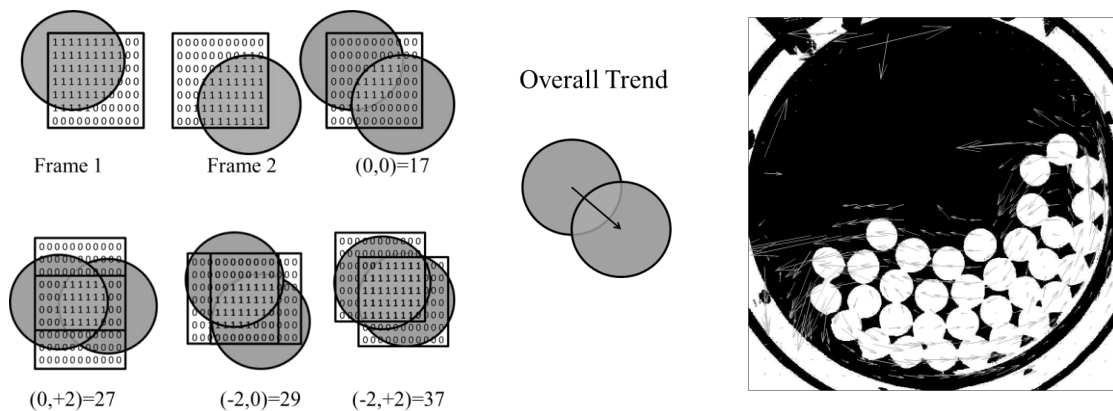


Figure 2: Experimental Study Setup

Methods. Most early studies qualify granular flow from experimental set-ups like the one in this report utilizing PIV or Particle Image Velocimetry to both qualify and quantify granular material motion. From this method, familiar looking images like the one shown below (in Figure 3-2) use

vector plots superimposed over images to visually describe the flow while also providing data to be analyzed. PIV begins with a set of images with traceable particles, which all move within a relatively uniform fluid motion and do not radically change in qualities, such as shape, size and color, between frames. PIV functions through the utilization of interrogation windows. Between frames, like the ones shown in (Figure 3-1) below, images are correlated by transposing the integration window vertically and laterally to find probable path and speed resulting in a velocity vector for the given window. By keeping all particles within similarly sized interrogation windows and preventing particles from traversing into or out of a single window in a given time step, sets of image data can be used to form high resolution gradient fields.



Figures 3-1 and 3-2: The images on the left show the before and after photos of a particle moving through the interrogation window. As images are translated, the binary addition of their pixels will result in either increasing or decreasing sum values. After comparing correlation values from various transpositions probable path emerges. The image on the far right shows a processed result of PIV with arrows signifying general velocity trend at a point.

While our studies began with an initial foray into PIV, we ultimately used an algorithm built upon its architecture called PTV, or Particle Tracking Velocimetry, to begin characterization. While there are a multitude of PTV software packages available, this study builds off PTVlab (Brevis W; 2011), a Matlab add-on to PIVlab (the process outlined in Figure 4). While PIV is an excellent tool for measuring gradient flow fields, it did not allow for the tracking of media. While PIV can be used to ensemble average a flow, Particle Tracking Velocimetry (PTV) gives a tracking identity to every particle within a space and can give properties of an individual particle through space at any given time in addition to all of the PIV benefits mentioned above. PTV accomplishes this is by correlating each of the particles in addition to each of the frames.

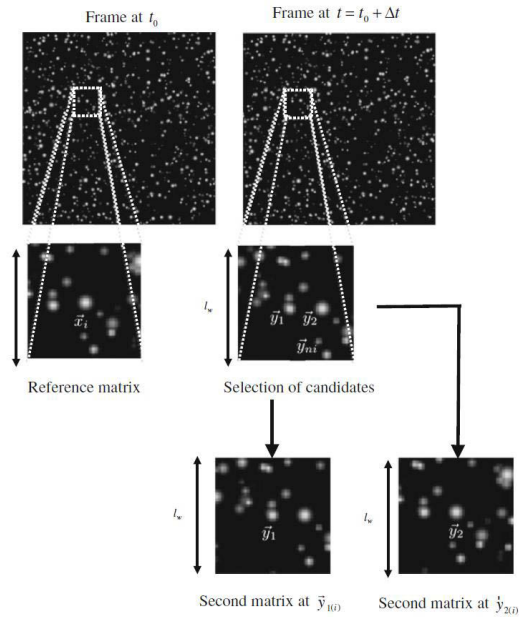


Figure 4: A description of the algorithm used by PTVlab which functions via relaxation and cross correlation.

This correlation takes place in two steps: cross correlation and relaxation. Relaxation uses a velocity data taken from a particle’s last known trajectory to make an educated guess, assuming minimal acceleration, as to a particle’s new location given a constant velocity and path. Cross Correlation finds neighbors that have similar properties (shape, size and color) to match a particle’s identity between frames.

The final tool used was an adaptation of a preexisting method, often used in the medical field to adjust for organ movement when comparing MRI scans. Image registering, which works in a manner similar to both PIV and PTV, utilizes the values of pixels to determine when images match. Each pixel in a matrix was represented by a number, 0-255 (black to white). Two images are then converted into this numeric format before one is rotated with appropriate scaling and precautions. This prevents a loss of information as square matrixes are rotated and made to fit within the same bounds. If images were known to be a perfect match, the maximum value is obtained by multiplying each overlaying photo-matrix value.



Figure 5: On the left an identical apple is superimposed over an identical apple mismatched by 90 degrees, and on the right the two images are matched to give a visual representation of a registered image.

Data Processing. Images taken from the Photron camera were processed through a four-step method shown in Figure 6. Images were first fed through a built-in circle finding algorithm in Matlab which could locate and find particles of particular size before exporting an image with clear particle locations. From this point, the prepared images were processed in PTVlab to identify and track each of the particles in the flow field. In order to minimize misidentification of particles, the camera frame-rate was increased to ensure any given particle moved no more than one-half of its diameter per frame. Data from this process gave every particle's path and translational velocity at each point. Once each particle was identified, the image was cropped using a circular mask, which only leaves a given particle; this process was repeated for all particles. An example is presented in Figure 7. In order to estimate a particle's rotation, the second image, Figure 7-2 for example, is digitally rotated a known increment and registered with the first un-rotated image, Figure 7-1. For any two successive images, this process is repeated over angles: $-8^\circ < \theta < 8^\circ$. The rotation with the maximum cross-correlation is assigned as the rotation for that grain over the interval of time between images. While this process ignored rotation in the x- and z-directions, this issue will be addressed in future work.

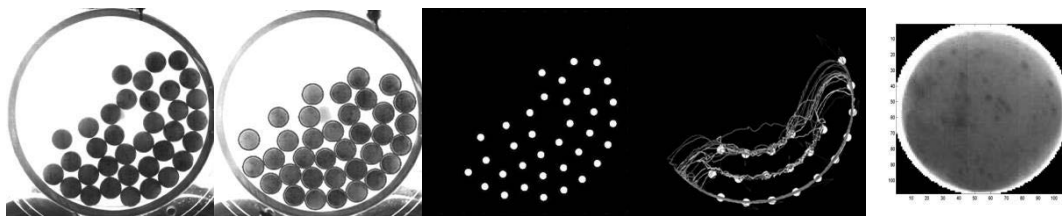


Figure 6: From left to right: raw image, image with located particles, easy to track recreation, PTV, individual masked for registering.

Unlike the stock apple image shown in the methods section, images in this study were not perfect matches-being before and after shots of the same particle. Therefore, while perfect correlation was not expected, peak correlation meant that a significant amount of particle features correlated.



Figures 7-1 and 7-2: This piece of media has a counterclockwise rotation which took place in the timespan of 5 frames. Images collected during rolling (15% Fill – Froude #0.14).

From this data-providing particle identity, velocity, and rotation results of previous studies were duplicated and further results were compiled.

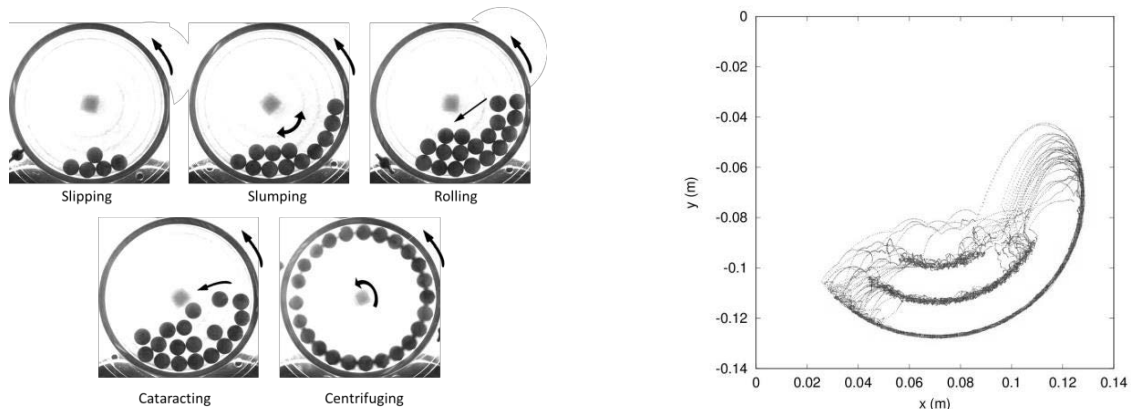
Results

Important Constants. To simulate and allow for the repeatability of research, the following table of constants showcases the various constants and properties possessed within experiments. Care was taken in experimentation to remove media which possessed certain characteristics, such as size, which fell as an outlier amongst other media to preserve relative uniformity in experiments.

Table 1: Parameters taken from the Experimental Setup

| Parameter (Marb/Marb) * | Value | Parameter (Marb/Drum) * | Value | Other Parameters | Value |
|----------------------------|--------|----------------------------|----------|------------------------|-----------|
| Young's Modulus | 64 GPa | Young's Modulus | 2.96 GPa | Marble Density | 2.23 g/cc |
| Poisson's Ratio | 0.2 | Poisson Ratio | 0.43 | Marble Diameter | 15.875 mm |
| Coefficient of Restitution | 0.97 | Coefficient of Restitution | 0.73 | Internal Drum Diameter | 13.97 cm |
| Coefficient of Friction | 0.9 | Coefficient of Friction | 0.43 | *Marb for Marble | |

Characteristic Modes. Of the six commonly recorded flows, findings in this study clearly recognized five. The most difficult modes to distinguish between were that of cascading and cataracting, made difficult due to the relative diameter of aggregate with respect to drum diameter. Slipping was defined by a low angle of repose. Slumping, like slipping, was defined by a point when aggregate “clings” to the rotating surface for a moment, before slipping back down the side in an oscillatory fashion. Rolling occurred when particles began to slide over the exposed upper surface aggregate. Cataracting is defined when the mass of particles begin to separate from the main flow. Finally, centrifuging occurred during complete loss of tumbling behavior as particles were flung outward and remained on the edge of the rotary tumbler.



Figures 8-1 and 8-2: Images were collected for the following modes: Slipping (4% Fill – Froude #0.56), Slumping (10% Fill – Froude #0.09), Rolling (15% Fill – Froude #0.14), Cataracting (15% Fill – Froude #1.44) and Centrifuging (20% Fill – Froude #9). In the second figure, Cataracting particles are plotted with respect to position.

Figure 8-2 illustrates the formation of two boundary layers, one at the top surface and one toward the bottom. Grains in contact with the drum are imparted with velocity due to frictional drag, which is dictated by the friction and weight of the grain bed. The slump angle is dictated by how much kinetic energy the grains in the drum accumulate. As grains cascade down the free surface and meet the drum they are swept under the grain bed by the rotating drum. This is in contrast to grains near the center of the grain bed, which are near motionless. Thus, some grains continue to circulate while others remain nearly motionless toward the center of the grain bed.

Total Energy. Within a given system, the identification of the movement and transformation of energy within mass finishing devices remains a unified goal, yielding critical insight into its overall efficiency. The most common form of energy associated within a rotary tumbler is translational energy, but rotational energy plays a consistent role as media not only moves through the flow, but has a tendency to tumble while doing so.

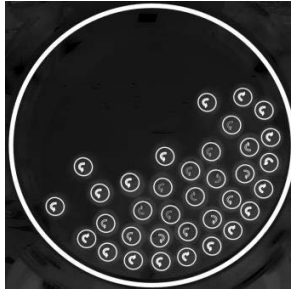


Figure 9: The image above is an artistic rendition of rotational force chains as generated within a rotary drum spinning counterclockwise; each particle affecting an opposite rotational force upon its neighbors.

To begin, plots of the characteristic depth of a particle, as a function of non-dimensional transverse, stream-wise, and rotational velocities, were generated. Transverse refers to x-component of particle velocity, while stream-wise is the y-component. Rotational non-dimensional numbers are the ratio of a particle's rotation rate with respect to the drum's rotation rate. Within the non-dimensional plots, it can be seen that slipping and slumping are characterized by particles that do not change their bed depth over time, being fixed to a location, staying in set locations within the bed depth. It is hard to tell whether the drum was rotating in the clockwise or counter clockwise direction. In the stream-wise velocity graphs of rolling and cataracting, as media travels away from the drum wall, particles begin to travel with a clear velocity bias, betraying the counterclockwise rotation of our drum as particles rush across the exposed upper surface towards the point of lowest potential. Transverse velocity graphs show that, as particles reach the surface, they tend to accelerate as they are pushed from the main flow and, in the cases of cataracting, crash back onto the exposed surface. Finally, the centrifuging or phase space plots show the effects of gravity and drum shape as particles begin to accelerate or decelerate depending on their location within the flow.

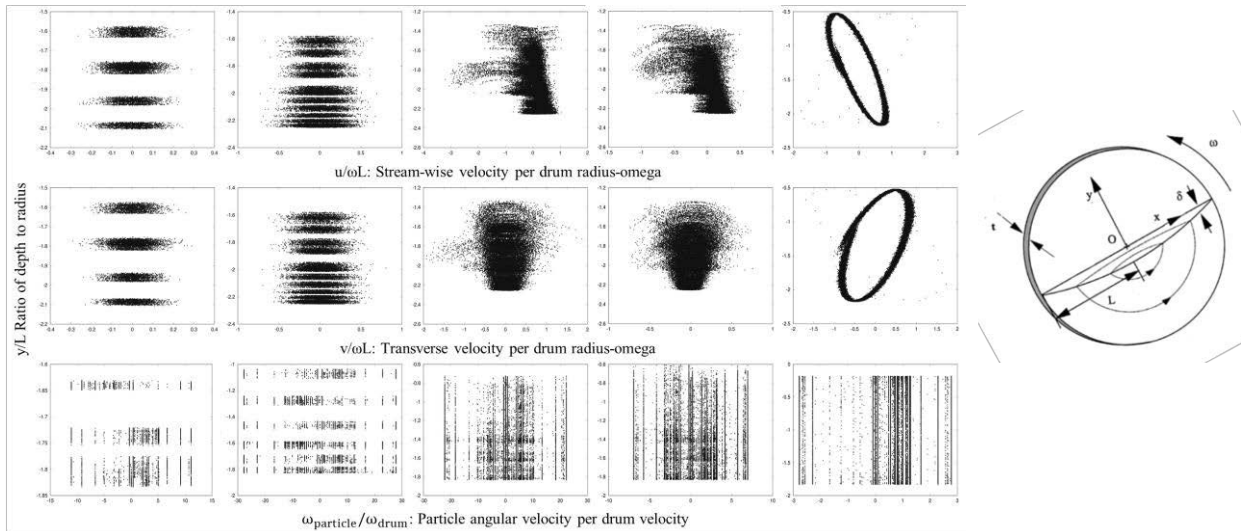


Figure 10: Plot of all particles: depth to radius as a function of stream-wise (top) and transverse (center) velocity per radius-omega, and particle angular velocity (bottom) per drum velocity at the conditions noted in Figure 8. Plots of non-dimensional translational velocities matched trends observed in a larger tumbler (Nitin Jain; 2002).

Histograms show the occurrences of certain energy, rotational or transverse, as well as give an indication of which type of energy contributes to the description of a certain system. As shown below, it follows that slipping, marked by particle spinning in place, would have high rotational

energy and low translational energy, while cataracting, in which particles are flung onto the sides of the tumbler wall, would have high translational energy and little to no rotational energy.

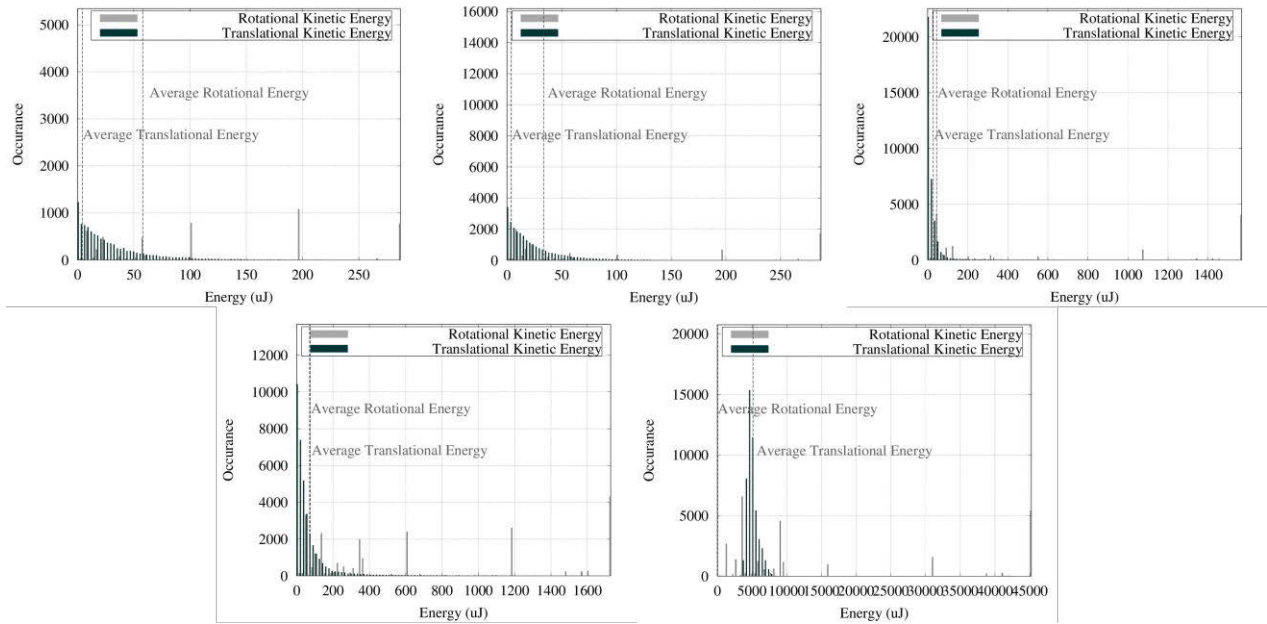


Figure 11: Histograms of translational and rotational energy occurrences at characteristic modes noted in Figure 8.

Finally, total energy plots (Figure 12) took a single system of 18 marbles with a percentage fill and varied the drum speed, which resulted in variable Froude numbers. From these data sets, rotational and translational energies were summed and plotted against the input Froude number. From this, energy could clearly be seen to increase as a function of drum speed, as expected. Dividing these results each by total energy, rotational energy can be seen contributing the majority of energy at lower energy states, while translational energy begins to play a more important role once rolling commences. Between rolling and centrifuging, both energy types vie for dominance over the system with clear evidence that optimization of granular flow is a plausible study for industry.

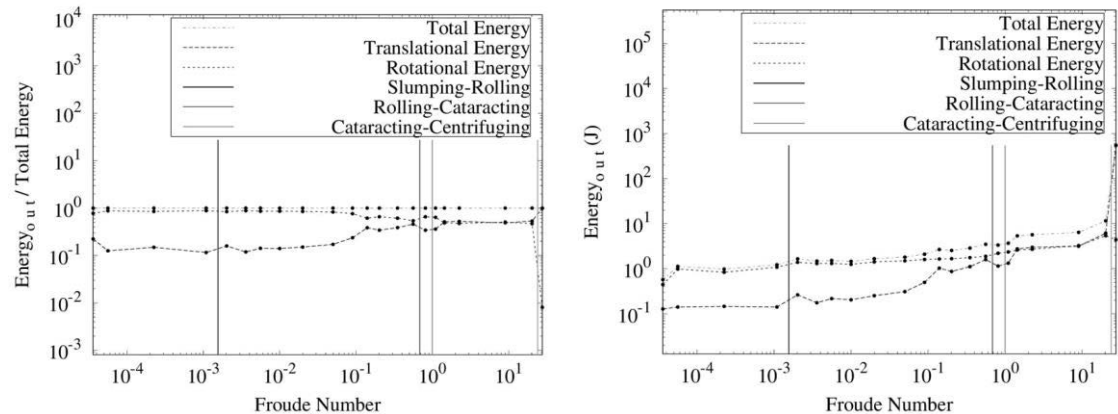


Figure 12: The plot on right shows energy over four seconds of time at a constant 15% fill as a function of Froude number while the one on the left charts translational and rotational energy over total measured energy as a function of Froude number.

Conclusions

Results of previous studies closely corresponded to past insights. Using methods derived from those in the past, in coordination with available equipment, a method was created to measure rotation of individual particles within a two-dimensional granular flow. Bro-chains were an exciting scientific phenomenon that added to the existing idea of force chains. Force chains, in the statics sense, should take place normal to the points of contact on neighboring particles. In dynamics, knowledge of friction between particles makes it clear that forces will also occur tangential to a particle's surface resulting in rotational influences in particle interactions, i.e. bro-chains. In industry, the grinding and polishing of media is an incomplete science. Knowledge of particle interaction was used to machine items. However, aside from general recommendations of fill and speed, the understanding seemed incomplete. Processes that are not fully optimized imply room to decrease media consumption, increase effectiveness and decrease costs.

Overall, it was noted that the study of granular material motion worked well in the context of a companion study, demonstrating that by using a mathematical model for a physical system, one could save time and money by predicting and informing design. Similarly, the characterization of the physical model informed simulations by advising algorithmic adjustment. While having access to a local computer cluster to help to speed calculations, these computations still took the vast majority of experimental and simulation time. To keep data collection and processing efficient, one should use minimal GUI interaction and run in parallel for efficient use of all cores.

Future areas of work into granular materials for the benefit of science include: the tracking of all individual particles within a 3D environment via 3 Axis Gyroscopes or augmenting tracer particles within a three-dimensional flow field to glean rotation in all three axes. In contribution to industry, it has been noted that the processes, which remove the chips and flash off commercial products, represent a secondary application of the knowledge gleaned. Goals in this case would be to maximize the energy used to process materials, while decreasing the amount of media utilized by manipulating fill, media type and speed. It is within these ideas, a few of many, that research completed in this study could be applied to a next stage.

References

- Bendicks, C. "Improved 3-D Particle Tracking Velocimetry with Colored Particles." *Journal of Signal and Information Processing* 02.02 pp 59-71, (2011)
- Brevis W, Niño Y and Jirka GH. "Integrating cross-correlation and relaxation algorithms for particle tracking velocimetry." *Experiments in Fluids*, 50 (1), pp 135-147. ISSN 0723-4864. (2011)
- Florent Pignatel, Caroline Asselin, Lucas Krieger, Ivan C. Christov, Julio M. Ottino, and Richard M. Lueptow. "Parameters and scalings for dry and immersed granular flowing layers in rotating tumblers" *PHYSICAL REVIEW E* **86**, 011304. (2012)
- Homeniuk, Darren LN, David S. Nobes, and David J. Wilson. "Three-Dimensional Particle Tracking Velocimetry." *The Canadian Society for mechanical Engineering*. University of Alberta. T6G 2G8 (2010)
- Nitin Jain - J. M.Ottino - R. M.Lueptow. "An Experimental Study of the Flowing Granular Layer in a Rotating Tumbler." *Physics of Fluids* 14.2 (2002)
- Pengfei Chen, Julio M. Ottino, Richard M. Lueptow. "Subsurface granular flow in rotating tumblers: A detailed computational study." *PHYSICAL REVIEW E* 78, 021303 (2008)
- T. Deng, M.S. Bingley and MSA Bradley. "The influence of particle rotation on solid particle erosion rate of metals." *Wear* 256, pp 1037-1049, (2004)
- Valle, Romero. "Numerical Modeling of Granular Flows in Rotary Kilns." Thesis. Delft University of Technology. Literature Survey. (2012)
- Warr, S., Jacques, G. T. H. & Huntley, J. M. "Tracking the translational and rotational motion of granular particles: use of high-speed photography and image processing." *Powder Technol.* 81, pp 41–56, (1994)

A study on Select Solar Cell's Voltage Output at High Altitudes Using a Weather Balloon

Jalal M. Nawash, Rebecca Holzer, Rebekah Taylor and Jacob Bogenschuetz

Department of Physics, University of Wisconsin - Whitewater

Abstract

The Voltage output of select solar cells was monitored as a function of altitude up to approximately 93,000 feet. A weather balloon was used to carry the solar cells to the required altitude. Two launches were accomplished to acquire data for analysis. Data collected also included the altitude, temperature and pressure. The voltage signal of the used solar cells depended largely on temperature. It was discovered that the voltage signal of the solar cells has a complex relationship with altitude. Temperature had a significant influence on the magnitude of the voltage signal at lower altitudes, but this influence may have declined at higher altitudes.

Introduction

Solar cells have become very popular in many applications, including providing electricity for houses, businesses and some cars. The solar cell industry has grown even faster in the past years due to the increasing demand for alternative sources of energy to fossil fuels. Solar energy is clean and lasts as long as the sun shines. Many researchers are dedicated to increasing the efficiency of solar cells for further applications. NASA's green aviation goals are to support fuel-efficient flight planning and to reduce aircraft fuel consumption, emissions, and noise. NASA's Ames Research Center has been working on reducing carbon footprint around the planet for decades. In addition to the environmental impact, switching to solar energy will have a positive economical influence. For example, the United States government has plans to fly light solar cell-powered drones at high altitudes for days at a time without the need to refuel. Doing this with a conventional plane would be expensive.

In this paper, a high altitude weather balloon was used to monitor the voltage output signal of solar cells at high altitudes. The efficiency is mostly calculated by dividing the output energy by the input energy. However, in this project, the changes in voltage output signal under a constant sunlight input is a sufficient indication of the efficiency changes. In recent years, there have been an increased number of investigations to address the effect of altitude on solar cells, but many more are still needed. Payloads carried by balloons can be equipped with devices and electronic equipment to record several types of data during the balloon ascent and descent. Temperature, pressure and other weather elements might have an effect on the efficiency. Two balloon launches were completed to collect data.

Hundreds of balloons are sent to the upper atmosphere every year around the planet [1] and weather balloons have been utilized in many different aspects of physics research. Some of this research has involved measuring the cosmic rays at high altitudes [2] and studying the various effects of weather on electrical and magnetic properties of high altitude ranges under several solar conditions [3,4,5]. Weather balloons were also employed to investigate the electric and magnetic fields generated in substorms [6]. In Wisconsin, Elijah High Altitude Balloon Payload Program launches

This project was funded by WSGC and the College of Letters and Sciences at University of Wisconsin - Whitewater

balloons every year. One of their projects in recent years was to study mercury pollution at high altitudes [7]. Most investigators use balloons for weather studies, but few researchers have studied solar cell measurements [8].

Weather balloons are usually launched to near space altitudes, between 60,000 feet – 120,000 feet. Most balloons carry a global positioning system (GPS) device to help locate the balloon payload after the balloon bursts and falls under the influence of gravity. Depending on the altitude the balloon ascends to, the trip up and down can take between one and three hours or more. Due to the rotational kinematics of earth, the landing location of the balloon will be to the east of the launching site. However this drift is also subjected to weather patterns and can range between 50 miles to 125 miles.

Photovoltaic (PV) cells or solar cells are mostly comprised of semiconductor crystals. Unlike conductors, semiconductors can conduct electricity only if the crystal was exposed to a certain voltage difference or provided with energy in a form of heat or light. What dictates this behavior is the energy band gap (E_g) [9]. Electrically, materials in general, have two energy bands separated by a gap. The lower band, where the electrons exist, is known as the valance band, while the upper band is called the conduction band. The energy separation between them can range from zero eV to a number of electron Volts. In conductors, the two bands overlap and $E_g = 0$ eV which allows electrons to be free to conduct electricity. In semiconductors however, the separation between the two bands does not allow electrons to conduct electricity. The conducting electrons, which are found in the valance band, have to receive a quantized beam of energy that is equal to the energy gap E_g , as a result, the electrons jump from the valance band to the conduction band. When the electron becomes part of the conduction band population, it can move freely from one part of the crystal to another and thus conducts electricity. In semiconductors, E_g is small, $0 < E_g < 3$ eV or 4 eV. Semiconductors can either be made out of pure crystals, such as those made from silicon (E_g at room temperature = 1.11 eV [10]) or Germanium (E_g at room temperature = 0.67 eV [11]). Mixing and synthesizing some materials or elements can also produce semiconductors. If $E_g > 4$, it is known as an insulator and the material does not conduct electricity.

When electrons are mobilized from one region to another, they leave behind an excess of positive charge known as holes; this region is called “p”. The region they end up in has an excess of negative charge is known as “n”. A semiconductor that has these two regions forms what is known as the p-n junction diode. Since making the first solar cell in the late 1940s, the efficiency of single p-n junction crystalline silicon devices are now approaching the theoretical limiting efficiency of 37.7%. However, the new multiple layer solar cells have a theoretical limit of 86% It is well known that the design and the shape of the solar cell platform have a noticeable effect on the efficiency at high altitudes [1].

Procedure

There are three main parts of the weather balloon; these parts are connected together via non-stretchable strong lightweight ropes. The upper part is a rubber balloon (Kaymont KCI TX3000 weather balloon) that is made out of latex or synthetic rubber (neoprene). This balloon was inflated by helium until it had the sufficient buoyant force required to lift off the payload.

The second part of the weather balloon was the parachute, which was connected directly to the balloon using a rope and a U-shaped knot that was tightened by zip ties. The purpose of the parachute was to bring the payload back to the ground at a low and safe terminal velocity.

The third part was the payload itself, which was attached to the parachute using several ropes. The payload consisted of two Styrofoam boxes, one inside the other, to ensure that the fragile measuring instruments were protected. Had the payload landed on water, the extra Styrofoam also would have kept it afloat. The contents of the payload included two GoPro cameras to capture photos and videos. One camera was set to take pictures through the bottom of the box and the second one was placed on the side and recorded video footage. Two Track-it DataLoggers and one Spot GPS Tracker were mounted on the inside cover of the box. An Eagle Flight Computer, which measured weather elements and location (latitude and longitude) was placed on the cover outside the box. Some hand warmers were placed inside the box, which also contained the batteries to power instruments. Two PowerFilm MPT6-150 Solar Cells (3" X 4") were mounted on the outside part of the box cover. Both cells were placed inside a transparent plastic sealed top. The voltage signal from each cell was recorded independently. The temperature and pressure sensors were also placed inside the sealed plastic top. See Figure 1.

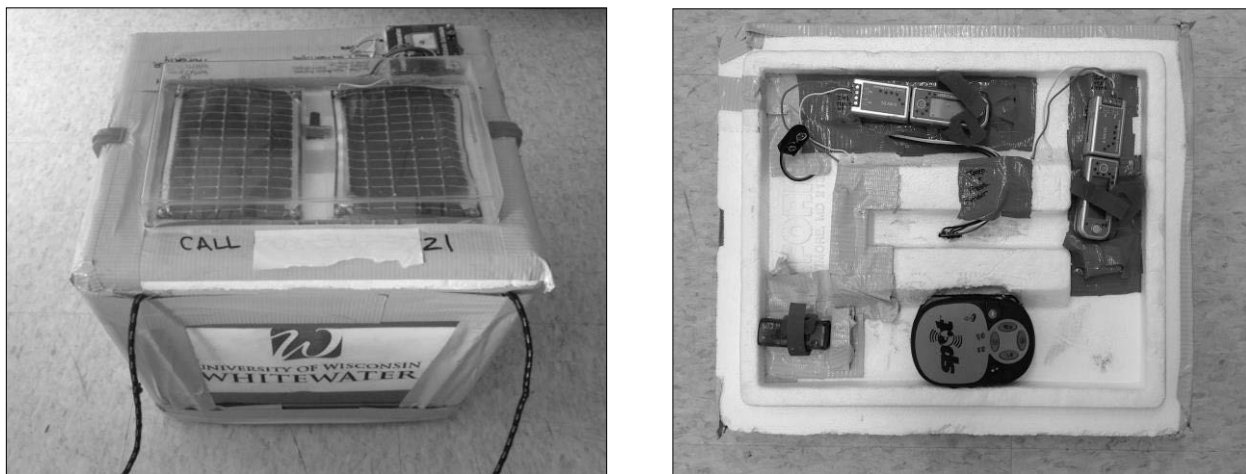


Figure 1. Photo of the payload and the cover of the box. The temperature and the pressure sensors were placed between the two solar cells under the sealed transparent cover (left). Some sensors, data loggers and the GPS were placed on the inside of the cover (right).

Prior to the launch, the measurement devices carried in the box were tested for proper function. Both launches used the same apparatus and design shown in Figure 1. The two launches were performed in Wisconsin on sunny days in August 2013 and April 2014. The choices for launch sites and dates were dictated mostly by weather. The flight predictor free website (predict.habhub.org) was chosen to trace the projected path of the balloon from launch to landing. The Spot GPS Tracker and Findmespot.com website were used to trace the actual trajectory of the balloon from launch to landing. See Figure 2. Once the launching location was chosen, the balloon was filled with Helium until it had sufficient force to lift up both the parachute and the payload.

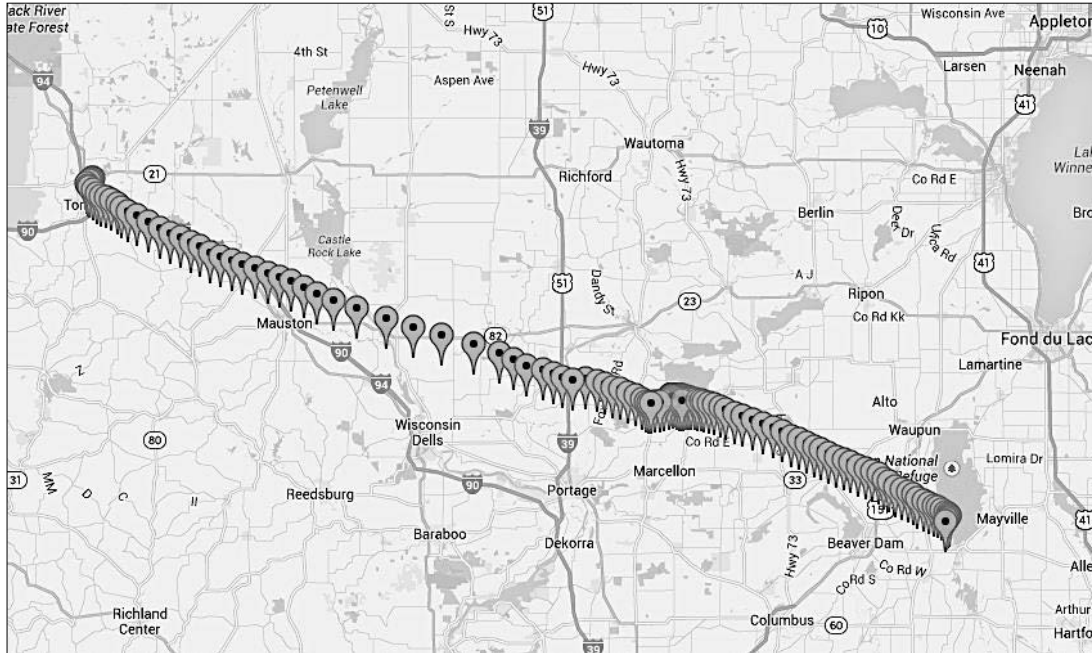


Figure 2. Actual trajectory of the second lunch was constructed by Spot GPS Tracker and Findmespot.com.

Results and Analysis

It was determined in the laboratory that these types of solar cells have voltage outputs that are highly dependent on temperature. As the temperature increased the voltage signal value decreased. The voltage signal was also tested on the ground when the cells are directly under the sunlight and when they are 3 feet within the shadow of a building. It was noticed that the voltage signal decreases by about 10% when it was in the shade. This test was necessary to understand how the voltage signal reacts when the solar cells come underneath the shaded areas created by the balloon/parachute. Impact tests were also conducted to check the validity of the parachute when the load hit the ground.

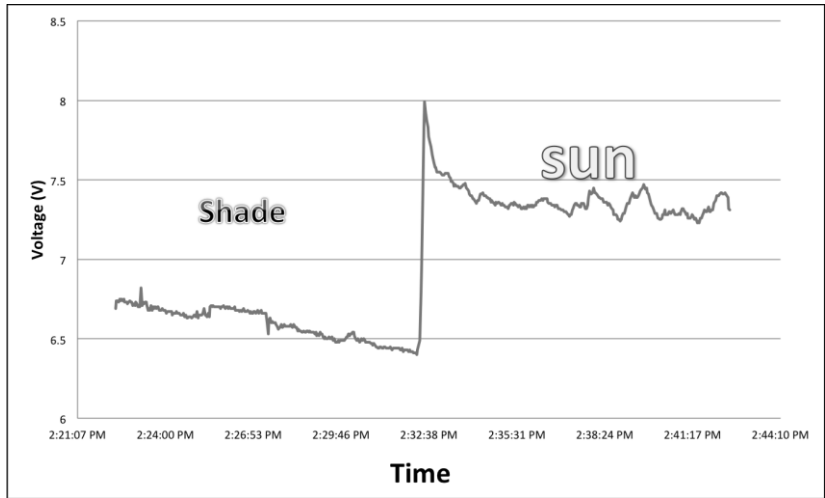


Figure 3. The solar cell voltage signal. The left side is in the shade and the right side is under the sun.

The first launch, in which a lot of data was acquired and analyzed, was used as a learning experience to help perfect the second launch. No major problems were recorded for the first launch, however, the temperature sensor and the video camera failed

In the second launch, temperature, pressure, altitude, voltage signals and other data were collected and analyzed. Figure 4 (left) shows the pressure for the entire flight. From this graph, it was clear to see that the ascending trip took almost twice the time of the descending one (less than an hour). Figure 4 (right) shows the temperature inside the sealed transparent chamber, where the solar cells were, as a function of time for a complete flight. It appeared that the temperature increased to a maximum value of 73 °C (~163 °F). This unexpected high temperature might have resulted from the combination of the hand warmers that were placed inside the box and the greenhouse effect created by the sun's rays on the tightly sealed small transparent chamber. Both graphs started counting time 0.75 hours before the launch and kept recording till about 0.25 hours after landing.

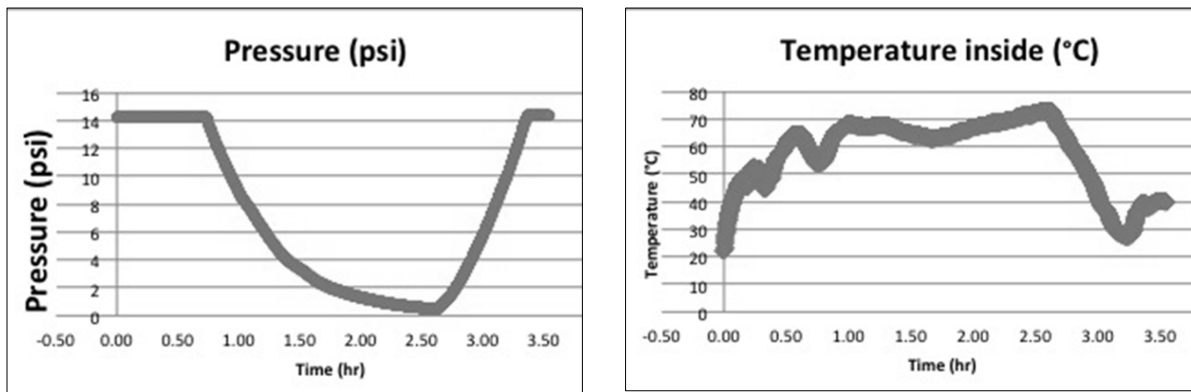


Figure 4. Pressure (left) and temperature (right) as a function of time for the complete trip.

In Figures 5 and 6, graphs of the temperature (°F) and voltage (V) for the ascending trip only are shown as a function of time. These two graphs are to the same scale. Both the temperature and voltage signals exhibited a uniform pattern. As was expected from the tests performed on the solar cells on the ground, it was realized that the voltage signal decreased when the temperature increased.

From the graphs and at the very start of the ascending trip, the voltage signal increased slightly as a response to the decrease in temperature, which was expected. This occurred immediately after the launch and at a very low altitude. During this period, the maximum voltage output was recorded for the whole trip. Then, as the temperature increased to 150 °F, the signal dropped accordingly. The temperature increase continued, but at a slower rate, and output signal responded slightly to this change by slowing down the decrease rate, as can be seen at about 15,000 ft. After this point and between 0.25 hours to 0.65 hours, the temperature made a slight decrease then returned to the previous level. Although this temperature fluctuation can be seen affecting the voltage signal between 15,000 ft. to 21,000 ft., the slight change (in the voltage signal) in this altitude range could also be the result of the slower temperature increase rate that occurred earlier.

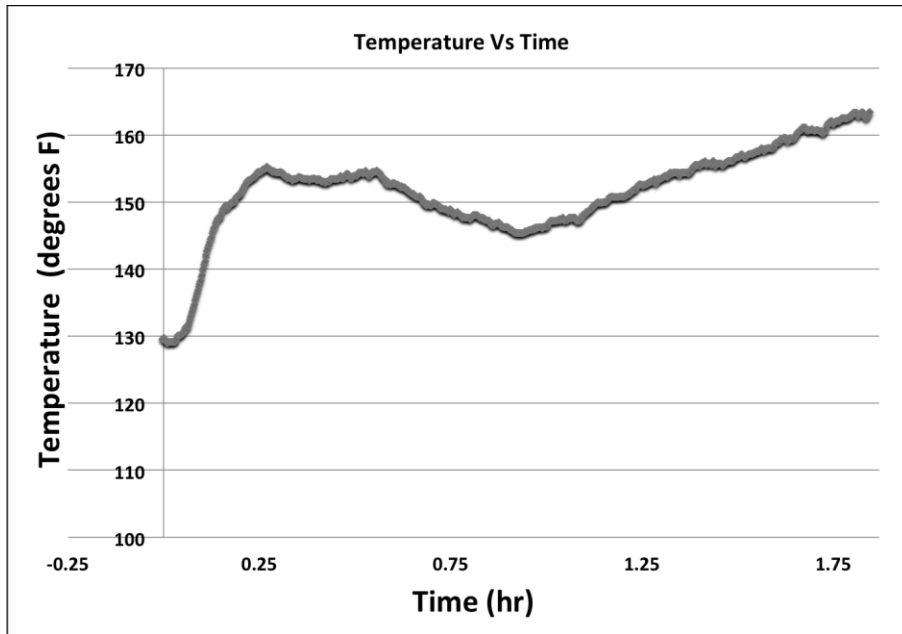


Figure 5. Temperature ($^{\circ}\text{F}$) for the ascending trip only as a function of time.

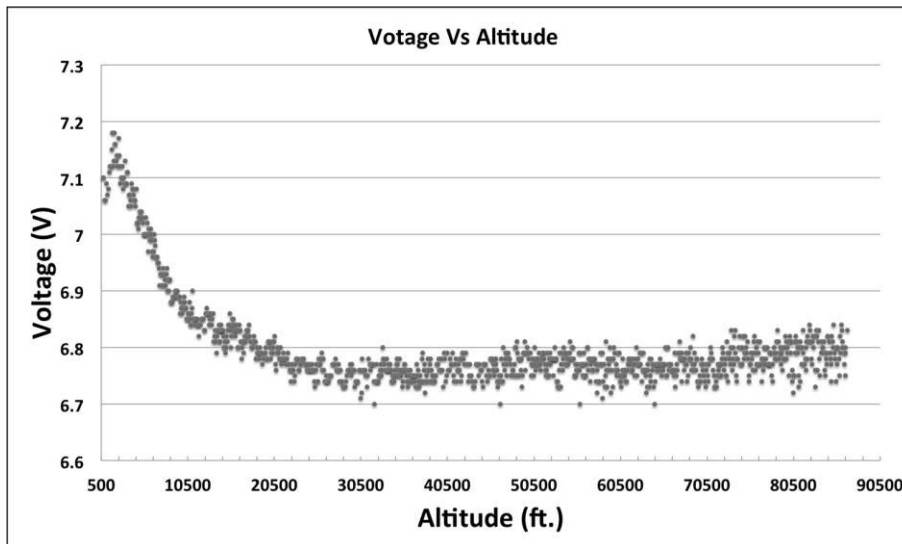


Figure 6. Voltage for the ascending trip only as a function of time. These two last figures were to the same scale.

Finally, at the long range defined between 0.65 hours to 1.87 hours, the temperature decreased to 145°F after one hour (of the flight time) then gradually increased to 163°F . In Figure 6, this is shown in altitudes above 25,000 ft. In this full region although the voltage signal was slightly affected, it is a far less reaction than those seen at lower altitudes. For example, the temperature increased by a large percentage between the time one hour and 1.87 hours and the signal barely changed. The indirect relationship between temperature and voltage seemed to fade away at those altitudes. One explanation to that is the rate at which the voltage signal increased as altitude increased was the same rate it has decreased due to temperature's increase, this combined effect forced the voltage signal to plateau when it should decrease. This leads to the conclusion that voltage output signal had increased when the balloon was at an altitude above 45,000 ft. Another

explanation is that above 45,000 ft., temperature fluctuations do not have an influence on the voltage signal for these types of solar cells.

The voltage output signal was also analyzed during the ascending part of the flight. See Figure 7. Both voltage (stars) and temperature (solid line) displayed a uniform pattern where temperature and voltage are in an ideal indirect relationship.

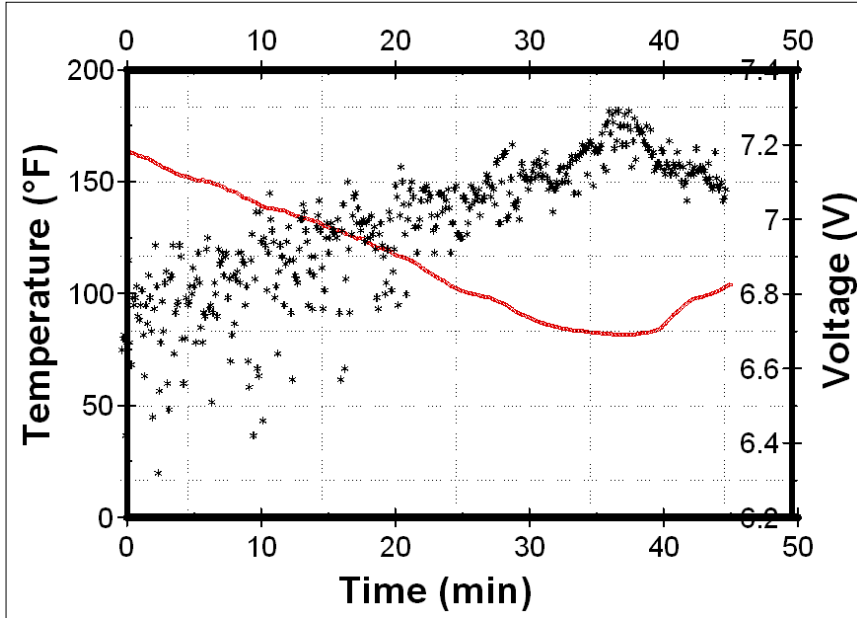


Figure 7. A plot of voltage and temperature (solid line) during descend, as a function of arbitrary unit.

Finally, a summary of the two launches is shown in Table 1.

| | Launch # 1 | Launch #2 |
|---|---|--|
| Date | August 28, 2013 | April 26, 2014 |
| Maximum Height (ft.) | 93200 | 80215 |
| Length of the flight (hr.) | 2.8 | 2.6 |
| Max voltage signal (regardless of temperature) | ~ 34000 ft. | ~1000 ft. |
| Notes | Video and temperature sensor did not function | Temperature went up more that expected |
| | Pictures were captured when Balloon popped | Balloon popped after cameras died |

Table 1. A summary of the two launches.

Conclusion

The output voltage signals of select solar cells were monitored and recorded as a function of altitude using a weather balloon. It was not clear if signal was influenced by the change in altitude at lower elevations, as the influence of temperature on the efficiency is very evident, as discussed previously. It was also found that the signal plateaued above 45,000 ft. This could be the result of increasing temperature and altitude. But since an increase in temperature was proven to cause the voltage signal to decrease, a flattened signal output might be explained as a result of an increasing voltage signal.

Future work will include using more than one type of solar cells to obtain a universal conclusion. If a sealed transparent chamber should be used to enclose solar cells, then a temperature regulator to keep the temperature constant inside is a must. This will lead to more reliable data to better understand how the voltage signal changes as a function of altitude, especially above 45,000 feet.

Acknowledgments

The authors would like to thank Wisconsin Space Grant Consortium (WSGC) for funding this project. We are also grateful for the College of Letters and Sciences and the Office of Research and Sponsored Programs at University of Wisconsin – Whitewater for funding and supporting this work. Many thanks and appreciation go to students Alexander Neumann and Charles Simonet who started working on this project long before it was funded.

References

- [1] G Romeo, G Frulla, and E Cestino, Design of a high-altitude long-endurance solar-powered unmanned air vehicle for multi-payload and operations, Special Issue Paper 199.
- [2] G. Basini and M. Ricci, Balloon measurements of cosmic ray muon spectra in the atmosphere along with those of primary protons and helium nuclei over midlatitude, Phys. Rev. D 60, 1999.
- [3] H. S. Hopfield and Tropospheric, Effect on Electromagnetically Measured Range: Prediction from Surface Weather Data, Radio Science Vol. 6, NO. 3, 1971,
- [4] R. H. Holzworth, High latitude stratospheric electrical measurements in fair and foul weather under various solar conditions, Journal of Atmospheric and Terrestrial Physics, Volume 43, Issue 11, 1981.
- [5] J.J. López-Moreno, G.J. Molina-Cuberos, R. Rodrigo, M. Hamelin, and K. Schwingenschuh, Polar ionic conductivity profile in fair weather conditions: Terrestrial test of the Huygens/Hasi-PWA instrument aboard the Comas Sola balloon, Journal of Atmospheric and Solar-Terrestrial Physics, Volume 63, Issue 18, 2001.
- [6] T. J. Rosenberg, J. R. Benbrook, D. Detrick, D. L. Matthews, M. J. Rycroft, M. A. Saunders, W. R. Sheldon, and E. A. Bering, Electric Fields, Electron Precipitation, and VLF Radiation During a Simultaneous Magnetospheric Substorm and Atmospheric Thunderstorm, Journal of Geophysical Research, Vol. 85, No. A1, 1980.

[7] <http://www.uwgb.edu/WSGC/default.aspx>

[8] F. W. Sarles, W. C. Haase, and P. F. McKenzie, Balloon Flight Instrumentation for Solar Cell Measurements, *Rev. Sci. Instrum.* 42, 1971.

[9] W. D. Callister and D. G. Rethwisch, *Materials science and engineering: an introduction*, John Wiley & Sons, 2009.

[10] J. D. Holmes, K. P. Johnston, R. C. Doty, B. A. Korgel, Control of Thickness and Orientation of Solution-Grown Silicon Nanowires *Science*, Vol. 287 no. 5457, 2000.

[11] B. G. Streetman and S. Banerjee *Solid State electronic Devices* (5th ed.), New Jersey: Prentice Hall. p. 524. (2000).

Design of a Lunar Solar Wind Volatiles Extraction System

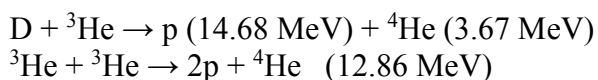
Aaron D.S. Olson, John F. Santarius, Gerald L. Kulcinski

Engineering Physics Department, University of Wisconsin-Madison, Madison, WI

Two devices are being developed as part of a project to demonstrate the extraction of helium-3 and other volatiles from lunar regolith. The first is an implantation system to embed helium ions into JSC-1A lunar regolith simulant and the second is a counter flow heat pipe heat exchanger for the subsequent diffusion of the helium out of the regolith. This will simulate the previously proposed acquisition of helium-3 from the Moon for use in nuclear fusion reactors on Earth. Preliminary designs of both of these systems are discussed.¹

I. Introduction

Of the various volatile materials available on the Moon, there is potentially only one that has significant value back on Earth. Helium-3 (^3He), if used as fuel in a nuclear fusion reactor, could become a significant lunar export for power generation around the world. The nuclear fusion reactions using ^3He :



are promising for commercial future fusion reactors due to their high energy output and their low emission of neutrons, higher energy conversion efficiency, increased safety and potential ease of maintenance compared to the more studied deuterium-tritium (DT) fuel cycle. Unfortunately, there is not enough terrestrial ^3He to support its use for power generation.¹ It was realized in 1985 that there is $\sim 10^6$ tonnes of ^3He embedded in the lunar regolith from over 4 billion years of the Moon being bombarded by the solar wind. The seminal article tying lunar ^3He to fusion development was published by researchers at the University of Wisconsin-Madison's Fusion Technology Institute (FTI) in 1986.² Three designs of lunar ^3He miners have been developed at the FTI: the Mark-I, II, and III (M-1 through M-3).³⁻⁵ The



Figure 1. Illustration of the Mark I helium-3 lunar volatiles miner³ (Credit: John Andrews)

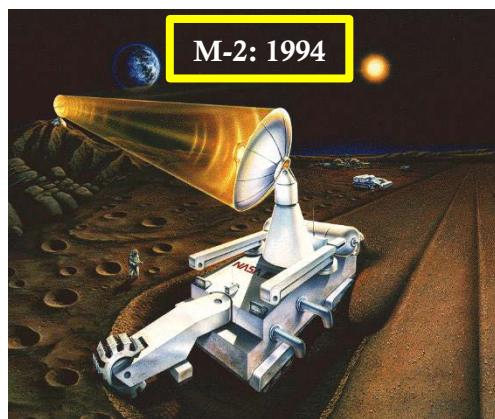


Figure 2. Illustration of the Mark II helium-3 lunar volatiles miner⁴ (Credit: I. Sviatoslavsky)

The Wisconsin Space Grant Consortium (WSGC) graciously provided funding in support of the work presented in this paper. The Greatbach Foundation and Grainger Foundation were also instrumental in support of this work.

most recent of these designs was completed in 2006. The M-3 miner was designed to return 33 kg of ^3He to Earth each year after excavating to 3 m depth over a 1 km² area. This would be enough to fuel one ~400 MWe fusion power plant. The 33 kg/yr collection rate assumes a 10 ppb ^3He grade (by mass) and that the miner only operates during 90% of the lunar daytime (3942 hours/year). It is thought that the ^3He grade in the undisturbed maria regolith should actually be closer to 20 ppb⁶ and with this in mind, the collection would be closer to 66 kg/yr. The other solar wind volatiles (H_2 , ^4He , CO_2 , CH_4 , N_2 , H_2O), which diffuse out of the regolith with heating, could also be collected for the life support needs of astronauts anywhere in cislunar space or beyond (water, oxygen, atmosphere, food growth) and/or fuel for spacecraft. These other volatiles are present in the lunar regolith in much higher concentrations than ^3He as seen in Table 1, and in a mining operation where each miner collects 66 kg/yr of ^3He , these volatiles could be collected to support hundreds of people in space.⁷ The M-3 miner design employs a continuous volatile extraction process where regolith is excavated with a bucket wheel excavator before entering the internal processing portions of the miner. Inside the miner, regolith is beneficiated in a series of sieves, screw conveyors and a fluidized bed so that only particles larger than 100 microns are rejected. Particles smaller than 100 microns enter a heating system where the volatiles are evolved by diffusion out of the regolith.

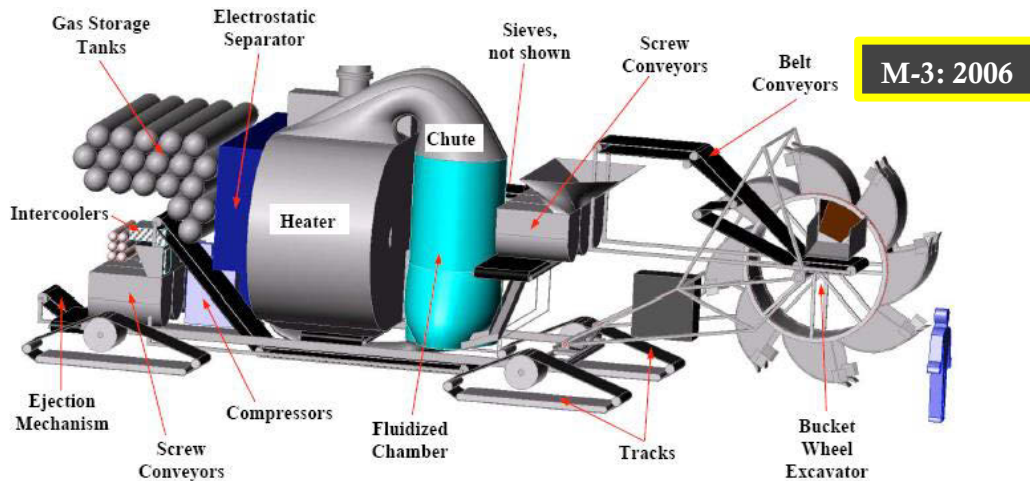


Figure 3. Model of the interior components of the Mark III helium-3 lunar volatiles miner⁵ (Credit: M. Gajda)

Table 1. Volatiles Products of Heating Mare Regolith to 700 °C

| Volatile | Mass evolved per tonne of regolith mined (g)* | Mass evolved per kg of ³ He evolved (kg) | Mass extracted (tonnes/yr)** |
|--|---|---|------------------------------|
| H ₂ | 43 | 6100 | 201 |
| ⁴ He | 22 | 3100 | 102 |
| ³ He | 0.007 | 1 | 0.066 |
| H ₂ O | 23 | 3300 | 109 |
| N ₂ | 4.0 | 500 | 16.5 |
| CH ₄ | 11 | 1600 | 53 |
| CO | 13.5 | 1900 | 63 |
| CO ₂ | 12 | 1700 | 56 |
| *After beneficiation, 450 kg of regolith is heated | | | |
| ** With 20 ppb and 1258 tonnes/hr excavation | | | |

The heating system is effectively a counter flow heat pipe heat exchanger that consists of preheater, supplemental heater, and recuperator sections of heat pipes. Concentrated solar energy is transferred to the supplemental section of heat pipes from a solar collector. The heating system brings the temperature of the <100 micron regolith particles up to 700 °C from an inlet temperature of 30 °C to evolve the embedded volatiles while also recuperating heat from the waste regolith, in the recuperator section, before it exits the heating system. Using Apollo 11 sample 10086.16, it was shown that heating maria regolith from Mare Tranquillitatis up to 700 °C releases 85% of the trapped ³He.⁸ To produce 33 kg/yr of ³He (assuming 10 ppb) at an energy recovery efficiency of 85%, 12.3 MWt is required from the solar collector for a 157.3 kg/s mass flow rate of processed regolith. A total of 21,500 1.5 cm diameter heat pipes, with their 1 m long condenser sections acting as the preheater and their 1 m long evaporator sections acting as the recuperator, would be required. The working fluid in the heat pipes varies with depth in the heating system from water in the lowest temperature rows of heat pipes (near the inlet) progressing to mercury, potassium and eventually sodium next to and in the supplemental heater section. The pressure inside of the heating system was chosen to be 20 kPa. The gas in the heating system is the released volatile gas mixture, which is mostly H₂ and ⁴He. Figure 4 illustrates the concept of the heat pipe heat exchanger for the Mark series of ³He and lunar volatiles miners. The heating system is approximately 5 m in length, 2 m in width and 3 m in height. It is estimated to be ~9 tonnes. Figure 5 shows the model of the heat exchanger where the 21,500 heat pipes that make up the heating system are shown at three different viewing scales.

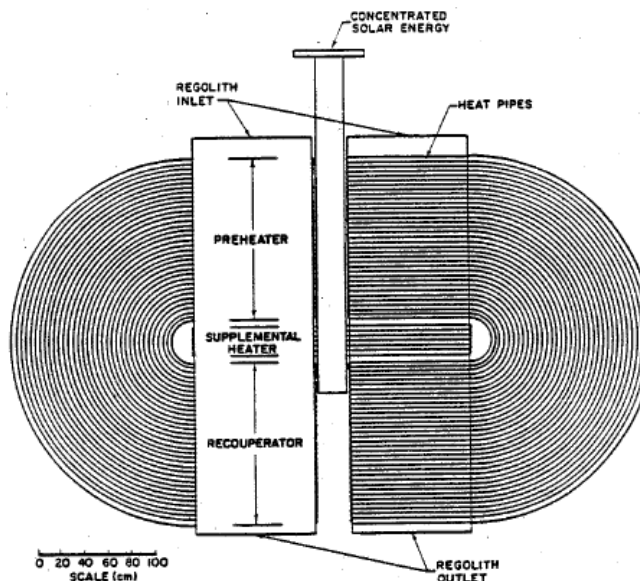


Figure 4. Illustration of the heat pipe heat exchanger designed for the Mark series of helium-3 lunar volatiles miners.³ The system is scaled to heat 157 kg/s of regolith from 30 °C up to 700 °C.

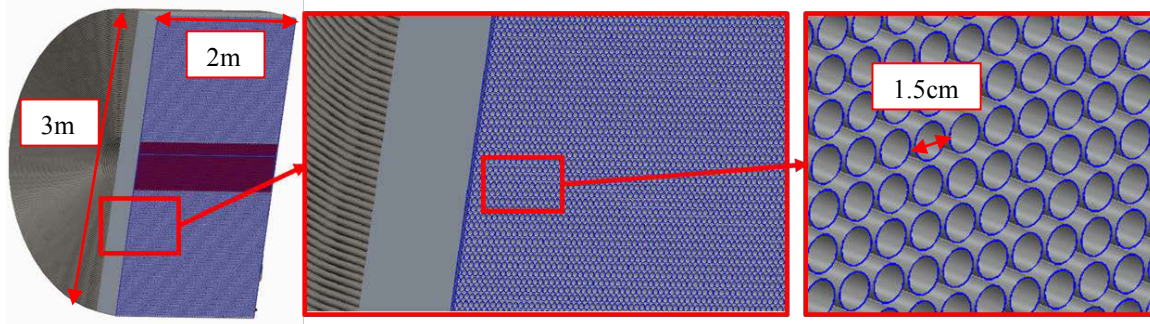


Figure 5. Model of the Mark series miners' heating system on three different viewing scales, demonstrating the size of the system relative to an individual heat in the system.

II. Small Scale Heat Pipe Heat Exchanger

Currently at the FTI, work is being done to demonstrate the process of acquiring ^3He from lunar regolith on a small scale, which could lead to eventual large scale acquisition for future nuclear fusion reactors. The extraction technique described above is the design baseline for the demonstration system. In lieu of a solar concentrating system to provide heating power to the heating system, electrical resistance heating (Joule heating) will be used for simplicity. A 1:1000 scale

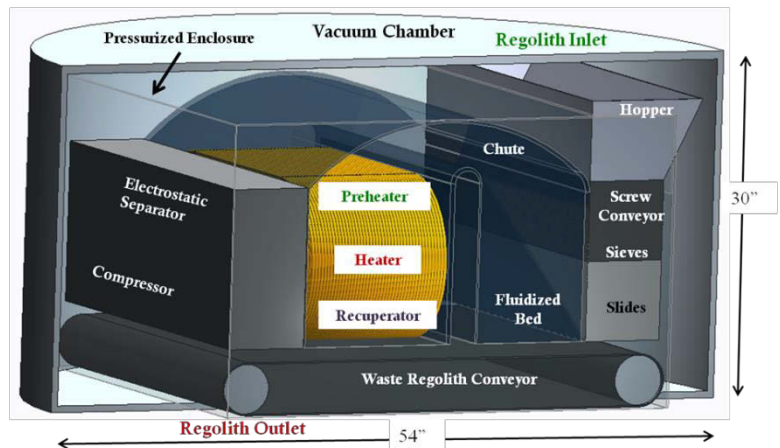


Figure 6. Concept of a demonstration lunar volatiles extraction system with a heat pipe heat exchanger heating system

compared to the M-3 was selected for an initial demonstration system. This means that the demonstration unit will need to heat a regolith mass flow rate (\dot{m}) of 0.157 kg/s. With this mass flow rate known, the heating system design comes down to determining the required heat transfer area for a given heat exchanger configuration. The aforementioned heating system configuration is a counter flow heat exchanger with a capacity ratio of unity because the regolith going through the preheater has the same specific heat as the regolith going through the recuperator. The number of thermal transfer units (NTU) for a heat exchanger such as this can be determined as a function of effectiveness (ϵ) using the standard formula shown in Eq. (1) below.⁹ Effectiveness is the ratio of heat transfer in the heat exchanger to the maximum possible heat transfer while NTU is a heat exchanger's total thermal conductance (UA) over its capacitance rate, \dot{C} , as seen in Eq. (2). Total thermal conductance is the inverse of total thermal resistance (R_{tot}) and the capacitance rate is simply the product of the mass flow rate and the specific heat (C_p) of the regolith.

$$NTU = \frac{\epsilon}{1 - \epsilon} \quad (1)$$

$$NTU = \frac{UA}{\dot{C}} \quad (2)$$

In this case the effectiveness is the same as the prescribed energy recovery efficiency, and thus the heat exchanger's total conductance can be directly determined with Eq. (1) and Eq. (2). The effectiveness of 85% was kept from the full scale M-3 design, but could be varied in future demonstrations. Heat pipe effective thermal conductivities can be 3 to 4 orders of magnitude larger than the best solid conductors (e.g., copper).¹⁰ With this in mind, the thermal resistance of the heat pipes has been neglected in the calculation of total thermal resistance. The only resistance taken into account is that due to convection heat transfer at the condenser (preheater section) and the evaporator (recuperator section) surfaces of the heat pipes. The condenser and evaporator surface areas (A_{pre} and A_{rec}) have to be equal for the heat exchanger to operate as intended, and thus the total thermal resistance can be described as shown in Eq. (3). The heat transfer coefficient (h) can be determined from an appropriate Nusselt number (Nu) correlation. For this configuration the Dittus-Boelter correlation was used as seen in Eq.(4) with the Reynolds number (Re) and Prandtl number (Pr) defined as in Eqs. (5). The hydraulic diameter (D_h) for the flow paths in the heat pipe arrangement was calculated as shown in Eqs. (5) with the distance between outer walls of consecutive columns of heat pipes (δ) and the evaporator section length of a heat pipe (L_{pipe}). The regolith bulk density (ρ) used is 1700 kg/m³, and the specific heat of the regolith used is 800 J/(kgK). The thermal conductivity (K) of the bulk regolith was taken to be 0.4 W/(mK) by augmenting thermal conductivity values measured for JSC-1A simulant at 25 kPa in air.¹¹ In a H₂ and ⁴He environment at 20 kPa, the bulk regolith thermal conductivity should increase like Deissler and Boegli showed for similar granular materials.¹² The viscosity of the flowing regolith was taken to be 2.1x10⁻⁴ (Pa s) as Sviatoslavsky used.³

$$(UA)^{-1} = R_{tot} = \left(\frac{1}{hA_{pre}} \right) + \left(\frac{1}{hA_{rec}} \right) = \frac{2}{hA} \quad (3)$$

$$Nu = 0.023Re^{4/5}Pr^{2/5} = \frac{hD_h}{K} \quad (4)$$

$$Re = \frac{\rho U_{avg} D_h}{\mu} \quad Pr = \frac{C_p \mu}{K} \quad D_h = \frac{2\delta L_{pipe}}{\delta + L_{pipe}} \quad (5)$$

The calculation of the Reynolds number requires the average velocity (U_{avg}) of the bulk regolith through the heat pipe matrix. A capillary model, for flow through paths in a porous medium, was used to model the flow between the heat pipes and estimate the average regolith velocity for a given average flow area (A_{avg}) and effective gravitational pressure drop ($\frac{dP}{dz}$) as shown in Eqs. (6).¹³ The effective gravitational pressure drop was simply taken as the product of the height that the regolith falls from the heating system inlet to the supplemental heater section (H_{pre}), with the gravitational acceleration on Earth (g) and the density of the bulk regolith simulant over the effective flow path length (L_{eff}) through the preheater section of the pipe matrix.

$$\dot{m} = \rho U_{avg} A_{avg} = \frac{\pi \rho D_h^4}{128 \mu} \left(\frac{dP}{dz} \right) \quad \left(\frac{dP}{dz} \right) = \frac{\rho g H_{pre}}{L_{eff}} \quad (6)$$

The counter flow heat exchanger and capillary flow model relations presented above allow for the solution of a heat pipe arrangement given appropriate bounds on the system's overall height (H), heat pipe diameter (D) and condenser/evaporator section length (L_{pipe}). An optimum (mass-minimized) configuration was determined in which the number of heat pipe columns (N_{col}) and rows (N_{row}) were determined as well as the inter-pipe distance across a row. The number of columns was rounded up to 7, the number of rows was rounded up to 17, and δ was found to be ~ 1 mm. For simplicity, the supplemental heater section uses heating rods of the same diameter as the heat pipes. Assuming that all of the heating rods' external surface area is at the same temperature (T_s) of 800 °C, the number of required electrical resistance heating rods can be determined by dividing the total length that the regolith needs to flow between the heating rods (H_{supp}) to reach its peak temperature of 700 °C by the pipe diameter. The length is calculated using an internal pipe flow model with the same hydraulic diameter presented above as shown in Eqs. (7).¹⁴ The perimeter (per) of the flow path between the heating rods is the product of twice the number of heat pipe columns and the sum of the heat pipe evaporator section length and inter heat pipe distance, also shown in Eqs. (7). The result was rounded up to 2 rows of electrical heating rods.

$$T_{outlet} = (T_{inlet} - T_s) \exp\left(\frac{-(per)hH_{supp}}{\dot{c}}\right) + T_s \quad per = 2N_{col}(L_{pipe} + \delta) \quad (7)$$

The entire heating system mass is 5.4 kg (excluding the heat pipe working fluid) with heat pipes of stainless steel wall material, 1.5 cm diameter and 0.25 mm thickness and solid stainless steel heater rods also with 1.5 cm diameter. The heat pipe and heating rod configuration is shown on the left of Figure 7. A CFD model of the bulk regolith flow and heat transfer through the heat pipe matrix was created to compare to the analytical results. The model takes into account the tortuosity of the flow path, the varying effective flow channels between the heat pipes, and a varying heat transfer coefficient through the pipe matrix as well. A velocity magnitude contour plot resulting from the CFD model is shown in the center of Figure 7. A temperature contour plot of the regolith through the heat pipe matrix is shown on the right in Figure 7. The velocity results of the CFD model match that of the capillary model in the vertical flow paths through the pipe matrix within 10%. The CFD model's thermal results confirm that regolith will reach a maximum temperature of 700 °C and therefore release the anticipated amount of implanted volatiles.

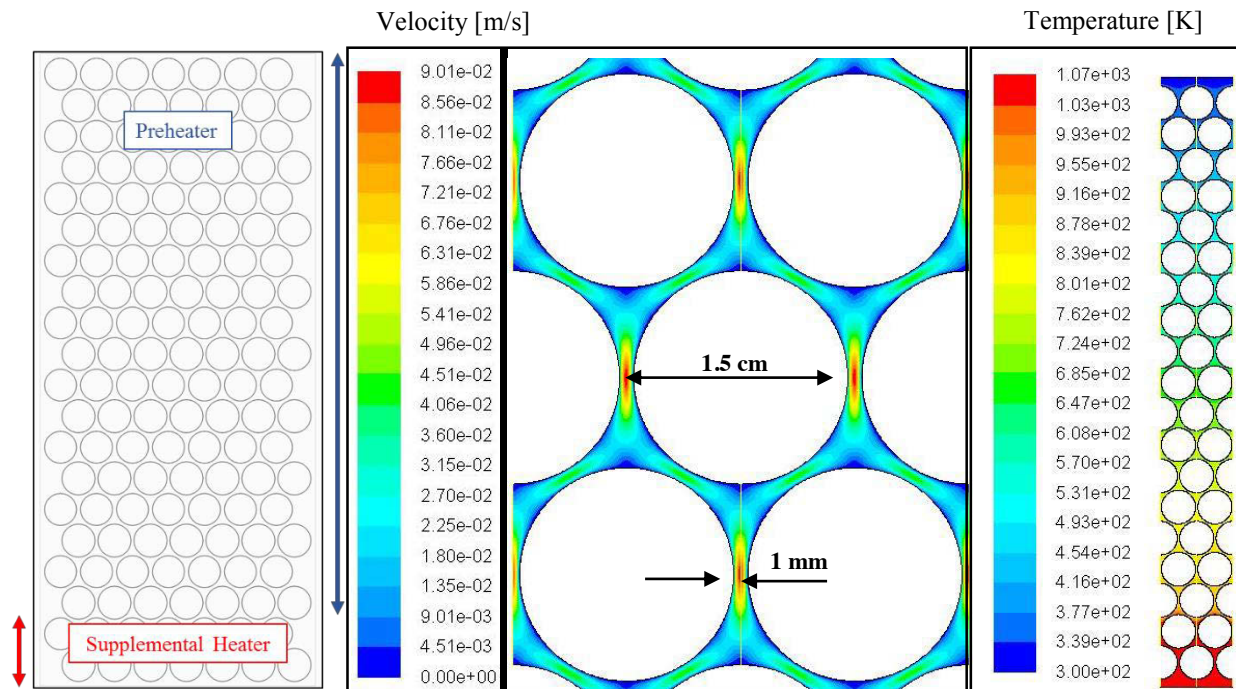


Figure 7. Heat pipe arrangement in the preheater and supplemental heat exchanger sections (left), contour plot of bulk regolith velocity through the heat pipe matrix (center) and a contour plot of the temperature variation of the regolith with depth through the scale heat pipe heat exchanger (right).

Modifications to the CFD model will allow for particle tracking, where the percentage of particles actually reaching the maximum temperature can be determined, and more accurate results that take into account the cohesiveness that may develop amongst the regolith particles as they flow through the heating system. There is a significant amount of work remaining before this demonstration heating system can be constructed and tested. Beyond the model modifications described above, in depth analysis on the individual rows of heat pipes will need to be completed. In the foregoing heat exchanger analysis it was assumed that all of the heat pipes provide the same amount of heat to the regolith. This will almost certainly not be the case due to the differences in the operational characteristics of heat pipes with different working fluids. A revised design will take this into account along with the transient behavior of the heating system, so that an estimate for the startup time and energy can be determined as a function of the overall system's energy recovery efficiency. The movement of the regolith prior to the heat exchanger inlet and after the heat exchanger outlet will also need to be taken into consideration. The instrumentation of the demonstration unit must also be developed. It is envisioned that a residual gas analyzer will be used to monitor the evolution of volatiles out of the regolith while thermocouples probes will gather temperature measurements at various locations inside of the heat exchanger.

III. Implantation of Helium into Regolith Simulant

Before demonstrating the evolution of ^3He out of regolith simulant, simulant that is embedded to a known concentration must be available in order to gauge the performance of the extraction system. Beyond the Apollo and Lunakhod lunar soil samples, there is no regolith or regolith simulant that has already been implanted with solar wind volatiles that is available for

experimental studies. An implantation device is being developed to implant helium-4 into batches of JSC-1A simulant. Helium-3 will only be used after the device's operational performance is completely tested in order to keep costs down. Of the numerous known implantation techniques, implantation by a dc plasma discharge was chosen for this implantation device because of its relative simplicity. In a dc glow discharge an electrical potential, or voltage, is held between two parallel electrodes (plates) under a controlled pressure environment. Empirical results have given curves of the required breakdown voltage (V_b) to start the glow discharge as a function of the product of pressure and distance between the electrodes for a given gas.¹⁵ These curves are referred to as Paschen curves. For helium ions to implant in regolith simulant with approximately the same average energy as the helium ions do on the lunar surface², an ~8 kV potential is required. Using this as the breakdown voltage, a pressure-distance product (Pd) can be determined from Eqs. (8). It should be noted that Paschen curves are nonlinear and that there are actually two different pressure-distance products that could initiate the glow discharge at an 8 kV breakdown voltage. To avoid the additional cost of using a high vacuum system for the implantation device, the larger pressure-distance product of 933 Pa-m was selected. The preliminary design utilizes an available borosilicate glass bell jar as the vacuum chamber. The chamber is 21 cm in inner diameter and 28 cm in cylindrical height with a hemispherical dome. The size restrictions of the bell jar led to a plate spacing of 10 cm, which in turn determined a pressure of 9.33 kPa (70 Torr) for the helium inside of the chamber. The concept of the implantation device is that regolith will be implanted when it flows out of a wedge shaped hopper and between the electrodes as shown in Figure 8.

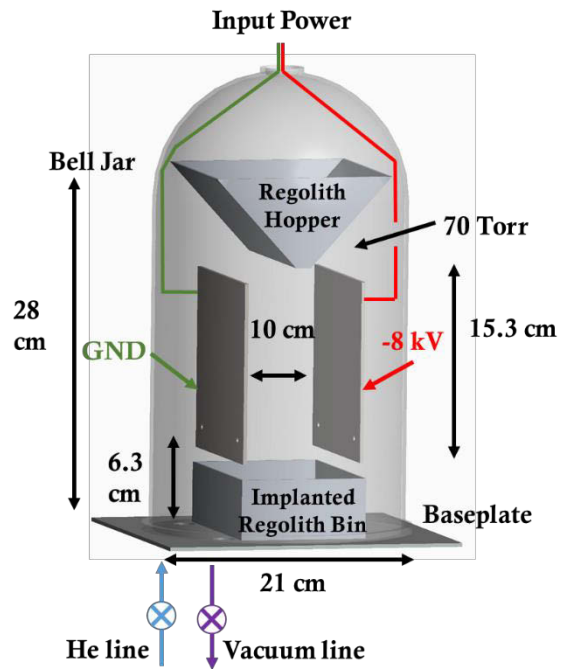


Figure 8. Concept of a dc plasma discharge implantation device for lunar regolith simulant

It should be noted that Paschen curves are nonlinear and that there are actually two different pressure-distance products that could initiate the glow discharge at an 8 kV breakdown voltage. To avoid the additional cost of using a high vacuum system for the implantation device, the larger pressure-distance product of 933 Pa-m was selected. The preliminary design utilizes an available borosilicate glass bell jar as the vacuum chamber. The chamber is 21 cm in inner diameter and 28 cm in cylindrical height with a hemispherical dome. The size restrictions of the bell jar led to a plate spacing of 10 cm, which in turn determined a pressure of 9.33 kPa (70 Torr) for the helium inside of the chamber. The concept of the implantation device is that regolith will be implanted when it flows out of a wedge shaped hopper and between the electrodes as shown in Figure 8.

$$A'Pd \exp\left(-\frac{B'Pd}{V_b}\right) = \ln\left(1 + \left(\frac{1}{\gamma_{se}}\right)\right) \quad A' = 2.1 \text{ Pa}^{-1}\text{m}^{-1} \quad B' = 57.75 \frac{\text{V}}{\text{Pa}\cdot\text{m}} \quad \gamma_{se} = 0. \quad (8)$$

It is important to consider the electron collision probability with the regolith simulant between the electrodes. If the probability of collision (P_{coll}) is too high, the discharge will not sustain itself. This will occur if the flow of regolith between the electrodes is too dense. Porosity in the regolith flow between the electrodes plates can be achieved by introducing a sieve at the hopper's outlet orifice and through the use of a gate mechanism that slides under the orifice to limit flow. With an appropriate number density of regolith particles (n) between the plates at any given time, the mean free path (λ) of electrons through the regolith particles will be sufficiently large to keep the electron collision probability ≤ 0.5 , which should keep the discharge going. The relationship between the mean free path and collision probability is shown in Eq. (9) where the cross section

of the regolith particles (σ) is set by the average diameter (D_p) of the JSC-1A simulant, ~100 microns.

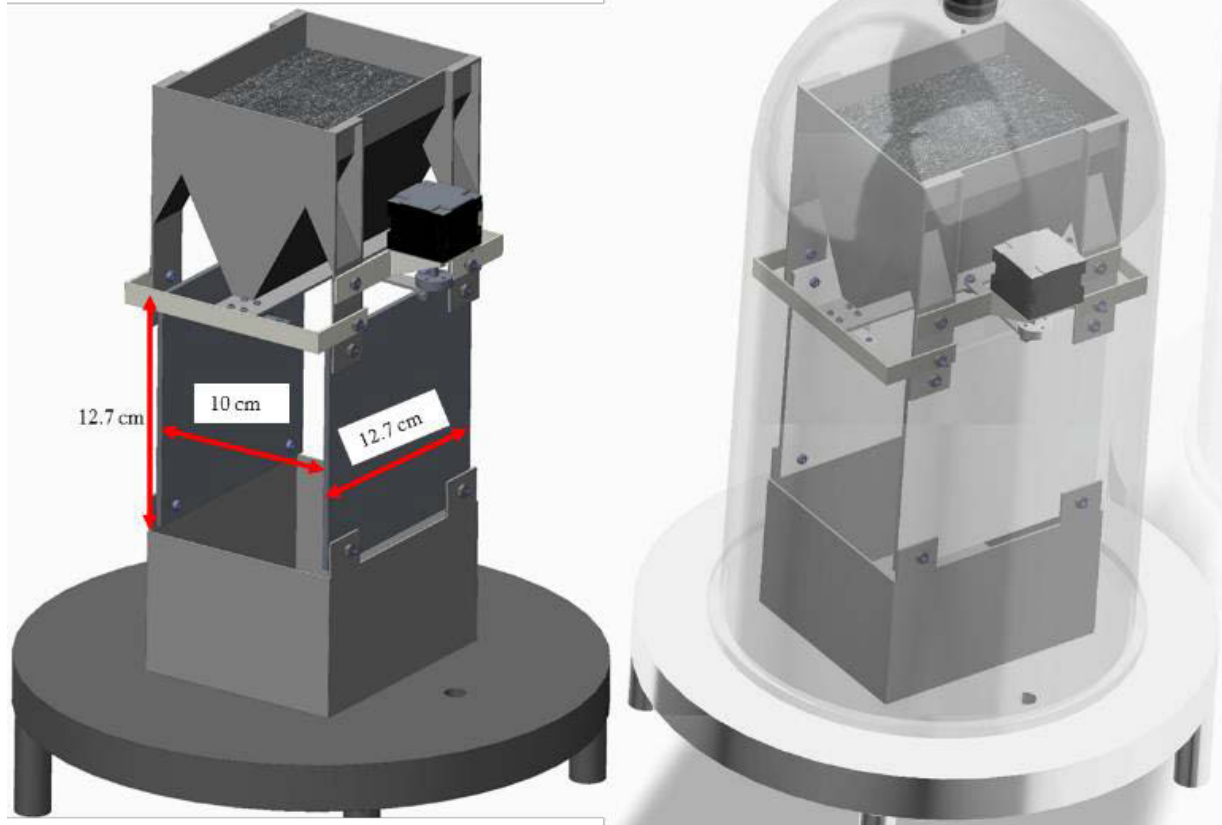


Figure 9. Preliminary design of a dc glow discharge implantation system for regolith simulant

$$P_{coll} = 1 - \exp\left(-\frac{x}{\lambda}\right) \quad \lambda = (n\sigma)^{-1} \quad \sigma = \pi D_p^2$$

One configuration that could allow the discharge to persist, and therefore the implantation of helium into the JSC-1A simulant to occur, is shown in Fig. 9. This configuration uses a stepper motor to control a gate mechanism of the hopper and has a #140 size standard sieve mesh that allows particles <106 microns to pass and blocks out 65% of the cover hopper orifice.

IV. Conclusion

A significant amount of progress has been made toward the goal of demonstrating the process of extracting ^3He from lunar regolith in a manner that could eventually support future nuclear fusion reactors. The general parameters of the aforementioned heat pipe heat exchanger have been established such as the heat pipe arrangement and geometry. CFD simulation of the flow through the heat pipe matrix shows that the regolith will indeed reach the required temperature to release 85% of the embedded ^3He . The preliminary design of the implantation system has been developed.

The parameters of the dc glow discharge that will implant helium into the regolith have been chosen and the supporting structural and vacuum elements of the system were discussed. Attention has been paid to the electron collision probability, which will determine whether the discharge continues when regolith is falling between the electrode plates of the discharge.

References

- 1 Wittenberg, L. J., "Terrestrial Sources of Helium-3 Fusion Fuel- A Trip to the Center of the Earth," *Fusion Technology*, vol. 15, 1989.
- 2 Wittenberg, L. J., Santarius, J. F., and Kulcinski, G. L., "Lunar Source of He-3 for Commercial Fusion Power," *Fusion Technology*, vol. 10, 1986, p. 167.
- 3 Sviatoslavsky, I. N., and Jacobs, M. K., "Mobile Helium-3 Mining and Extraction System and Its Benefits Toward Lunar Base Self-Sufficiency," *Wisconsin Center for Space Automation and Robotics Technical Report (WCSAR-TR) AR3-8808-1*, 1988.
- 4 Sviatoslavsky, I. N., "The Challenge of Mining He-3 on the Lunar Surface: How All the Parts Fit Together," *Space 94, The 4th International Conference and Exposition on Engineering, Construction and Operations in Space, and The Conference and Exposition/Demonstration on Robotics for Challenging Environments, February 26 - March 3, 1994, Albuquerque NM Also: WCS*, 1993.
- 5 Gajda, M., "A Lunar Volatiles Miner," University of Wisconsin-Madison, M.S. Thesis, 2006.
- 6 Schmitt, H. H., "Return to the Moon," *Return to the Moon*, Praxis, 2005, p. 89.
- 7 Olson, A. D. S., "The Mark IV: A Scalable Lunar Miner Prototype," *International Astronautical Congress 2013, Beijing, China, IAC-13.A3.2B.7*, 2013.
- 8 Gibson Jr., E. R., and Johnson, S. M., "Thermal Analysis-Inorganic Gas Release Studies of Lunar Samples," *2nd Lunar Science Conference Vol. 2*, 1971, pp. 1351–1366.
- 9 Nellis, G., and Klein, S., "Heat Exchangers," *Heat Transfer*, 2009, p. 857.
- 10 Thermacore, "Heat pipe and thermal management solutions, Thermacore," *Thermacore.com* Available: <http://www.thermacore.com/thermal-basics/heat-pipe-technology.aspx>.
- 11 Yuan, Z. G., and Kleinhenz, J. E., "Gas Phase Pressure Effects on the Apparent Thermal Conductivity of JSC-1A Lunar Regolith Simulant," *41st International Conference on Environmental Systems*, 2011, pp. 1750–1757.
- 12 Deissler, R. G., and Boegli, J. S., "An Investigation of Effective Thermal Conductivities of Powders in Various Gases," *Transactions of American Society of Mechanical Engineers*, vol. 81, 1958, pp. 1417–1425.
- 13 Fan, L. S., and Zhu, C., "Ch.5. Basic Equations," *Principles of Gas Solid Flow*, 1997, p. 224.
- 14 Nellis, G., and Klein, S., "Ch. 5. Internal Forced Convection," *Heat Transfer*, 2009, p. 686.
- 15 Lieberman, M. A., and Lichtenberg, A. J., "Ch. 14. Direct Current (DC) Discharges," *Principles of Plasma Discharges and Materials Processing*, 2005, p. 545.

Human Factor Analysis of Light Emitting Diode Technologies for Cabin

Lighting in Manned Space Flight Applications

Todd H. Treichel¹

Orbital Technologies Corporation, Madison, Wisconsin 53717

Advantages of transitioning to Light emitting diode (LED) technologies in spacecraft are reduced mass, reduced occupied volume, reduced power, improved color control, longer operating life, and lower cost associated with power consumption and disposal. According to Brainard et al (2012) newly designed U.S. spacecraft, and ISS fluorescent tube replacements, must utilize LEDs in lieu of traditional artificial light sources to take advantage of technology improvements. Light emitting diode technologies remain a controversial technology in the aerospace industry, where commercial manufacturers are the only source for procurement.

The first portion of this research effort was performed to investigate commercially manufactured LEDs, by measuring light output quality to see if the LEDs will meet NASA and DOD reliability requirements. The second portion of the research pertains to this paper for 2014 which applies to LEDs with the highest reliability from the first portion of the this research. A randomized block design has been constructed for evaluating human factor effects using soft white light, emitted from LEDs and a NASA qualified ISS fluorescent.

Nomenclature

| | |
|----------------|------------------------------------|
| <i>COTS</i> | = commercial off the shelf |
| <i>DOD</i> | = department of defense |
| <i>GLA</i> | = general luminaire assembly |
| <i>HI-REL</i> | = high reliability |
| <i>ISS</i> | = international space station |
| <i>LED</i> | = light emitting diode |
| <i>LUX</i> | = lumens per meter squared |
| <i>MIL</i> | = military |
| <i>ORBITEC</i> | = orbital technologies corporation |
| <i>QML</i> | = qualified manufacturers list |
| <i>QPL</i> | = qualified parts list |
| <i>WSGC</i> | = wisconsin space grant consortium |

¹ Systems Engineer, Space Center, 1212 Fourier Drive, Madison, Wisconsin, USA.
The author acknowledges Wisconsin Space Grant Consortium for making this research possible.

Introduction

Technology in the electronics industry changes rapidly and engineers within the aerospace industry do not always have access to new technology due to high-reliability (HI-REL) requirements established in DOD and NASA procurement standards. Engineers designing for commercial products can experiment with new technologies with little or no restrictions in design component selection. Military and aerospace engineers are required to

manage product designs by making component selections from DOD and NASA approved part lists, where specific components have been tested extensively and heritage field data is cataloged for quality and reliability performance. New electronic technologies are being developed and by the time these technologies become available on a DOD quality parts list (QPL) or quality manufacturer's list (QML), the technology may have been replaced or improved in the commercial markets, thus making it difficult for aerospace engineers to select state-of-the-art design components without extensive testing. In 2013 WSGC member university UW-Madison was instrumental in providing mechanical engineering support where commercial LEDs were extensively tested in accordance with QML and NASA environmental requirements and deemed suitable for use in space flight applications. This paper covers phase two of LED industry/academic partnership for evaluating human factors for habitable spacecraft.

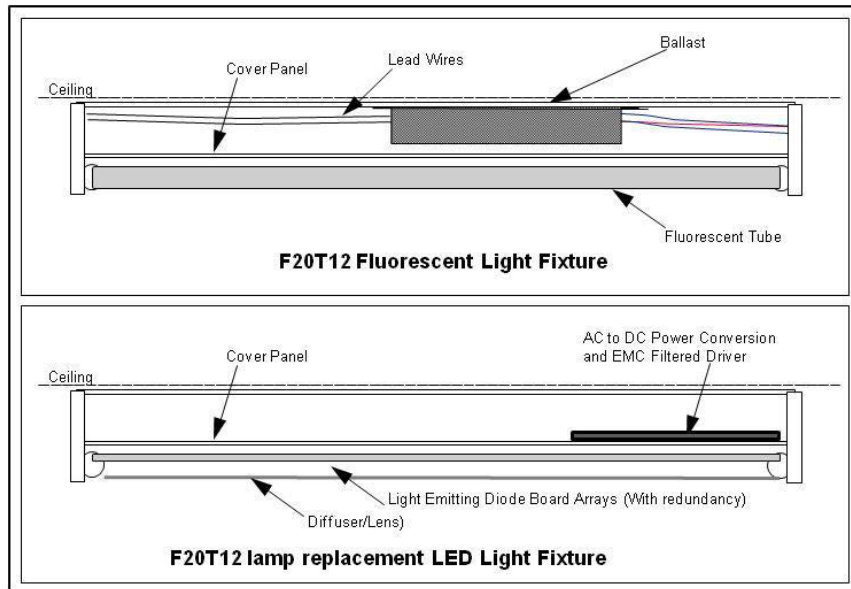


Figure 1. Schematic of fluorescent light replaced with LED technology.

Light Emitting Diodes

Light emitting diodes are semiconductors that convert electrical energy into light energy. The color of the emitted light is designed into a specific semiconductor material composition for each component where individual LEDs may be selected for mixing of colors to obtain a desired color of light output. Light emitting diodes are classified into ultraviolet, visible, and infrared wavelengths depending on the technological application (Lenk & Lenk, 2011). Figure 2 illustrates the broad spectrum of white light critical to the suitability of human habitation in space that relies on 100 percent of artificial light.

Development of high-power LED technology involves challenges for design engineers in that LED lighting devices are subject to high temperatures that must be properly managed. Increased junction temperatures of the LED chip, causes stress on associated material and may cause earlier than expected light output degradation which will lead to an operational failure. Lenk and Lenk (2011) described two primary methods for producing high intensity white-light using LED technology: (1) one is to use individual LEDs that emit the three primary colors of red, green, and

blue, and mix the three colors to produce white light, and (2) is to use a phosphor material to convert monochromatic light from a blue or ultraviolet (UV) LED to broad-spectrum white light. The latter of these two primary LED lighting methods is applicable to the investigation discussed herein (mixing three primary colors of red, green, and blue).

Light emitting diode technology can provide the military and space community with advantages when compared to the current use of incandescent light sources including: (a.) lower power consumption, (b) improved reliability by use of redundancy, (c) improved ruggedness for harsh environments, (d) lighter weight, (e) smaller size, (f) improved control over color and brightness and, (g) faster switching. Figure 1 illustrates the differences between a fluorescent light fixture, commonly used in military applications such as US Navy vessels, and the smaller, and lighter weight LED technology which may be retrofitted into an existing fluorescent light fixture.

Purpose of Investigation

The International Space Station (ISS) contains fluorescent light technologies for illuminating the astronauts' research and living environments. NASA engineers have built a case for replacing fluorescent lighting with LED technology due to advantages such as: (a) lower heat generation, (b) lower power consumption, (c) less weight, (d) greater resistance to damage, (e) less toxic material, (f) elimination of fluorescent tube disposal, and (g) improved reliability. The fluorescent lamp technology on ISS is aging and there is an acceleration of failures which require replacement, due to a deficiency of NASA flight qualified fluorescent units, LED technologies provides an opportunity for retrofitting the ISS with lighting that has improved efficiency, no mercury, and improved reliability (Brainard et al., 2012). Little is known about which commercially available LED components are the most robust in accordance with aerospace requirements. This information will prove useful for future commercial space applications which may include both vehicles and habitable structures.

Howard, LaTasha, and Patrick (2010) revealed that NASA qualified fluorescent lights have failed more than three times the expected failure rate on the ISS. The high failure rate is of major concern to ISS program managers because the quantity of available spares are diminishing to a point where there will not be enough suitable replacements to coincide with the planned life of the ISS (Howard et al., 2010). President Barack Obama announced on January 8, 2014 that the ISS mission life has been extended to 2024 and that a qualified LED lighting source for replacement of existing fluorescents is of high importance. In July 2013 a search of approved parts listings published by NASA and DOD yielded no suitable sources for HI-REL selection of LED products intended for use in space and military applications. Unavailability of qualified LED

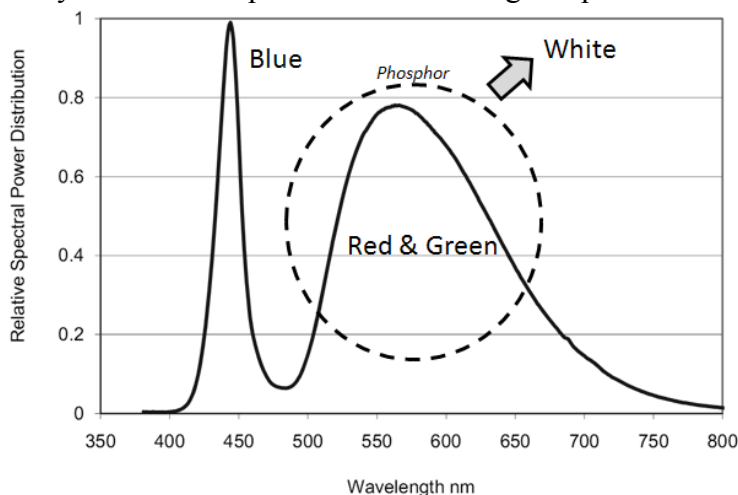


Figure 2. Broad-spectrum white light color distribution model.



Figure 3. Current NASA qualified fluorescent General Luminaire Assembly (GLA) procured for human factors

components prohibits spacecraft designers from utilizing the advantages offered by new technologies for integration into future manned space vehicles and space habitats (Lindenmoyer & Stone, 2010).

The research problem for this study is a government and private aerospace industry problem involving how LEDs cannot replace existing fluorescent lighting in manned space flight vehicles until such technology meets DOD and NASA requirements for manufacturer reliability, color reliability, robustness to environmental test requirements, and degradation effects from operational power, while providing comfortable ambient light free of fatigue, eye strain and/or headache in astronauts (Brainard et al., 2012; Meras et al., 2011). Commercial space designers are required to manage space flight designs in accordance with parts selections made from qualified parts listings approved by DOD and NASA agencies for reliability and safety (Lindenmoyer & Stone, 2010). Barriers for LED implementation involve challenges with aerospace engineers not having DOD or NASA qualified LED components to select from when referencing U.S. government qualified parts lists. Without researching these issues, the benefits of LED lighting including improved color control, longer operating life, lower cost associated with power consumption and disposal cannot be realized (Lenk and Lenk, 2012).

Spacecraft designed for human habitability must include accommodations that involve total human emersion into the habitat for extended periods of time (days and months); where on earth a particular human-habitat can be exited and reentered at random intervals (Hersman & Fowler, 2009). Light emitting diodes are considered an unproven technology in the aerospace industry and require further research and testing (Meras et al., 2011).

The purpose of this quantitative experimental study is to determine to what extent commercial LEDs can suitably meet NASA requirements for manufacturer reliability, color reliability, robustness to environmental test requirements, and degradation effects from operational power, while providing comfortable ambient light free of eyestrain to astronauts in lieu of current fluorescent lighting. Having selected two commercial LED manufacturers, as a result of the 2013 research WSGC grant, the second phase in this 2014 study is in progress and currently testing for human factor effects resulting from LEDs used for habitable task lighting inside a manned spacecraft. The three independent variables are: (a) ISS fluorescent, (b) white LED, and (c) blue LED that diffuses white light. The dependent variable is the overall satisfaction score recorded by human subjects exposed to experimental conditions. A randomized block design, as described by Montgomery (2013), shall be employed to test human factor effects of soft white light, created from LEDs (white light from white LEDs or blue LED light converted to white light) and a NASA qualified ISS fluorescent (see Figure 3Error! Reference source not found.), on human subjects to test whether white or blue LEDs cause retinal fatigue and eye strain. A total of 18 human subjects are planned for a laboratory experiment exposing each subject to experimental conditions, simulating space vehicle use. Participants are presently being recruited from University of Wisconsin - Madison, University of Wisconsin -Platteville, University of Wisconsin - Milwaukee, and other

WSGC affiliate institutions of higher learning. Data from this study will be used to assign LEDs a NASA TRL rating for technology readiness quantification that may be used by commercial and government personnel when designing space flight vehicles.

This WSGC 2014 research is in progress at the time of the publishing of this paper. Human subjects are currently being subjected to two hours of uninterrupted exposure to either fluorescent or LED light sources. The researcher has randomized the test conditions and is currently asking human subjects to perform that involves detailed assembly using detailed instructions that involve discernment of colors. Upon completion of the test duration the test subjects are asked to fill out a survey about their experience. Lighting factors tested in the human experiment are human response to existing fluorescent light technology used on the ISS and two LED technologies selected from a factorial experimental design. The LED technology for white light and blue light are used to represent the highest reliability for each of the two colors. Figure 4 illustrates three lighting conditions administered in the quality of light survey (using LEDs characterized from the results of the 2013 WSGC grant research effort) where the same human subjects will be exposed to the three factors for two hours each.

Table 1. Completely randomized block design showing random order of participants and factors.

| Human Subject | Factor Setting | | |
|---------------|----------------|---|---|
| | A | B | C |
| a | 1 | 3 | 6 |
| b | 4 | 2 | 9 |
| c | 7 | 8 | 5 |

Table 1 illustrates a randomized block design containing randomized numbers in each cell to show an example of run order. Experimental blocks are A, B, and C where each human subject is exposed to each factor at some point in the experiment. The design is replicated four times using three different human subjects during each experimental replication. To assure research validity and reliability, each human subject is exposed to each factor on different test days (where possible)

to remove bias from potential fatigue, boredom, and other unintended influences caused by continuous exposure to the designated test environment. A ground based capsule has been constructed (simulating the Boeing CST-100 capsule) for the purpose of maintaining a

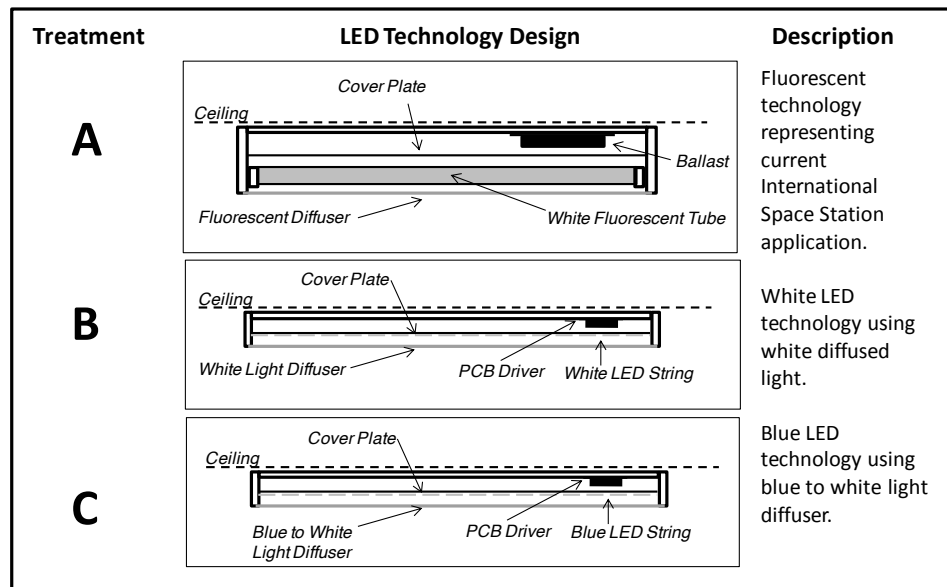


Figure 4. Schematic of fluorescent and LED experimental factors.

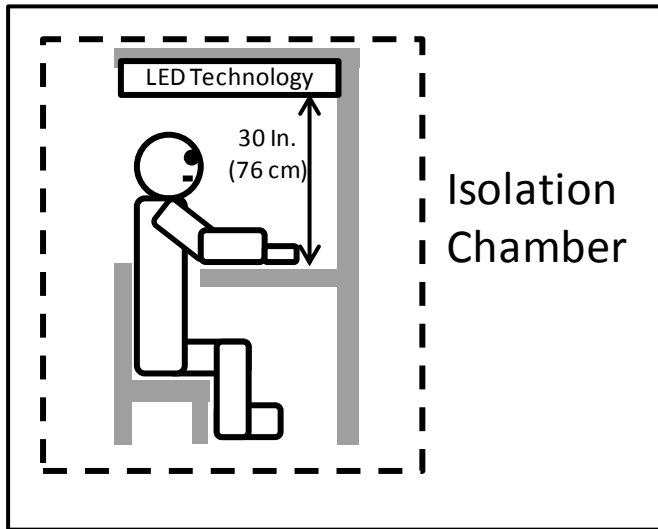


Figure 5. Schematic of isolation chamber for testing fluorescent and LED experimental factors.

of actual component or system in a space environment (Mankins, 2009). The space environment may be achieved through laboratory testing which is represented in this analysis by subjecting LED technologies to NASA specified environmental stresses as an experimental factor. This research will examine the suitability of commercial LEDs for human space flight use in accordance with a technology readiness level of seven. Level seven TRL is a NASA rating achieved by successfully demonstrating that new technology suitably meets intended function while being subjected to rigors of the space flight environment (Mankins, 2009). This project will examine needed research in a literature gap in evaluating the unknown effects of LED lighting that may be adverse to astronaut long term living in a space habitat reliant on 100% artificial light.

consistent and relevant test environment that reduces any potential for introducing experimental bias across all human subjects.

The problem addressed by this research is that LED technologies remain a controversial technology in the aerospace industry, where commercial manufacturers are the only source for procurement. Aerospace engineers tasked with design and development activities of space flight hardware, will be required to manage to the NASA technology readiness level (TRL) system (Yiyuan et. al, 2011). A TRL level seven is achieved with successful demonstration



Figure 6. Ground based isolation chamber for testing fluorescent and LED experimental factors.

Conclusion

The problem addressed by this research is that LED technologies remain a controversial technology in the aerospace industry, where commercial manufacturers are the only source for procurement. Aerospace engineers tasked with design and development activities of space flight hardware, will be required to manage to the NASA technology readiness level (TRL) system (Yiyuan et. al, 2011). A TRL level seven is achieved with successful demonstration of actual component or system in a space environment (Mankins, 2009). The space environment may be achieved through laboratory testing which is represented in this analysis by subjecting LED technologies to NASA specified environmental stresses as an experimental factor. This research will examine the suitability of commercial LEDs for human space flight use in accordance with a technology readiness level of seven. Level seven TRL is a NASA rating achieved by successfully demonstrating that new technology suitably meets intended function while being subjected to rigors of the space flight environment (Mankins, 2009). This project is currently in the process of examining needed research in a literature gap in evaluating the unknown effects of LED lighting that may be adverse to astronaut long term living in a space habitat reliant on 100% artificial light.

Cohen et. al (2011) stated that a robust LED system does no good to the user if the selected technology creates glare, resulting in unwanted eye strain and other effects which are undesirable for task lighting purposes when applied to a human user environment. This research will investigate selected LED technology and the effects on human subjects which support a business decision to use or not to use LED technology on future manned space flight applications. Research results will assist design engineers in making informed decisions about component selection in accordance with mission goals for safety, reliability, and compliance with human factor requirements. This research is empirically risky in that there may be an unexpected hypotheses result where the current ISS fluorescent light may be recommended as the better choice for astronaut health. A final publication of research findings will be presented at the WSGC 2015 Space Conference.



Figure 7. Joe Klopotic from WSGC member institution University of Wisconsin - Madison.

Acknowledgement

The author would like to thank the Wisconsin Space Grant Consortium for their support of this academic partnership and recognize the University of Wisconsin –Madison and mechanical engineering student Joe Klopotic (see Figure 7) who was instrumental in configuring the LED test prototypes and was offered full time employment at Orbital Technologies Corporation in Madison, Wisconsin. Mr. Klopotic is currently employed at ORBITEC as a mechanical engineer as a result of this research effort.

References

- Brainard, G. C., Coyle, W., Ayers, M., Kemp, J., Warfield, B., Maida, J., Bowen, C., Bernecker, C., Lockley, S. W., & Hanifin, J. P. (2012, April). Solid-state lighting for the international space station: tests of visual performance and melatonin regulation. *Acta Astronautica*. doi:10.1016/j.actaastro.2012.04.019
- Cohen, F. B., Martinsons, C., Vienot, F., Zissis, G., Barlier, S. A., Cesarinin, J. P., Enouf, O., Garcia, M., Picaud, S., & Attia, D. (2011, July). Light emitting diodes for domestic lighting: any risks for the eye? *Progress in Retinal and Eye Research*, 30 (4), 239-257. doi:10.1016/j.preteyeres.2011.04.002
- Hersman, C. & Fowler, K. (2009, October). Best practices in spacecraft development. *Mission Critical and Safety Critical Systems*. 1 (3), 269-460. doi:10.1016/B978-0-7506-8567-2.00005-6
- Howard, R. L., LaTasha, T., & Patrick, J. (2010, July). Manned pressurized rover lighting. *Earth and Space*, 1-8. doi: 10.1061/40830(188)122
- Jiank, H., Rodngues, L. F., Bell, S., Kortenkamp, D., & Capristan, F. (2011, April). Prediction of reliability for environmental control and life support systems. *Journal of Spacecraft and Rockets*, 48 (2), 336 – 345. doi:10.2514/1.44792
- Lindenmoyer, A., & Stone, D. (2010, April). Status of NASA's commercial cargo and crew transportation initiative. *Acta Astronautica*, 66(6), 788-791. doi:10.1016/j.actaastro.2009.08.031
- Lenk, R., & Lenk, C. (2011), *Practical lighting design with leds*. Hoboken, NJ: John Wiley and Sons, Inc.
- Mankins, J. C. (2009, December). Technology readiness assessments in retrospective. *Acta Astronautica*, 65(10), 1216-1223. doi:10.1016/j.actaastro.2009.03.058
- Meras, P., Cooper, M., Dillon, R. P., Forouhar, S., Gontijo, I., Liebe, C. C., & Shapiro, A. (2011, March). Qualification and selection of flight diode lasers for the NUSTAR space mission. *IEEE Xplore*, 1-11. doi:10.1109/AERO.2011.5747388
- Yiyuan, Z., Tangwen, Y, Dayong, D., & Shan, F. (2011, November). Using tlx to evaluate the flight deck design in design phase of aircraft. *Procedia Engineering*, 17(4), 77-83. doi:10.1016/j.proeng.2011.10.010

24th Annual Wisconsin Space Conference

PART THREE

Biosciences and Geosciences

“Hands-on” Remote Sensing of Physical Models in Exploration of Surficial Processes¹

Jeffrey J. Clark

Department of Geology
Lawrence University

Abstract

The goal of this work is to create an interactive, data-rich learning environment that will enhance student understanding of remote sensing principles and surficial processes. In service of this goal a data acquisition system consisting of common consumer electronics (e.g. a digital camera and Microsoft Kinect) was used to monitor temporal and spatial changes in a scale model of a fluvial setting. Analysis of these data allows students to track landform evolution in response to changing inputs and boundary conditions. These scale-model observations of surficial processes can be also compared to full-scale planetary landscapes.

Introduction

A common way of engaging students with the sciences in the laboratory setting is through experimentation. But experimentation is challenging in the earth sciences because the temporal and spatial scales involved make direct observation of many geological processes problematic. Physical models, however, allow us to greatly compress the temporal and spatial scales, make direct observations, visualize processes, and control the inputs and boundary conditions allowing us to create “what if” scenarios. The advent of inexpensive data acquisition instruments such as digital cameras and the Microsoft Kinect™ allow us to easily and inexpensively take frequent detailed measurements of these models. Moreover, the familiarity of these everyday consumer electronic devices provides a bridge to discussion of applications of the more sophisticated space-based remote sensing assets monitoring Earth and other planets.

Remotely sensed data is ubiquitous in the technologically-based world we live. We encounter remotely sensed data on the news in the form of satellite imagery of clouds and water vapor, we use digital maps and imagery our smart phones to find restaurants, and we can now view the entire surface of Mars using Google Earth™. However, few people realize where these data come from and how it is processed for our use. Another goal of this work therefore is to familiarize students with the principles of remote sensing by having them collect and analyze their own data.

The laboratory activities based on the use of remote sensing of physical models and of planetary surfaces described below provide a dynamic and exciting learning environment, which is vital for engaging the student scientist and developing scientific habits of mind. Data-rich environments like those developed here establish a context for exploration, and require students to quantify observations, propose explanations, test ideas, and communicate their results (AAAS, 1989; NRC, 1997). The open-ended research questions enabled through investigation of physical models also hone critical thinking skills and motivate students to take ownership of the material

¹ Funding provided by NASA’s Higher Education Program and distributed through the Wisconsin Space Grant Consortium. Additional funding provided by the Lawrence University Excellence in Science Fund.

(AGU, 1997). At its best, participation in discovery-based laboratory exercises enhances the students' ability to relate to, analyze, and understand real world data and processes they are investigating (Boyer Commission, 1998). These student experiences are essential as we train the next generation of scientists and a technologically literate work force.

Work on this project began in the summer of 2013 and continued throughout the 2013-14 academic year. The modeling environment and data acquisition system was developed over the summer and laboratory activities and quantitative exercises were developed for two courses offered during the academic year. The sections below describe these activities in detail.

Modeling Environment and 2013 Summer Work (4 students)

We used a 2.5 meter-long, 1.2 meter-wide and 0.20 meter-deep soapstone table as the base of the flume. The table can be tilted to slopes of ~5% (Figure 1). Water is supplied to a constant head

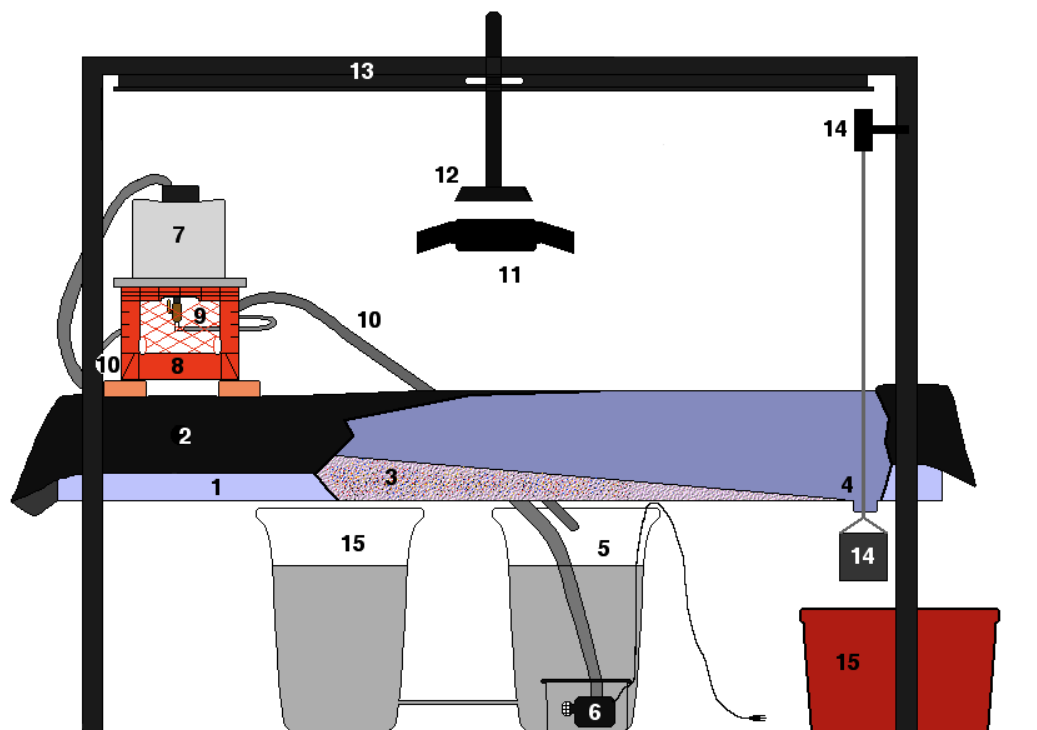


Figure 1 – Schematic diagram of flume components.

- 1 Flume base – soapstone.
- 2 Impermeable liner over flume base
- 3 Ground plastic “sediment” on top of liner
- 4 Drain and weir
- 5 Reservoir: holds water to be circulated through the system
- 6 550gph pump inside filter box
- 7 Constant Head Tank
- 8 Constant Head Tank Stand (2x4s and milk crate)
- 9 Valve at base of head tank to control discharge to flume.
- 10 Discharge Tube, Dispersion Mechanism, and Overflow Tube
- 11 Lighting: 2X3000W-equivalent LED arrays
- 12 Kinect and DSLR
- 13 2” circular steel pipe frame supports soapstone and used to mount instrumentation
- 14 Sediment Weigh Mechanism (Load cell, chain, and sieve)
- 15 Additional reservoirs

tank via a 550gph pump. The water drains to the back to pump reservoir for recirculation. The sediment in the flume consists of ground thermoset plastic (Figure 2). This is a durable material that has two distinct advantages over quartz/feldspathic sands. The first is that it has a specific gravity of 1.55. The lower density (~ 58% of quartz) means that it will move more easily. The other advantage is that the plastic is color-coded by size, which means that we can use digital color photography and image processing to quickly determine the surface composition. The data acquisition system consists of a Microsoft Kinect™ which is used to take 3-D images and a 20MP digital color camera (DSLR) which is used for color photography and provides the images for textural analysis. An 8” diameter by 8” deep circular sieve with a mesh size of 0.074 mm collects the sediment that passes out the drain. The sieve is suspended by a chain and connected to a data-logging load cell which allows us to track sediment evacuation from the system over time. The collected sediment can be mechanically sorted and the size distribution of bulk transport can be determined.

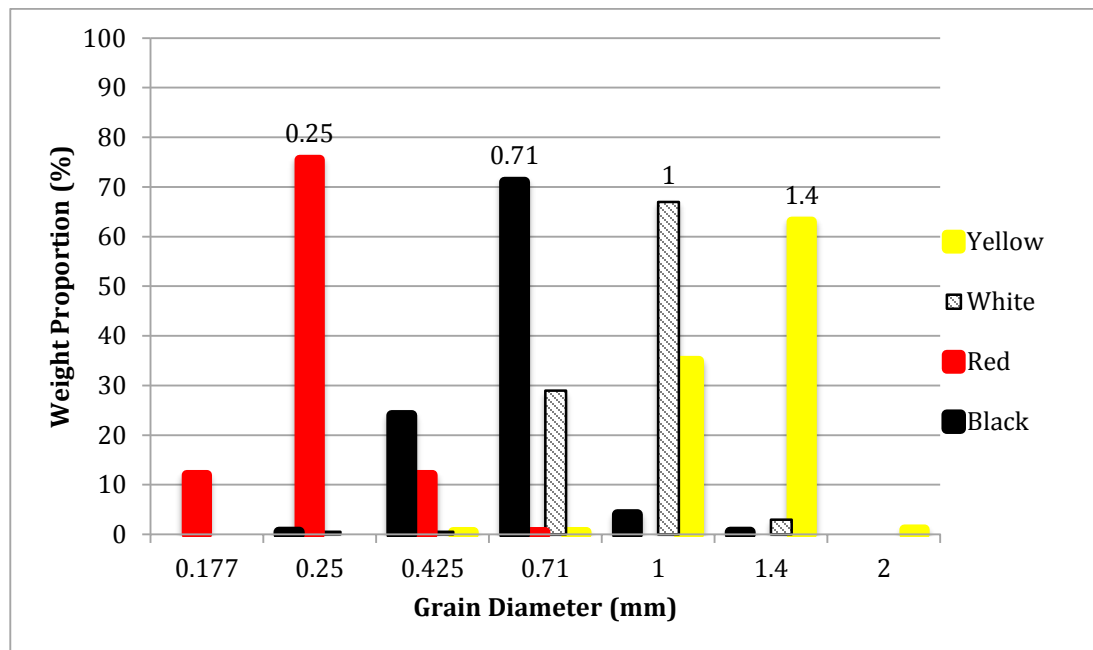


Figure 2. Sediment size distribution of colored sediment.

In the summer of 2013, a team of four students worked to develop a modeling environment which could be used to simulate fluvial processes. One student designed and built the constant head tank to control the input of water and calibrated the force gage to record sediment flux. Another was responsible for developing protocols to turn the color digital photography into texture maps based on sediment color. A custom data acquisition program was developed by another student to tap the Kinect’s data stream and to set intervals to record and time stamp data using protocols outlined by Mankoff and Russo, 2012. The fourth student measured planform metrics of terrestrial and Martian alluvial meanders such as wavelength, width, and radius of curvature and developed curves for comparative purposes (Figure 3). At the summer’s end these efforts were compiled into a user manual for the flume and a protocol was developed for efficient and inexpensive processing and analysis of the data. The following activities were developed.

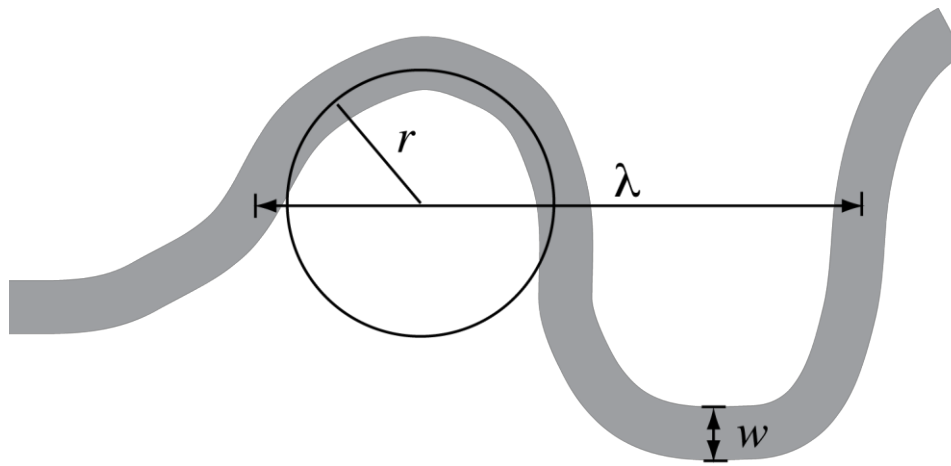


Figure 3. Schematic diagram of meander metrics measured. Where w is the channel width at bankfull, λ is the wavelength and r is the radius of curvature. Image from Richeson.

Course Activities

Several activities were built around the concepts of using hands-on remote sensing techniques as an inroad to exploration of space-based remote sensing and on comparing surficial processes on Mars and Earth. The activities were incorporated into two courses as described in the following sections.

Course 1: GEOL 360 – Earth Surface Processes (12 students)

Two labs have been developed for this course related to this project. The first involves comparing meander characteristics (Figure 3) from aerial imagery of Earth and Mars. We used the measurement tools in ArcGIS (ESRI, 2011) for our work, but it could have easily been done in GoogleEarth or any location aware image processing program. The advantage of ArcGIS is that terrestrial imagery can be accessed easily via ArcGIS Online (www.arcgis.com/home/) and spatially referenced Martian imagery from the university of Arizona's HiView application (www.uahirise.org/hiview) can be downloaded. (The resolution of imagery in GoogleEarth – Mars is too coarse for analysis of smaller channels.) Previous work on terrestrial streams has shown strong correlations between meander wavelength (λ) and channel width (w), and meander wavelength and radius of curvature (r) (Leopold and Wolman, 1960 and Williams, 1986). Martian channels also exhibit strongly correlated relationships between these metrics, though there are a few caveats to keep in mind. Martian meanders, for example, are relict features and true channel widths of alluvial channels on Mars are unknown because the floodplains have been eroded away by wind leaving the coarser channel beds in relief (Pain and Ollier, 1995). Nonetheless students can compare the terrestrial metrics and correlations with those of Martian channels and speculate on past Martian climate and environment.

In the second lab activity students simulate sediment transport dynamics and resultant landform evolution in response to changing input conditions. Stream systems will change in response to changes in base level, valley slope, or the supply of water and sediment to the reach. The changes in input variables, in turn are caused by larger drivers such as regional tectonics and climate change. The modeling system developed here is highly adaptable allowing us to simulate changes from any of these drivers. For example, increasing the weir height will simulate a rise in base level, which can be driven by subsidence, normal faulting, or eustatic adjustment due to climate

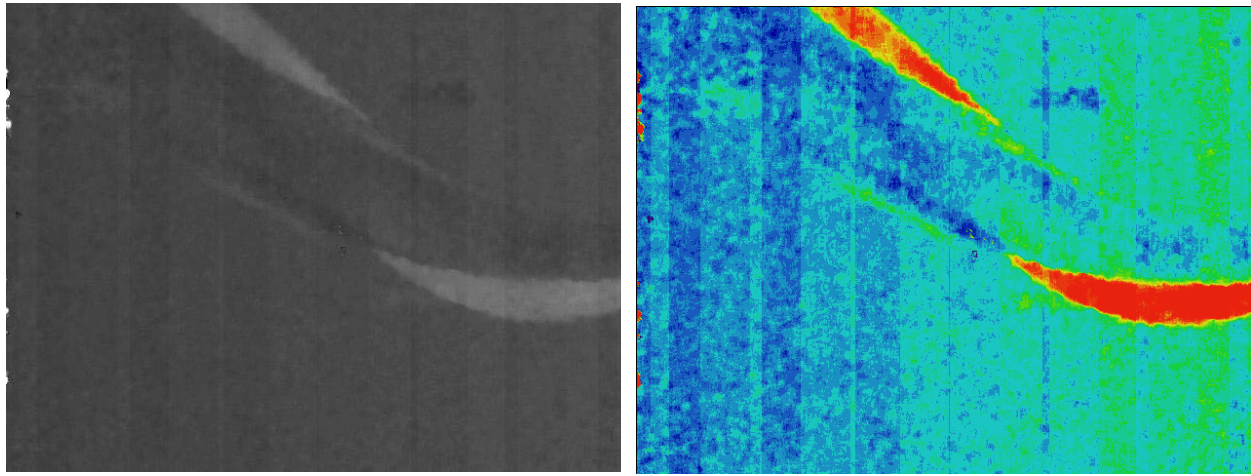


Figure 5 – Time differenced image showing areas of erosion at cutbanks shown as white regions in the grey scale map to the left and orange-red in the heat-map image to the right.

The color digital camera images are in a raster format called a Portable Pixel Map (ppm). We use the 20MP camera rather than the color image from the Kinect because the red and black grains are not visible in the 640X480 Kinect image. The images can be viewed and analyzed in FIJI and a FIJI plug in called “Weka Segmentation” (Hall and others, 2009) allows us to classify the image based on color (Figure 6). From these classified images we can determine the proportion of each color that makes up the surface of an area of interest. The ability to track surface textural changes over time combined with areas of erosion and deposition allows the students to see how erosion may leave behind coarse material and how material fines on the inner portion of the meander bends. These are observations they can also make in the field, but using the model allows them to see the sorting develop, whereas in the field we can only see the results of the sorting.

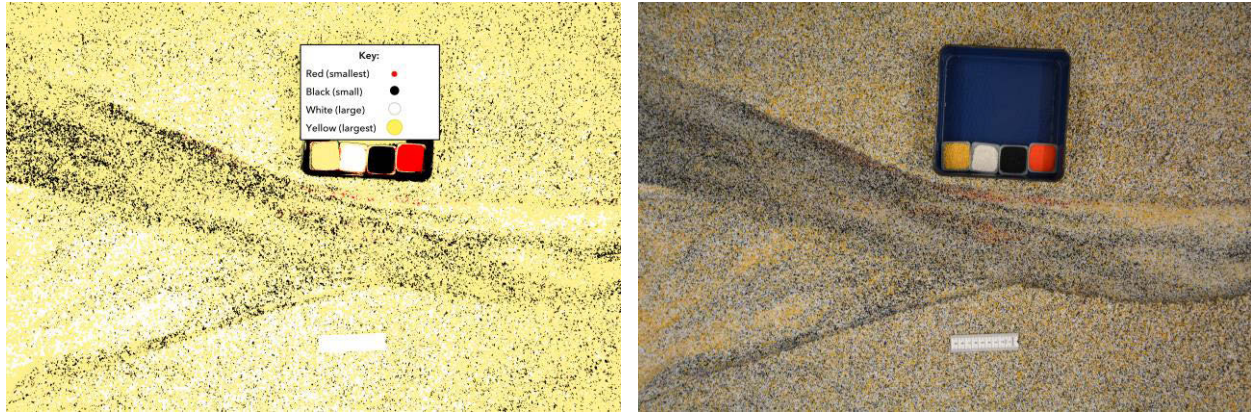


Figure 6 – Classified image of color sediment (left) and original color image (right). The classified image is used to calculate the proportion of area covered by each size class (color) of sediment. Reference samples of each color and a millimeter scale are included in each image.

At its core, the Weka Segmentation is a supervised classification routine where the user selects areas of known composition tells the computer what they are e.g. “forest”, “cornfield”, or in our case “red sediment”. Then the computer uses algorithms to sort each pixel into one of the user-selected categories (e.g. red, white, black, yellow). Though we have the capabilities of developing robust statistics on the quality of the classification, this is beyond the scope of this particular

course, so we use a visual trial and error iteration to get most of the target pixels classified correctly.

Course 2: GEOL 220 - Remote Sensing and GIS (12 students)

Any introductory textbook on remote sensing will include a discussion of system parameters or resolutions (e.g. spatial, temporal, radiometric and spectral) as well as system operational characteristics (active or passive, scanning or framing). To reinforce these concepts and to understand the tradeoffs among them we use the Kinect and a digital camera as examples of remote sensing instruments. The Kinect, for example, is an active framing system. However, it does not use time of flight to measure distance like conventional RADAR and LiDAR. For each instrument the students develop a spec sheet and compare them to the operations page of space-based assets (for example see the HiRISE specs - www.uahirise.org/teknikos.php). Comparisons of the cameras from the Viking orbiters give students a new appreciation for how far technology has come. Students also take the system specs (e.g. CCD array size and focal length) from the DSLR and determine the spatial resolution of a pixel at a known distance. Then they are asked to evaluate how the field of view and resolution change as the focal length changes. They can verify their calculations by simply looking at the live field of view and importing the images into image processing/viewing software such as FIJI (Schindelin and others, 2012) or ArcGIS (ESRI, 2011). This exercise drives home the trade-off between spatial resolution and field of view.

Students are also engaged with important image processing techniques as they analyze the data taken from the Kinect and DSLR. The raw data has several artifacts such as infrared shadow and striping (for example Figure 5) which need to be removed through the application of various filters before analysis. Students rarely encounter such errors when browsing remotely sensed imagery because those images have already been corrected, so this gives them first hand experience with what happens behind the scenes. It is also an opportunity to explore the effects of different filters and to think about which one is best for vertically oriented artifacts. Students then need to calibrate the vertical and horizontal scales and classify the images using the Weka Segmentation procedure already described (e.g Figure 6). These are authentic image processing techniques that are made relevant because the students took their own data using devices.

These activities are metered out over several class periods and feedback is provided. Additionally we make frequent reference to these exercises as we discuss the design and application of remote sensing platforms such as MODIS and HiRISE. As part of a final exam students are given a problem that asks them to determine a) if the Kinect can resolve the red sediment grains (mean diameter = 0.25mm) and b) the optimal height from which to hang the digital camera to provide maximal coverage of the model flume while still being able to resolve the finest, red particles. Both of these questions require application of concepts learned earlier in the course and demonstrate mastery of the material.

Learning Outcomes

Due to our small sample sets (n=24), and lack of a control group we rely on authentic assessment techniques to evaluate the effectiveness of our learning outcomes. Below each goal is discussed.

It is surprising considering the number of technologically savvy students, how few understand the fundamental constraints and uses of remotely sensed data. It is perhaps even more surprising that

students in spatially dependent fields such as geology and environmental science are little better informed. Although one of the primary goals of this project was to introduce students in traditionally field-based disciplines to applications of remote sensing, this project far exceeded my expectations. The main benefit came from using common consumer electronic devices and casting them as remote sensing instruments. For example students were excited to learn how their digital cameras work and this motivated them to persevere through fairly complex problems - such as optimizing our remote sensing system and quantifying topographic changes in the model.

The comprised of the physical model and novel remote sensing system required students to engage directly with data collection, data reduction, and data analysis – all with goal of better understanding surficial processes. Although no quantitative data was collected to show improved quantitative reasoning, working through the problems and labs themselves was excellent practice. And students demonstrated ability to apply concepts learned both within and across courses. For example, students in the surficial processes class were asked to apply a new sediment transport law (aeolian rather than fluvial) to a new environment – Mars. Completing this problem requires that students understand the fundamental driving forces and how they differ in the two environments. By and large students did well on this problem. However, the most exciting gains were those by the students who took both courses.

The three students who took both courses benefitted the most because the each course used the technology in a different way and with different goals. In remote sensing, the main goal was learning the technology and the techniques, whereas in the surficial processes course the instrumentation was secondary and study of the processes was primary. Students who had remote sensing first were able to apply what they had learned and carry it over to the surface processes class. The most gratifying thing was that they also eagerly assisted other students with the analysis of terrestrial and model landforms. This ‘accidental’ peer teaching was very effective and generated additional interest in the remote sensing course. Likewise remote sensing students became interested in surficial processes and physical modeling, so much so that a special topics course on physical modeling was created and will be offered in the 2014-15 academic year.

Future Work

Though this work was successful, the image processing activities in the surficial processes class took much longer than anticipated. As a result we didn’t have time to introduce a similar module on mass wasting. Rather that material was covered in the field and classroom. However, there is potential to reconfigure the class to run with two labs a week, which would allow enough time to expand the hill slope processes portion of the class and to incorporate modeling activities and remote sensing data. If time resources allow, the course will be offered as a double lab in 2015-16. I am also exploring with a colleague developing a version of the river modeling labs that would be appropriate for introductory geology. This will entail substantially simplifying the data processing so that students can focus on the processes demonstrated rather than image correction protocols.

References

American Association for the Advancement of Science (AAAS), 1989, Project 2061, Science for all Americans,

AAAS Press, Washington, DC.

American Geophysical Union (AGU), 1997, Shaping the future of undergraduate earth science education: Innovation and change using an earth system approach, Washington, DC.

The Boyer Commission on Educating Undergraduates in the Research University, 1998, Reinventing Undergraduate Education: A Blueprint for America's Research Universities, Carnegie Foundation for the Advancement of Teaching, Princeton, NJ.

ESRI (Environmental Systems Resource Institute). 2011. ArcMap 10.1. ESRI, Redlands, California.

Hall, M., Frank, E., Holmes, G., Pfahringer, B., Reutemann, P., and Witten, I., 2009, The WEKA Data Mining Software: An Update, SIGKDD Explorations 11(1).

Leopold, L.B., and Wolman, M. G., 1960, River Meanders, Bulletin of the Geological Society of America, 71:769-794.

Mankoff, K. D., and Russo, T. A., 2012, The Kinect: A low-cost, high-resolution, short-range 3D camera, Earth Surface Processes and Landforms Online. 11p.

National Research Council (NRC), 1997, Science Teaching Reconsidered: A Handbook Committee on Undergraduate Science Education, National Academy Press, Washington, DC.

Pain, C.F., and C.D. Ollier, 1995, Inversion of relief - a component of landscape evolution, . Geomorphology, 12(2):151-165.

Richeson, D., (<http://divisbyzero.files.wordpress.com/2009/11/meander.png>), accessed 7/29/2014.

Schindelin, J., Arganda-Carreras, I., Frise, E., Kaynig, V., Longair, M., Pietzsch, T., Preibisch, S., Rueden, C., Saalfeld, S., Schmid, B., Tinevez, J., White, D., Hartenstein, V., Eliceiri, K., Tomancak P., and Cardona, A., 2012, Fiji: an open-source platform for biological-image analysis, Nature Methods 9(7): 676-682.

Williams, G. P., 1986, River Meanders and Channel Size, Journal of Hydrology, 88:147-164.

Assessment of Ecosystem Photosynthetic Parameters along Two California Climate Gradients

Sean DuBois¹

University of Wisconsin – Madison, Nelson Institute for Environmental Studies

Abstract: Improving coupled Earth system models of current and future climate requires robust observations that accurately provide parameters and observations for evaluation across spatial scales relevant for the model. Photosynthetic parameters $V_{c_{max}}$ and J_{max} help to characterize the ability of vegetation to assimilate carbon, a required parameter in most land surface modules of climate models. Remote sensing, flux tower data, and field measurements were collected to develop a methodology to estimate the variability in these parameters across diverse landscapes in Southern California and the Sierras, regions experiencing prolonged drought which is expected to become more common in the future. $V_{c_{max}}$ maps were generated with NASA hyperspectral airborne AVIRIS imagery by scaling up leaf level measurements to the canopy and evaluated using flux tower data for nine sites across California. These maps illustrate the expected temporal and spatial changes in the parameter. However, $V_{c_{max}}$ estimated from inverse modeling of flux tower data did not fall in the range found in field measurements. The methods developed in this study expand the applicability of imaging spectroscopy in estimating ecosystem metabolism.

Introduction

Increases in atmospheric carbon dioxide are well documented in the past century (Hofmann et al., 2006) and the resulting change in regional climates are predicted to have impacts on local vegetation, especially for Mediterranean climate systems, through changes in precipitation (Breshears et al., 2005). Vegetation shifts resulting from a changing climate have already been quantified in California (Kelly & Goulden, 2008). Meanwhile, there is a need to provide higher accuracy and increased spatial resolution data to models in order to better estimate ecosystem parameters during times of increased vegetative stress (Vargas et al., 2013). Significant uncertainty exists in our ability to model global photosynthesis and its sensitivity to future climate change.

Recent work by Serbin et al (2012) has indicated strong evidence for the ability to use hyperspectral imaging collected from high altitude airborne missions to detect photosynthetic rates. Spectroscopy was used to predict leaf metabolic properties $V_{c_{max}}$, the maximum rate of carboxylation of the enzyme RuBisCO, and J_{max} , the maximum rate of electron transport necessary to regenerate the RuBP, across ecosystems. A robust relationship between spectra and leaf was developed that is applicable to a wide range of environmental conditions and vegetation types. However, there lacks systematic observations for how leaf level photosynthetic rate constants vary with time and how they scale from leaf to canopy.

Our research in this project assessed the potential to make spatially explicit estimates of $V_{c_{max}}$ and J_{max} from remote sensing that can be scaled to predict seasonal canopy assimilation across large

¹I would like to acknowledge the WSGC Graduate Fellowship for the financial assistance which allowed me to conduct this research. Additional financial and technical support was provided by the Nelson Institute for Environmental Studies, and ASD inc/ PANalytical Boulder. I also want to thank Ankur Desai (UW-Madison), Phil Townsend (UW-Madison), Shawn Serbin (Brookhaven National Lab) and Andrew Jablonski (UW-Madison) for their contributions to this project.

areas. These two traits are used to predict photosynthetic capacity using an often employed biochemical model (Farquhar et al., 1980; Farquhar and von Caemmerer, 1982). Field measurements were made to calibrate concurrently collected remote sensing images. Eddy covariance flux tower data – a widely used method to measure ecosystem carbon, water and energy fluxes (Baldocchi and Meyers, 1998) – were used to evaluate the scaling up of leaf level estimates to the canopy. Understanding the spatial variability in these traits will allow for more robust model inputs and thus predictive capacity. The principle objectives of this project were to make maps illustrating the spatial and temporal variations in $V_{c_{max}}$ across a wide range of vegetation, and to evaluate these models using data collected from flux towers located in these ecosystems. This report summarizes research conducted under partial support of the WSGC Grad fellowship. The fellowship allowed for the study of annual variation in the flux data, including the drought signal, and presentation of these findings to an international audience at the Global Land Project Meeting in Berlin, Germany.

Methods

Site descriptions. The flux tower sites used in this study comprise two climate gradients, one located in southern California (transecting the San Jacinto Mountains) and the other in central California (rising from the San Joaquin Valley into the Sierra Nevada Mountains). The use of sites located along these climate gradients allows for numerous ecosystem types to be studied in relatively close space, ensuring the results from this study to be applicable and replicable in other regions.

The southern California climate gradient covers the vegetation types grassland, coastal sagebrush, and an oak-pine forest on the western slope of the San Jacinto Mountains, and pinyon-juniper woodland, chaparral scrubland and desert scrub located on the eastern slope (Kelly & Goulden, 2008). The Sierra climate gradient is comprised of the three sites oak/pine woodland, ponderosa pine forest, and mixed conifer forest (figure 1).

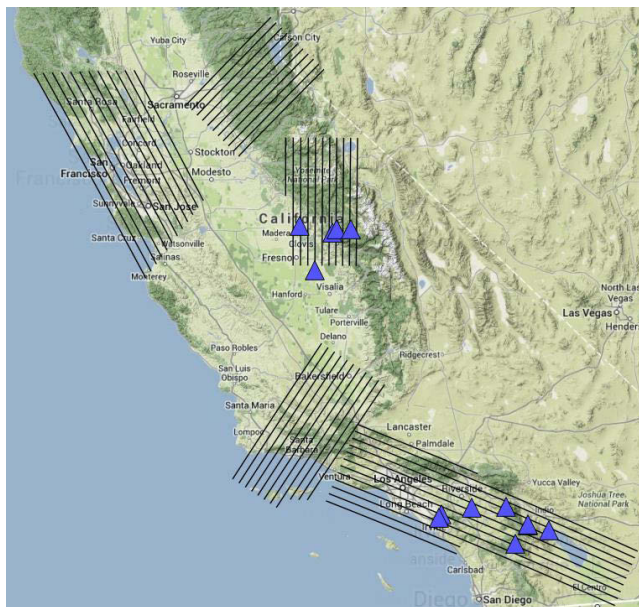


Figure 1: Location of the core study sites found within the five HypSPIRI campaign flight boxes. The southern sites comprise the southern California climate gradient, while the northern lie along the Sierra gradient.

woodland, chaparral scrubland and desert scrub located on the eastern slope (Kelly & Goulden, 2008). The Sierra climate gradient is comprised of the three sites oak/pine woodland, ponderosa pine forest, and mixed conifer forest (figure 1).

Remote sensing collection. The two climate gradients used in the study were flown by the NASA high altitude E-2 aircraft collecting imaging spectroscopy and thermal imagery using the AVIRIS (Airborne Visible/Infrared Imaging Spectrometer) and MASTER (MODIS/ Advanced Spaceborne Thermal Emission and Reflection Radiometer Airborne Simulator) sensors (see figure 1). Flights were conducted at least once a season and timed to capture maximum variation in the ecosystems (figure 2). NASA provided processed

reflectance imagery which were topographically corrected and corrected for bidirectional reflectance distribution function. AVIRIS has a spectral resolution of around 10 nm and covers the electromagnetic range of 414–2447 nm. Using a partial least-squares regression (PLSR) modeling approach similar to Serbin et al. (2014), maps of $V_{c_{max}}$ were generated for the areas around each flux tower (see figure 3).

In conjunction with the airborne measurements, ground-based measurements of canopy LAI and clumping, leaf reflectance, temperature, nutrient status, stomatal conductance, and photosynthetic CO₂-response were conducted at two southern sites and 3 Sierra sites in the spring and summer of both 2013 and 2014. These field measurements were designed to collect data for the calibration of remote sensing products. The field measurements coincided with AVIRIS and MASTER overflights.

Flux Data Collection. Eddy covariance flux tower compute net ecosystem exchange (NEE) of trace gases, energy and momentum based on the turbulent conservation equation for fluids (Baldocchi and Meyers, 1998). NEE can be computed from high-frequency (> 10 Hz) covariation of vertical wind and tracers on towers, collected using the methods and instruments described in Goulden et al. (2012). NEE observations were aggregated into half hourly estimates, as were other meteorological parameters including air temperature and solar flux.

Collection of eddy covariance data on sloped terrain presents issues due to potential vertical movement of air via cold air drainage instead of turbulent flow. Our sites, located along an elevational climate gradient and thus sloped terrain, are impacted by this issue and require specific quality control. Filtering of low friction velocities (u^*) was performed to remove data collected during periods of low turbulence.

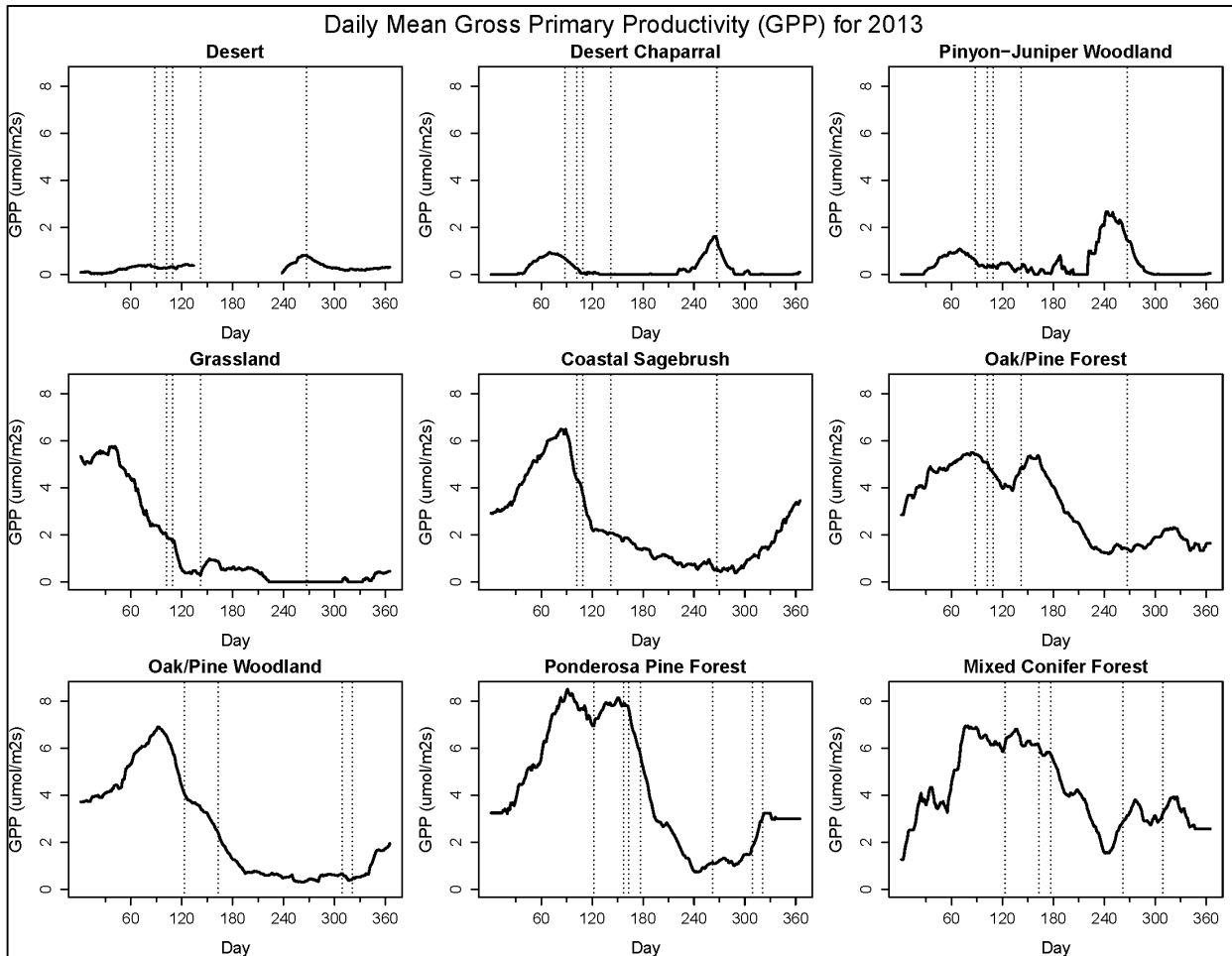
In order to generate a complete time series after removing data during the quality control process, we filled missing data points using the Desai-Cook gap filling model (Cook et al., 2004; Desai et al., 2005). This model was applied to the u^* filtered data, utilizing the 30 minute values for NEE, photosynthetically active radiation (PAR), air temperature and site location. The model uses a variable moving-window mean diurnal variation method to estimate missing meteorological data, with the window size depending on the completeness of the dataset.

The Eyring function (Cook et al., 2004; Eyring, 1935) was applied to the filled data to estimate ecosystem respiration (R_{eco}). Gross Primary Productivity (GPP) was modeled from the difference between the 30 minute modeled R_{eco} and the original NEE data. The computed GPP was fit to a Michaelis-Menton reaction rate equation (Falge et al., 2001; Ruimy et al., 1995) in order to fill gaps. The full time series of R_{eco} and GPP was then used to estimate NEE and fill gaps in the original dataset.

Estimates of $V_{c_{max}}$ from flux tower data were made from inverse modeling a Farquhar-based photosynthesis model following the method described in Wolf et al. (2006). The model was computed using filtered and gapfilled NEE along with meteorological data collected at the flux

tower site. Estimates were made for multiple sites, using data from approximately four or five days depending on site conditions and quality of the extended data.

Analysis. GPP estimated from NEE data was used to categorize ecosystem growing seasons. As our sites covered a variety of climatic zones and precipitation-dependent vegetation types, growing seasons and thus peak productivity do not align across sites. Comparing GPP between sites and AVIRIS collection dates allow for the remote sensing data to be put in the context of each sites' growing season.



Results

California Climate. The Southern California transect can be divided into three climate categories: (i) coastal, which includes coastal sage and grassland, (ii) southern interior, consisting of desert,

Figure 2: GPP for all sites from 2013 with AVIRIS imagery dates indicated by the vertical dashed line. GPP follows the precipitation regime, with maximums often following times of peak precipitation. The AVIRIS imagery captures a range of productivity levels for each site, but misses maximum productivity for the xeric and coastal sites, most likely due to drought causing the growing seasons to retreat into the cooler months.

desert chaparral, and pinyon-juniper woodland, and (iii) southern montane for the oak/pine forest. The coastal sites receive most of their annual precipitation in the cooler winter months before an often dry and warm summer. The southern interior sites are the most xeric, with low precipitation usually in the late winter or spring, and intermittent throughout the rest of the year. The southern montane also receives its most significant rainfall in the winter and early spring, but has moderate temperatures relative to the other southern sites.

The Sierra sites are categorized as central interior (oak/pine woodland) and montane (ponderosa pine and mixed conifer). All sites receive most of the annual precipitation in winter and spring, and at a lesser rate during the rest of the year. The montane sites experience cold winters and moderate summers, while the central interior has moderate winters and warm summers. California is currently enduring severe drought conditions since the 2012 calendar year (US Drought Monitor, 2014). This is evident in our data, as annual precipitation has steadily declined since 2011 (see figure 4). All sites in which we examined previous years' data exhibited a

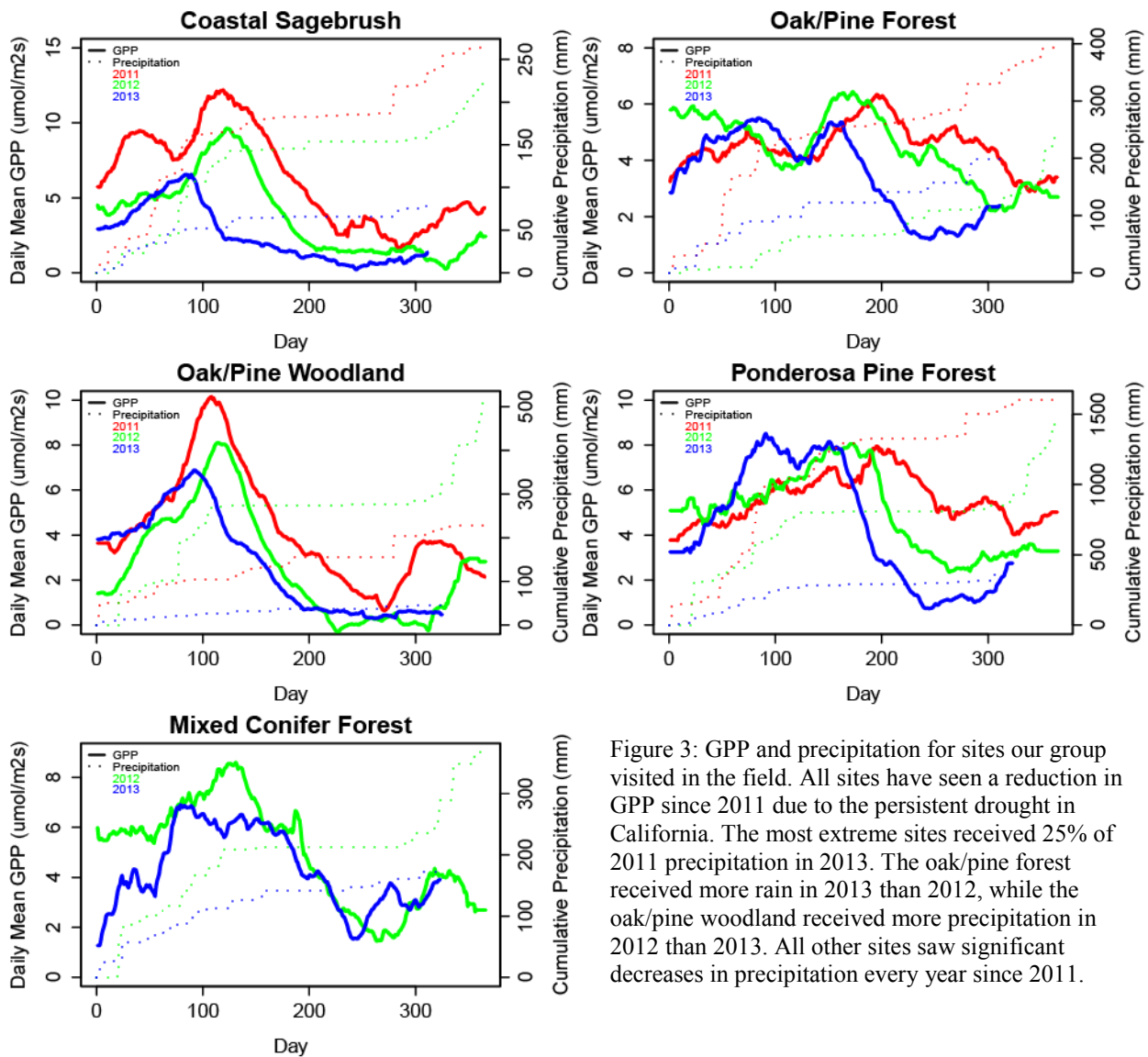


Figure 3: GPP and precipitation for sites our group visited in the field. All sites have seen a reduction in GPP since 2011 due to the persistent drought in California. The most extreme sites received 25% of 2011 precipitation in 2013. The oak/pine forest received more rain in 2013 than 2012, while the oak/pine woodland received more precipitation in 2012 than 2013. All other sites saw significant decreases in precipitation every year since 2011.

decreasing trend in precipitation, with 2013 data often signaling drier conditions than the first year of the drought in 2012. The drought tends to deviate most strongly from previous years' rainfall records in the spring, when the wet season usually delivers a significant portion of the annual precipitation for the southern sites. During drought years, the spring increase in rainfall either did not occur or the magnitude of rainfall was significantly decreased.

Ecosystem carbon fluxes. The most xeric sites (desert, desert chaparral, and pinyon-juniper woodland) have a bimodal growing season (figure 2), caused from two predominant precipitation periods occurring in 2013. These events directly resulted in times of increased production. The mesic sites are categorized as having predominately a single peak in productivity occurring in late winter or spring. The single peak is caused by precipitation events and low water demand in the cooler winter months.

Due to the continuous nature of flux tower measurements compared to the irregular remote sensing campaigns, it is necessary to contextualize the imagery with the eddy covariance measurements. The numerous overflights often were able to categorize annual variability by collecting at periods of both maximum and minimum productivity. However, the sites characterized by maximum GPP occurring in late and early spring (grassland, coastal sagebrush, and oak/pine woodland) reached peak productivity before the first AVIRIS flight of the year. Comparing spectra-derived estimates of photosynthesis must take into account the differences in growing seasons between vegetation types.

V_cmax Inversion. Inverse modeling of the Farquhar photosynthesis model using flux tower data provided V_cmax and LAI estimates for multiple vegetation types in the footprint of each flux tower. The estimates for all sites in 2013 were far below those measured from leaf chamber gas exchange.

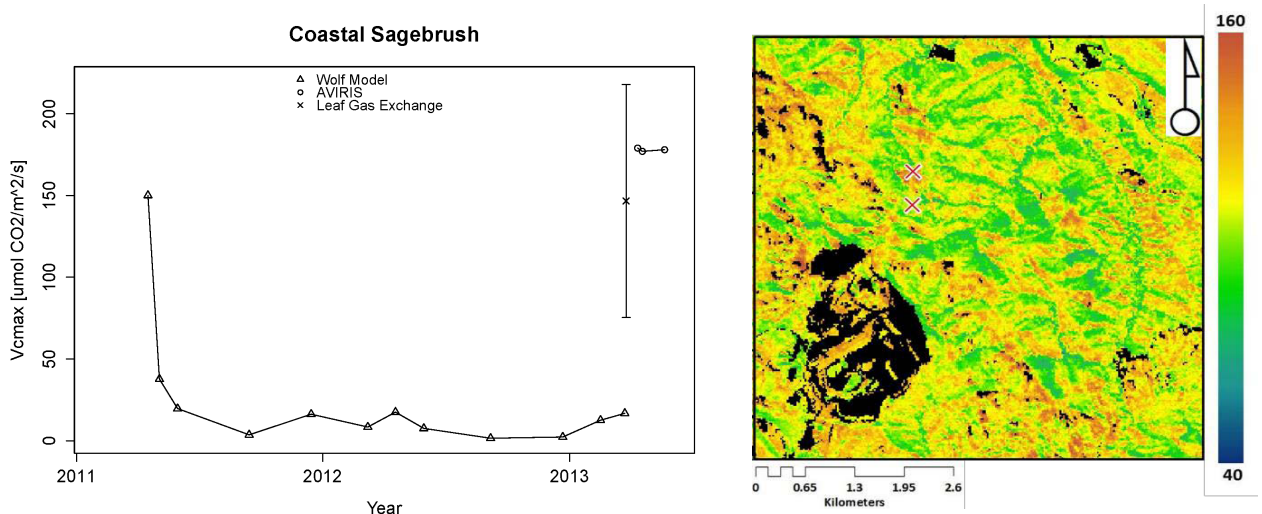


Figure 4: V_cmax values for coastal sagebrush. *Left:* comparison of estimates from the Wolf approach for modeling V_cmax from flux data and AVIRIS image, and measured field values for all dominant species. During drought conditions, the Wolf approach yields much lower estimates compared to pre-drought. However, the estimates from AVIRIS imagery are within the range measured in the field. *Right:* Map of V_cmax from 2013 spring for the coastal sage (north red marker) and grassland (south red marker). Variation in the parameter is high across the landscape.

In order to determine the variability of $V_{c_{max}}$ estimates from the flux tower data, estimates were made going back to 2011. Figure 3 shows a comparison of estimated $V_{c_{max}}$ from the flux tower data, the AVIRIS imagery, and the calculated range of values from leaf chamber gas exchange measurements for the coastal sage site. 2011 estimates of $V_{c_{max}}$ (150 $\mu\text{mol CO}_2/\text{m}^2/\text{s}$) were closer to those collected in the field in 2013 (ranging from 74 to 300 $\mu\text{mol CO}_2/\text{m}^2/\text{s}$ for all dominant species). Preliminary estimates from the AVIRIS imagery are also near the average $V_{c_{max}}$ estimate from field data.

Discussion and Conclusion

This often preceded a significant decrease in summer and fall GPP. The one site that did not follow this trend was the oak/pine woodland, which received higher rainfall in 2012 than in 2011. There is a clear discrepancy between the flux data and the other two methods for estimating $V_{c_{max}}$. Although there are no field measurements in 2011, the Wolf estimated $V_{c_{max}}$ is around the expected value for the coastal sage site during springtime. Even throughout 2012 and 2013, there is variation in the $V_{c_{max}}$ estimate, but it does not reach levels often associated with viable ecosystems. Comparing this to the AVIRIS map of $V_{c_{max}}$, the spatial heterogeneity of $V_{c_{max}}$ does not include such low estimates. Our initial analysis shows that drought reduces the ability of the models used in the inversion to correctly predict ecosystem photosynthetic properties, which is concurrent with previous studies (Vargas et al., 2013). Given the decrease in $V_{c_{max}}$ estimates during the transition between pre-drought to drought conditions, we suggest that the Wolf approach does not accurately estimate $V_{c_{max}}$ during periods of high water stress for our sites. However, $V_{c_{max}}$ estimates are correlated with GPP modeled from flux data ($r=0.70$), and although the estimates do not reach levels measured in the field, the model still captures annual changes in productivity.

The flux tower data provides a long-term view that places the airborne field experiment imagery into context and provides a justification for long-term satellite based sensing of plant photosynthetic rate. The most important observation from tower data is the impact drought currently has on the Californian vegetation. All sites have seen a decrease in annual GPP, with most sites peak GPP reduced as well. Furthermore, peak productivity for the southern sites and some Sierra sites moves to earlier in the year when it is cooler and wetter. A common theme among sites is the drastic reduction in late season GPP. Peak productivity is often affected, but the largest decrease occurs in the summer and fall due to the reduced spring rainfall that historically provided some of the necessary moisture during the times of high water demand in the summer months. Thus, both maximum and minimum GPP are reduced due to the ongoing drought.

Eddy covariance flux measurements were used to inform ground and airborne data collection. Annual variations in vegetation productivity are captured in the flux data. In order to maximize effectiveness of field and airborne campaigns, estimates on timing of vegetation maxima and minima should guide these efforts. During the 2013 campaign, maximum productivity at the grassland and sage sights were missed by AVIRIS flights (figure 2). This appears to be caused in part by the drought, as the GPP maximum has retreated to earlier in the year. Future flights will be

adjusted in order to ensure the capture of the GPP range at each site by making predictions based on previous years' data.

Conclusion. Flux tower measurements were employed to evaluate the ability to scale $V_{c_{max}}$ estimates from the leaf to the canopy level. The inverse modeling technique to derive $V_{c_{max}}$ from the flux tower data was inadequate at predicting reasonable estimates due to the ongoing drought in the western U.S. Flux tower measurements and modeled GPP offer important observations which can inform remote sensing data collection due to the continuous collection, but are limited in spatial coverage. Long-term and high spatial resolution of ecosystem metabolism data is only possible with satellites equipped with imaging spectrometers.

Future work. Flux tower modeled GPP does appear to be a viable alternative to evaluating the spectroscopy scaling issue. It is possible to model GPP from the spectra-derived photosynthetic parameters, so this will be the preferred method for evaluating remote sensing $V_{c_{max}}$ estimates. In addition to the ongoing drought impacting productivity in California, other anthropogenic pollution including ozone is known to have negative impacts on vegetation. Ozone pollution will be compared to annual productivity and is expected to explain certain seasonal and annual variation during times of high pollution.

References

Baldocchi, D., and T. Meyers (1998), On using eco-physiological, micrometeorological and biogeochemical theory to evaluate carbon dioxide, water vapor and trace gas fluxes over vegetation: a perspective, *Agricultural and Forest Meteorology*, 90(1-2), 1-25, doi:10.1016/s0168-1923(97)00072-5.

- Breshears, D. D., et al. (2005), Regional vegetation die-off in response to global-change-type drought, *Proceedings of the National Academy of Sciences of the United States of America*, 102(42), 15144-15148, doi:10.1073/pnas.0505734102.
- Cook, B. D., et al. (2004), Carbon exchange and venting anomalies in an upland deciduous forest in northern Wisconsin, USA, *Agricultural and Forest Meteorology*, 126(3-4), 271-295, doi:10.1016/j.agrformet.2004.06.008.
- Desai, A. R., P. V. Bolstad, B. D. Cook, K. J. Davis, and E. V. Carey (2005), Comparing net ecosystem exchange of carbon dioxide between an old-growth and mature forest in the upper Midwest, USA, *Agricultural and Forest Meteorology*, 128(1-2), 33-55, doi:10.1016/j.agrformet.2004.09.005.
- Drought Monitor (2014), U.S. Drought Monitor California, accessed August 2014 at <http://droughtmonitor.unl.edu/Home/StateDroughtMonitor.aspx?C>
- Eyring, H. (1935), Activated complex in chemical reactions, *Journal of Chemical Physics*, 3, 107-115, doi:10.1063/1.1749604.
- Falge, E., et al. (2001), Gap filling strategies for defensible annual sums of net ecosystem exchange, *Agricultural and Forest Meteorology*, 107(1), 43-69, doi:10.1016/s0168-1923(00)00225-2.
- Farquhar, G. D., and S. v. Caemmerer (1982), Modelling of photosynthetic response to environmental conditions, *Encyclopedia of plant physiology. New series. Volume 12B. Physiological plant ecology. II. Water relations and carbon assimilation. [Lange, O.L.; Nobel, P.S.; Osmond, C.B.; Ziegler, H. (Editors)]*, 549-587.
- Farquhar, G. D., S. V. Caemmerer, and J. A. Berry (1980), A BIOCHEMICAL-MODEL OF PHOTOSYNTHETIC CO₂ ASSIMILATION IN LEAVES OF C-3 SPECIES, *Planta*, 149(1), 78-90, doi:10.1007/bf00386231.
- Goulden, M. L., R. G. Anderson, R. C. Bales, A. E. Kelly, M. Meadows, and G. C. Winston (2012), Evapotranspiration along an elevation gradient in California's Sierra Nevada, *Journal of Geophysical Research-Biogeosciences*, 117, doi:10.1029/2012jg002027.
- Hofmann, D. J., J. H. Butler, E. J. Dlugokencky, J. W. Elkins, K. Masarie, S. A. Montzka, and P. Tans (2006), The role of carbon dioxide in climate forcing from 1979 to 2004: introduction of the Annual Greenhouse Gas Index, *Tellus Series B-Chemical and Physical Meteorology*, 58(5), 614-619, doi:10.1111/j.1600-0889.2006.00201.x.
- Kelly, A. E., and M. L. Goulden (2008), Rapid shifts in plant distribution with recent climate change, *Proceedings of the National Academy of Sciences of the United States of America*, 105(33), 11823-11826, doi:10.1073/pnas.0802891105.
- Ruimy, A., P. G. Jarvis, D. D. Baldocchi, and B. Saugier (1995), CO₂ fluxes over plant canopies and solar radiation: a review, *Advances in Ecological Research*, 26, 1-63, doi:10.1016/s0065-2504(08)60063-x.
- Serbin, S. P., D. N. Dillaway, E. L. Kruger, and P. A. Townsend (2012), Leaf optical properties reflect variation in photosynthetic metabolism and its sensitivity to temperature, *Journal of Experimental Botany*, 63(1), 489-502, doi:10.1093/jxb/err294.
- Serbin, S.P., A. Singh, B.E. McNeil, and P.A. Townsend (2014), Spectroscopic determination of leaf morphological, nutritional, and biochemical traits for northern temperate and boreal tree species, *Ecological Applications*. doi: 0.1890/13-2110.1
- Vargas, R., et al. (2013), Drought Influences the Accuracy of Simulated Ecosystem Fluxes: A Model-Data Meta-analysis for Mediterranean Oak Woodlands, *Ecosystems*, 16(5), 749-764, doi:10.1007/s10021-013-9648-1.
- Wolf, A., K. Akshalov, N. Saliendra, D. A. Johnson, and E. A. Laca (2006), Inverse estimation of V_c(max), leaf area index, and the Ball-Berry parameter from carbon and energy fluxes, *Journal of Geophysical Research-Atmospheres*, 111(D8), 18, doi:10.1029/2005gd005927.

Testing for wildfire feedbacks in forests of the US Northern Rockies

Initial Report

Brian J. Harvey

Ecosystem and Landscape Ecology Lab, Department of Zoology, University of Wisconsin

Abstract. Understanding the complex responses of forested landscapes to changing fire regimes is critical for predicting land-cover patterns under a warming climate. Using decades of existing NASA satellite imagery and extensive field-calibration data on burn severity I tested whether successive forest fires in the Northern Rocky Mountains interact through feedbacks, and identified factors that are more likely to lead to two successive high-severity (stand-replacing) fires. Feedbacks among wildfires depended on forest type and interval between the first and second fire. Feedbacks in wildfire severity shifted from negative to positive with increasing elevation and with interval between two fires. Areas characterized by two successive stand-replacing fires were in subalpine forests at higher elevations, shallower slopes, and northeasterly aspects where the interval between fires was longer. Further analyses are underway, and results will identify when and where fire-catalyzed shifts in vegetation are occurring or are likely to occur with continued climate change and altered fire regimes.

Introduction

Understanding regional wildfire patterns is becoming urgent as the climate continues to warm and worldwide fire activity steadily increases (Flannigan et al. 2009). In the western US, fire frequency and annual area burned have increased since the mid-1980s in association with a warmer and drier climate (Westerling et al. 2006), and trends are particularly strong in forests of the N. Rocky Mountains (Morgan et al. 2008) where qualitative shifts in fire regimes are projected by the mid-21st century (Westerling et al. 2011). Tracking changes to fire regimes is necessary to further understand global change (Turner 2010), forecast changes to ecosystem services (Adams 2013), and inform US resource management (Stephens et al. 2013). Because of the spatial and temporal extent of wildfires, remote sensing data acquired from NASA satellites provide the most consistent and comprehensive information about these changes, but regional studies of changing fire regimes are lacking.

For many forested regions, a major consequence of increased wildfire activity is a decrease in the fire rotation (the time required to burn an area equal to a landscape of interest; (Baker 2009)). Most N. Rockies forests are adapted to regenerate after stand-replacing fires that occur every 100-300 years (Romme and Despain 1989, Barrett et al. 1991, Barrett 1994, Higuera et al. 2011), and wildfire activity was historically limited by the frequency of climate conditions suitable for fire initiation and spread. Simulations predict that continued warming and drying of the region over the next century could decrease fire rotations to ~ 30 years by the year 2050 (Westerling et al. 2011), but a key unknown is whether sequential fires occurring over a short period (i.e.,

Supported by the Dr. Laurel Salton Clark Memorial Graduate Fellowship Award from the Wisconsin Space Grant Consortium. Additional funding for field data collection and equipment was provided by the Joint Fire Science Program, the US National Park Service / George Melendez Wright Climate Change Fellowship, the Meyer Research Award from the Department of Zoology, University of Wisconsin - Madison.

“reburns”) may interact through feedbacks that affect subsequent fire activity. Reduced burnable fuel following one fire may impose a negative feedback on fire severity (impacts of fire on the ecosystem) in a second fire (Collins et al. 2009, Parks et al. 2014). Alternatively, abundant growth of flammable vegetation following fire may cause a positive feedback on fire severity, where severely burned areas in one fire may be prone to burning severely again in a second (Thompson et al. 2007, Holden et al. 2010, van Wagendonk et al. 2012).

If a second stand-replacing fire occurs before the trees regenerating from the first fire reach reproductive maturity, vegetation may transition from forest to non-forest (e.g. shrubland or grassland) because of failed tree recruitment after the second fire (Brown and Johnstone 2012, Pinno et al. 2013) (Figure 1). The factors that contribute to severe reburns in the N. Rockies are unknown, but critical for understanding potential broad-scale changes across forested landscapes.

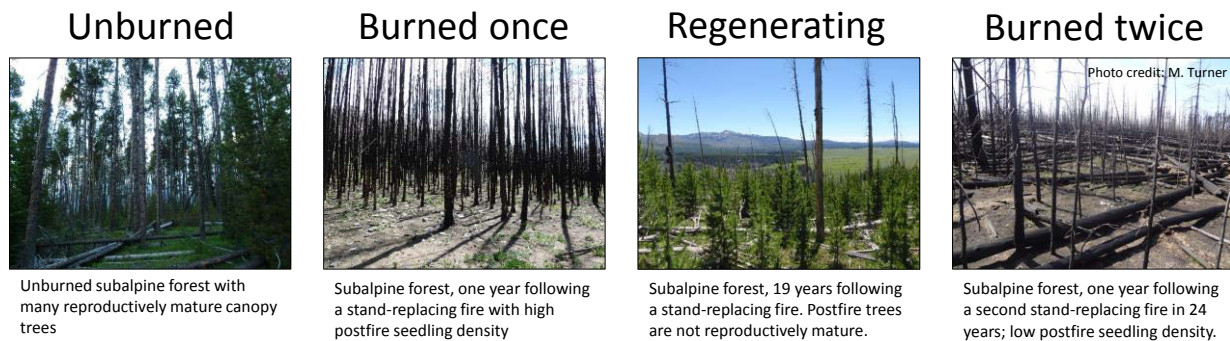


Figure 1. Chronosequence illustrating temporal progression from a mature forest that has not burned in 100-300 years (left) to a recently burned forest with abundant postfire seedling regeneration (middle left) to a regenerating forest 19 years after fire (middle right) that then burns again at high-severity before the regenerating trees are reproductively mature. Photo credits: Brian J. Harvey and Monica G. Turner.

Methodological advances over the last several decades have improved the ability to track burn severity and post-fire recovery over space and time (see Lentile et al. 2006 for a review). The widespread availability of satellite data through the Landsat Thematic Mapper (TM) archive and projects such as the Monitoring Trends in Burn Severity (MTBS; www.mtbs.gov) (Eidenshink et al. 2007) have enabled analyses of regional fire trends (Miller et al. 2008, 2011, Dillon et al. 2011), but many studies are limited in their regional inference because they lack field data to calibrate burn severity indices (Miller et al. 2009).

In this study, I use remote sensing and field data to test for feedbacks among recent forest fires in the Northern Rocky Mountains in areas that have burned twice between 1984 and 2010, to ask the following research questions: (1) Is the severity of successive forest fires (fires occurring in the same location within 24 years) related through positive or negative feedbacks? What combination of factors leads to two successive stand-replacing forest fires? In answering these two questions, I test two hypotheses. First, I hypothesize that negative feedbacks among wildfires will be strong in low-elevation forests where postfire fuels regenerate slowly, whereas feedbacks will be weaker in mid-elevation forests and positive in subalpine forests, where postfire fuels can quickly regenerate. Second, I hypothesize that successive stand-replacing fires will more likely occur in areas characterized by subalpine forests with adaptations to high-severity fire, cool/wet climate conditions following the first fire, and protected topographic positions.

Methods

Study Area. The N. Rockies study region follows the US EPA ecoregions 15,16,17 and 41 (<http://www.epa.gov/wed/pages/ecoregions.htm>), stretching from northwestern Wyoming to the US/Canada border at the northern tip of Idaho (Figure 2). Forests are conifer dominated and vary compositionally with elevation, moisture, and latitude (Baker 2009). Historical fire regimes include low-frequency, high-severity regimes in higher elevation and mesic forests to moderate-frequency, mixed-severity regimes in lower elevation forests (Arno 1980, Baker 2009). Between 1984 and 2010, a total of 733 named forest fires larger than 200 ha occurred in the study area, burning 3,872,568 ha in total. Out of this total, 438,075 ha have burned twice, with intervals between fires ranging from one to 23 years (Figure 2).

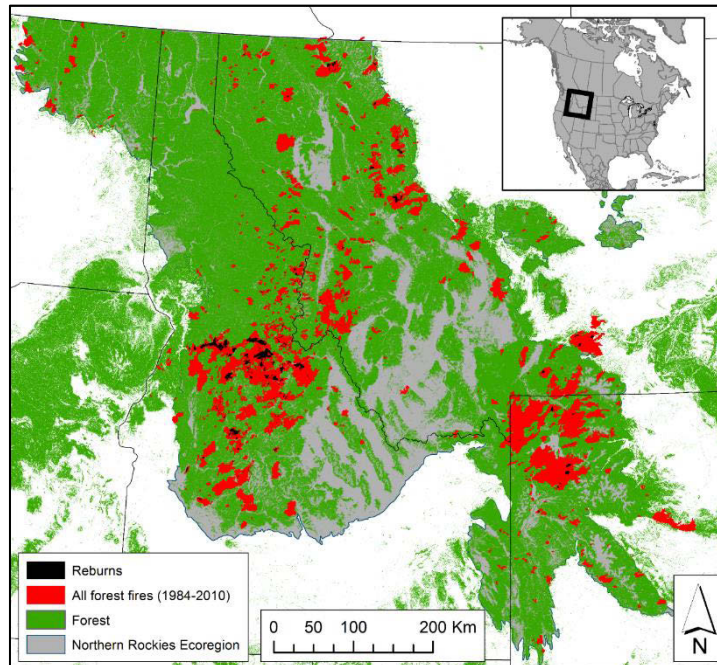


Figure 2. Map of study area with the Northern Rockies Ecoregion outlined in gray, forested areas shaded in green, all forest fires occurring in the study period in red, and all areas that burned at least twice during the study period in black.

Data acquisition and preparation. Fire-severity maps for all large fires (> 200 ha) burning in the study area (1984-2010) were extracted from the MTBS database (Eidenshink et al. 2007) and assembled into a regional fire severity atlas. To facilitate comparison of burn severity across multiple fires, the relative differenced normalized burn ratio (RdNBR; (Miller and Thode 2007)) that accounts for differences in pre-fire biomass was used to compare burn severity in the first and second fires for each location that has burned twice. Field data from 371 plots were used to calibrate burn-severity indices to field measures of burn severity using established protocols. Field measures of burn severity showed strong correlations (Pearson's r from 0.75 to 0.88) with RdNBR. Topographic data were acquired from the USGS National Elevational Dataset, forest type data were acquired from LANDFIRE (LANDFIRE 2014), and climate data were available from existing downscaled (12 km x 12 km) monthly data generated for the N. Rockies (Westerling et al. 2011). Using ArcGIS, I extracted the following variables from each of 2,249 systematically distributed points separated by at least 400m: burn severity in the first fire

(RdNBR), burn severity in the second fire (RdNBR), interval between fires (years), dominant forest type (subalpine, mid montane, lower montane), elevation (m), slope (deg.), NE Index (0-2, reflecting solar radiation), and regional moisture deficit (MD) (mm) in the year following the first fire and the year of the second fire. Field calibration data (Harvey et al., in prep) were used to determine areas of stand-replacing fire (greater than 90% tree mortality).

Data Analysis. To analyze feedbacks between successive fire events, I evaluated the relationship between burn severity in the first fire and burn severity in the second fire for two time intervals between fires (1-10 yrs or 11-23 yrs). Analyses were also separated for each forest type because of expected differences among forest types. Using all sampled pixels, I calculated the mean and 95% confidence interval for fire severity in the first and second fire in each forest type and interval combination. I interpreted negative feedbacks to be reflected by high severity in the first fire leading to low severity in the second fire, or vice versa. Positive feedbacks would be reflected by high severity in the first fire leading to high severity in the second fire, or vice versa.

To test for factors associated with two successive stand-replacing fires, I tested for significant differences between values for biophysical variables (forest type, elevation, slope, NE index, interval between fires, MD the year of the second fire, and MD the year after the first fire) between areas that burned twice where only the first fire was stand-replacing (i.e., second fire was lower severity) and areas that burned twice where both fires were stand-replacing. I used Chi-square tests to test for differences among forest types and non-parametric Wilcoxon signed-rank test for continuous variables. All analyses were performed using the R statistical software (R Development Core Team 2012).

Results and Discussion

Wildfire feedbacks in different forest types. Initial results suggest that feedbacks among successive fires differed depending on the forest type (Figure 3). Lower and mid-elevation forests were characterized by negative feedbacks, meaning that fire severity was higher in the first fire and lower in the second fire (Figure 3). For both forest types, the negative feedback was stronger with shorter intervals between fires (reductions in fire severity of 40% and 37%, in lower and mid-elevation forests, respectively) likely because of the time required to regenerate sufficient fuel following the first fire. Over longer intervals, negative feedbacks in low and mid elevation forests were weaker (reductions in fire severity of 21% and 11%, in lower and mid-elevation forests, respectively), as the effect attenuates when fuels are less limiting to fire severity. Contrasting this, subalpine forests exhibited positive feedbacks, where fire severity in the second fire was only 9% lower in short interval (1-10 yr) reburns but was 10% higher when intervals were 11-23 years (Figure 3).

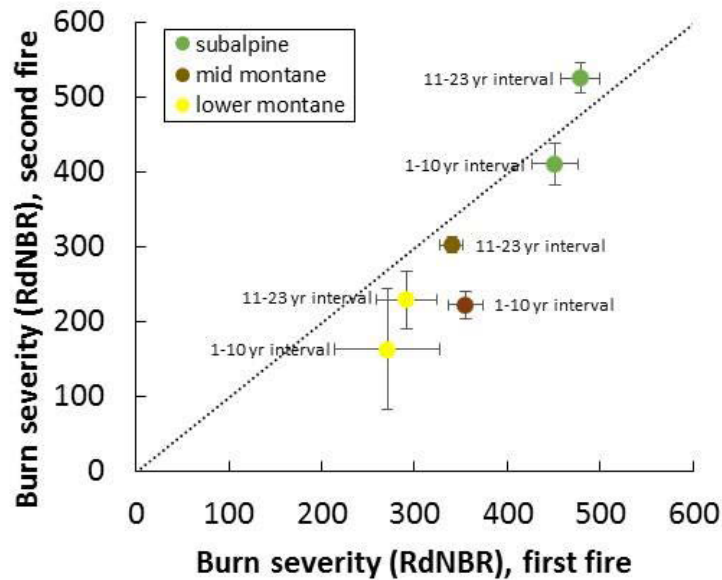


Figure 3. Relationship between fire severity in the first fire and fire severity in the second fire for all plots that burned twice during the study period. Points are means with 95% confidence intervals for all plots in each combination of forest type and interval between fires.

Factors leading to successive stand-replacing fires. Initial results suggest that vegetation and topographic setting both influenced the likelihood that an area that burned once as a stand-replacing fire, if burned a second time, would burn again as stand-replacing fire. Subalpine forests were more likely to burn as stand-replacing fire twice, whereas lower and mid-montane forests were less likely to experience two stand-replacing fires (Figure 4).

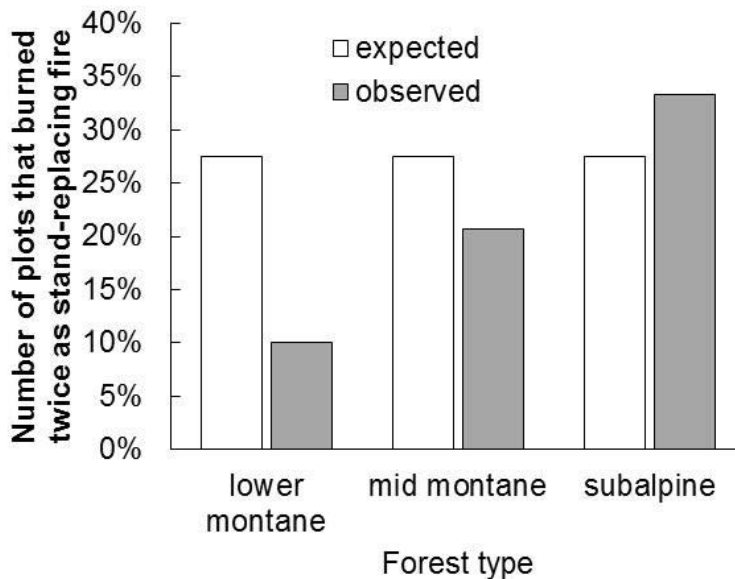


Figure 4. Observed vs. expected percentage of plots burning twice as stand-replacing fire in each forest type. Observed data deviated significantly from the expected under the null hypothesis of no difference among forest types ($X^2 = 33.33$, $P < 0.001$, Chi-square test of association).

Physical variables also influenced the likelihood that an area that burned once as stand-replacing fire, if burned again, would burn as stand-replacing fire in a reburn. Areas that burned twice as stand-replacing fire had higher elevation, shallower slopes, more northeasterly aspects, and longer intervals between fire events than areas that burned once as stand-replacing and then were not stand-replacing (i.e., much lower severity) in the second fire (Figure 5). Climate variables (MD) were not significantly different between areas that burned once at stand-replacing severity and those that burned twice as stand-replacing (Figure 5).

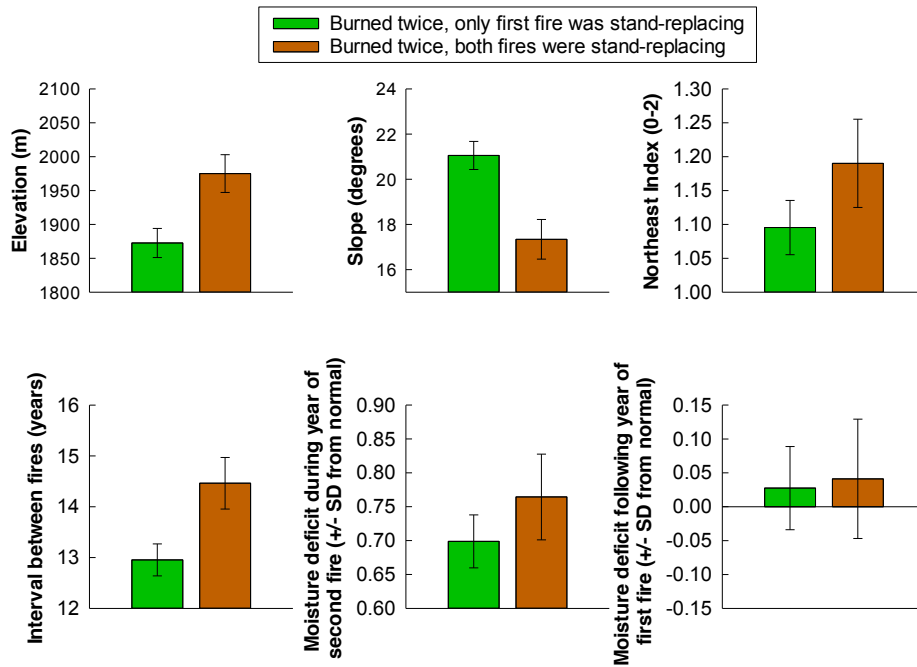


Figure 5. Comparisons for each biophysical variable among plots that burned twice as stand-replacing or burned twice, but only the first fire was stand-replacing. Bars are means and error bars are 95% confidence intervals.

Conclusion and ongoing work

The strength and direction of feedbacks among successive fires differed among forest types, with negative feedbacks in lower elevation and mid-montane forests and positive feedbacks in subalpine forests. Areas that were most likely to experience successive stand-replacing fires were subalpine forests at higher elevation, northeasterly aspects, gentler slopes, and where the interval between fires was longer. These factors all relate to high capacity for fuels to regenerate quickly after the first stand-replacing fire.

This report presents preliminary results, but research is continuing on this project. To determine whether successive, short-interval fires impair forest recovery, I will compare the normalized differenced vegetation index (NDVI) for the first three post-fire years in areas that burned twice at stand replacement to determine whether NDVI is lower in the first three years following the second stand-replacing fire than first fire. To control for differences among post-fire climate years, I will also compare areas within fires that burned twice at stand-replacement to areas that burned once at stand replacement (in the second fire only). I expect forest recovery will be

impaired in areas experiencing two stand-replacing fires. This will be indicated by significantly lower NDVI values in the first three years following the second fire compared to areas that only experienced a single fire at stand-replacement, similar to findings in other systems (Malak and Pausas 2006).

References

- Adams, M. A. 2013. Mega-fires, tipping points and ecosystem services: Managing forests and woodlands in an uncertain future. *Forest Ecology and Management* 294:250–261.
- Arno, S. F. 1980. Forest fire history in the Northern Rockies. *Journal of Forestry* 78:460–465.
- Baker, W. L. 2009. *Fire ecology in Rocky Mountain landscapes*. First edition. Island Press, Washington, D.C.
- Barrett, S. 1994. Fire Regimes on Andesitic Mountain Terrain in Northeastern Yellowstone-National-Park, Wyoming. *International Journal of Wildland Fire* 4:65–76.
- Barrett, S. W., S. F. Arno, and C. H. Key. 1991. Fire regimes of Western larch - lodgepole pine forests in Glacier National Park, Montana. *Canadian Journal of Forest Research-Revue Canadienne De Recherche Forestiere* 21:1711–1720.
- Brown, C. D., and J. F. Johnstone. 2012. Once burned, twice shy: Repeat fires reduce seed availability and alter substrate constraints on *Picea mariana* regeneration. *Forest Ecology and Management* 266:34–41.
- Collins, B. M., J. D. Miller, A. E. Thode, M. Kelly, J. W. Wagtendonk, and S. L. Stephens. 2009. Interactions among wildland fires in a long-established Sierra Nevada natural fire area. *Ecosystems* 12:114–128.
- Dillon, G. K., Z. A. Holden, P. Morgan, M. A. Crimmins, E. K. Heyerdahl, and C. H. Luce. 2011. Both topography and climate affected forest and woodland burn severity in two regions of the western US, 1984 to 2006. *Ecosphere* 2:1–33.
- Eidenshink, J., B. Schwind, K. Brewer, Z.-L. Zhu, B. Quayle, and S. Howard. 2007. A project for monitoring trends in burn severity. *Fire Ecology* 3:3–21.
- Flannigan, M. D., M. A. Krawchuk, W. J. de Groot, B. M. Wotton, and L. M. Gowman. 2009. Implications of changing climate for global wildland fire. *International Journal of Wildland Fire* 18:483–507.
- Higuera, P. E., C. Whitlock, and J. A. Gage. 2011. Linking tree-ring and sediment-charcoal records to reconstruct fire occurrence and area burned in subalpine forests of Yellowstone National Park, USA. *Holocene* 21:327–341.
- Holden, Z. A., P. Morgan, and A. T. Hudak. 2010. Burn severity of areas reburned by wildfires in the Gila National Forest, New Mexico, USA. *Fire Ecology* 6:77–85.
- LANDFIRE 1.2.0. 2014. Environmental Site Potential layer. U.S. Department of Interior, Geological Survey. [online] Available: <http://www.landfire.gov/viewer/> [2014, June 30].
- Lentile, L. B., Z. A. Holden, A. M. S. Smith, M. J. Falkowski, A. T. Hudak, P. Morgan, S. A. Lewis, P. E. Gessler, and N. C. Benson. 2006. Remote sensing techniques to assess active fire characteristics and post-fire effects. *International Journal of Wildland Fire* 15:319–345.
- Malak, D. A., and J. G. Pausas. 2006. Fire regime and post-fire Normalized Difference Vegetation Index changes in the eastern Iberian peninsula (Mediterranean basin). *International Journal of Wildland Fire* 15:407–413.
- Miller, J. D., E. E. Knapp, C. H. Key, C. N. Skinner, C. J. Isbell, R. M. Creasy, and J. W. Sherlock. 2009. Calibration and validation of the relative differenced Normalized Burn

Ratio (RdNBR) to three measures of fire severity in the Sierra Nevada and Klamath Mountains, California, USA. *Remote Sensing of Environment* 113:645–656.

- Miller, J. D., H. D. Safford, M. Crimmins, and A. E. Thode. 2008. Quantitative evidence for increasing forest fire severity in the Sierra Nevada and Southern Cascade Mountains, California and Nevada, USA. *Ecosystems* 12:16–32.
- Miller, J. D., C. N. Skinner, H. D. Safford, E. E. Knapp, and C. M. Ramirez. 2011. Trends and causes of severity, size, and number of fires in northwestern California, USA. *Ecological Applications* 22:184–203.
- Miller, J. D., and A. E. Thode. 2007. Quantifying burn severity in a heterogeneous landscape with a relative version of the delta Normalized Burn Ratio (dNBR). *Remote Sensing of Environment* 109:66–80.
- Morgan, P., E. K. Heyerdahl, and C. E. Gibson. 2008. Multi-season climate synchronized forest fires throughout the 20th century, Northern Rockies, USA. *Ecology* 89:717–728.
- Parks, S. A., C. Miller, C. R. Nelson, and Z. A. Holden. 2014. Previous Fires Moderate Burn Severity of Subsequent Wildland Fires in Two Large Western US Wilderness Areas. *Ecosystems* 17:29–42.
- Pinno, B. D., R. C. Errington, and D. K. Thompson. 2013. Young jack pine and high severity fire combine to create potentially expansive areas of understocked forest. *Forest Ecology and Management* 310:517–522.
- R Development Core Team. 2012. R: a language and environment for statistical computing. R Foundation for Statistical Computing, Vienna, Austria.
- Romme, W. H., and D. G. Despain. 1989. Historical perspective on the Yellowstone Fires of 1988. *BioScience* 39:695–699.
- Stephens, S. L., J. K. Agee, P. Z. Fulé, M. P. North, W. H. Romme, T. W. Swetnam, and M. G. Turner. 2013. Managing Forests and Fire in Changing Climates. *Science* 342:41–42.
- Thompson, J. R., T. A. Spies, and L. M. Ganio. 2007. Reburn severity in managed and unmanaged vegetation in a large wildfire. *Proceedings of the National Academy of Sciences* 104:10743–10748.
- Turner, M. G. 2010. Disturbance and landscape dynamics in a changing world. *Ecology* 91:2833–2849.
- Van Wagtendonk, J. W., K. A. van Wagtendonk, and A. E. Thode. 2012. Factors Associated with the Severity of Intersecting Fires in Yosemite National Park, California, USA. *Fire Ecology* 7:11–31.
- Westerling, A. L., H. G. Hidalgo, D. R. Cayan, and T. W. Swetnam. 2006. Warming and earlier spring increase western US forest wildfire activity. *Science* 313:940.
- Westerling, A. L., M. G. Turner, E. A. H. Smithwick, W. H. Romme, and M. G. Ryan. 2011. Continued warming could transform Greater Yellowstone fire regimes by mid-21st century. *Proceedings of the National Academy of Sciences* 108:13165–13170.

Size differences of the post-anoxia, biotic recovery brachiopod, *Dyoros* sp., in Hughes Creek Shale (Carboniferous), Richardson County, Nebraska.

Daryl Johnson and Rex Hanger

Dept. of Geography & Geology

University of Wisconsin-Whitewater

Whitewater, WI 53190

Abstract. Two localities of the Carboniferous Hughes Creek Shale in southeastern Nebraska contain both fossiliferous limestones and shales, as well as black shales interpreted as being deposited under anoxic conditions in ancient oceans. Fossils within strata above the anoxic layers represent life that had recovered from a local killing event. Examining the killing/recovery patterns on expanded, regional scales is made difficult due to the relative lack of good exposures between outcrops. Previous miscorrelations have occurred for the Hughes Creek Shale in two established collecting localities separated by only a few kilometers. Specimens of the brachiopod fossil, *Dyoros* sp., abundant at both localities were compared using the size frequency distributions of their length measurements. Null hypotheses of the equality of the medians and equality of the overall distributions were not able to be rejected, adding support to the current accepted interpretation of correlation for the two localities, allowing for future use of both for examining killing/recovery of life on expanded geographic scale.

Introduction

The Hughes Creek Shale of southeastern Nebraska is a Carboniferous Period (~350-290 million years ago) rock unit that has been interpreted to contain evidence of several intervals of anoxia, or low/no oxygen in the oceans in which they were originally deposited. The anoxic episodes are shown as black-colored shales that are devoid of fossil remains. For the Hughes Creek Shale the anoxic episodes were regional in scale probably covering only several 100km². Even so, they are a good, small-scale model for the larger (global?) existence of anoxia during mass extinction events, such as at the end of the Permian Period (~250 million years ago), while the “normal” limestones and shales deposited above them (and containing fossils) indicate how life and environments recover afterwards.

Before testing any hypotheses of mass extinction and recovery, it is necessary to show that rocks in geographically separated locations can be correlated, or shown to be coeval. Locality 5 of Pabian and Diffendal (2003) is assumed to be correlative to their Locality 10, but they correctly note that it was only a few years before thought to be from a different formation, and several million years younger (Holterhoff and Pabian, 1990). Correlative rock units in this study are assumed to contain fossils with the same size characteristics. In order to test a hypothesis that Localities 5 and 10 are correlative, the size frequency distributions of one of the most distinctive and well-preserved species, the brachiopod *Dyoros* sp., were statistically compared.

Significance for Astrobiology

Anoxic events as preserved in the stratigraphic record on Earth are related to space science via the interdisciplinary sciences of Astrobiology and Exobiology. The current guidelines for NASA-supported studies of this type are the Astrobiology Roadmap (Des Marais et al., 2008). This paper addresses GOAL4 – “Understand how life on Earth and its planetary environment have co-evolved through geological time. Investigate the evolving relationships between Earth and its biota by integrating evidence from the geosciences and biosciences that shows how life evolved, responded to environmental change, and modified environmental conditions on a planetary scale.” Objective 4.3 within GOAL 4 is to investigate the effects of extraterrestrial and terrestrial events upon the biosphere, with research based on the fossil record of life and its activities. Evidence of the timeliness of such studies is the fact that a complete session, entitled, “Oxygen and Evolution: Looking to the Past” was devoted to anoxic black rocks and their associated fossils in the most recent Astrobiology Science Conference 2012 (NASA, 2012).

Location

Carboniferous age rocks are sporadically exposed in road and stream cuts throughout southeastern Nebraska. Localities 5 and 10 (Figure 1) are both road cut exposures of the Carboniferous rocks in Richardson County, Nebraska, separated by approximately 10 miles of geographic distance. The land cover between the two localities is mostly agricultural, making exact correlations, and even formation identification, difficult.

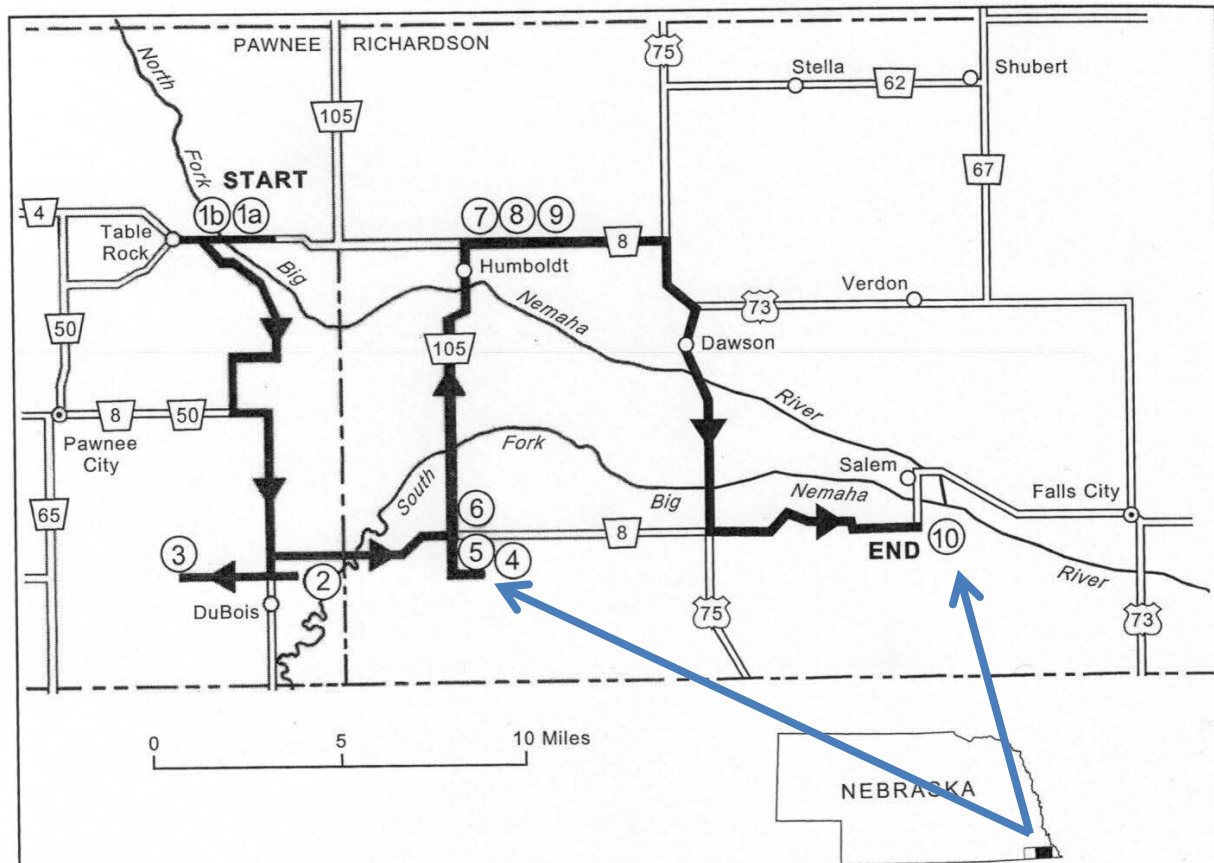


Figure 1 – Locality map of Carboniferous localities in southeastern Nebraska (adapted from Pabian and Diffendal, 2003). Localities 5 and 10 are indicated with arrows.

Methods

Specimens of *Dyoros* sp. were collected in the field using both surface collection and bulk sampling methods. These have been shown previously to be an efficient method of maximizing species richness and biomass values. Both localities (5 and 10 of Pabian and Diffendal, 2003) were sampled for equal duration over relatively equal surface areas. In addition, the field collections were supplemented by previously collected specimens from the same sampling localities now deposited in the University of Wisconsin-Whitewater Invertebrate Paleontology collections. All *Dyoros* sp. specimens (N=103 from Loc. 5; N=257 from Loc. 10) were identified, sorted from the other taxa, counted, and measured for length and width (Figure 2) using digital calipers.

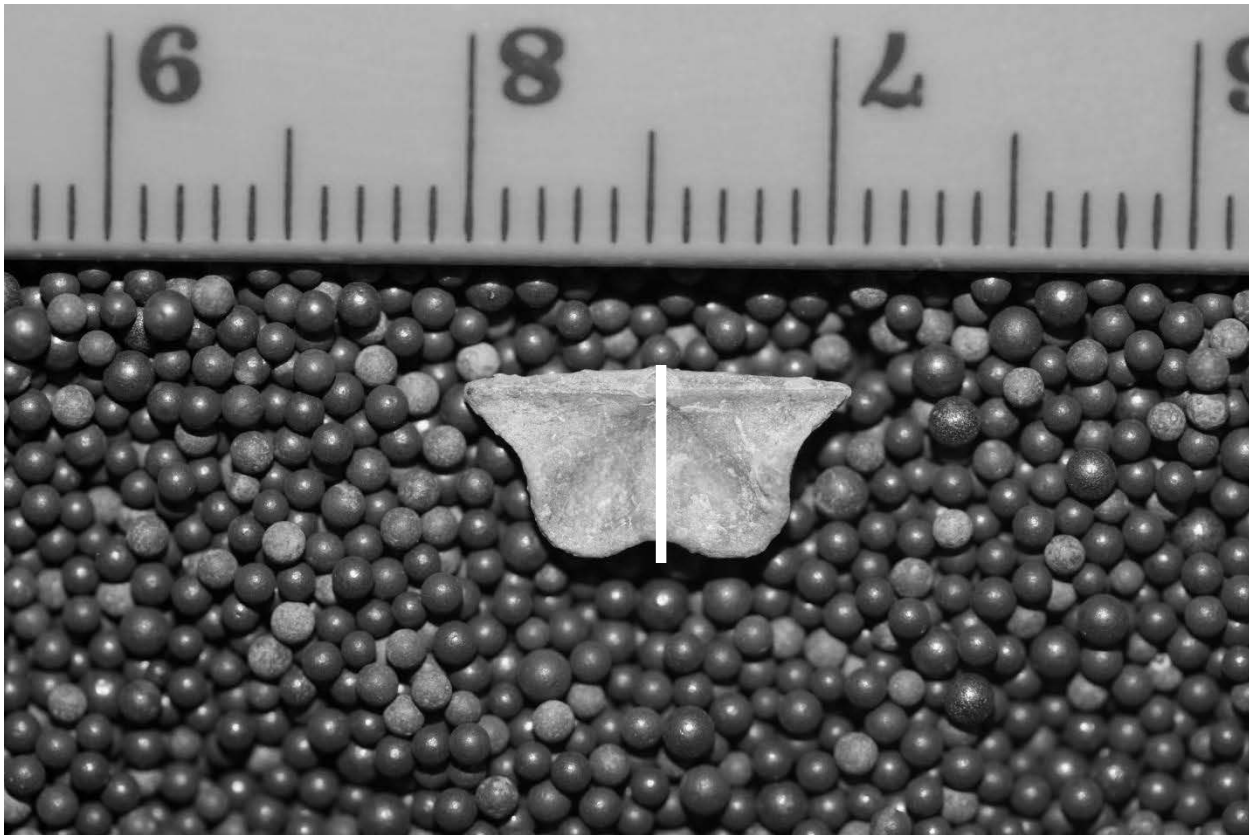


Figure 2 – Ventral view of *Dyoros* sp. from the Hughes Creek Shale. White bar indicates the standardized length measurement for all individuals. For the individual shown, length = 12.73mm.

All statistical analyses were performed using the software package, PAST (Hammer et al., 2001). Measurements of the length of unbroken specimens were log-transformed as is standard in biometric analyses (Zelditch et al., 2012) and tested for normality using the Shapiro-Wilk test. The Mann-Whitney U and Kruskal-Wallis tests were used to test hypotheses of equality of medians, and the Kolmogorov-Smirnov test was used to test a hypothesis of equality of distributions for the two sampling localities.

Results

Though both the distributions for Localities 5 and 10 appear normally distributed (Figure 3), Shapiro-Wilk tests for their normal distribution are rejected for Locality 5, $p(\text{normal}) = 3.009e^{-05}$; but not for Locality 10, $p(\text{normal}) = 0.06558$. Since at least one of the distributions is not normal, non-parametric statistical tests were used for further testing.

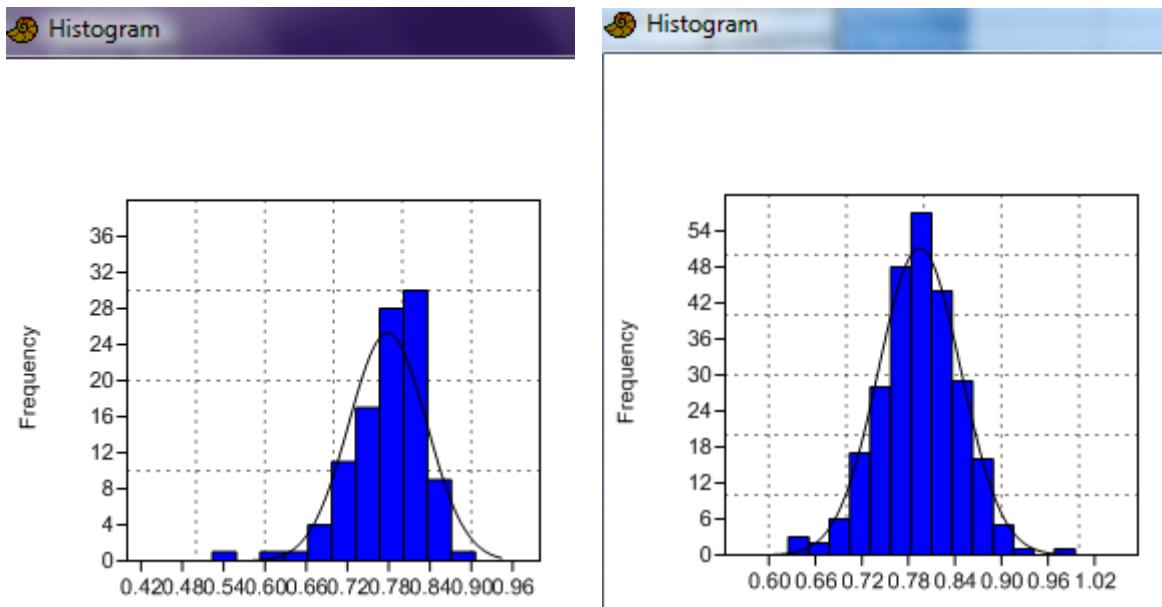


Figure 3 – Size frequency distributions for log-transformed mm length measurements (x-axis) of *Dyoros* sp. at Locality 5 (right) and Locality 10 (left).

Both the Mann-Whitney U and the Kruskal-Wallis are used with non-normal distributions tests for a null hypothesis that two samples are taken from populations with equal medians. Values greater than 0.05 would fail to reject such hypotheses, and thus one could not say that the medians of the two distributions had different medians. Both the Mann-Whitney ($p=0.05217$) and the Kruskal-Wallis ($p=0.0521$) fail to reject the null hypothesis.

The Kolmogorov-Smirnov can test a null hypothesis of equality of overall distributions for non-normal data. For a null hypothesis that the two samples are taken from populations with equal distributions, p values greater than 0.05 will fail to reject, and one could say that the two samples had different distributions. The Kolmogorov-Smirnov ($p=0.1563$) thus fails to reject the null hypothesis.

Discussion and Conclusions

Body size is an important population characteristic for all marine animals, but especially so for suspension feeding organisms, such as the brachiopod *Dyoros* sp., because the size of the body has a direct effect on the availability of food particles moving around an obstructive skeleton (Humphries, 2007). In general, larger body sizes can be viewed as a positive factor in feeding, with increased size meaning increased size of flow (and thus, food) vortices shed around a suspension feeding organism. If the ambient environment were different in the original seas existing at Localities 5 and 10, such as would be expected if the two localities were not coeval,

then the expectation would be that this should be reflected in different body size distributions between localities for populations of the same species, like *Dyoros* sp.

At the community level, body size distribution has proven useful in describing variation both within and between modern (Robson et al., 2005) and ancient (Payne, 2005) communities. The relative body size distributions of any member species may control the species composition and relative abundances, influencing community function. Again, if Localities 5 and 10 were not coeval, then the expected, different body size distributions of suspension feeding species like *Dyoros* sp. would produce cascading effects throughout numerous species of the communities, which are simply not observed for Localities 5 and 10.

The failure to reject null hypotheses of the equality of medians (Mann-Whitney and Kruskal-Wallis tests) and equality of distributions (Kolomogorov-Smirnov test) supports the correlation of Localities 5 and 10 of the Hughes Creek Shale. This then fails to reject an informal hypothesis that the two localities preserve coeval beds of strata. The rejection of the earlier interpretation of Holterhoff and Pabian (1990) by Pabian and Diffendal (2003) is supported by the evidence presented here.

Confident that Localities 5 and 10 are indeed coeval, they can both be used in aggregate to examine the recovery of marine fauna after recovery after a small-scale anoxic event covering at minimum, the ~10 mile distance between them. Both localities are highly fossiliferous, and their summed diversities and body size distributions for all taxa, including *Dyoros* sp., as shown here, add to their robustness as an astrobiologic model for the extinction and recovery of taxa during larger-scale extinctions.

Bibliography

Des Marais, D., J. A. Nuth, III, L. Allamandola, A. P. Boss, J. D. Farmer, T. M. Hoehler, B. M. Jakosky, V. S. Meadows, A. Pohorille, B. Runnegar and A. M. Sporman. 2008. The NASA Astrobiology Roadmap. *Astrobiology*, 8(4): 715-730.

Hammer, O., Harper, D. A. T. and Ryan, P. D. 2001. PAST: Paleontological statistics software package for education and data analysis. *Palaeontologica Electronica*, 4(1): 1-9.

Holterhoff, P. and R. K. Pabian. 1990. Paleoenvironmental implications of a pyritized molluscan fauna from the Bennett Shale Member, Red Eagle Formation (Lower Permian), Richardson County, Nebraska. *The Compass*, 67(1): 35-46.

Humphries, S. 2007. Body size and suspension feeding, Pp. 16-32, In Hildrew, A., D. G. Raffaelli and R. Edmonds-Brown (eds.), *Body Size: The Structure and Function of Aquatic Ecosystems*. Cambridge University Press, Cambridge, England.

NASA. 2012. <http://abscicon2012.arc.nasa.gov/abstracts/>

Pabian, R. K. and R. F. Diffendal, Jr. 2003. Late Pennsylvanian and earliest Permian cyclic sedimentation and paleoecology in southeastern Nebraska. In Niemi, T. (ed.) Geologic Field Trips in the Greater Kansas City area. Missouri Geological Survey, Special Publication, pp. 35-52.

Payne, J. L. 2005. Evolutionary dynamics of gastropod size across the end-Permian extinction and through the Triassic recovery interval. *Paleobiology*, 31(2): 269-290.

Robson, B. J., L. A. Barmuta and P. G. Fairweather. 2005. Methodological and conceptual issues in the search for a relationship between animal body-size distributions and benthic habitat architecture. *Marine and Freshwater Research*, 56: 1-11.

Zelditch, M., D. Swiderski and H. D. Sheets. 2012. *Geometric Morphometrics for Biologists; A Primer*. Second Edition. Elsevier, Amsterdam, 478pp.

24th Annual Wisconsin Space Conference

PART FOUR

Team Projects

2014 WSGC Elijah High-Altitude Balloon Payload Project

Final Report

August 15, 2014

Jadee Kellogg¹, Madeline Lambert², Danny Ochoa³, Evan Schilling³, Michael Stefik⁴, Michael Wiznitzer³

¹Ripon College, ²University of Wisconsin-La Crosse, ³Milwaukee School of Engineering, ⁴University of Wisconsin-Milwaukee

Abstract

The purpose of this paper is to discuss the development and findings of the experiments performed on the high altitude balloon payload. After some bonding time in the beginning of the summer, the team got together and decided on the four following experiments: Atmospheric Electric Field, Breakdown Voltage, IR Imaging, and Solar Efficiency/Payload Spin. Subsequently, research and fabrication began which involved learning new skills such as Arduino programming, 3-D modeling, foam cutting, and more. The launch was successful, and the results retrieved were more or less what were expected. This internship opportunity proved to be an amazing learning experience for the team which will be valued for each of their future career experiences.

Introduction

The objective for the team this summer was to design experiments to send up in a high altitude balloon, and successfully collect and analyze data from said experiments. The team was given a budget, size and weight restrictions, and then given free reign as to what they wanted to research. The team decided on four projects: Atmospheric Electric Field, Breakdown Voltage, IR Imaging, and Solar Efficiency/Payload Spin.

Payload Structure

In order to safely house the experiments, two unique payload structures were designed and constructed. The two capsules, shown in Figure 1, were both constructed with an interior birch aircraft plywood frame and an exterior shell made of polystyrene insulation. The capsules were then wrapped in an aluminized mylar foil which insulates the capsules during the flight.



Figure 1: Primary capsule (top right) & secondary capsule (bottom left)

Thank you to WSGC for the financial support, and Dr. Farrow for the guidance.

The primary capsule had a cylindrical shape with a one foot diameter and was one foot tall. This capsule also featured a passive stabilization ring. For the ring, a forty-eight inch diameter hula hoop was used. Because the hula hoop had a much larger diameter than that of the payload, it significantly increased the moment of inertia of the capsule, which led to a substantial decrease in the rotational velocity of the payload. The stabilization ring was supported by two fiberglass dowels which also held on the conductive spheres for the electric field experiment.

In order to determine the minimum size of the beams in the frame, an estimation was done using a cantilever beam with a length equal to that of the radius of the payload. The following equation for bending stress was used:

$$\sigma = \frac{-m \frac{h}{2}}{\frac{1}{12}bh^3}$$

where m is the maximum bending moment (60 in-lb), σ is the average maximum stress, in our case 6114.356 psi (Handbook of Finnish Plywood), b is the thickness of the plywood (3/16 in), and h is the plywood width, which we are solving for. This calculation yields a minimum width of 0.56 inches. Based on this width, the frames for the two capsules were designed. The primary capsule was broken into two halves. The frames for the top and bottom halves are shown in Figure 2 and Figure 3 respectively.



Figure 2: Primary capsule upper frame



Figure 3: Primary capsule lower frame

The four pegs which protruded down from the upper frame meshed with the extrusions on the ring of the lower frame and held the two halves together. The sheet metal pieces on the rings of the two frames supported the fiberglass dowels that ran through the payload and also served as part of the locking mechanism. Located around the vertical ribs of the frame were “shelve” features that served as an attachment point for the electronics board. The electronics board in the primary payload held all of the electronics for the experiments, as well as a few sensors which recorded the dynamic motion of the payload, as well as atmospheric data.



Figure 4: Secondary capsule lower frame



Figure 5: Secondary capsule lid

The lower frame and lid for the secondary capsule are shown in figure 4 and figure 5 respectively. The platform on the lower section supported the breakdown voltage electronics. The supports protruding out from the platform corresponded with the slots on the lid and locked the two together. A bolt was then run through the hole in the lid and lower section and prevented the two parts from coming apart.

Atmospheric Electric Field Experiment

Electric fields surround us everywhere. They do many useful things for us in the form of electricity, but are not directly observable through any of our senses. As such, they require specialized equipment to measure and visualize them. Figure 6 shows a depiction of “Earth’s Electrical Environment” (National Research Council, 1986), providing an idea of how unique and varied the electric fields are that exist in our atmosphere.

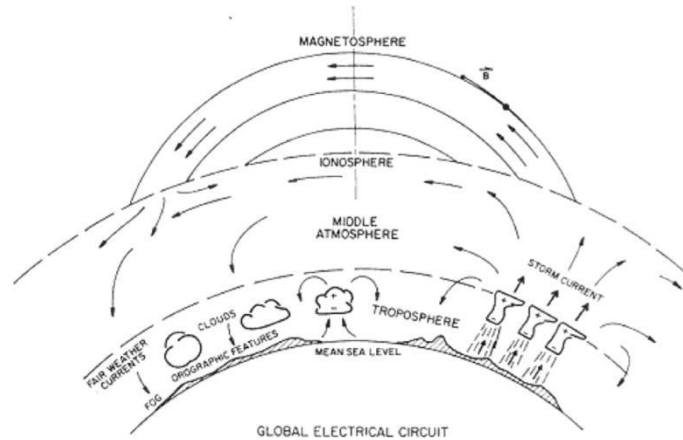


Figure 6: Schematic of electrical processes in the global electric circuit

Purpose: Balloon-borne atmospheric electric field measurements have been taking place since the late 1960s. A common method developed, known and documented as the “double Langmuir probe technique” (R. H. Holzworth and E. A. Bering III, 1998), is used for performing these measurements. Our team sought to replicate the aforementioned method to successfully construct an electric field measuring setup and use it to visualize the field above southern Wisconsin during the balloon flight.

Method: After analyzing an overview of the method, the team set out to design custom hardware in order to build a device capable of performing electric field measurements on our payload. This began with a simple simulation of the technique, which helped us gain insight into how it worked physically. This simulation, performed in the Falstad 2D Electrostatics Applet, is shown on the right in Figure 7.

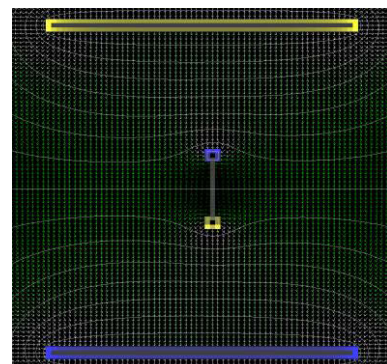


Figure 7: Falstad electric field simulation

From this simulation, the team was able to visually see the basic principle of the method: a voltage potential, produced by the electric field forcing a separation of charge, develops across the probes. If a differential voltage measurement is done using an instrument op-amp with the two probes as the positive and negative terminals, a voltage difference that is proportional to the field strength in that direction is obtained. To get a final magnitude value, the voltage difference is simply divided by the separation length, giving us Volts/Meter. The direction can be obtained by watching the rotation of the probes about their vertical axis; whatever the magnetic direction is at the time of a voltage difference maximum, that is the direction of the field (maximums occur when parallel to the electric field gradient, minimums when perpendicular).

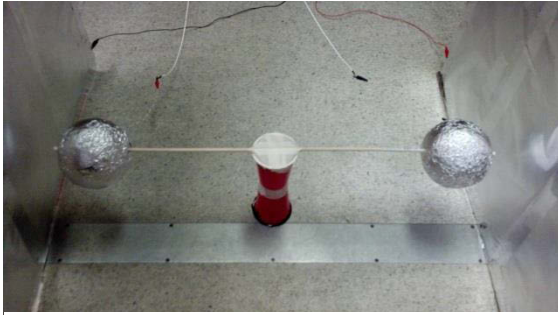


Figure 8: The test setup used to verify the technique

A test setup was then constructed. This consisted of an INA116 as the instrument op-amp, an LM324 used as a 2nd order low-pass filter (10Hz cutoff), two Styrofoam spheres covered in aluminum foil connected by a wooden dowel as the double probes, and two RG188A/U coaxial cables to connect the probes to the instrument op-amp. Two large metal plates (3x3' area) built using aluminum foil and cardboard were used to generate a test electric field. This whole setup was placed within a Faraday cage and is pictured above in Figure 8.

After an external field was applied to the large metal plates using a function generator, a received signal was picked up on the probes and plotted on an oscilloscope. A square wave was successfully received but with ramped planes shown in Figure 9;



Figure 9: Square wave received on scope

this was due to the small but noticeable input leakage (advertised on the order of 10^{-15} amps but measured in lab to be at 10^{-13} amps).

Results: The electronics were placed within a shielded 3d printed enclosure; this enclosure was then put inside of the main payload and hooked up to the payload data logger. The final probes were Styrofoam spheres covered with conductive carbon spray separated at 1 meter by a fiberglass boom. The final setup can be seen in Figure 10.



Figure 10: Final payload assembly with field probes

Once the analog data was obtained, a program was written in Python using Enthought Canopy to generate electric field vectors of a certain magnitude at each altitude. Yaw rotation data was taken from the on-board IMU in order to find the direction of the field. Figure 11 shows the final output; the

altitudes are listed in feet, the magnitudes in Volts/Meter, and the direction in magnetic degrees (0° is magnetic north).

The plot shows we were successful in what we set out to do; a definite trend in the high-altitude data is shown, indicating that a field was detected. The magnitude did not correspond to what we see in scientific papers on the subject, but this gain error could likely be adjusted for future flights to give us more accurate data.

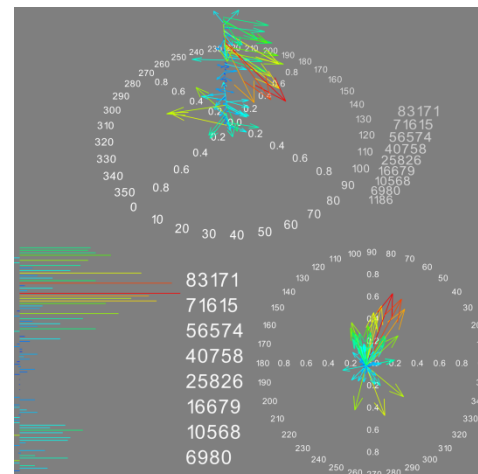


Figure 11: Visualization of the atmospheric electric field

Breakdown Voltage Experiment

Purpose: Breakdown voltage is a property innate to insulators. When the correct voltage is applied, the insulator begins to conduct electricity. This is especially important to take into account with high voltage circuits, as sparking may occur between components if the breakdown voltage of air is exceeded between them. The breakdown voltage spark gap experiment was designed to test the effect of the changing atmospheric conditions with the differing altitudes on the breakdown voltage of air.

Method: Using Paschen's Law, $V = \frac{Bpd}{(C + \ln(pd))}$, where p is the pressure in torr, d is the gap length in centimeters, and B and C are constants specific to the different substance, a Paschen's curve was calculated as an estimate for the breakdown voltage of air at high altitude with a half centimeter gap (Figure 12). In order to reach the appropriate voltage, approximately 1000 volts was required. Given the size and weight restrictions, creative measures had to be taken as to how to produce that voltage. A circuit similar to the one shown in Figure 13 was used, replacing the Geiger tube with the spark gap, and removing the speaker. The spark gap was constructed using two wooden spheres covered in copper tape, mounted on a 3D printed stand. Using a nine volt battery as the power source, a CCFL inverter and voltage doubler were responsible for ramping up the voltage. A digital potentiometer was put into the circuit and controlled via an Arduino nano. It took one minute and 32 seconds to ramp up to the 900 volt maximum, and three minutes and 37 seconds to be brought back down to its minimum voltage, 208. A delay was then set before repeating the cycle. For the first six repetitions of the cycle, this delay was ten minutes. Afterwards, the delay was then set to two minutes. The interrupt function of Arduino coding was utilized so that every time a spark occurred, the time stamp was put into the EEPROM of the nano. In order to protect the nano from a large voltage spike, two resistors were placed in the circuit to bring down the voltage to the manageable five volts maximum. An opto-isolator and an op-amp were also used to further isolate the nano from the high voltage.

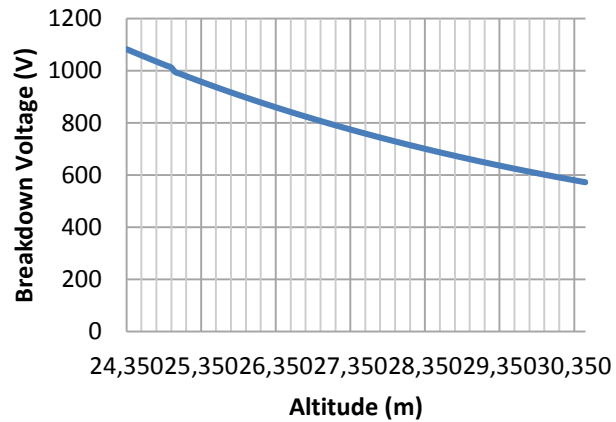


Figure 12: Chart of Breakdown Voltage vs. altitude with a half centimeter gap length

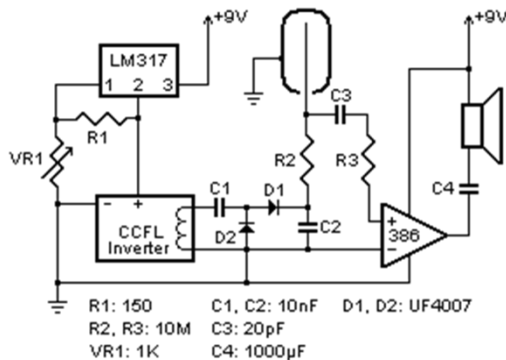


Figure 13: Similar circuit to the one used for the breakdown voltage experiment, found at <http://adammunich.com/geiger-muller-tubes/>

Results: Using a separate Arduino code, the EEPROM was read back. It contained one time stamp at 45 minutes and 17 seconds into the flight. After further examination of GPS data (shown in Figure 14), this was found to correspond to an altitude of approximately 28,346 meters, or about 93,000 feet. Using Paschen’s Law and the pressure data from the payload electronics, the calculated breakdown voltage at the time the spark occurred was 848.6 volts.

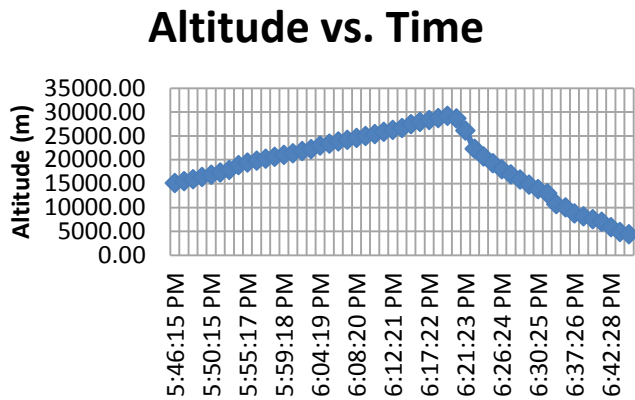


Figure 14: Graph of GPS data collected by secondary tracking payload

The actual voltage at this time was 840. This could be due to humidity or moisture entering the payload container, or various other environmental factors.

One spark is not enough to draw reliable or precise conclusions. If the experiment were flown again, the delay time could be shortened, as could the gap length, to allow for more sparks to occur. However, the one data point retrieved did correlate with the predictions made, which is promising for any future attempts at recreating the experiment.

Infrared Imaging

Purpose: The Infrared (IR) imaging project was developed with the goal of analyzing plant and crop health at various altitudes. This experiment was conducted using a Canon camera which utilized special software to take time lapse photos. An external filter system was also built with both visible and IR imaging filters. Crop health can be tracked after the IR and visible light images are combined to form a Normalized Difference Vegetation Index (NDVI) picture.

Method: The initial step of the project was working with the Canon A1200 camera. The Canon A1200 was chosen because the other camera possibility, the Canon A495, failed to properly allow the desired time lapse function to work. The Canon A1200 cooperated with the preferred method, the Canon Hacker Development Kit (CHDK) software, and the software was successfully downloaded onto it, in order to give the camera time lapse functionality. CHDK was programmed to take pictures every four seconds for the duration of the flight. The camera also had its internal IR blocking filter removed so the external filters could be used. The two filters, visible and infrared, were designed to be mounted externally from the camera and controlled by a Servo motor using the Arduino Mega. A camera housing was designed to have three main functions: to securely hold the camera, to serve as an attachment point for the servo motor, which was mounted externally from the main housing using a sheet metal bracket and small bolts to firmly hold it in place, and to house and protect the filters, which were mounted into a filter switching mechanism that slid within the camera housing. This mechanism functioned using two arms; one connected to the Servo, and the other connected to the filter mount. After watching how the Servo rotated the mechanism, the proper initial and final angles were chosen. Both the camera housing and the filter switching mechanism were 3D printed using the MakerBot 2X. When ready to run the experiment, CHDK and the filter switching mechanism were manually

synced. Electronically syncing up the Arduino and Servo with the CHDK software was researched extensively and there was no practical method to align both systems in time. As added protection, four hand warmers were included in the payload to keep the camera warm enough to take pictures throughout its entire flight.

Final data and results: On launch day, while other balloon preparations were being made, the four hand warmers were attached to the payload's interior frame. When the electronics were ready to be turned on, the Servo was activated and the camera's CHDK program was manually synced with the rotations. Once finished with the camera preparations, the payload was then passed along so other experiments could be initiated. This is believed to be the cause of our malfunctioning filter switching mechanism. Since no visible light images were obtained throughout the flight, the mechanism must have become blocked with debris while sitting on the ground before the launch. In order to use the data we had gotten, in the form of IR pictures, Google Earth Images were used as the comparable visible light picture. This, of course, is not an accurate method to analyze the plant health in the area of Mt. Horeb on the day of the launch. However, as the Google Earth Images used were only a couple months old, the NDVI pictures are a representation of the expected results. Below, Figure 15, is an IR picture our camera took during flight. The picture on the right, Figure 16, is the visible light picture taken from Google Earth. After combining the two pictures using the proper formula, in a photo editing program named Gimp, we came up with the NDVI picture, Figure 17.



Figure 15: IR picture taken during flight

Figure 16: Google Earth picture

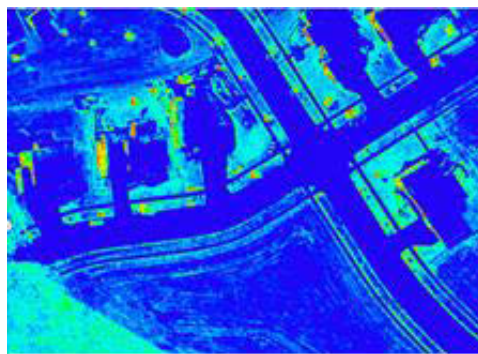


Figure 17: NDVI picture

The trees along the edge of the street are a yellow/orange. Some people's yards are a brighter blue than others. The idea is that the warmer the colors, the healthier the area should be. The houses and the concrete are a dark blue because they do not produce any heat. Although it cannot be confirmed that these results are 100% accurate, the general concept was proved.

Solar Cell Experiment

Purpose: As technology becomes more advanced, much research is put into energy conservation so that people can save money and the world can become a greener place. One such method is the use of solar cells to convert the sun's light into usable energy. The goals of this experiment were to explore how efficient solar cells are in this converting process relative to altitude and temperature and also how effectively they can be used to measure rotation of an object.

Method: Efficiency is calculated by dividing the solar cell output power by the amount of the sun's light that is hitting the solar cell, as described in the equation: $\eta = \frac{P_{output}}{P_{input \times Area}}$ (Honsberg & Bowden). As these particular solar cells used for the experiment were 73x74mm rated 3.6V at 50 mA, it was calculated that the maximum rated power they could produce was 0.18 watts, for an efficiency of about 3.33%, assuming a resistance of 72 ohms and that the sun's intensity was 1000 watts/m² on Earth's surface. This resistance was calculated by dividing the rated current by the rated voltage using Ohm's law and was also verified experimentally to be the optimal resistance where the solar cells produced the maximum power. Due to the molecular processes that occur in a solar cell, it was hypothesized that solar cells would become more efficient at colder temperatures, which means that the efficiency should peak between 50-60,000 feet in Earth's atmosphere where it's the coldest, almost negative 70°C (Solar Cell Efficiency, 2009). It was also assumed that the efficiency would generally increase with altitude, since there would be less sunlight absorption the higher up in Earth's atmosphere (Andrew, 2011). It should be noted the sun's intensity was always assumed to be 1,000 watts/m² regardless of altitude, so it was only presumed the efficiency would increase due to higher power output of the solar cells. This might not actually reflect the actual efficiency of the solar cells, since even though the power output could be higher, the efficiency could nevertheless still be lower. For future endeavors, the solar irradiance should also be measured with altitude.

The spinning behavior of the payload was determined by mounting four solar cells, one in each direction, on the payload at 45° angles. This angle was chosen for two reasons. One is the fact the efficiency of the solar cell is greater when placed in the most optimum angle towards the sun (which in August in Madison is about 55° from the vertical at solar noon which was near the time of the launch) (Solar Angle Calculator, 2014). The other was so that the solar cells would be sufficiently angled enough that only one of the four solar cells would have the maximum output voltage at any given time. The idea would be then to keep track which of the four solar cells had the maximum output voltage, which would then be able to be processed to output if the payload was turning counterclockwise or clockwise. Additionally, a graph of the rate of rotation would also be generated and compared to the one generated by the IMU (Inertial Measurement Unit) for comparison to see if they looked the same as was hypothesized.

Final data and results: The flight was fairly successful, and the hypotheses for the solar experiments were confirmed for the most part. The efficiency results are shown below in Figure 18 and were calculated by only pulling the power values generated from the solar cell that was directly facing the sun during the flight (the cell that had the highest power value of the four solar cells).

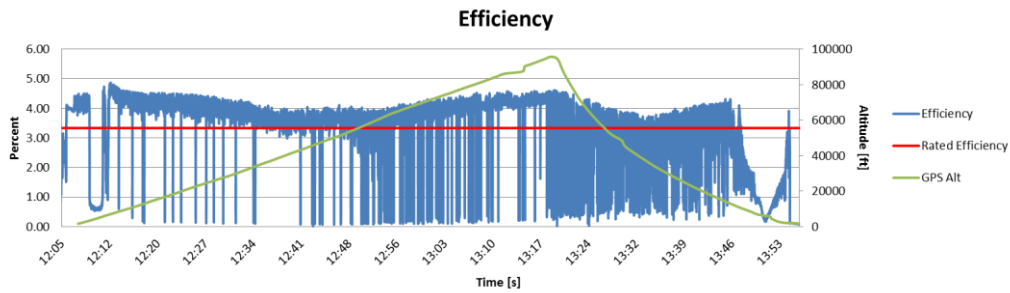


Figure 18: Relationship between efficiency and altitude over time

The red line symbolizes the rated efficiency of the solar cells which was at around 3.33%. As can be clearly seen, the efficiency was above that for the entire flight, ranging between 4 and 4.8%. It peaked near 7,000 ft. at 4.87%, when the payload reached its highest altitude at around 96,000 ft. at 4.61% (which makes sense due to higher sunlight intensity), and also at 14,000 ft. at 4.31% but not at the other expected range between 50 and 60,000 feet. Unfortunately, the temperature sensor output skewed results because of the hand warmers inside the payload, so the data could not be used to see if the temperature was actually colder at those altitudes. One theory could be the fact that the optimum solar angle mentioned before was not constant throughout the flight and was at its optimum only when the payload reached 7,000 ft. on the way up and 14,000 ft. on the way down. To get more accurate results, a solar tracker can be used to keep the solar cell at the optimum angle towards the sun, and the actual temperature of the solar cell can be monitored as well.

The other experiment proved to be an effective method of measuring payload spin and rate of rotation. The results are shown below in Figures 19-21:

Spinning Behavior

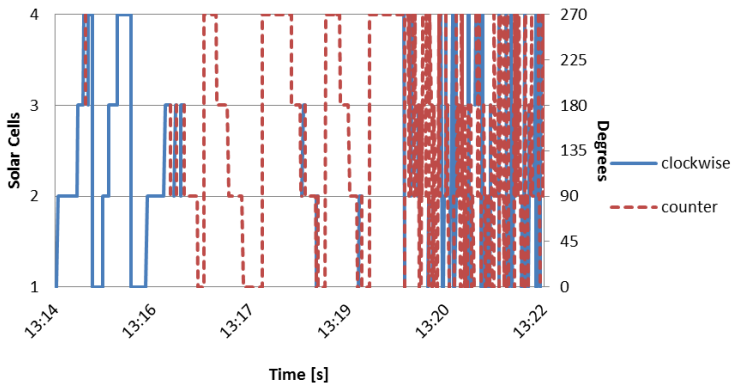


Figure 19: Solar cell spinning behavior

Voltage Change Rate from Solar Cells

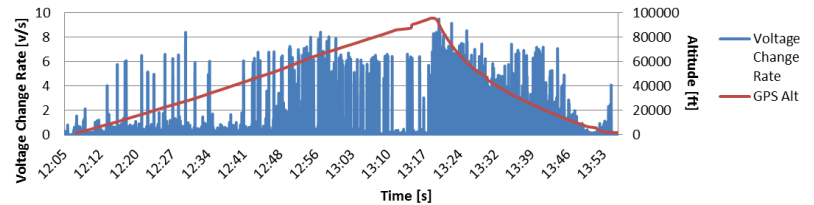


Figure 20: Results generated from solar cells

Rotation Rate from IMU

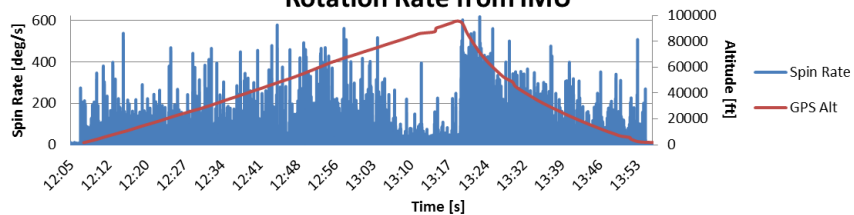


Figure 21: Results generated from IMU

As shown above in Figure 19, one can see at what points the payload turned and if it was turning counterclockwise or clockwise. It can also be observed that the balloon popped at 1:19pm because that is when it begins to spin rapidly. Figures 20-21 show that the rate graphs generated

from the solar cells and the IMU are very similar, proving that using solar cells to measure rotation rate is a feasible method.

Conclusions

Each of the separate experiments achieved their objectives. With the specified alterations to each part of the project, better and more accurate results could be obtained with another launch. All in all, the project went well, with all the team members collaborating to ensure its success.

References

- Andrew. (2011, March 2). "Natural Frequency." Retrieved August 7, 2014, from Solar Radiation: <http://naturalfrequency.com/wiki/solar-radiation>
- "Enthought: Scientific Computing Solutions," Enthought, Retrieved July 2014, from <https://www.enthought.com/products/canopy/>
- Falstad, P., "Falstad Math and Physics: EM Static Applet," Retrieved July 2014, from <http://www.falstad.com/emstatic/index.html>
- Handbook of Finnish Plywood*,
http://www.upm.com/cn/products/plywood/Documents/Handbook_EN.pdf
- Holzworth, R.H. & Bering III, E. A., "Ionospheric Electric Fields From Stratospheric Balloon-Borne Probes," *Measurement Techniques in Space Plasmas: Fields*, vol. 103, Washington, SC, American Geophysical Union, 1998, pp. 79-84.
- Honsberg, C., & Bowden, S. (n.d.). "PV Education." Retrieved July 6, 2014, from PVeducation.org: <http://pveducation.org/>
- "Insulator Breakdown Voltage." All About Circuits. Retrieved June 2014, from http://www.allaboutcircuits.com/vol_1/chpt_12/8.html
- Munich, Adam. (2012). "Geiger-Müller Tubes." Retrieved June 2014, from <http://adammunich.com/geiger-muller-tubes/>
- National Research Council, The Earth's Electrical Environment, Washington, DC: The National Academies Press, 1986.
- "Paschen's Law." Retrieved June 2014 from <http://www.donbot.com/Enerbot/LENR/LENR5-Engine/LEN019PaschenzLaw.html>
- Solar Angle Calculator. (2014). Retrieved July 6, 2014, from Solar Electricity Handbook: <http://solarelectricityhandbook.com/solar-angle-calculator.html>
- Solar Cell Efficiency. (2009). Retrieved July 6, 2014, from Solar Power information: <http://www.solarpower2day.net/solar-cells/efficiency/>

The Onset of Normal Field Instability in a Ferrofluid in a Reduced Gravity Environment.

Krull, Brendan; Rundle, Tessa; LeCaptain, Kevin; Barhite, Justin; Gear, Amelia
Carthage College Physics Dept.

9/14/14

Abstract

A ferrofluid is a magnetic liquid comprised of nanoscale ferrous particles suspended in a low-viscosity carrier fluid. When subjected to a magnetic field, the surface of a ferrofluid deforms into peaks and valleys along the magnetic field lines. The onset of surface deformation is called the normal field instability. The theory describing the NFI identifies a critical magnetic field below which no magnetically driven surface deformations occur. The critical field depends on the gravitational acceleration and, according to the theory, should disappear as local gravitational acceleration approaches zero. While there have been previous demonstrations of the normal field instability in a reduced gravity environment, data has been inconclusive on the existence of a critical magnetic field in reduced gravity. For our work, we designed a sounding rocket payload for a suborbital rocket mission. Our experiment incorporates a ferrofluid sample and a uniform magnetic field which can be varied across a discrete range of values to observe surface deformations at different applied fields. During the microgravity portion of the rocket's flight, we obtain video of the ferrofluid's behavior and compare it to data taken in Earth's gravity. A team of five undergraduate students designed and built the payload that will characterize the role of gravity in setting the critical magnetic field strength for the onset of the NFI. Data will be used to further understanding of ferrofluid behavior in a microgravity environment to advance its use in various space-based applications.

Mission Requirements and Description

Our objective was to record video of a ferrofluid's response to various external magnetic fields in microgravity and compare it to the response on Earth. Additionally, we expected to find a difference between the critical fields required to induce the deformation in microgravity in Earth's gravity. To do this, at least one video of the ferrofluid's deformation through a series of magnetic field levels in microgravity would have to be collected. A magnetometer would record the magnetic field level being applied at each specific time.

In order to have liquids aboard our flight, our experiment needed to be inside of a secondary containment vessel, to protect the other experiments in case of a leak. The Rocksats team from the previous year had a secondary containment vessel made, so our experiment had to fit inside that space.

Previous work done by Friedrichs and Engel^[1] theorizes the effect of gravity on the deformation of ferrofluid in a magnetic field.

We would like to thank Dr. Kevin Crosby for his supervision during the project, as well as the generous support from the Wisconsin Spacegrant Consortium.

The critical magnetic field for a ferrofluid is shown in equation 1, assuming an infinite plane of ferrofluid with an arbitrary depth d being acted upon by a magnetic field H perpendicular to the ferrofluid plane.

$$H_{c,\infty} = \sqrt{\frac{(1 + \chi)(2 + \chi)\sqrt{g\rho\sigma}}{\chi^2\mu_0}} \quad (1)$$

The critical magnetic field of the ferrofluid is determined by the magnetic susceptibility χ , ferrofluid density ρ , ferrofluid surface tension σ , the applied gravitational acceleration, and the permeability of free space.

The distinction between the magnetic field H and the magnetic field B is that H is the measurement of magnetic field strength used for magnetic dipoles, and would be used to calculate the force between, say, two bar magnets. H is relevant in this case, because a ferrofluid is analogous to many tiny interacting bar magnets. B is the magnetic field that would come from a current-carrying wire. In order to create a magnetic field H inside the ferrofluid, we would need to apply the proper outside magnetic field B . The conversion between these two is shown in equation 2, which is accurate to within 5%.^[1]

$$B = \mu_0(1 + \chi)H \quad (2)$$

When the magnetic field H is above the critical magnetic field, waves begin to form on the ferrofluid's surface. The separation between the peaks of these waves is governed by their wave number k .

$$k_{c,\infty} = \sqrt{\frac{\rho g}{\sigma}} \quad (3)$$

Equation 3 describes the wave number for a ferrofluid when the magnetic field H is equal to H_c . This is equal to $\frac{2\pi}{\lambda}$, where λ is the peak separation at the critical magnetic field.

Using values of susceptibility and surface tension for our ferrofluid found at MIT^[2], the equations suggest that the critical magnetic field B for the ferrofluid is between 22.8 and 27.1 G, and that the peak separation λ at the critical magnetic field is between .24 and .33 mm.

According to this equation, during microgravity, the ferrofluid would be expected to form peaks when exposed to any magnetic field.

Payload Design

Our payload was designed to record the reaction of a ferrofluid once a constant magnetic field was applied. We decided to use a pair of Helmholtz coils to produce the magnetic field. Helmholtz coils produce a nearly uniform magnetic field between them when they are positioned at a distance equal to their radius away from each other. We decided this was the best option because it would allow for a constant magnetic field while still allowing for clear visibility of the ferrofluid. At the center of the coils we needed a small capsule containing the ferrofluid. After testing the ferrofluid in different containers, we determined that it would be necessary to use a glass container to prevent the ferrofluid from staining the container and making the deformations difficult to see. We then decided to position 2 small cameras on the same plate as the ferrofluid container to record video during the experiment. Initially, we wanted to obtain videos at a side view and a top view, but after deciding on a container with an opaque lid, we decided to put both cameras on the same plate as the ferrofluid and get two views of the capsule.

In order to power the experiment we would house all of the electronics and batteries at the top. The only major design change came after it was discovered that the operational amplifiers could not source enough current to power the coils without overheating itself. We then decided to use relays to control power to the coils.

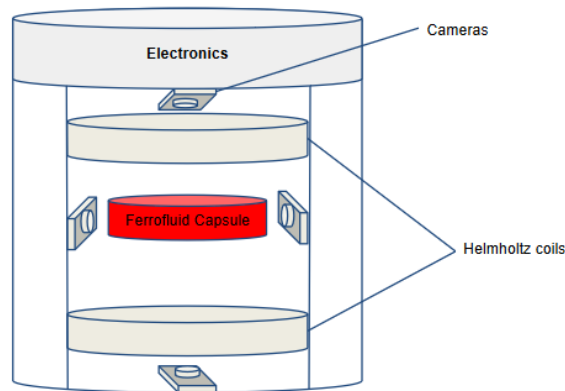


Figure 1. Initial payload design concept.

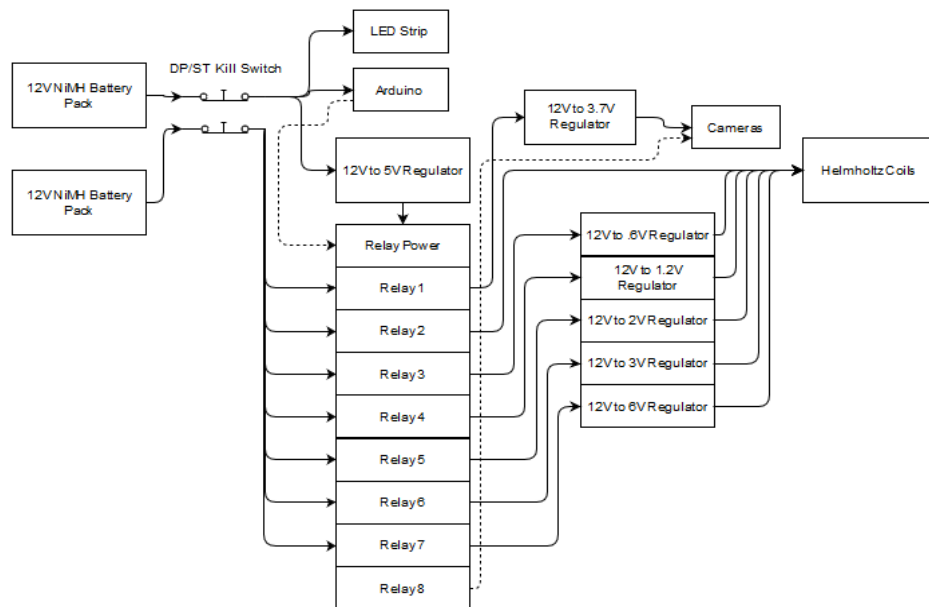


Figure 2: Electronics Block Diagram. Dashed lines show digital signals. Solid lines show power lines.

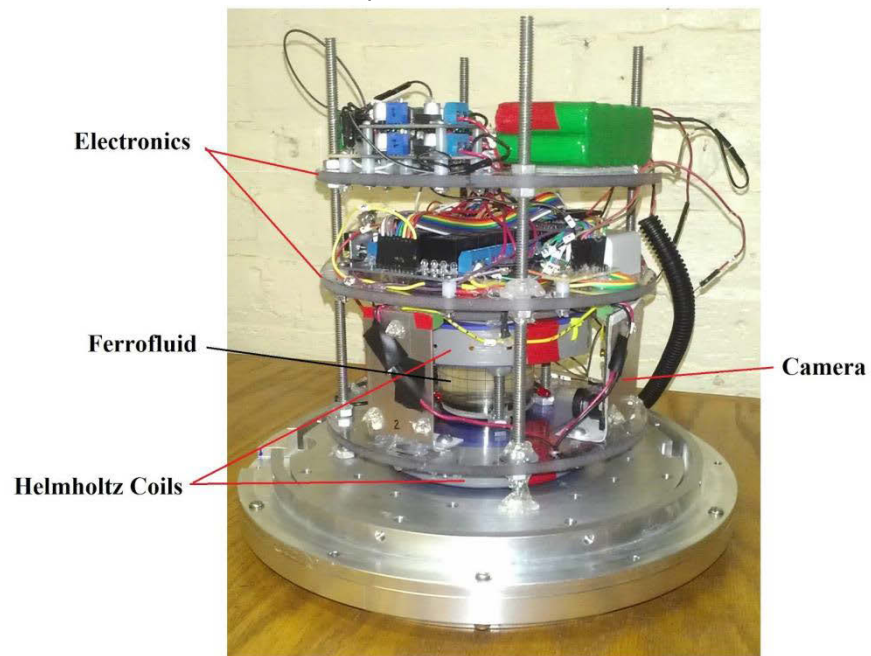


Figure 3: Final payload design.

Testing Results

We ran several tests with individual components of our experiment before integrating to ensure that each subsystem would function correctly. Our electrical components (voltage regulators, relays) were tested on their own to ensure they could be used for the purpose we intended. Our Helmholtz coils were tested after construction to verify that heat generated from running the coils for an extended period of time would not affect other electrical components. We tested our magnetometer at different placements, because our magnetometer could only measure magnetic fields between -8 and 8 Gauss and would saturate if placed too close to the magnetic field. We also tested our cameras at several locations in order to have the best possible view of the ferrofluid container. We tested the focus of the cameras to determine the best setting for getting a clear view of the ferrofluid and grid lines on the container. Because the experiment needed to be well lit in order to see the ferrofluid deformation, we ran multiple test runs for different LED placements. The LEDs were placed in the optimal position for lighting the ferrofluid while reducing the amount of glare on the glass container.

Other experiments on the Rocksat-C flight were designed to measure the Earth's magnetic field, which required the installation of steel plates to dissipate the magnetic field in the direction of the other experiment. We determined the magnetic field falloff using one, two, and three steel shielding plates and concluded that the use of three plates would be the best option to minimize the chance of our produced field interfering with another experiment.

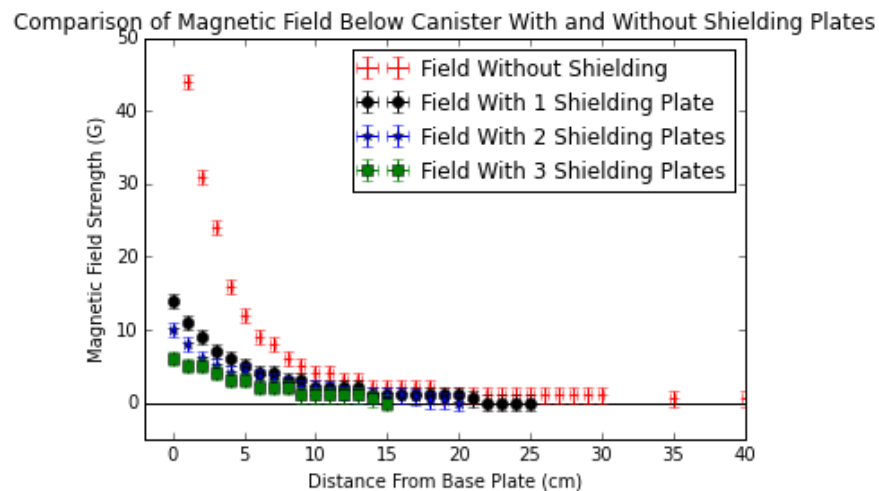


Figure 4: Graph of measured magnetic field below experiment, comparing multiple shielding plates.

After we tested each of our components individually, we ran a series of full mission simulations. With these tests, we ensured that the Arduino was triggering all events at the proper time and the SD cards could read and write correctly. Some simulations were run without secondary containment and the Rocksat-C canister so team members could monitor

LED status and visually confirm that the simulation was running as planned. We also ran several mission simulations inside secondary containment to obtain video used as ground data.

Mission Results

Our payload failed to carry out its mission. After de-integration, the experiment was discovered to have turned on without executing the program. Further testing showed that the most likely cause of this failure occurred right at launch. The SD card was most likely jarred by the force of launch, and this caused the Arduino's code to crash. This was an oversight in testing.

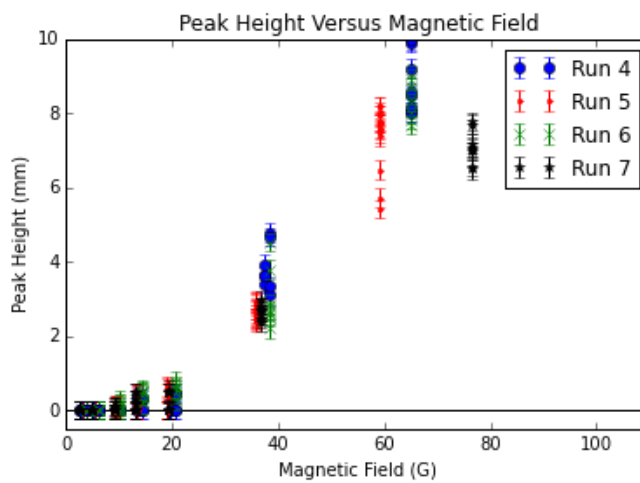


Figure 5: Graph of ferrofluid height vs magnetic field in 1g

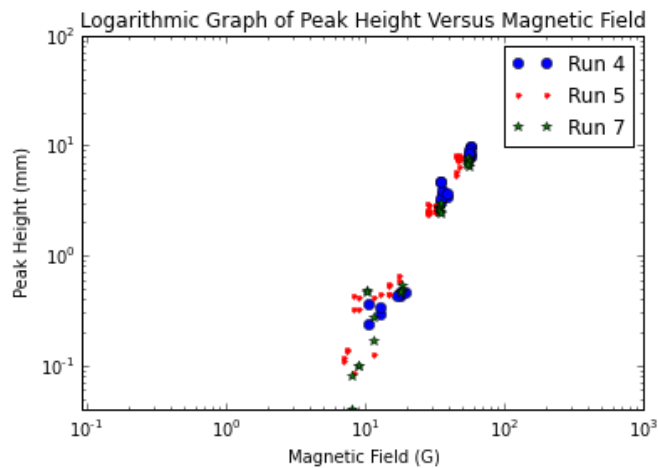


Figure 6: Logarithmic graph of ferrofluid height vs magnetic field in 1g

Analysis of the ground data, intended to serve as a comparison point against the zero-g data, revealed that our ferrofluid begins to deform under an applied magnetic field of approximately 15 G. Our calculations predicted that the onset of Normal Field Instability would occur under an applied magnetic field between 22 and 27 G in 1-g, which is close to, but not the same as, our experimental value.

Because we failed to collect zero-g data, we do not have any data to analyze in order to determine the onset on Normal Field Instability in a microgravity environment, and thus cannot determine if the onset occurs under a lower applied magnetic field as predicted.

Conclusions

Our experiment could use more detail in its ability to select magnetic field levels. An experiment that would build on this one would need to be able to select many more magnetic field levels so that we could obtain more data points near the calculated onset of normal field instability, to determine the accuracy of our calculations and obtain a more precise experimental value.

Because we did not obtain any zero-g data, we are not able to determine the onset of normal field instability in our ferrofluid in microgravity conditions, nor compare our ground data to data obtained in zero-g.

Potential Follow-up Work

Due to the nature of our payload's failure, it could be run as is on next year's RockSat flight, however, a number of potential improvements could be made.

The ferrofluid container could be improved. Our Helmholtz coils had to be placed farther apart than we would have liked in order to accommodate our container, and a custom container could be made to fit our specifications.

In a future project, it would be very important that a more continuous sample of magnetic field levels could be captured. Since we had to use relays to control the application of magnetic field levels, we had to decide on a very discrete set of magnetic field levels, making it difficult to pinpoint the field level where we first see normal field instability. If we could sweep through a range of magnetic field levels, it would be much easier to pinpoint the onset of normal field instability.

The experiment can be modified to fly on other rockets or on zero-gravity flights.

[1] Friedrichs, Rene, and Andreas Engel. "Pattern and Wave Number Selection in Magnetic Fluids." *Physical Review E* 64 (2001)

[2] Amin, Shahrooz, Shihab Elborai, Se-Hee Lee, Xiaowei He, and Markus Zahn. "Surface Tension Measurement Techniques of Magnetic Fluids at an Interface between Different Fluids Using Perpendicular Field Instability." *Journal of Applied Physics* 97 (2005)

Team Whoosh Generator
2014 WSGC Collegiate Rocket Competition

Kirsti Pajunen, Eric Johnson, James Ihrcke, Stephan Skibinski, Kathryn Baisley

Department of Mechanical Engineering, Milwaukee School of Engineering

Abstract

The objective of the 2014 Wisconsin Space Grant Consortium (WSGC) Collegiate Rocket Competition is to design, build, and fly a single-stage, high-powered rocket to accurately reach an apogee of 3000 feet, along with design restrictions and two added design objectives. The rocket must use a motor as specified by WSGC, have a maximum length of 72 inches, have a body tube diameter between 4 and 6 inches, use a flight data recorder provided by WSGC, and be safely recovered in a flyable condition by an electronically deployed parachute system. Also, a system in addition to the altimeters already on board must be implemented that records data which can be used to find the rocket's velocity and acceleration during ascent. Finally, the time to rocket recovery must be minimized.

Included in this report are design details considered, anticipated performance, photos of constructed components, and flight results.

Team Whoosh Generator thanks the Wisconsin Space Grant Consortium (WSGC) for the funding to make this project possible.

1.0 Rocket Design and Construction

The following subsections will detail the airframe design, nosecone and fin design, rocket stability, electronics bays, pressure relief considerations, and recovery method.

1.1 Motor selection. Several different motors were available for use in the competition. In order to determine which motor would work best, a MATLAB program was run. The code uses the thrust curves of the various motors, the propellant masses, the drag coefficient of the rocket, and also the outside diameter of the rocket. All possible motor choices for the competition were placed in the code and a plot of possible rocket masses versus altitude of the rocket's flight was created. This is shown in Figure 1 for a diameter of 5 inches. To achieve an altitude of 3000 feet and still have room for the extra mass added from the Alternate Velocity Measurement System (AVMS), which is described later, a large motor was necessary. The chosen motor was the Cesaroni K454 because it was the lowest power motor that would achieve an apogee of at least 3000 feet and allow for extra weight, with a total rocket weight (without fuel) of around 16 pounds.

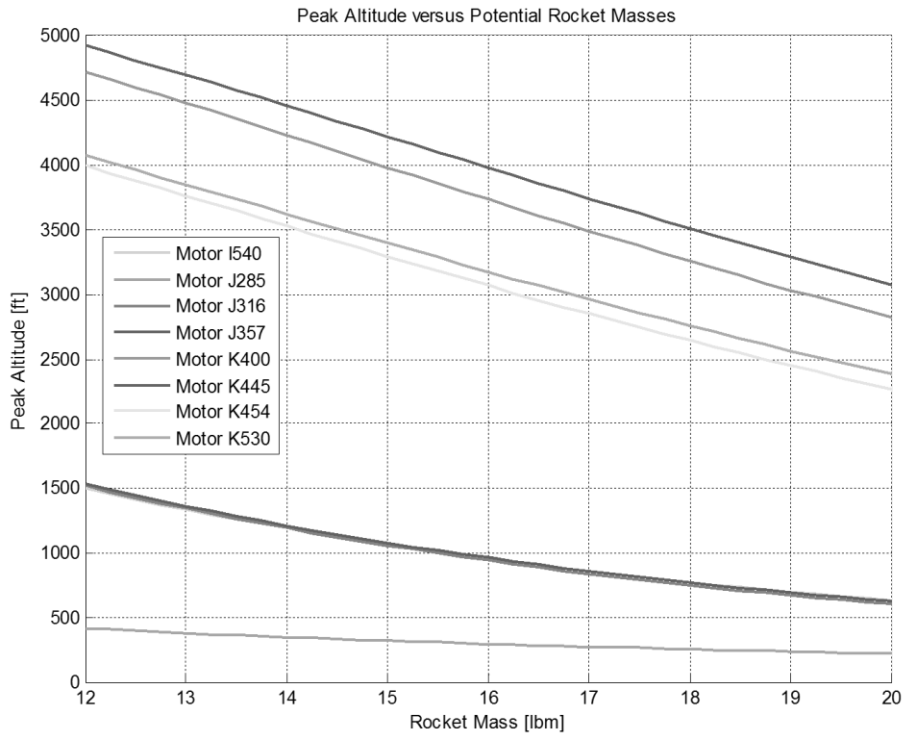


Figure 1: Altitude versus Rocket Mass for each Motor Option

1.2 Airframe design. The body tubes could be selected from several different kinds of materials, including cardboard, fiberglass, and PVC. Cardboard was selected as the body tube material for the rocket because of its simplicity, strength, price, and ease of cutting and drilling. Cardboard has proven to work well from previous years' rockets.

The rocket's diameter was determined using the same MATLAB code used to determine the motor. The possible rocket body diameters for the competition were between 4 to 6 inches. Since the body tubes are normally available in one inch increments, diameters of 4, 5, and 6 inches were run along with the MATLAB code. It was determined that a 5 inch diameter body tube would cause the rocket to have an apogee closest to 3000 feet and still be flexible with the mass of the rocket. Unfortunately the team was unable to find cardboard tubing that was available at 5 inches in

diameter. The closest to the 5 inch diameter tubing without going down to 4 inches or up to 6 was 5.54 inches in diameter. Inputting 5.54 inches into the program still proved this to be a viable option, so this was chosen for the rocket.

The body tube lengths were heavily dependent on the design restriction of a maximum total rocket length of 72 inches. OpenRocket, a free rocket design software program, was the primary software used to design much of the rocket. OpenRocket was used to calculate optimum body tube lengths. It was found that the lower body tube (to house the motor mount and drogue parachute) would have a length of 25.5 inches. The upper body tube (to house the main parachute) would have a length of 16.5 inches. These lengths help to bring the rocket to an apogee of approximately 3000 feet, with favorable centers of gravity and pressure. The total length of the rocket is 65.5 inches, which is below the 72 inch restriction.

1.3 Nose cone. After choosing a body tube size of 5.54 inches, nose cone options were limited to a 5.38 inch diameter. Only two durable plastic options were found with an ogive shape, both made by LOC Precision Rocketry; the PNC Short and the PNC Long. With the short length measuring 13 inches and the long length measuring 21 inches, the 13 inch length was chosen in order to maximize the available space for electronics bays, parachutes, and other miscellaneous items while remaining inside of the maximum overall rocket length. The ogive shape was chosen because it has a low coefficient of drag which will allow for a higher apogee with the increased weight of the payloads.

1.4 Fins. The fins are the main component that determines the location for the center of pressure on a rocket and therefore the stability of the rocket. The design of the fins was determined by placing different shapes and sizes of fins in OpenRocket until a stable ratio between the center of gravity and center of pressure was obtained. It was determined to use 4 fins spaced evenly around the rocket. The fins chosen were C-08 G-10 fiberglass fins from Public Missiles shown in Figure 2. The fins were attached to the rocket using through-the-wall construction with epoxy fillets on each contact surface.

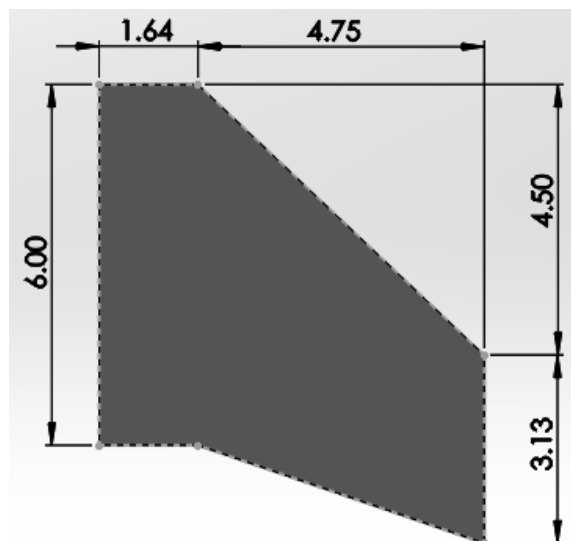


Figure 2: Fin Dimensions

1.5 Rocket stability. The relationship between the center of pressure (CP) and center of gravity (CG) is one of the most important relationships in high-powered rocketry. The center of pressure is defined as the point at which aerodynamic forces on the rocket are centered. The center of gravity is the location at which the whole weight of the rocket can be considered to act as a single force. The ratio between the locations relative to the rocket diameter can be used to predict the stability of the rocket during flight. Generally, the center of gravity must be at least one (but not more than two) body tube diameters in front of the center of pressure.

The center of pressure and center of gravity were determined for this design using the OpenRocket software. The results were then compared against the results using Barrowman’s Theory, and the two agreed acceptably.

The following assumptions were made during the derivation of Barrowman’s theory for predicting the center of pressure (Barrowman, 2014):

- 1) The flow over the rocket is potential flow.
- 2) The point of the nose is sharp.
- 3) Fins are thin flat plates.
- 4) The angle of attack is near zero.
- 5) The flow is steady and subsonic.
- 6) The rocket is a rigid body.
- 7) The rocket is axially symmetric.

The rocket design presented in this paper did violate some of these assumptions, particularly assumptions 2, 6, and 7. However, the theory was still applied with the understanding that minor uncertainties will be present as a result.

Table 1 shows the locations of the CP and CG and the caliber stability at ignition and at burnout according to the OpenRocket simulation.

Table 1: Locations of CP and CG (In Inches from Nose Cone Tip)

| | CP | CG | Stability (Caliber) |
|----------------------|------|------|---------------------|
| Ignition | 47.9 | 41.3 | 1.19 |
| Motor Burnout | 47.9 | 39.4 | 1.53 |

From this analysis, it can be concluded that the rocket will be stable during the entire ascent portion of the flight.

1.6 Lower payload bay. The Lower payload bay was made from a 5.372 inch OD tube that is reinforced with a 5.24 inch OD stiffy tube. It was 6.5 inches long and since the outer diameter of it was 5.372 inches, it fit perfectly into the 5.38 inch ID airframe. A small piece of airframe, measuring 1.5 inches in length, was cut from a body tube and epoxied in the center of the payload bay to turn the bay into a coupler. Two barometric altimeters were used in the payload bay a RRC2 mini used in previous years and an ALTS25 given to the team at the Altimeter Conference. These altimeters will be used to deploy the drogue and main parachutes as well as record the altitude of

the rocket. The payload bay also holds the Raven III (WSGC flight data recorder) along with two 9 volt batteries that will power the previously mentioned electronics. Two key switches were placed 180 degrees apart on the payload bay to allow easy arming of devices on the launch pad. One key switch is for turning on the WSGC flight data recorder and the other is for arming both altimeters. Terminal blocks were placed at either end of the bay to allow easier attachment of black powder charges on launch day. The assembled payload bay is shown in Figure 3.

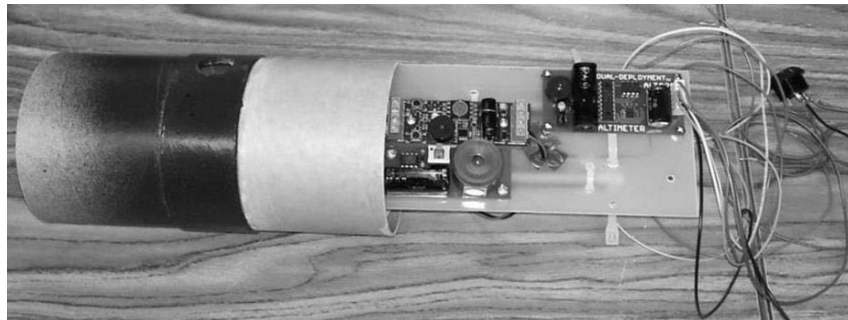


Figure 3: Lower Payload Bay Assembly

1.7 Alternate velocity measurement system (AVMS). A requirement of this year’s competition was to record data that can be used to find the rocket’s velocity and acceleration during its ascent using a device other than the altimeters used for electronic deployment of the parachutes.

The design that was chosen involves calculating the velocity using the drag force on the main nose cone. An aluminum rod was attached to the nose cone and rested on a force sensor. The device works using a pressure sensor that can read between 0 and 1000 pounds of force depending on the size of the resistor used in its amplifier circuit. The pressure sensor is a variable resistor that will decrease in resistance as the force applied to the sensor goes up. The pressure sensor feeds into an analog pin on an Arduino Uno board with an Ethernet shield attached to it. The pressure sensor is shown in Figure 4. The Arduino Uno reads the voltage across the pressure sensor and then saves it to a micro SD card inserted on the Ethernet shield. This voltage has a known relationship to the force being applied to the pressure sensor, which was calibrated. The Arduino Uno also has a piezo buzzer attached to one of its digital pins that beeps at a regular interval to show the force sensor is connected and recording data.



Figure 4: Pressure Sensor for AVMS

The payload bay that houses the AVMS has 2 fiberglass boards in it to support the electronics. The electronics that are housed in the upper bay are the force sensor, the force sensor’s amplifier circuit, the Arduino Uno with attached Ethernet Shield, the Garmin GTU 10 Global Positioning System, and three 9-Volt batteries: two used for the force sensor’s amplifier circuit, and one used to supply power to the Arduino Uno. The force sensor’s amplifier circuit and the Arduino Uno will be turned on at the launch pad using key switches. The boards are centered around an aluminum rod running from the nose cone down to the force sensor. Conduit is attached to the bottom bulkhead to guide the aluminum rod in the bay. The nosecone is free to move down one eighth of an inch but a

removable pin in the aluminum rod stops the nose cone from going upwards. A diagram of the upper bay without the boards or electronics is shown in Figure 5.

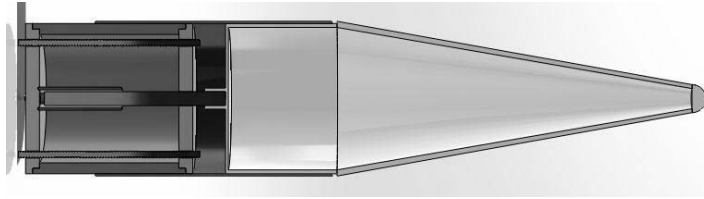


Figure 5: AVMS Setup

The voltage across the pressure sensor was recorded and related to the force applied using the sensor's calibration. The velocity was found using the drag force equation shown in Equation 1.

$$F_d = \frac{1}{2} \rho V^2 C_d A \quad (1)$$

where F_d is the drag force on the nose cone, ρ is the density of air, V is the velocity of the rocket, C_d is the coefficient of drag of the nose cone, and A is the cross sectional area of the nose cone. The velocity was solved for as shown in Equation 2.

$$V = \sqrt{\frac{2F_d}{\rho C_d A}} \quad (2)$$

Using Equation 2 and the recorded data on the SD card, the velocity of the rocket's ascent was determined.

1.8 Pressure relief. The two barometric altimeters used to deploy the drogue and main parachutes require static pressure port holes. Static port holes are required for pressure equalization between the air inside the bay and the outside air during flight. This is very important since the parachutes could be deployed too early or too late if the static port holes are not the correct size. The general rule for port hole sizing is to use a 1/4 inch diameter hole (or equivalent area if multiple smaller holes are used) for every 100 cubic inches of bay volume. It is also recommended to use at least three holes spaced evenly around the body tube to help negate the effects of crosswinds.

The diameter of the lower payload bay is 5.38 inches and the inner length of the bay is 5.75 inches. This yields a volume of 130.7 cubic inches. The diameter of a single port hole is equal to 0.24 inches with an area of 0.047 square inches. Three holes were drilled into the payload bay each with a diameter of 0.141 inches spaced 120 degrees apart.

During the rocket's ascent the atmospheric pressure surrounding the rocket decreases. In order to relieve the pressure, a quarter inch hole was drilled into both the upper and lower body sections of the rocket. If these holes are not present the higher pressure inside the rocket could cause the rocket to separate and deploy its parachutes early.

1.9 Recovery. The rocket used a dual deployment system. This means the rocket deploys a small drogue parachute at apogee and then a main parachute at a lower altitude to minimize the drift of

the rocket allowing easier retrieval of the rocket. A 24 inch drogue chute that deploys at apogee and a 60 inch main SkyAngle Classic parachute that deploys at 600 feet were used. The rocket has a descent rate of 18 feet per second once the main chute has opened. Two altimeters were used for redundancy to ensure the parachutes deploy. The parachutes are shown in Figure 6.



Figure 6: Drogue and Main Parachutes

2.0 Anticipated Performance

The anticipated performance of the rocket was simulated using two programs: MATLAB and OpenRocket. The results of both simulations were compared to estimate the performance of the rocket on launch day. The following sections detail these simulations.

2.1 MATLAB Simulation. The primary assumptions made were that the rocket would be launched vertically and that the rocket would follow a vertical flight path. Additionally, standard temperature and pressure were assumed to determine air density, which was also assumed to be constant throughout the range of flight.

A MATLAB simulation for the rocket's flight performance that was used in previous years and improved upon this year was run. The function was designed to perform the following:

- 1) Load thrust data obtained from ThrustCurve.org.
- 2) Interpolate thrust curve for more discrete steps.
- 3) Calculate change in mass resulting from burnt propellant.
- 4) Calculate velocity from the combined impulse from drag, gravity, and thrust.
- 5) Calculate altitude and acceleration from velocity.

The rocket simulation function operates in the following way.

The velocity of the rocket was determined from the previous momentum plus the impulse. This relationship is shown in Equation 3:

$$m_i v_i + F_i \Delta t = m_{i+1} v_{i+1} \quad (3)$$

Where F_i is the net force acting on the rocket and Δt is the time step between calculations. The net force acting on the rocket during ascent is expressed in Equation 4:

$$\begin{aligned}
 F_{net} &= F_{grav} + F_{drag} + F_{thrust} \\
 &= m_i g + \frac{1}{2} \rho v_i^2 C_d A + T_i
 \end{aligned}
 \tag{4}$$

where ρ is the density of air, C_d is the coefficient of drag, A is the frontal cross sectional area of the rocket, and T_i is force from the motor. Substituting Equation 4 into Equation 3 and solving for v_{i+1} yields:

$$v_{i+1} = \frac{1}{m_{i+1}} \left[v_i m_i + \frac{1}{\Delta t} (T_i - m_i g - k v_i^2) \right]
 \tag{5}$$

Where:

$$k = \frac{1}{2} C_d A$$

Acceleration was calculated using Newton's second law which is expressed in Equation 6:

$$a_i = \frac{F_i}{m_i}
 \tag{6}$$

The trapezoidal method for approximating the area under a curve was used to calculate the altitude of the rocket during the flight. The simulation calculated the altitude, velocity, and acceleration versus time for the flight until apogee, based on the assumptions as stated in the Assumptions and Limitations section. The drag coefficient for the MATLAB simulation was found in OpenRocket. The drag coefficient used was 0.41.

2.2 OpenRocket. OpenRocket is a free, open source, software similar to RockSim. It is capable of calculating acceleration, velocity, and position data. This is done while accounting for variables including: elevation, wind speed, and the effects of individual components on performance. Also included in the program is the ability to construct full to-scale schematics of the rocket design. From this schematic the CP and CG can also be approximated.

OpenRocket was the main source used in designing the rocket. The rocket was modeled entirely in the program, providing a way to design and calculate proper lengths of body tubes, optimal fin and nosecone designs, rocket weights, acceptable locations of the CP and CG, and drag coefficients.

2.3 Flight Predictions. The peak altitude, acceleration and velocity for both simulation methods are shown in Table 2.

Table 2: Maximum Flight Predictions

| | OpenRocket | MATLAB |
|--|------------|--------|
| | | |

| | | |
|---------------------------------------|------|------|
| Altitude (ft) | 3012 | 2996 |
| Velocity (ft/s) | 462 | 465 |
| Acceleration(ft/s²) | 201 | 197 |

3.0 Results

Simulations were run to design and estimate flight performance of the rocket. The two programs that were used were OpenRocket and MATLAB code written by the team. Actual flight data was recorded using a Raven 3 flight data recorder provided by WSGC. The flight of the rocket matched well with the estimates of both simulations. A comparison between predicted and measured results is shown in Table 3.

Table 3: Flight Performance Comparisons

| | Apogee (ft) | Maximum Velocity (ft/s²) | Maximum Acceleration (ft/s²) |
|--------------------------------------|--------------------|--|--|
| MATLAB | 2996 | 465 | 197 |
| OpenRocket | 3012 | 462 | 201 |
| Actual | 2967 | 400 | 228 |
| Percent Error From Actual (%) | | | |
| MATLAB | 1 | 16 | 14 |
| OpenRocket | 1 | 16 | 12 |

Predicted and actual acceleration data is shown in Figure 7.

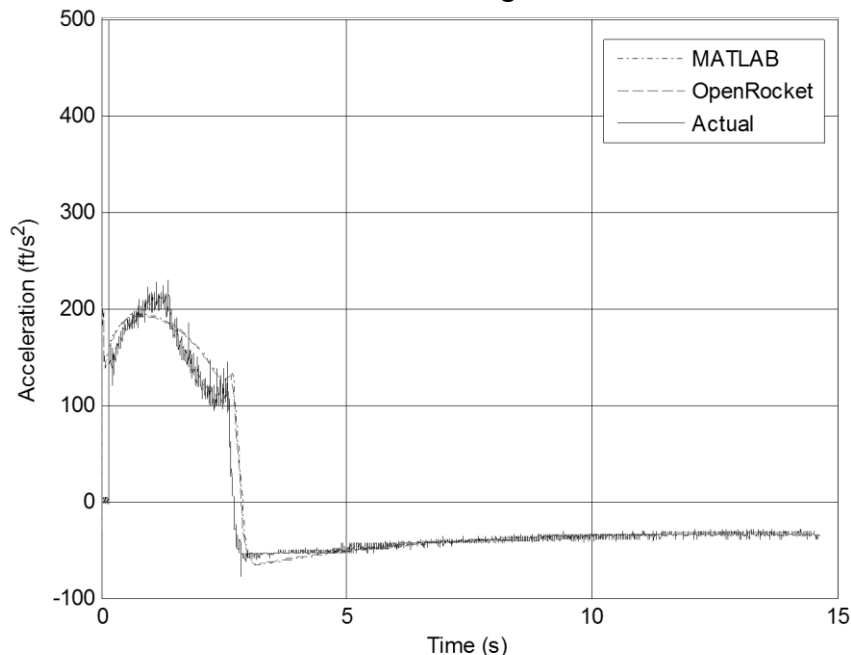


Figure 7: Comparison between Predicted and Actual Acceleration
Velocity data from the AVMS is shown in Figure 8.

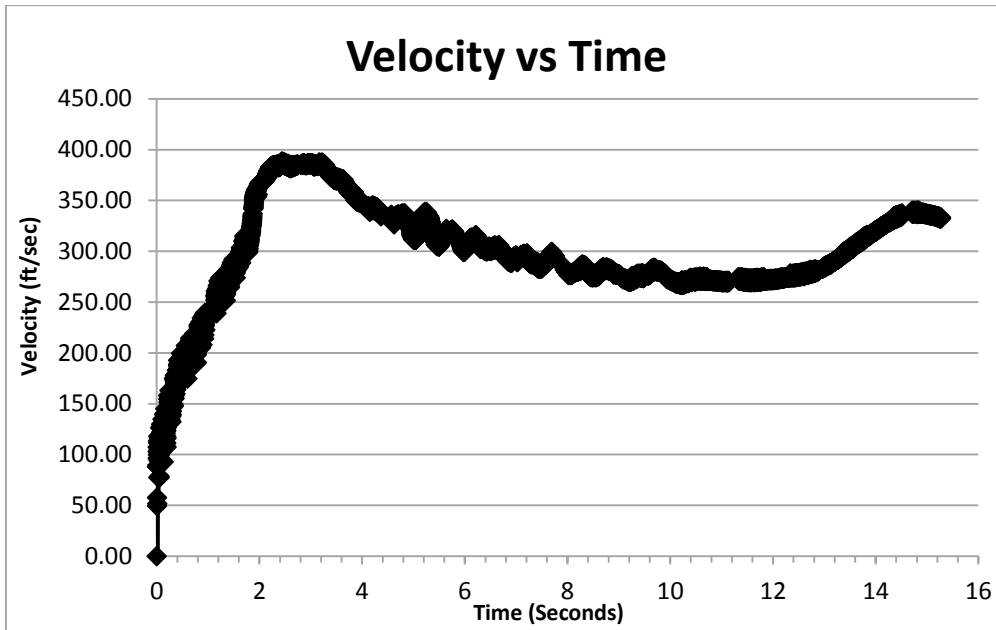


Figure 8: Velocity Data from AVMS

From Figure 8 it can be seen that the velocity data from the AVMS has a steady increase while the motor is burning. The velocity begins to decrease as the rocket approaches apogee. There is some noise in the data near apogee probably due to the nose cone rattling on the force sensor. The calculated maximum velocity by this method was 388.17 ft/s compared to the actual maximum velocity of 400 ft/s.

The time to apogee was about 14.5 seconds, which was as predicted. The rocket undershot the desired altitude of 3000 feet by 33 feet. This was fairly good because MATLAB predicted an apogee of 2996 feet and OpenRocket predicted 3012 feet. Since the actual apogee and these two predicted values had a percent error of 1%, the simulations were good representations of the actual flight. The undershoot was expected because there was a burst of about a 15 mile per hour wind right before the rocket launched. This caused the rocket to reach below the expected apogee.

4.0 Conclusion

The rocket was successfully recovered in a flyable condition in compliance with the competition rules. The software utilized for this design predicted the altitude of the rocket to an exceptional margin given the uncertainties present in the launch and design. The AVMS recorded velocity data closely matched the actual data showing that this method works as a possible alternative to recording the velocity using accelerometers. Lessons learned through this design will be incorporated into future competitions by returning team members.

5.0 References

Barrowman, James. "The Theoretical Prediction of the Center of Pressure." (1966). Apogee Rockets. Web. 13 Apr. 2014.
 <http://www.apogeerockets.com/downloads/PDFs/barrowman_report.pdf>.



Pioneer Rocketry
2014 WSGC Collegiate Rocket Competition

Maria Smiles, Trent Cybela, Jacob Ellenberger, Luke Sackash

Society of Physics Students: University of Wisconsin-Platteville

Abstract

The objective of the 2014 Wisconsin Space Grant Consortium (WSGC) Collegiate Rocket Competition was to design a one-stage high-powered rocket that could accurately reach an apogee of 3,000 feet and then be recovered timely and safely and in a flyable condition. The competition also required two methods of determining velocity through the use of onboard electronics.

Overall, the performance in the 2014 WSGC Collegiate Rocketry Competition was a success. The rocket used for competition, *Pioneer - I*, reached an apogee of 3094 feet. The time took to recover the rocket was approximately ten minutes. The apogee reached and recovery time, combined with our presentation, design report, post-flight report, and educational outreach services put us into first place for this year's competition¹.

The following report details the design, construction, and flight of Pioneer Rocketry's 2014 Competition Rocket *Pioneer - I*. Pioneer Rocketry is composed of undergraduate students from the University of Wisconsin - Platteville. This report will detail:

- Competition Parameters
- Rocket Design and Construction
- Anticipated flight Performance
- Post Flight Results

¹ WSGC 2014 Rocketry Competition Handbook

Pioneer Rocketry would like to thank Wisconsin Space Grant Consortium, the University of Wisconsin-Platteville, Duane Foust, and the Society of Physics Students-UW Platteville for their support through our many endeavors.

1.0 Competition parameters

According to the competition parameters handbook for the 2013-2014 WSGC Collegiate Rocket Competition, student teams will compete to design a one-stage, high-powered rocket that will as accurately as possible achieve an apogee of 3000 feet and be recovered safely and in flyable condition. The rocket shall carry onboard instrumentation sufficient to perform post-flight analysis in categories concerning the rocket's velocity, acceleration, and altitude. Teams will devise at minimum two methods by which the rocket will record these parameters during flight. The time to recover the rocket will also be used to calculate the results¹.

Flight Mission

- Capture flight performance using more than one type of measurement system
 - Speed vs. Altitude
 - Acceleration vs. Altitude

More than one type of measurement system allows for cross-verification of the flight performance.

Flight Apogee Requirements

- Target Apogee 3000 feet
 - Max - 3500 feet
 - Min - 2500 feet

Parachute Deployment

- Electronic Dual-Deploy required
- Motor ejection charge backup required

Rocket Limits

- Body Diameter
 - Min - 4 inches
 - Max - 6 inches
- Length
 - Max - 84 inches

Rocket Motor

- Each team must select one of the following Cesaroni motors:
 - 38 mm I-540; J-285; J-316; J-357
 - 54 mm K-400; K-445; K-454; K530

2.0 Rocket design and construction

This following section will go into details into the physical parameters of the rocket design as well as the components used in the rocket's interior.

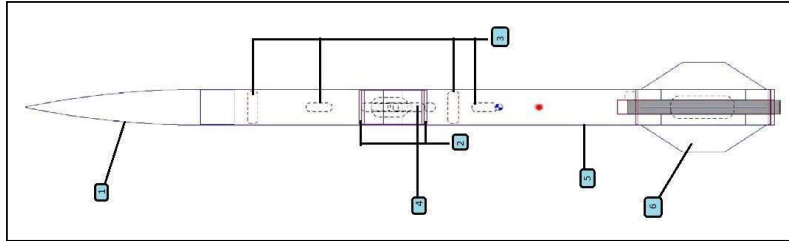


Figure 1: Pioneer-I Diagram

2.1 Nosecone The nosecone selected for Pioneer-1 was a 16.75 inch polypropylene design from Public Missiles Ltd. The shape of the nosecone is a tangent ogive. The tangent ogive nosecone was selected because it offers a good trade-off between stability and drag characteristics. We have previous experience using tangent ogive nosecones from other rockets which had been used as practice and verification platforms.

2.2 Control & stability systems Last year's rocket had mountable tube-fins that would be attached to the payload section of the rocket to increase drag and lower the maximum altitude. For this year's rocket it was decided not to control altitude using drag but rather through a system of interchangeable weights (or ballast). Using an interchangeable weighting system the weight of the rocket can be varied to control its flight. These weights will be attached to either the upper and lower avionics bay bulkheads. Through the process of placing variable weights along the interior length of the airframe, the stability and flight characteristics can be altered.

2.3 Recovery systems Per the competition parameters, Pioneer-1 operates on a dual deploy parachute system including one drogue and one main chute. Commonly, HPR parachutes are made from a single cut of ripstop nylon, which when deployed opens into a parabolic shape. A notable feature of our parachutes are that they are completely hemispherical, and also employ spill holes in their centers. "Squidding" is a term used for when a parachute fails to inflate fully, and instead ripples as the rocket falls. Though more expensive, hemispherical chutes should allow for a comparable descent rate relative to a parabolic chute, and reduce the chance of squidding. This is achieved by eliminating slack cloth, and allowing "through the chute" airflow by means of the central spill holes.

The drogue chute is to fire at apogee, and is housed in the booster section of the rocket. Safe recovery of high powered rockets mandates certain decent rates for each stage of parachute deployment in order to mitigate shock load while airborne, and impact trauma at landing. The drogue chute should allow the rocket to descend at approximately 55-60 feet per second (fps). Under both drogue and main chutes, the descent rate should slow to around 20 fps. Proper parachute sizing depends primarily on dead weight after motor burnout (6.7 lbs). Through this, along with experience from prior launches, the parachute sizes were determined. The shock cord which tethers the rocket after parachute deployment is made from a tubular nylon material with a nominal break strength of approximately 3100 lbs.

2.4 Avionics bay The avionics (AV) Bay is composed of a nine inch paper coupler tube and two birch plywood bulkheads. Housed inside the coupler is a birch-wood sled to which the electronics systems are mounted. Besides housing the electronics, the AV Bay also couples together the upper and lower rocket sections.

2.5 Airframe By using the J-357 motor, initial simulations predicted a significant overshoot of the target altitude. To increase the mass of the rocket prior to the addition of weighted rings, it was decided to make the rocket as large as possible by designing it to be just under the maximum length of six feet. For the airframe material, Quantum Tubing (QT) was selected from Public Missiles. QT is a proprietary material similar to PVC, and offers several preferable qualities that were felt to be ideal for the competition; mainly it's resistance to water damage, and relatively high fatigue and impact strength. Moisture resistance was especially important given the amount of marshland surrounding the competition launch zone.

2.6 Fins Pioneer-1 was designed to incorporate the use of four fins with a symmetrical trapezoidal rounded shape. This shape was adopted to reduce the possibility of damaging fins upon landing. Additionally, this shape helps with ease of assembly. To reduce the fin span and maintain the designed center of pressure (CP) the number of fins used was increased from three to four. The fins are designed as symmetrical trapezoids with a chord of 12 inches and a span of 3 inches. They are made of 0.125in aircraft grade birch plywood and are attached to both the motor tube and body tube. The connections between fins and the body tube are reinforced with thickened epoxy fillets and six ounce fiberglass fabric. This fin selection gives a dry stability caliber of two and a wet caliber of one. It is hoped that having this minimal stability caliber will help reduce the effects of weather cocking.

2.7 Weighting system In order to adjust the estimated altitude of the rocket, it is equipped with a system to adjust its overall weight and CG. This is accomplished using specially designed stainless steel plates which are attached to either ends of the avionics bay (figure 1). The plates were designed to not interfere with the various components inside the airframe. Plates with different weights are produced using a common shape but with various thicknesses. The plates were cut precisely using a CNC water jet table owned and operated by UW Platteville.

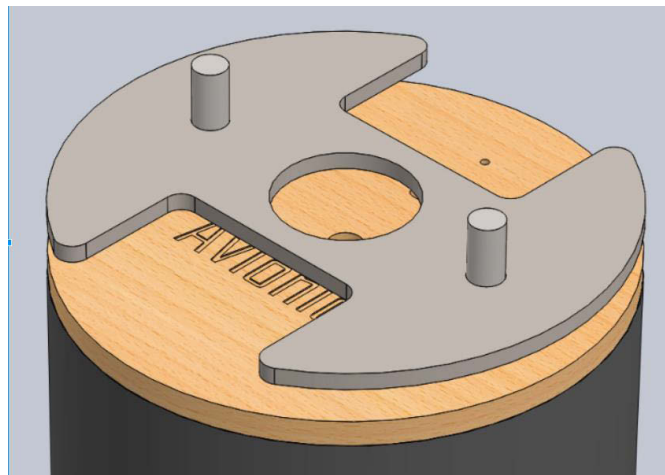


Figure 2: Pioneer-I Variable Weighting System

2.8 Rocket construction When constructing a rocket many things must be considered; most notably, the materials and fabrication methods used. To accurately attach the fins the *Tip to Tip Fin Jig* was used (<http://www.jrocket.com/ttjig.shtml>). This jig both orients the fins with either 90 or 120 degrees of separation and provides a flat, supportive surface for applying a layer of fiberglass.

For this competition the team was granted access to the university's new laser cutter. This tool has provided the capability to rapidly prototype and test parts for the rocket. The laser cutter also provided the ability to make entirely custom parts which accurately fit the rocket body, most notably centering rings, bulkheads, fins and avionics sled. The ability to produce multiple designs proved especially beneficial when building the avionics sled. The laser cutter has proved very useful and we are looking forward to using to build future rockets.

Selection of a body tube material for construction is a critical decision which was made early in the design process. When building two previous rockets, problems were encountered with the standard phenolic tubing ripping and tearing at certain points such as rivet locations and shear pin holes. To combat this a product called Quantum Tubing marketed by Public Missiles was settled upon for the body tube. QT is resistant to the ripping and tearing that the phenolic tubing was subject to, but had its drawbacks; QT is nearly twice the price as phenolic tubing. It also expands and contracts with changes in temperatures. This in mind, much consideration was needed when designing some components in hopes that on launch day no material failures

2.9 Avionics The avionics bay on Pioneer-1 houses four systems including two of the teams own design, as well as the measurement system provided by the Wisconsin Space Grant Consortium for the Intercollegiate Rocketry Competition. The team decided to use the Raven III, Big Red Bee 900MHz, a Raspberry Pi, and a system built around the Freescale Freedom development board. The Raven III, which is the same device used by Space Grant to take their own measurements of our flight performance, will be our primary means of recording flight as well. This device is also used to deploy both of our parachutes. The team adopted the Raven III as compared to other systems such as the Adept, which was used in previous year's competition rocket. The system was chosen for its ease of use and customizability. The Big Red Bee is a GPS coordinate transmitter designed for being used to track and locate rockets.

2.9.1 Secondary velocity measurement Our second method of data logging is a custom solution built around the microcontroller FRDM-KL25Z, a development board by Freescale. Last year the team used Flight Trac, a custom built data logger designed and constructed by team member Weston Woolcock; this year instead of refining that system the team felt that it would be advantageous to migrate to the freedom platform. The Freedom platform was chosen because of multiple advantageous qualities. The board has a 32-bit ARM processor, which is capable of running on a very low amount of power. This quality will help to reduce the amount of batteries we will need to fit in to our avionics bay. The board also has an Arduino compatible pin layout which allows developers to utilize the large amount of hardware for the Arduino platform. It is part of the Mbed platform which allows access to a wealth of code created by an active community of developers and a development environment all from within a web browser. Finally team member Luke Sackash already had experience with this board. In order to collect data, an electronic barometer is used to measure air pressure which is then used to calculate altitude with

very low error. The Altitude is recorded with respect to time so that velocity and acceleration can then be calculated for Pioneer-1's flight.

2.9.2 GPS positioning The Big Red Bee sends the rockets GPS coordinates over a 900 MHz radio signal to a handheld radio device that is stationed at the launch site. Members of Pioneer Rocketry have developed software to interpret these coordinates and log them so that later a flight path can be reconstructed. The software developed also converts the coordinates received into a more user friendly format, allowing the team to briskly locate and retrieve the rocket. In preliminary flights the GPS proved extremely useful allowing for recovery of a rocket that would have otherwise been lost in the marshland of Bong Recreational Area.

2.9.3 Raspberry Pi and video

The final piece of hardware included is a Raspberry Pi and its camera peripheral to capture and store in-flight video. The raspberry pi is powered by a homebrew voltage regulated power supply. An SD card is loaded up with a Debian Linux distribution tailored specifically for the raspberry pi. At boot up, the camera module will begin to capture video. The captured video is then saved to the SD card. For next year's build there are hopes to take further advantage of the processing power the Pi for more advanced inflight data logging as well as exploring other possible uses.

3.0 Anticipated performance

Pioneer Rocketry's airframe designs depend heavily on the collection of empirical data. However following the current competition timeline it became impractical to construct and test the competition rocket prior to launch day. Because of this, PR has utilized simulation programs to help with design. The simulation program used was OpenRocket. This was the first time PR had used this program, and for this reason, we conducted three test flights prior to competition verify the software's accuracy. We tested a several different construction techniques and rocket designs, and referenced our flight data to the results given in OpenRocket (table 1). Data was taken for altitude, descent velocities, and acceleration.

There were a total of three test flights used to verify simulation results, two 38 mm Hi-tech rockets and one Torrent rocket. For the 38mm Hi-tech rockets one with a H-120 and the other with a H-152 motor, simulations were run in OpenRocket and the simulation data recorded. The rockets were then launched on Saturday, February 22nd, 2014 at Richard Bong State Recreation Area, and data was collected from those launches. The data from the Torrent rocket launch was deemed unusable due to a rapid unexpected disassembly (RUD). When comparing actual and simulated results, the predictions from our simulations matched the data collected on the launch day. Actual apogee was in both cases within a few hundred feet of predicted, proving that OpenRocket is a viable simulation program to use in the design of a rocket.

Rocket Hi-Tech H-45, 38 mm

| Motor | Predicted Data | | | | Actual Flight Data | | |
|-----------------|-----------------|-------------|--------------------|-----------------|--------------------|--------------------|-----------------|
| | Stability (Cal) | Apogee (ft) | Time to Apogee (s) | Flight Time (s) | Apogee (ft) | Time to Apogee (s) | Flight Time (s) |
| Cesaroni H120 | 1.72 | 3333 | 11.8 | 177 | 3168 | 26.5 | 111 |
| Cesaroni H152BS | 1.7 | 3363 | 11.6 | 174 | 3441 | 12.5 | 171 |

Table 1: Predicted Data compared to actual data of two test flights of both Hi-Tech rockets

4.0 Projected flight performance

A rocket must perform under strict parameters and is best built with experience and extensive testing as opposed to simulation. This said, we have extensively tested two practice rockets prior to construction of the Pioneer-1.

High powered rockets from previous team builds which had achieved apogees near 3000ft were used as models for this year’s competition rocket. Given the anticipated weather conditions for April 5th 2014 Pioneer-1 was configured in the launch simulation software to overshoot the target altitude under perfect conditions. Our anticipated maximum altitude of 3256 feet is expected provided no wind and a vertical launch. To help us achieve the 3000 feet target accurately a weighting system was developed as explained above to help plan for changes in weather conditions. Estimates of peak acceleration from OpenRocket are about 13.2 G. We anticipate a peak acceleration of 34 G based on prior launch experience and the data recovered therein. Below is a graph showing the expected acceleration when compared to time from the simulation program OpenRocket and a graph showing the peak acceleration of a previous launch of the Super DX-3 rocket collected from a Raven altimeter.

4.1 Pressure and gravity diagrams By the insertion of weighted plates into the rocket airframe, the flight characteristics of the rocket can change on the fly. The ability to adjust the weight of the rocket allowed the team to achieve our target altitude under a variety of possible weather conditions. The weighting system allowed us to add ballast without significantly shifting the CG of the rocket.

5.0 Post-flight results

Our post flight data very closely matched what we had predicted from our simulations (figure 3); we had a few hiccups on launch day but we were able to quickly find solutions and apply fixes in the field.

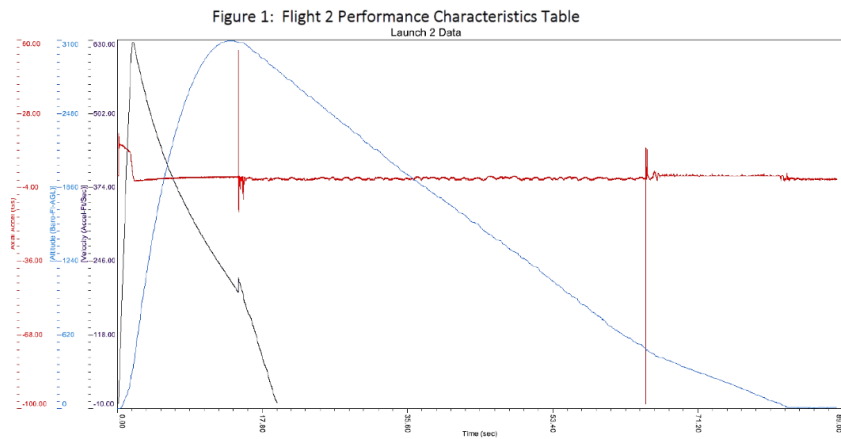


Figure 3: Flight 2 Performance Characteristics Graph

5.1 Data analysis & comparisons The predicted Apogee of 3018 feet was 76 feet below the measured apogee of 3094 ft from the second launch flight and the predicted maximum velocity was about 100 ft/s below the measured max velocity of 617 ft/s.

The predicted reasons for the discrepancy in apogee and maximum velocity may have been tied to the mass of the rocket. It is believed that there may have been a difference between the mass listed in OpenRocket and the actual mass at liftoff during flight-two. Changes were made to the mass of the rocket as a result of field repairs which took place after the first flight. It should be noted that the first launch (where mass was known) came in at an altitude closer to 3000 ft (2956 ft). Ballast was removed from the rocket for the second flight to compensate for the addition of epoxy and additional shock cord.

The predicted max acceleration was significantly different from the measured (table 2), overestimating by over 300 ft/s²; in addition, the predicted acceleration curve on the graph is significantly different from the measured acceleration line on the measured graph, being much higher overall. This might be due to measurement error.

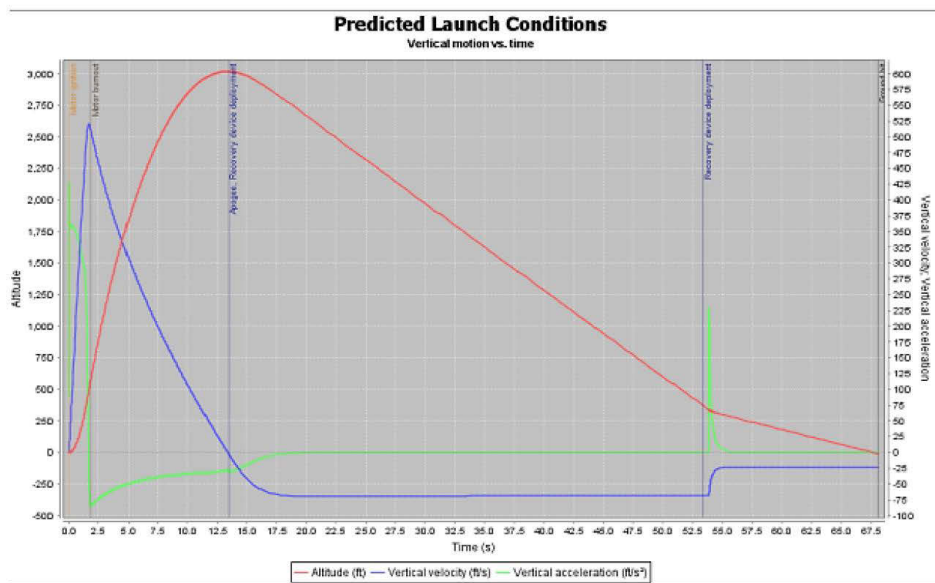


Figure 4: Flight performance characteristics from open rocket. The red line signifies the predicted altitude, the blue line signifies the predicted velocity, and the green line signifies the predicted vertical acceleration.

| Predicted Data | | | | | | Launch 2 Measured Flight Data | | | |
|----------------|-----------------|-------------|--------------------|---------------------|--------------------------------|-------------------------------|--------------------|---------------------|--------------------------------|
| Motor | Stability (Cal) | Apogee (ft) | Time to Apogee (s) | Max velocity (ft/s) | Max Accel (ft/s ²) | Apogee (ft) | Time to Apogee (s) | Max velocity (ft/s) | Max Accel (ft/s ²) |
| J357 | 1.14 | 3018 | 13.4 | 524 | 428 | 3094 | 17.73 | 617 | 55.61 |

Table 2: Flight performance characteristics

5.2 Performance of electronics systems

5.2.1 Expected outcomes The goal of our electronics bay was to capture in-flight video, log velocity and acceleration, and finally to send GPS coordinates our ground team. Our two methods of measuring velocity were intended to be our Raven III's accelerometer as well as a custom pressure logging system.

5.3 Actual outcomes

5.3.1 Overview From the start of the competition we noticed inconsistencies with our electronics bay. The GPS Board we had purchased was not being supplied a steady voltage and it was constantly restarting. Due to time constraints we were forced into our first launch without our active GPS system. By the time we had recovered our rocket we were confronted with the news that our in-flight video system as well as our pressure logging system had failed to log any data. Of the four systems we had on board, only one had properly functioned. As the rest of the team repaired the damaged rocket, the electronics team brainstormed solutions to fix the faulty avionics bay. We implemented a solution by rewiring the power supply of our failing in-flight video system to the GPS module. This was a big step in the right direction for our team. Not only were we able to secure a steady GPS signal, we also had a third method of calculating velocity secured. By the time our rocket was ready for a second launch; our GPS system was retrieving data properly (figure 5). The solution that we implemented ended up paying off. We ended up using the GPS coordinates as a velocity measurement, since the custom built system again failed to save coordinates.

5.3.2 Barometric measurement system Our secondary measurement system was supposed to log barometric pressure vs time to a flash memory chip which would then be sent to a computer via USB connection. The reason we used an external memory chip was to allow for the data to still be intact even if the board was power cycled (lost power). Our microcontroller could not write to its own memory. There was a problem in writing to and reading from the flash memory, however so no data was recovered from the device.

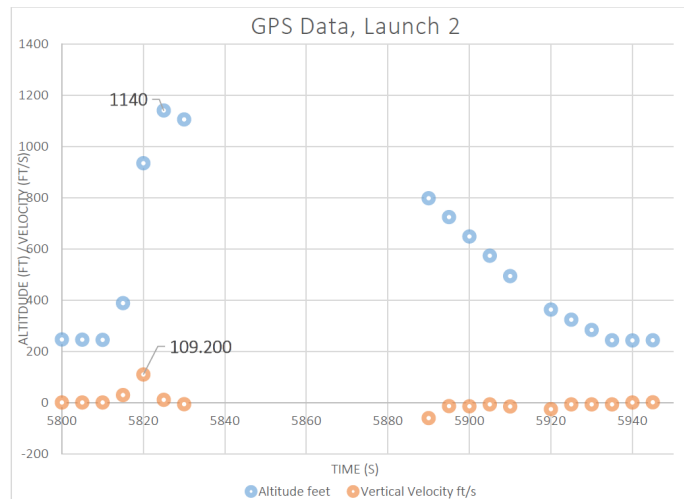


Figure 5: Flight-2 data as recorded by GPS system. The upper blue dots represent the altitude feet and the lower red dots represent the vertical velocity. Note the gaps between data packets, which in this case excludes data that would have marked flight-apogee.

6.0 Conclusion

The completion of Pioneer-1 brings a close to PR's second season as part of the WSGC intercollegiate rocketry competition. The challenge of designing a rocket capable of reaching the 3000 foot altitude while simultaneously logging data via a suite of onboard electronics has been met by the hard work and dedication of over twenty undergraduate engineering students. The larger airframe, extended avionics bay, additional data logging capabilities, and weight control systems integrated into Pioneer-1 are examples of our growth as a team, and our understanding in the fields of engineering and aerospace science.

PR's member base is not small, and for this reason is modeled differently than most contenders in this year's competition. Our intent is to become more than just an isolated group of rocketeers, but rather to be an integral part of our University's selection of student organizations. It is hoped that over the coming years PR will expand its membership, build more rockets, conduct more launches, receive more HPR certifications, and lend creditability to the use of aerospace applications as part of an undergraduate college curriculum. We are grateful to WSGC and Tripoli Rocketry for allowing us the opportunity to compete, and we look forward to the coming competition.



Figure 6: 2013-2014 Pioneer Rocketry Team

2014 HUNCH SPIDER

Jonathon Woods

East Troy High School NASA HUNCH

Program

HUNCH is an instructional partnership between NASA and high school, intermediate school, and middle school students. This partnership benefits both NASA and students. NASA receives cost-effective hardware, while students receive real-world hands-on experiences. The results of this cooperation is the inspiration for the next generation of researchers and space explorers. Our team was comprised of seven members: Eli Rand, Nicholas Nolting, Jonathon Woods, Luke Goetsch, Paul D'Amico, Joey Dominski, and Daniel Barr. Each member of our team had designated roles within the group, but we all worked together to advance towards goals and meet deadlines.

Goal

The task at hand was to design, and build an experiment to test in microgravity. As with each team coming up with their own unique experiment, our team went with trying to solve the problem of astronauts always losing tools that they are working with aboard the International Space Station. This has always been a challenging issue for astronauts in space due to the microgravity environment. This problem is a potential high risk due to when tools or parts float away as they can get lost, lodged somewhere, or even damage other equipment. By creation of our device we hope to improve the livability and ensure greater safety for astronauts in space.

Experiment

Our team went with the route of using RFID (Radio Frequency Identification) technology as the way to alert a user about an object leaving their vicinity. The experiment SPIDER (Spatial Proximity Identification Device for Environmental Reading) consisted of several parts. SPIDER's was made of an Arduino board, RFID board, Nano rack, antenna, and tag. These parts were for controlling/interpreting data, reading, housing the device, transmitting the signal/detecting the tag, and marking the tool, respectively. The program for SPIDER is on a continuous loop, searching for a signal from the RFID tag within a range of 3 feet (average arm reach). If the signal is lost it causes a blue light to flash at the user, alerting them of the objects movement.

Supported by Wisconsin Space Grant Consortium and the East Troy Education Foundation

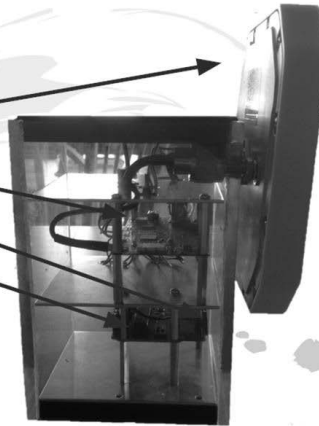
Diagram

Antenna (902-928Mhz)

RFID Module (Interprets Data)

LEDs (Indicate in/out of range)

Arduino Board (Utilizes Data)



Testing

Testing and data collection was done in two parts. The first part, ground testing, was done to ensure all parts of the experiment were working properly with one another, and that all bugs had been worked out of the program. This was done weekly over the course of three months before flight testing. Ground testing involved moving the RFID tag away from the antenna to find the best distance to signal ratio for the human arm reach and tweaking the program for consistency. The second part of testing was done during two reduced gravity flights. Each flight consisted of 30 parabolas, lasting between 30-15 seconds of micro-gravity. Each one of our tests was done during the 30-15 seconds of reduced gravity to procure the best results. Testing on the first flight involved moving the RFID tag at various angles within a NASA tested safety glove box. These angles were pre-measured out at 45°, 67°, and 90° from the antenna. The angles were tested because the antenna can only send and receive signals from items on a certain axis. We wanted to see how the angles would make the signal deteriorate as the tag was placed farther away from the axis directly perpendicular to the antenna face. Testing on flight two was made up of letting the tag float freely outside the glove box, and marking when the signal with the device was lost. The device was tested in free fall because we wanted to make sure it would be unaffected and to measure any affects that could have possibly arisen. There was no research done to test RFID in microgravity and we did not want to assume. All of this testing was done, on the reduced gravity flight, to ensure the reliability and effectiveness of the devices NASA could potentially put op on the ISS.

Supported by Wisconsin Space Grant Consortium and the East Troy Education Foundation

Outcome

During both flights the testing was congruent with ground testing. The first experiment gave us consistent data that from 90° to 45° the average distance decreased by 30%. This means that our current model is only practical if the tag is within about a 45° angle from the axis perpendicular to the face of the antenna. Staying constant with how SPIDER was programmed, the device lost signal with the tag within the 3 foot radius when at a 90° angle to the antenna. In the future we're planning on furthering our use with RFID technology. We have many ideas about the next steps we want to take with the project; these include but are not limited to: an omnidirectional antenna to have a wider area for detection, several antennas for detecting location or direction of travel, and lastly fractal antennas which give you more powerful antennas within the same space.

Supported by Wisconsin Space Grant Consortium and the East Troy Education Foundation

WSGC Collegiate Rocket Competition Report
Wombat 1
Team Night Skies
University of Wisconsin-Sheboygan
Grace Zeit, Christine Sutherland, Aaron Jarosh, Randy Lutz



WSGC

Table of Contents

| | |
|-----------------------------------|----|
| Rocket Design | 3 |
| Payload Design..... | 4 |
| Projected Flight Performance..... | 5 |
| Rocket Construction..... | 6 |
| Competition Flights..... | 7 |
| Doppler Shift Experiment | 8 |
| Pitot Tube Experiment | 11 |
| Conclusion..... | 14 |
| Closing | 14 |
| Budget | 15 |

Rocket Design

Our rocket is based on a Formula 98 rocket kit manufactured by Rocketry Warehouse. To meet our design requirements, we asked the manufacturer to make the following changes to the kit:

- Increase the booster airframe length by 2 inches.
- Increase the payload airframe length by 6 inches.
- Increase the motor tube length by 5 inches to accommodate a tail cone.

We also made the following modifications:

- Eliminated the switch band.
- Shortened the electronics bay by 1”.
- Shortened the nosecone by 1.5”.
- Reconfigured the shape of the fins.

After modifications were done by the manufacturer and ourselves, the rocket was essentially scratch built with only the centering rings and the bulkheads remaining from the original design.

The decision to base our design on an existing rocket kit versus a scratch built design was necessitated by budgetary constraints. The cost of the kit and modifications came to \$174.00. If purchased separately these same parts would have cost \$354.00. By basing our rocket design on an existing manufactured kit we realized a \$180.00 savings.

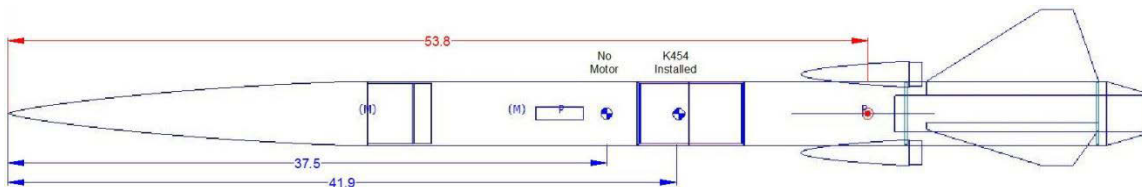


Figure 1: Basic Drawing of Rocket Design and Dimensions

Our final design is shown above. Critical design parameters are as follows:

- Diameter – 4”
- Overall Length – 71.5”
- Span diameter – 12.9”
- CP location – 53.8” from front of rocket
- CG₁ – 37.5” from front of rocket
- CG₂ – 41.9” from front of rocket
- Stability – 2.9 caliper with K454 motor

Payload Design

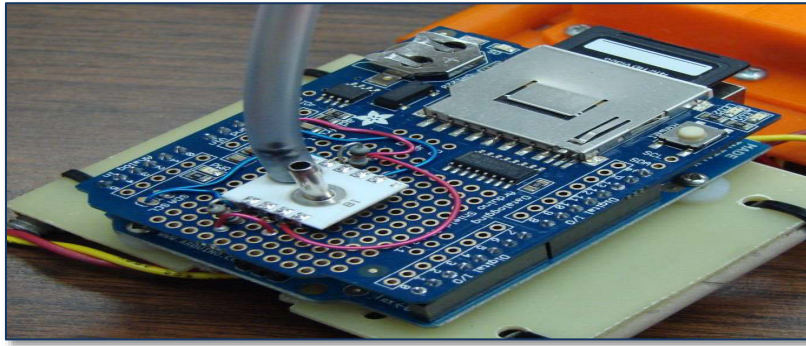


Figure 2: Differential Pressure Sensor

Our rocket contained two experimental payloads to assist us in determining its flight profile. Our first experiment used a pitot tube to determine the rocket's speed throughout the flight. The total pressure was sensed by the tube in the airstream outside the rocket and the static pressure was sensed in the altimeter bay. A differential pressure sensor manufactured by Silicon Microstructures Inc. converted the pressures to a digital signal. The differential pressure signal was read over its I²C bus, time stamped and stored on a flash card by an Arduino microcomputer. The data collected during the flight was downloaded and analyzed to calculate the rocket's velocity during the flight.

Our second experiment would attempt to determine the rocket's velocity using the Doppler Effect. Two piezo-electric sounders were mounted on opposite sides of the airframe to emit a 2700 Hz tone during the rocket's flight. We recorded the sound on the ground using a 20" parabolic microphone and a Zoom H1 digital recorder. After the flight we analyzed the recorded audio using an audio spectrometer software package which determined the shifted frequency of the emitted tone. From this frequency shift we were able to calculate the rocket's speed during flight.

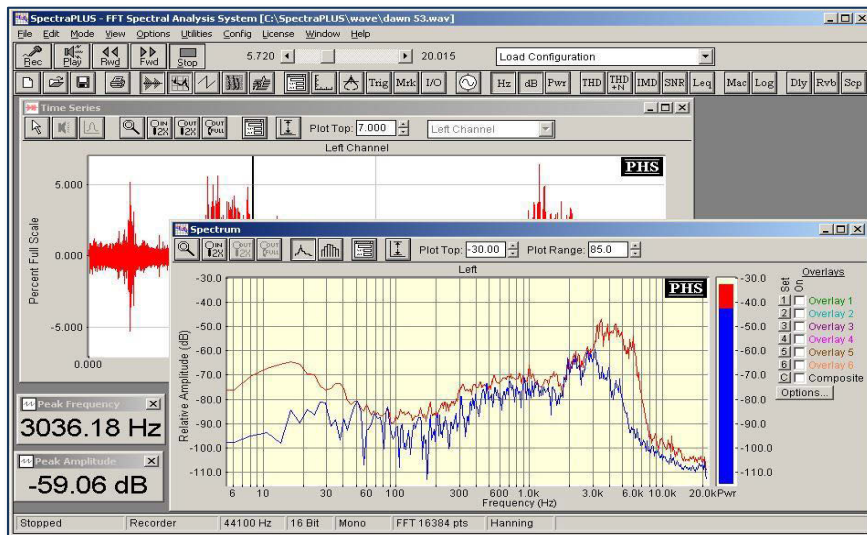


Figure 3: Recorded Data from Frequency Shift

Projected Flight Performance

After the rocket's construction was complete, it was weighed and the actual CG was measured. This data was added to our RockSim model to increase the accuracy of our flight simulations. RockSim predicted the following flight statistics when using a CTI K454 motor:

- Maximum acceleration: 223.7 Ft./s/s (7 g's)
- Maximum velocity: 312.2779 MPH
- Maximum altitude: 3,488 Ft.
- Time to burnout: 3.150 Sec.
- Time to apogee: 15.675 Sec.
- Optimal ejection delay: 12.525 Sec.

RockSim was also used to plot the predicted flight profile.

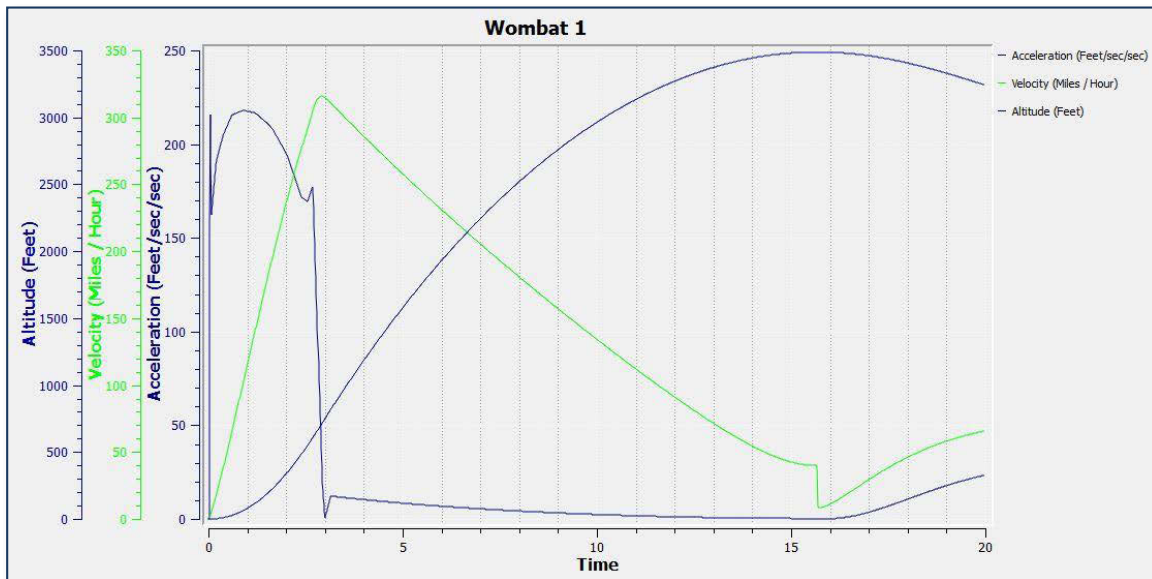


Figure 4: Projected Rocket Profile with RockSim Data

Rocket Construction



Figure 5: Fiberglass Tubing

With several pieces of fiberglass tubing, our adventure began. Starting with the fin can, we used a mixture of epoxy resin and hardener to hold together the individual pieces of the rocket. As an additional step, we also used expandable foam which was used to surround the motor tube and act as extra support for the fins.

We then began constructing the altimeter bay. For many on the team, this was the first experience they had with soldering.

Lastly, we assembled the nosecone and finished the rocket by drilling holes to relieve the pressure within the airframe. We also drilled holes to place sheer pins into the rocket, as a means to prevent drag separation.



Figure 6: Epoxy Adhesion to Tubing



Figure 7: Epoxy for Construction



Figure 8: Expandable Foam



Figure 9: Team Photo



Figure 10: More Epoxy Construction

Competition Flights

April 5, 2014, a day that will not soon be forgotten. It was warmer than usual, the kind of day one relishes after a long harsh winter. It was sunny and a crowd was beginning to gather. The cars were pulling in steadily, and by 9:00 am, Parking Lot E of the Richard Bong Recreational Area was flooded with the joyful exuberance of the day's fliers, judges, and spectators. Men, women, and children had come, from coast to coast, to this small park in Wisconsin to feast their eyes on one thing, the flight of the Wombat 1.

A ragtag team of Rocketeers approached the launch pad, rocket slung proudly over their shoulders; this was it. The crowd cheered their names as Team Night Skies walked ever forward, heads held high. The theme from *Chariots of Fire* played in synchrony with their footsteps. The rocket was quickly and calmly set up. The sounders were sounding, the altimeters were calculating, the Pitot tube was, was ... well, it was doing something, I'm sure, *pitoting, maybe... pressuring?* Regardless, this rocket was ready for liftoff! Fifteen minutes passed and in those fifteen minutes the Wombat 1 soared, popped its chutes, landed gracefully, and was hurriedly carried back to the judges. The data was slow to transfer. The crowd bit their nails; the nerves were beginning to creep up on them. This was their team; this was what they had come to see. Finally, the results were in, Team Night Skies had elevated to 3,051ft, a near perfect flight! No? That was the wrong altimeter, you say? The competition altimeter read higher than that? Oh, right, sorry about that then, "ahem"; what I meant to say was, Team Night skies had elevated to 3,348ft, which is still respectable and something that they're very proud of! At once, the nervous silence was overtaken by a deafening roar from the crowds. They had done it, ladies and gentlemen; Team Night Skies had really done it!

OK. So, I may have embellished a little bit of that story. But Team Night Skies really was and is a ragtag group of Rocketeers, and I really did hum the theme from *Chariots of Fire* as we walked out, and our rocket really did soar to 3,348ft, and, most importantly, we really did have as much fun as I tried to convey in that last paragraph. Thankfully, we were afforded the opportunity to fly a second time, achieving an even better altitude of 2,815ft and a much improved recovery time, roughly a twelve minute improvement. We were able to improve upon our initial flight with some quick thinking. We had to work with what we had available, so by adding some duct taped tools and padding it with gloves and pajamas we were able to reduce our altitude. Better still, both of our experiment, the Doppler shift and a Pitot tube, respectively, worked very well and closely resembled the data received via the Raven III altimeter, as will be shown in the following pages.

Doppler Shift Experiment

Experiment Design

This experiment attempted to determine the velocity of our rocket by measuring the Doppler shift of a tone emitted from two piezo-electric sounders on the rocket. The sounders were mounted on two sides of the rocket near the aft end. Each sounder emitted a ~3200 Hz tone at 100db. As the rocket accelerated off the launch pad, the emitted tone was recorded using a 20" parabolic microphone and a digital recorder. Data analysis was performed using audio spectrograph software and Excel.

Results

The recorded wave file was examined using an open source spectral analysis program called Spectran (www.weaksignals.com). The resultant waterfall graph is shown below.

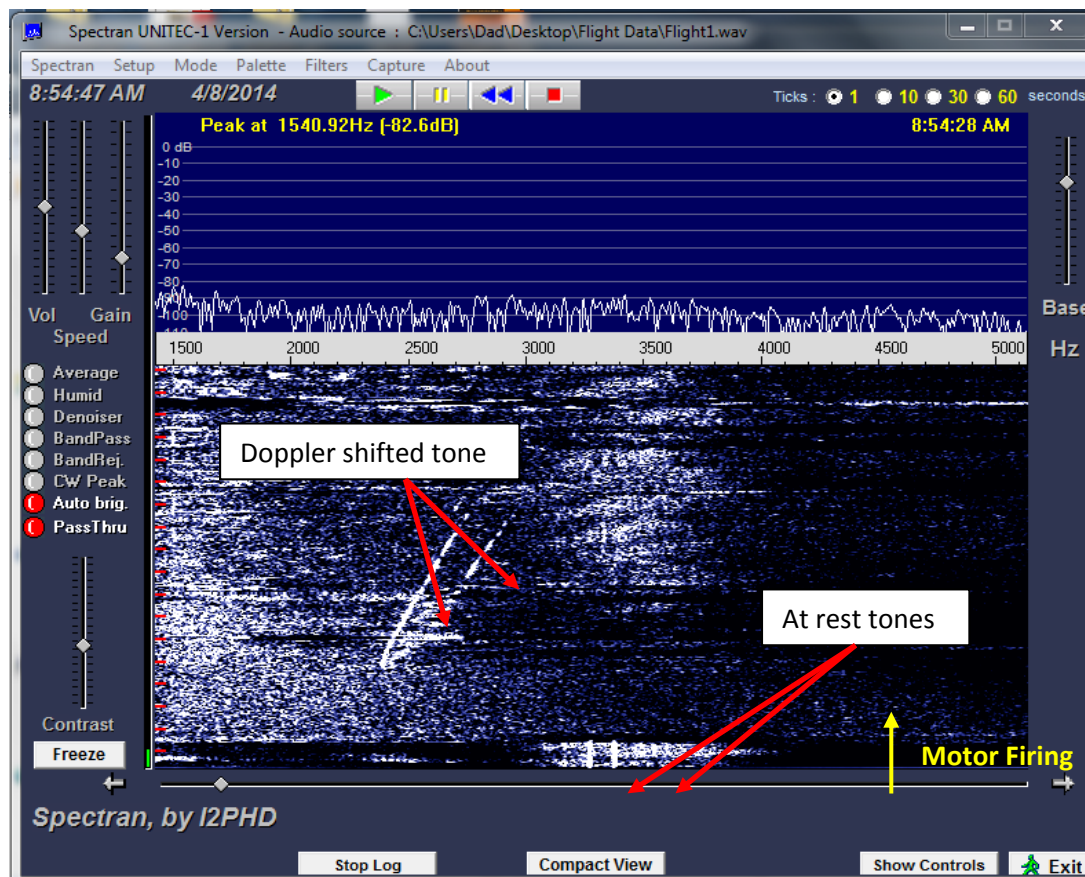


Figure 11: Doppler Shift Analysis Data

The program logs the peak frequencies and Excel was used to plot the results. The initial 3 seconds of audio were drowned out by the rocket motor noise. After nine seconds the rocket had arced over and the tones were no longer heard. The frequency data was converted to velocity using the formula $V = C * (F_s / F_o - 1)$ where:

- Fs = Frequency of the source
- Fo – Observed Frequency
- C = Speed of Sound
- V = Velocity

Excel was used to graph the resultant velocities.

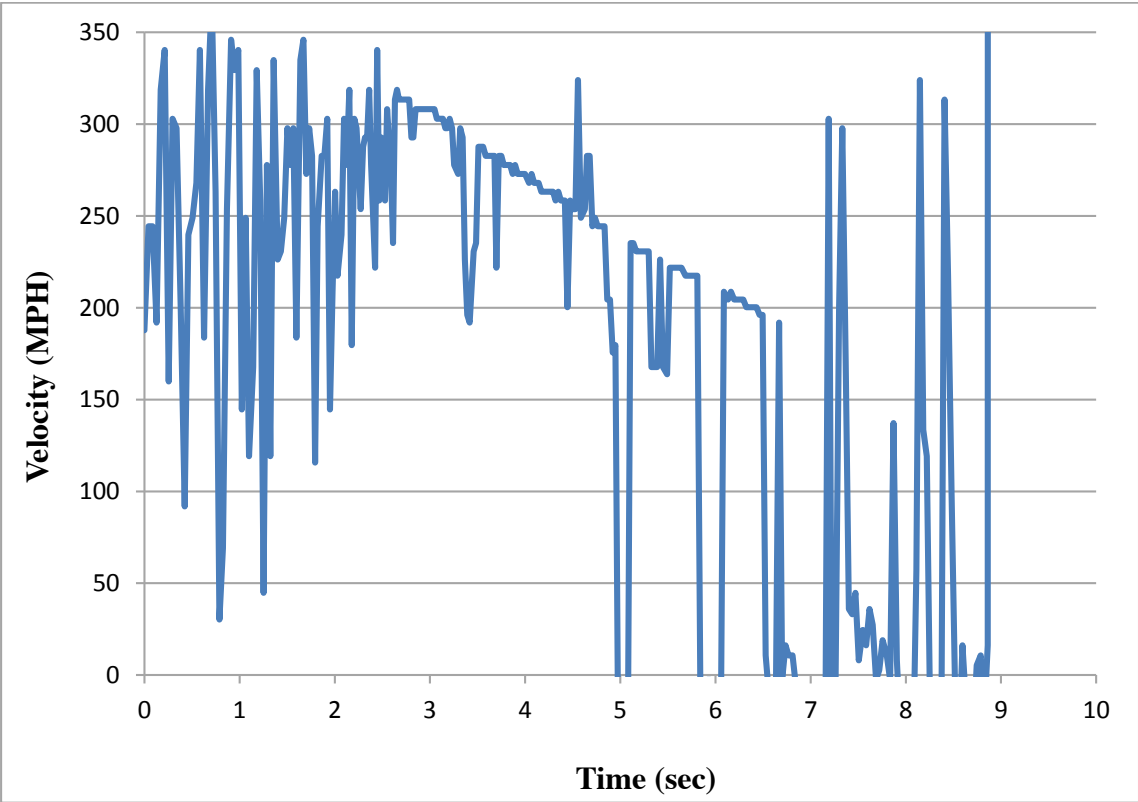


Figure 12: Graph of Velocity

Our initial comparison of the two data sets showed a substantial error in the Doppler data. Further analysis showed the error was due to the time it took for the sound emitted by the sounders to travel to the receiver. When the traverse time of the emitted signal was taken into account the error was eliminated.

The graphic below shows the two data sets overlaid on the same graph.

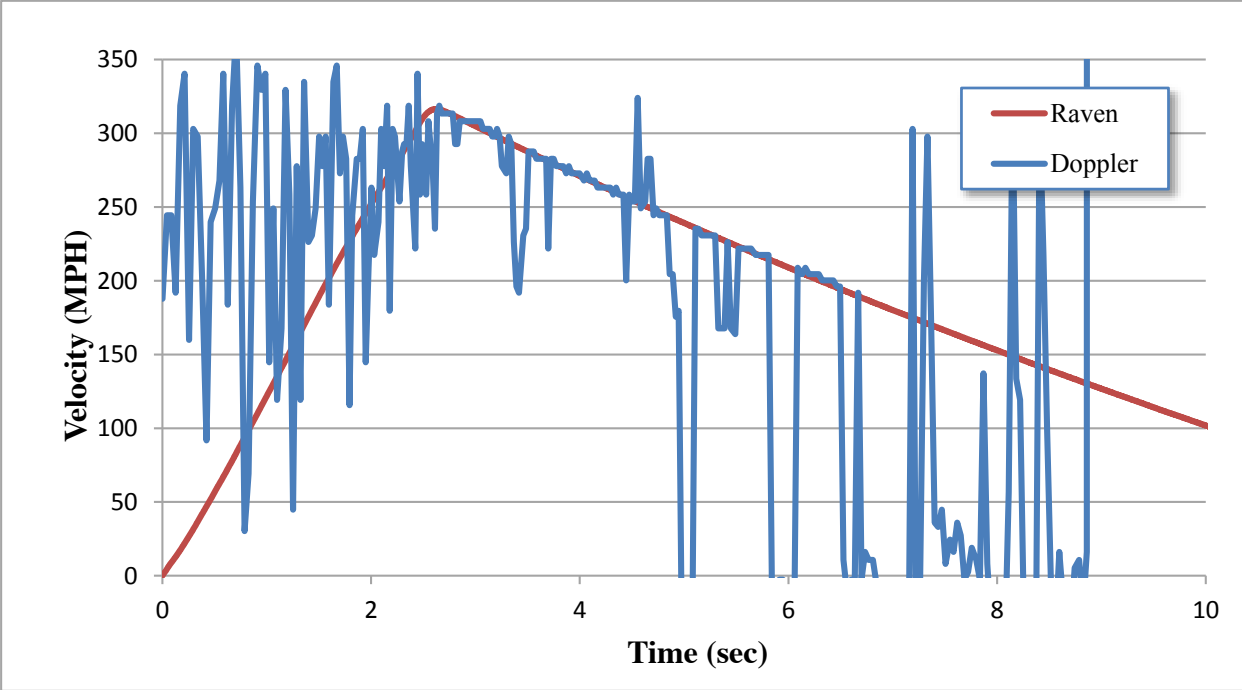


Figure 13: Comparison Chart of Raven and Doppler Data

As the chart shows, there is very strong correlation between the velocity data logged by the Raven altimeter and the Doppler data.

Pitot Tube Experiment



Figure 14: Arduino Microcomputer

Our second experiment also measured the rocket's velocity using a Pitot tube. A single port tube was placed outside the airframe to measure the dynamic pressure during the flight. The pressure from this tube was routed to the high side of a differential pressure transducer. The low side of the transducer was left open to sense the static pressure inside the altimeter bay. The resultant differential data was logged to a flash card using an Arduino microcomputer.

The differential pressure transducer was calibrated before the flight so we could convert the digital output of the transducer to engineering units. The resultant graph and transfer function are shown below.

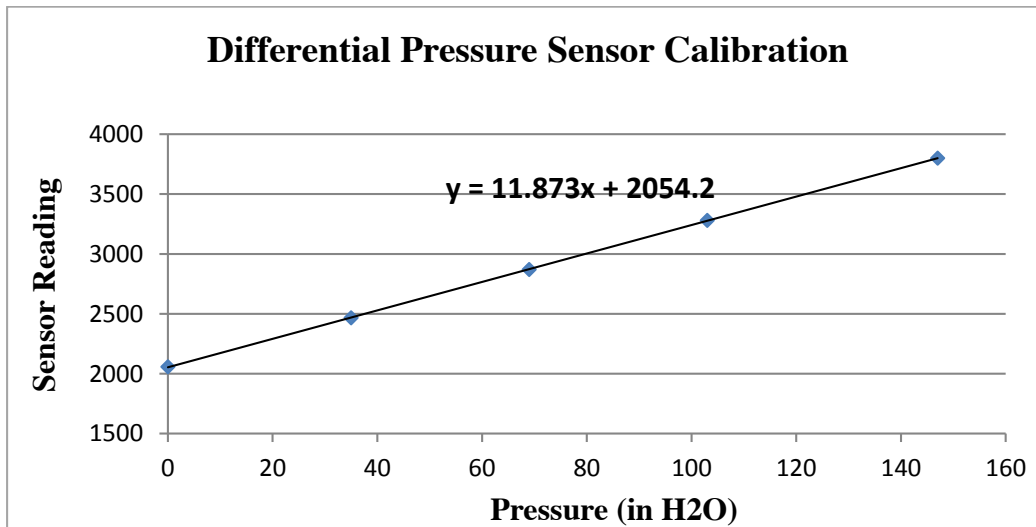


Figure 15: Preflight Calibration Data

Using this calibration data we could plot the Pitot tube pressure recorded during the flight.

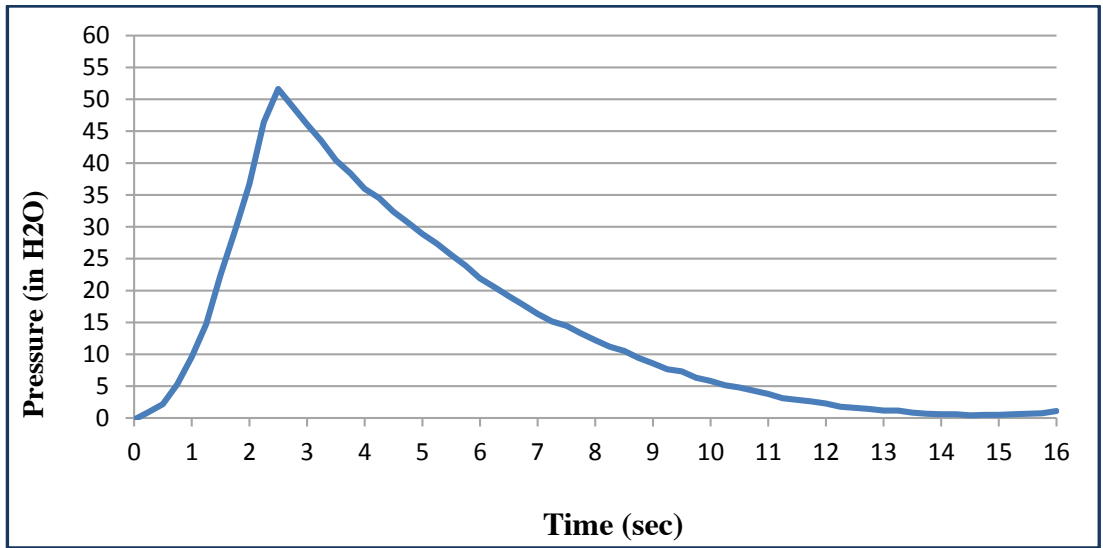


Figure 16: Pitot Tube Pressure During Flight

Next we converted the pressure data to velocity using the formula $V = \sqrt{\frac{2 * \Delta P}{\rho}}$ where:

V = Velocity

ΔP = Differential Pressure

ρ = Density of Air

Overlaying the Pitot tube velocity with the velocity reported by the Raven altimeter yielded an almost perfect match.

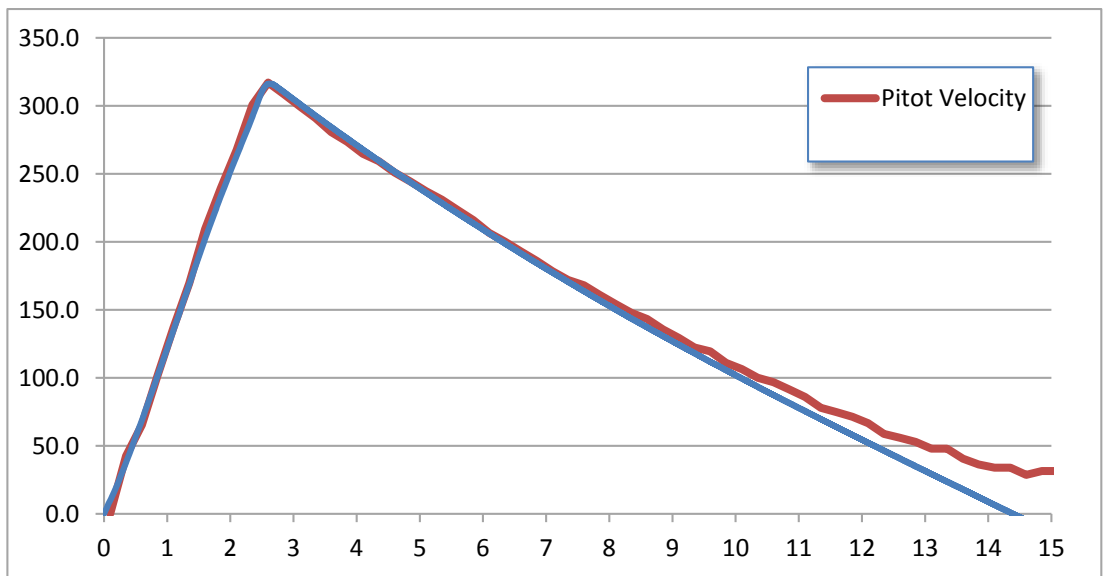


Figure 17: Comparison of Pitot tube Velocity to Raven Altimeter

Using the data from the Pitot tube, the rocket's acceleration and altitude was calculated. The calculated data was graphed with the corresponding data from the Raven altimeter and is shown below. Again there is strong correlation between the two data sets.

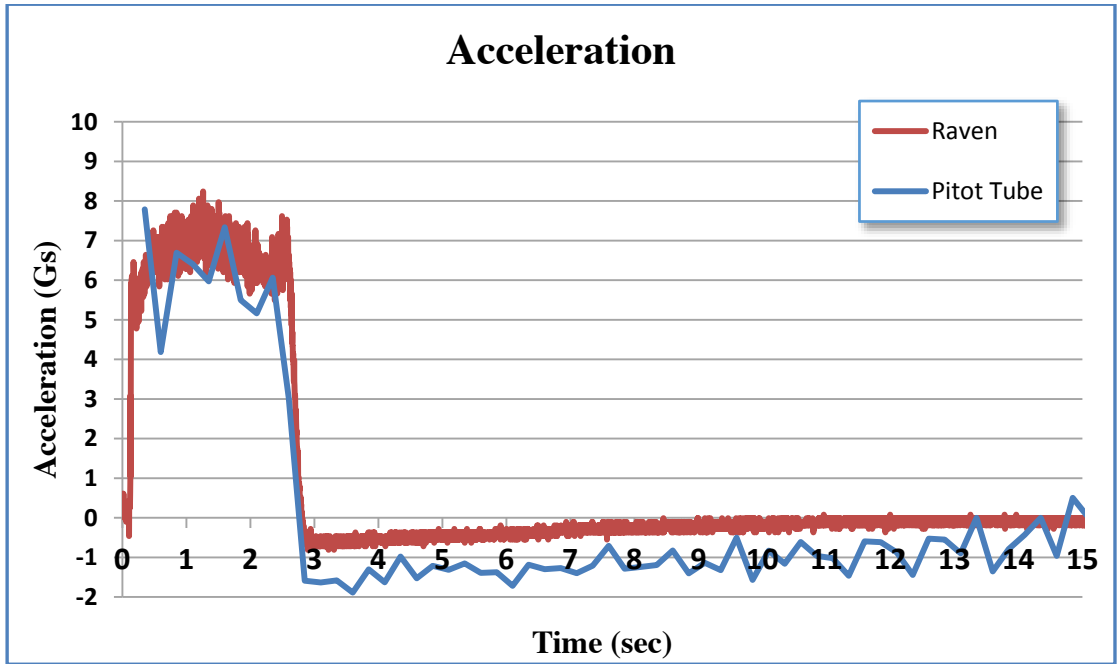


Figure 18: Acceleration Comparison of Raven and Pitot tube

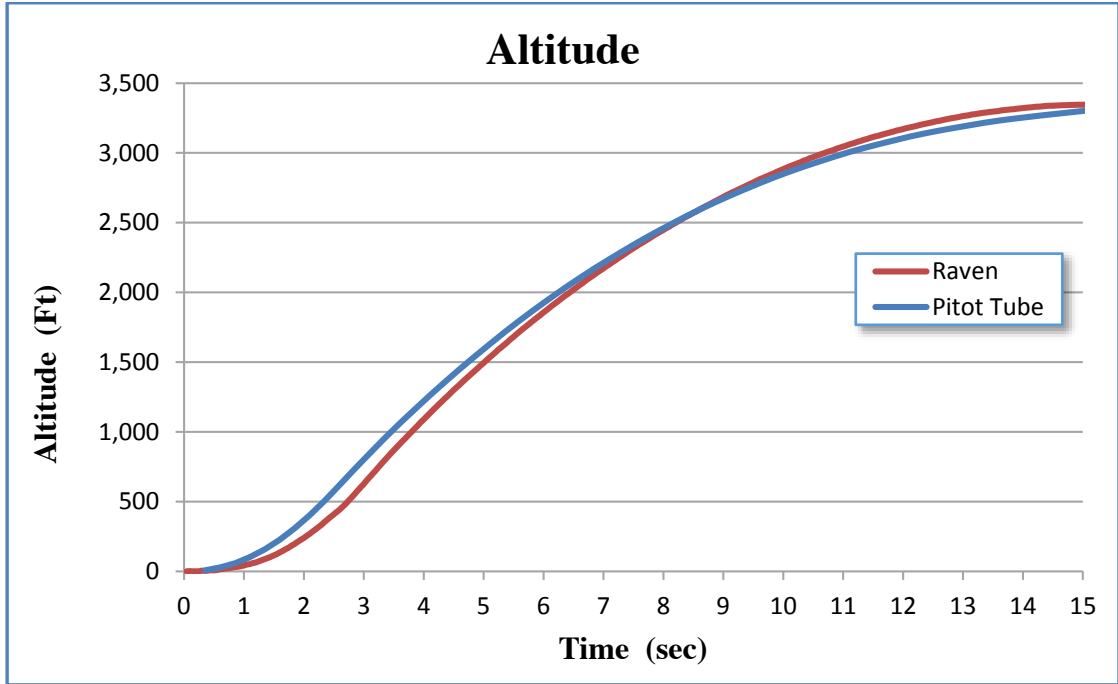


Figure 19: Altitude Comparison of Raven and Pitot tube

Conclusion

Data from both the Doppler and Pitot tube experiments matched closely to the data downloaded from the Raven altimeter. The Doppler experiment was hampered by the motor noise and the directional nature of the piezo-electric sounders but the limited data we collected provided a proof of concept for this technique.

Closing

Participating in the WSGC 2014 Collegiate High-Powered Rocketry Competition was a new and great experience for all members of Team Night Skies. This was a field of study that we had very little knowledge of prior to this competition. It gave us the opportunity to explore the fields of technology, science and innovation. Only one of us is majoring in the science field, so it was an expansive introduction into this field for our other two members and also gave our team a unique perspective. This competition also helped us develop our cooperation and interpersonal skills; working on a team and helping each of us to develop our leadership skills. Our team was also proud to be able to represent a gender that did not have much representation in this competition. We had two females on a team of three members. In addition, this has had a valuable experience for students who have an interest in working for NASA or any other company in the aerospace engineering sector. The entire competition was a great learning opportunity and experience and served as the platform from which we will continue to build our newly found love of rocketry.

It was an exciting process to see our rocket come to life. Each step along the way advanced our understanding and education of rocketry, from the starting stages, to the initial design plan, to the fabrication of our beloved Wombat 1, and finally being able to successfully launch our rocket. This was a truly life changing experience as, without this competition, we probably would have never gained this knowledge. This experience has led us to appreciate rocketry so much more than we ever would have expected, and we would like to extend a great thanks to all involved with this completion for presenting us with an opportunity to participate. Thank You.

Budget

University of Wisconsin - Sheboygan Rocket Competition Budget

Rocket

| | | | |
|-----------------------------|----|--------|-----------|
| Formula 98 rocket kit | | | |
| Standard Kit | \$ | 139.99 | |
| Manufacturer changes to kit | \$ | 35.00 | |
| Motor Retainer | \$ | 55.00 | |
| Shipping | \$ | 16.65 | \$ 246.64 |
| Altimeter | | | \$ 165.00 |
| Altimeter sled | | | \$ 30.99 |
| Misc. Hardware | | | \$ 50.00 |
| Lead ballast weights x3 | | | \$ 54.11 |
| 50" Parachute | | | \$ 79.95 |

Experiments

| | | | |
|--------------------------------------|--|--|----------|
| Pitot tube holder | | | \$ 29.44 |
| Power Connectors | | | \$ 3.99 |
| Differential Pressure Sensor | | | \$ 34.70 |
| Arduino data logger shield | | | \$ 32.24 |
| Cast eyebolt & tubing for pitot tube | | | \$ 17.83 |
| Piezo-electric sounder & batteries | | | \$ 16.77 |

Rocket Motor Reloads

| | | | |
|-----------------|----|--------|-----------|
| K454 Reloads x2 | \$ | 114.99 | \$ 229.98 |
|-----------------|----|--------|-----------|

| | | | |
|----------------------------|--|--|------------------|
| Total Budgeted Cost | | | \$ 991.64 |
|----------------------------|--|--|------------------|

24th Annual Wisconsin Space Conference

PART FIVE

Education and Public Outreach

Science Outreach at the BTC Institute - Aerospace Outreach Program & Special Initiatives Program

Barbara Bielec

BioPharmaceutical Technology Center Institute

Abstract

The BioPharmaceutical Technology Center Institute (BTC Institute) is a non-profit educational organization founded in 1993; located in Fitchburg, WI. During the summers of 2013 and 2014, the BTC Institute offered teacher training in biotechnology through two graduate education courses, *Biotechnology: The Basics* (2013 & 2014) and *Biotechnology: Beyond the Basics* (2013). Teachers of a wide variety of subjects with varied levels of teaching experience were active participants in this lab-based learning that provided teachers with training, background and curriculum materials including information about NASA and biotechnology. In addition to the teacher courses, the BTC Institute in partnership with the African American Ethnic Academy, Inc. (AAEA), a Madison non-profit organization, also offered "A Celebration of Life!", a science program for upper elementary and middle school students. The focus of the 2013 program was *Energy* and the focus of the 2014 program was *Flight*.

Aerospace Outreach Program

Introduction

Biotechnology: The Basics and *Biotechnology: Beyond the Basics* are week long summer courses offered by the Biotechnology Technology Center Institute (BTC Institute). *Biotechnology: The Basics* was held during the summers of 2013 and 2014; *Biotechnology: Beyond the Basics* was held during the summer of 2013. The primary goal of these courses is to provide middle school and high school teachers with the training essential to implementation of a laboratory-based biotechnology curriculum. This goal served as the guide in structuring each course, as well as in designing and implementing each activity. Both courses were offered for graduate education credits through Viterbo University and Edgewood College. All three course instructors are experienced teachers of biotechnology at the secondary level.

Three objectives of the National Space Grant Program are to:

- “Encourage interdisciplinary training, research and public service programs related to aerospace.” The need for quality STEM education training extends throughout many scientific disciplines, and as plans are made for humans to travel and someday live in space, biotechnology joins other technologies to support the “public service programs related to aerospace. Often students and teachers in the life sciences do not fully realize how biotechnology relates to NASA. One of the objectives for both courses was to highlight how biotechnology is and will be used in space exploration.

The BTC Institute is pleased to acknowledge the Wisconsin Space Grant Consortium Aerospace Outreach Program, the Wisconsin Space Grant Consortium Special Initiatives Program, the NASA Summer of Innovation Project, FOTODYNE Incorporated and the Wisconsin Environmental Education Board for their financial support.

- “Recruit and train U.S. citizens, especially women, underrepresented minorities, and persons with disabilities.” Enthusiastic well-trained STEM teachers are key to recruiting diverse future STEM professionals in “aerospace science and technology.” Making connections between biotechnology and NASA increases the pool of teachers and students who will help meet this objective since it also brings in life science teachers and the students that they teach.
- “Promote a strong science, mathematics and technology education base from elementary through secondary levels.” *Biotechnology: The Basics* and *Biotechnology: Beyond the Basics* help prepare teachers to provide “a strong STEM education base” utilizing current content and techniques. Classroom implementation of these content and techniques will enrich student learning which can “improve student academic outcomes.” (National Space Grant College and Fellowship Program, 2014).

Generating student interest in further STEM education and careers, including those at NASA, will require the efforts of all STEM educators, not just physics and space science teachers. Technology training that includes discussion of NASA resources and projects will help “raise the level of exposure and interest of K-12 teachers, students, and the general public in space, aerospace, and space-related science, design, or technology and its potential benefits; and/or increase interest, recruitment, experience and training of pre-college students in the pursuit of space- or aerospace-related science, design, or technology.” Training teachers from throughout the Midwest who teach a wide variety of students also helps “Improve the STEM pipeline by including underserved and/or underrepresented students in the project; or including the teachers who specifically teach those populations.” (Aerospace Outreach Program Request for Proposals 2014-2015).

Both courses included real-life examples of how biotechnology is utilized by NASA. For example, in the Summer of 2014 Dr. Eric Roden, Professor UW-Madison Department of Geoscience presented on how he uses biotechnology techniques in his bacterial research as part of the NASA funded Astrobiology Research Consortium . In addition, one of the requirements for teachers receiving a WSGC scholarship for *Biotechnology: The Basics* or *Biotechnology: Beyond the Basics* was to submit a 2-3 page summary report to the BTC Institute, at the end of the semester in which they implement discussion of NASA utilization of Biotechnology. Darcia Schweitzer, one of the 2013 WSGC teacher scholarship recipients reported the following.

Summary Report: Implementation of Classroom Discussion of NASA Utilization of Biotechnology
Darcia Schweitzer, Science Teacher Dodgeland High School, Wisconsin. May 2014

Description of how a discussion of NASA utilization of Biotechnology was implemented.

Students were introduced to NASA’s utilization of Biotechnology through reading the article, “Biotechnology-driven cell biology applications in microgravity: Summary of three test cases” (Kelleher, 2003). After students had read the article, we had a class discussion about the different ways biotechnology companies are cooperating with NASA to conduct research, particularly in the area of microgravity studies. Students were then asked to find another current article detailing a research project involving NASA and biotechnology. These articles were collected, copied, and distributed back, so that each student had a copy of each article. Students were asked to read the articles, and, again, participated in a class discussion of the various technologies and topics involved in biotechnology research through NASA.

Students then received a project assignment which required them to come up with a research proposal for NASA relating to biotechnology. I gave students guidelines for writing the proposal and discussed each section required in the proposal with students. Particular emphasis was placed on the "Introduction and Literature Review" section; students were advised to put the most effort into completing a thorough review of past and current research findings related to their proposed hypothesis and experiment. Students were given a week to complete a rough draft. I read each draft and provided students with feedback about how to improve their proposal. Students were then given an additional week to develop the final draft of their proposal; this was then graded as a project, using a simple scoring rubric. Students were asked to share a brief, informal presentation of their proposal with the class.

After completing the presentations, students had an opportunity to ask questions of other students and myself. Students then received a questionnaire requesting feedback about the unit. They were asked three questions: "What have you learned about NASA's utilization of biotechnology?", "What do you still want to know about NASA's utilization of biotechnology?", and "Do you think this was a worthwhile unit? Why/why not?" They responded in writing.

Student feedback on the discussion.

Overall, students felt that this unit was worthwhile; 75% of the class responded this way on the survey. One student expressed that they "gained knowledge on [a] real world situation in which biology is a key subject for studying and making advancements for mankind." Another stated, "We got to explore outside of what we would of originally learned and we got to get in depth into it." It seems that students really appreciated the opportunity to take the content of our course and not only see its real world applications, but also attempt to develop their own ideas and hypotheses about biotechnology in space. The minority that did not find the unit worthwhile stated that they were simply disinterested in the topic.

When asked what they learned about NASA's utilization of biotechnology, many students referenced the multitude of wide-ranging experiments that have been done and could be done. "NASA has completed numerous experiments to understand how single celled organisms and plant species may [be] impact[ed] by life in space," said one student. Students also mentioned the benefit to society of many experiments that have an impact on medical knowledge and treatments. One student recognized that, "new things are being discovered, and things are progressing because of NASA's work in space...this is helping the world's medical research."

Most students enjoyed learning about this distinctive niche for biotechnology research and utilization, as evidenced by the fact that many of them responded to the survey with further questions about NASA's involvement with biotechnology. Some sample questions from the students: "I want to know what NASA goes through in order to pick an experiment to do at the ISS." "I want to know what being one of the scientists that goes up in space is like." "What does NASA intend to do in the future with biotechnology?" I think I have sparked some interest in this topic that may be long-lasting, and even persist in the choices these students make for an area of study in college or a career. I found this unit enjoyable to teach to the students because the topic kept them engaged and they were really motivated by the experimental proposal project; three students who typically do not work hard during class and complete sub-par work were able to produce proposals that demonstrated their potential. As an educator, I cannot ask for much more than that.

Program Details

Biotechnology: The Basics (2013 & 2014) and *Biotechnology: Beyond the Basics* (2013) were one-week summer courses. Representing rural, urban, and suburban school districts, the attendees were teachers of a variety of subjects, including: middle school science, biology, biotechnology, agriculture, and chemistry. Class participants included teachers who had no previous training in biotechnology, as well as very experienced secondary teachers looking to update their knowledge of scientific content and techniques. Some of the teachers currently teach an independent biotechnology course; others incorporate biotechnology curricula within other life science,

chemistry or agriculture classes. Several teachers were looking for information to help them design and implement a biotechnology course for the first time.

For both courses, teacher participants were recruited through direct contact at the BTC Institute and a variety of teacher conferences; emails and electronic postings to several list-servs and websites; direct recommendation from UW-River Falls Agriculture Education Professor Timothy Buttles; and course listings in the Viterbo University and Edgewood College summer catalogs.

Table 1: Participants in *Biotechnology: The Basics* and *Biotechnology: Beyond the Basics*

| Teacher Course | Total Participants | High School Science Teachers | Agriculture Teachers. Often teach both high school and middle school | Other. Includes middle school teachers |
|--|--------------------|------------------------------|--|--|
| <i>Biotechnology: The Basics</i> 2013 | 9 | 3 | 4 | 2 |
| <i>Biotechnology: Beyond The Basics</i> 2013 | 7 | 5 | 1 | 1 |
| <i>Biotechnology: The Basics</i> 2014 | 7 | 5 | 2 | 0 |
| Total | 23 | 13 | 7 | 3 |

Attendance in these courses was largely due to scholarship funding provided by the Wisconsin Space Grant Consortium, the BTC Institute and FOTODYNE, Inc. Professional development funding is increasingly difficult for teachers to obtain, and the BTC Institute and the teachers who took the courses are very grateful for this support.

Topics and laboratory activities for *Biotechnology: The Basics* included: use of micropipettes, agarose gel electrophoresis, DNA extraction, restriction enzyme digestion, polymerase chain reaction (PCR), bacterial transformation, bioethics, genetic counseling, biotechnology and NASA, stem cells, biofuels and the Great Lakes Bioenergy Research Center, and careers and training in biotechnology.

Topics and laboratory activities for *Biotechnology: Beyond the Basics* included: PCR and transformation of the PTC gene, genetic identity testing, microarrays, science and social media, protein purification and detection, immunology, bioinformatics, biotechnology and NASA, bioprospecting and the Great Lakes Bioenergy Research Center, and, training and careers in biotechnology.

Implementation was consistently emphasized. How would teachers apply what they learned in their own classrooms? Resources included a comprehensive course binder for each teacher; laboratory protocols, classroom activities and power point presentations on a flash drive for each teacher; daily discussion and review of course topics and resources; and discussion of funding and equipment sources and tips for successful grant writing.

Each day teachers wrote a reflection detailing how they would integrate material into their curriculum and the challenges that they might face, including the resources they would need. These reflections were discussed the next day with the entire group. As a final project, each teacher

had to design and present a detailed and personalized curricular unit (lesson plan) that they intend to use with their students.

Results

Course evaluations were extremely positive for all three courses. For example, the 2014 *Biotechnology: the Basics* course evaluations included the following comments:

- I can't single out any [workshops] that were the most useful. I came here wanting to gain knowledge & all the workshops did that.
- I am very grateful for the scholarship, materials and the 2 awesome teachers we had. I also was really pleased with the low student/teacher ration. Also I was very happy to get my questions answered.
- I thought this was great. I had limited knowledge of the topic and fell good about where I am at now. I wouldn't change anything.
- I thought it [the course] was excellent, I really enjoyed the mix – lab discussion, content, guest speakers, etc., etc.
- Loved all the labs & hands-on activities.
- The course was outstanding – great feedback daily & all questions were answered. Review sheets each day were excellent way to received feedback.
- I received a plethora of resources, techniques and ideas!! Excellent week! Best weeklong class taken!! Thanks for everything!

Course evaluations also offered suggestions to improve the courses:

- More time to communicate with participants.
- [some] workshops were helpful but need to be a little shorter in length.
- Color code binder to find materials easier.
- Consider offering something for middle school teachers.
- Perhaps the lab protocols could be broken down into a flow-chart for the pre-lab discussion/directions.
- More structured teacher “share time”.

Course evaluations and daily reflections are used to improve courses year to year, as well as to address questions and concerns throughout the course. Next year several of the suggestions will be incorporated.

Conclusion

The enthusiasm demonstrated by our attendees is always inspiring. It consistently and clearly demonstrates the need for high quality professional development opportunities that have immediate relevance to the classroom. As stated by the National Science Board/National Science Foundation (NSB/NSF) in A National Action Plan for Addressing the Critical Needs of the U.S. Science, Technology, Engineering, and Mathematics Education System: “The United States possessed the most innovative, technologically capable economy in the world, and yet its science, technology, engineering, and mathematics (STEM) education system is failing to ensure that *all* American students receive the skills and knowledge required for success in the 21st century workforce.” In the action plan’s description of implementation it elaborates: “stakeholders should create professional development opportunities that deepen teachers’ content knowledge, inquiry experiences, pedagogical skills, and understanding of instructional materials and their use in the classroom. Retaining high quality STEM teachers depends on facilitating access to opportunities for professional development and intellectual growth throughout their careers.” (NSB/NSF 2007)

We are committed to offering quality professional development in STEM for teachers so that their students develop the STEM skills and knowledge needed for future success. We will continue to seek grant opportunities and new partnerships that will enable us to fund teacher scholarships and provide teachers with much-needed resources. The support provided by the Wisconsin Space Grant Consortium to design and implement these courses is greatly appreciated. The donations of instructor time and materials from Fotodyne, Promega, the Morgridge Institute for Research, Meriter Hospital, Madison Area Technical College, the Great Lakes Bioenergy Research Center and the UW–Madison Department of Geoscience Astrobiology Research Consortium are also key to our success. These partnerships, along with the options to receive graduate education credits through Viterbo University and Edgewood College, ensure the continuation of these essential opportunities for professional development.

Special Initiatives Program

Introduction

The primary goal of “*A Celebration of Life*” is to support the continued development of African American and other students’ interest in science, and to provide them with tools for success in school. A long-term goal continues to be increasing the number of minority students who successfully complete high school science courses, and who may eventually choose to pursue science, technology, engineering and math (STEM) careers. Extensive efforts are made to ensure participation of students from economically challenged families through the provision of scholarships and transportation.

Program Details

The program themes for 2013 and 2014 were *Energy* and *Flight*, respectively. The two-week weekday morning programs were held in June and July, the first session was for elementary students grades 3-5, the second session was for middle school students grades 6-8. For both sessions, hands-on activities, in outdoor, classroom and laboratory settings, were designed to engage students’ interest in science and STEM careers. This was accomplished through a series of activities about energy, flight, NASA projects and African American STEM professionals. Program activities reflect the Wisconsin Model Academic Standards for Science, which follow the form and content of the National Science Education Standards. Many of the educational activities were from the NASA Summer of Innovation Project (<http://www.nasa.gov/offices/education/programs/national/summer/home/index.html>, 2013).

Fifty-eight percent of the student participants were African American, and 69% of all participants belong to an underrepresented minority group. Many participants received scholarships and transportation to facilitate their participation in the program. A total of 72 students: 36 girls (50%) and 36 boys (50%), participated in developmentally appropriate learning.

Table 2: Gender and Ethnicity of Participants in *A Celebration of Life XVIII: Energy!* and *A Celebration of Life XIX: Flight!*

| Program | Total Participants | Girls | Boys | African-American | Hispanic | Other |
|----------------------------------|--------------------|-------|------|------------------|----------|-------|
| 2013 <i>Energy</i> Elementary | 19 | 8 | 11 | 11 | 0 | 8 |
| 2013 <i>Energy</i> Middle School | 18 | 10 | 8 | 12 | 1 | 5 |
| 2014 <i>Flight</i> Elementary | 14 | 6 | 8 | 7 | 3 | 4 |
| 2014 <i>Flight</i> Middle School | 21 | 12 | 9 | 12 | 4 | 5 |
| Total | 72 | 36 | 36 | 42 | 8 | 22 |

Specific topics for the summer 2013 *Energy!* and 2014 *Flight!* programs are listed below and many of the educational activities used were designed by NASA.

2013 *Energy!*

- types of energy
- energy for plants and animals
- renewable and nonrenewable sources of energy
- energy conservation
- current NASA projects related to energy, including space exploration
- historic and contemporary African American STEM professionals, including those affiliated with NASA

2014 *Flight!*

- basic principles of flight
- how birds fly
- constructing/testing aircraft and rockets
- current NASA projects related to flight, including space exploration
- careers in aviation
- historic and contemporary African American (STEM) professionals, including those affiliated with NASA

Each session also included a field trip and concluded with student presentations of selected activities to their peers, family members and other adult guests on the last day of each session. Students also shared their posters of African American STEM Professionals.

Results

Pretests and post-tests are administered as part of each AAEEA/BTC Institute summer science program as one indicator of students' learning. Overall, both elementary and middle school students showed an increased knowledge about energy, flight and African American STEM professionals. Some example questions and results are listed below.

In 2013 elementary students were asked to "Draw a food chain that shows how energy is transferred." On the pre-test, 81% (13/16) left this blank. On the elementary post-test, 67% (12/16) students could draw a food chain correctly and the other 33% could draw a food chain with some errors.

In 2013 middle school students were prompted: “The person in this picture is a STEM professional. What does STEM stand for?” On the pre-test, 73% (11/15) students left this prompt blank or gave an incorrect answer; on the post-test, 100% (16/16) could answer correctly.

Comments from the students who participated also speak to the impact of the program. When asked on the 2013 post-test, “Would you like to become a STEM Professional when you grow up? Why or why not?” elementary responses (spelling corrected) included:

- I would love to be a STEM Professional because I now know a lot about STEM.
- Yes, because I really like science.
- Sure why not I'd think it would be fun.
- I would love to be a STEM professional because it seems fun and I love helping people.
- Yes I would, because I will be helping the economy and create better energy sources.
- I would because I want to be a science leader and I love science.

On the 2014 elementary tests students were asked to “List any African American aviators (pilots or astronauts) or scientists, engineers or mathematicians that you know about.” Space was given for four answers. On the pretest only 1/13 (8%) students answered with the name of one African American STEM professional, the rest left the question blank. On the post-test all students (100%) listed four African American STEM professionals we had featured.

On the 2014 middle school tests students were asked, with an airplane diagram, to “Fill in the names of the 4 forces that act on an airplane.” On the pretest only 4/19 (21%) students could label either three or four forces correctly, on the post-test 14/16 (88%) could label all four forces correctly.

On the 2014 pretest and post-test middle school students were also asked: “Would you like a career in aviation or at NASA? Why or why not? Results are lists are listed below, spelling corrected.

Table 3: *A Celebration of Life XIX: Flight!* Middle School Responses to the prompt: “Would you like a career in aviation or at NASA? Why or why not?”

| Response | Pretest | Post-test |
|-------------------|---------|-----------|
| Yes | 4 | 9 |
| Maybe/ Don't know | 4 | 1 |
| No | 7 | 6 |
| No answer | 1 | 0 |
| Total | 16 | 16 |

- Aviation because they have good planes and they have candy but you can choose to be a pilot or not.
- Yes, because I'm fascinated with things that fly.
- I would like a job at NASA because I am more interested in Technology & Engineering.
- I think I would definitely consider it because I would love to experience actually flying, but I would probably be too scared.
- Yes, because now I know there are more jobs than astronauts, and some that I might like.
- Yes so I can fly in a plane with comfortable seats and get paid a lot of money.
- No because I really want to be a bone doctor and artist.
- Yes, because I always want to fly and see what space is like (what it looks like and the feeling of no gravity).
- No. I don't like to fly because I'm afraid of heights.
- No, I like the ocean better.
- I wouldn't be too interested in a career of aviation but working at NASA seems cool and awesome.
- I would like a career in NASA because I really wanted to go to space.

- I would want to be a pilot because it's fun, easy (except for bad weather and in the dark) and in the sky it looks like you can see the whole world!

Scientific content knowledge can be measured by the pretests and post-tests, providing information regarding one aspect of program assessment. Another key indication of success is the number of students who had participated in previous AAEA/BTC Institute programs, or who had family members who were previous participants. In the 2013 and 2014 summer programs, participants included 72 elementary and middle school students total. Of those 72 students, 53% (38/72) had previously participated, or have had family members who have participated. In the 2014 middle school program, of the 21 participants, 62% (13/21) had previously participated, or had family members who had participated. Eight of those 13 previous participants, all members of underrepresented minority groups, have participated for 3+ years!

The return rate of students, along with excellent attendance throughout both sessions, is solid evidence that this program is valued by the participants and their families. When students return for the third, fourth, fifth or sixth year, it is a strong indication of their interest in science programming.

Conclusion

The National Science Foundation (NSF) report, *Women, Minorities, and Persons with Disabilities in Science and Engineering: 2011*, noted that: "Underrepresented minorities [blacks, Hispanics, and American Indians] share of science and engineering bachelor's and master's degrees have been rising over the two decades since 1989, with shares of doctorates in these fields flattening after 2000. The greatest rise in science and engineering bachelor's degrees earned by underrepresented minorities has been in the social, computer, and medical sciences fields of study." However, this increase in STEM degrees still does not show equivalency with the population percentage of underrepresented minority groups in the U.S. population. From data presented in the NSF report African Americans comprised only 3% of the "Scientists and engineers in science and engineering occupations: 2006." The report concluded that: "The science and engineering workforce is largely white and male. Minority women comprise fewer than 1 in 10 employed scientists and engineers." (NSF, *Women, Minorities, and Persons with Disabilities in Science and Engineering: 2011*) Supporting African American educational opportunities in science is essential to helping increase the number of African American students who will ultimately go into baccalaureate and graduate programs in science.

A National Science Teachers Association feature article about science education programs that successfully engage underrepresented students describes the importance of culturally relevant content: "Teachers should discuss African-American scientists throughout the course, not just during Black History Month...Although textbooks may still lack adequate connections between science content and minority scientists, the internet is a great source to find individuals linked to specific stages of scientific development. Minority students will identify with these role models, and thus begin to personalize the science concepts and consider careers in science." (Bardwell and Kincaid, 2005). The AAEA/BTC Institute programs will continue to focus on African American STEM professional role models to help inspire students.

This approach is in alignment with the goal and objectives of the National Space Grant Program, 2010-2014. "The goal of the Space Grant Program is to contribute to the nation's science enterprise by funding education, research, and informal education projects through a national network of

university-based Space Grant consortia.” One of the objectives of the Space Grant Program is to: “Promote a strong science, technology, engineering, and mathematics education base from elementary through secondary levels while preparing teachers in these grade levels to become more effective at improving student academic outcomes.” A second objective is to: “Recruit and train U.S. citizens, especially women, underrepresented minorities, and persons with disabilities, for careers in aerospace science and technology.” (National Space Grant College and Fellowship Program [Space Grant] 2010-2014).

The support provided by the Wisconsin Space Grant Consortium helps the *A Celebration of Life!* summer science program meet both of these objectives, and the overall goal of the Space Grant Program. *A Celebration of Life!* has helped provide a “strong science, technology, engineering and mathematics education base” for both upper elementary and middle school secondary students. The exploration opportunities provided by the summer program enrich and enhance students’ scientific knowledge and associated skills. It is also essential for students to see themselves in those roles. Learning about historic and contemporary African American STEM professionals as part of an exciting hands-on science program assists in developing a diverse work force of problem solvers, scientists, inventors and engineers for “careers in aerospace science and technology.”

References

Aerospace Outreach Program Request for Proposals 2014-2015. Available at <http://www.uwgb.edu/WSGC/k12/announcements/ao.aspx>

Bardwell, Genevieve and Kincaid, Eric. The Science Teacher, February 28, 2005. *A Rationale for Cultural Awareness in the Science Classroom*. <http://www.nsta.org/publications/news/story.aspx?id=50285&print=true>

NASA Summer of Innovation Project, 2013. Available at http://www.nasa.gov/offices/education/programs/national/summer/education_resources/index.html

National Science Foundation, Division of Science Resources Statistics. 2011. *Women, Minorities, and Persons with Disabilities in Science and Engineering: 2011*. Special Report NSF 11-309. Arlington, VA. Available at <http://www.nsf.gov/statistics/wmpd/>.

National Science Board / National Science Foundation. A National Action Plan for Addressing the Critical Needs of the U.S. Science, Technology, Engineering, and Mathematics Education System, October 30, 2007. <http://www.nsf.gov/nsb/publications/2007/nsb1007.pdf>

National Space Grant College and Fellowship Program (Space Grant), 2014. <http://www.nasa.gov/offices/education/programs/national/spacegrant/about/index.html>

Teaching Teachers from Standards to Lessons

Coggin Heeringa

Crossroads at Big Creek, Inc. - Sturgeon Bay, WI

Abstract

Funds from Wisconsin Space Grant Consortium were used to provide scholarship stipends to upper elementary and middle school teachers, enabling them to take a continuing education class through the University of Wisconsin-Green Bay Education Outreach Program and/or participate in workshops sponsored by Crossroads at Big Creek. The objective of the class and workshops was to help teachers gain content knowledge and develop lessons aligned with the proposed Next Generation Science Standards.

Background

Crossroads at Big Creek is a 200-acre environmental preserve located in Sturgeon Bay, Wisconsin. Crossroads offers experience-based programs in science, history and the environment for learners of all ages. The Collins Learning Center is used for educational programs. The Astronomy Campus boasts a classroom building, and observatory, and a StarGarden-- an outdoor area dedicated to night sky viewing. The Door Peninsula Astronomical Society (DPAS) meets at Crossroads and often assists with or sponsors outreach activities.

Crossroads hosts about 100 school fields trips each year, but in addition to providing programs for Door County schools, Crossroads collaborates with the University of Wisconsin-Green Bay to offer teacher education, offering three to four one-credit classes annually to teachers from districts through northeast Wisconsin. At the same time, the 2014 Wisconsin Space Grant proposals were due, the Wisconsin Department of Instruction (DPI) announced that the Next Generation Science Standards would soon be available. Next Generation Standards are “rigorous, internationally benchmarked standards for K-12 science education... designed to identify science and engineering practices and content that all students should master in order to be fully prepared for college, careers and citizenship.” The release seemed a wonderful opportunity to introduce teachers to these new documents and help them develop lessons to bring the concepts alive in their classrooms. The University of Wisconsin-Green Bay Education Outreach coordinator was enthusiastic about the idea and encouraged Crossroads to submit a course syllabus, which was approved as a summer school offering for 2013.

The Door Peninsula Astronomical Society was planning an outreach event called “Celebrate the Sun” in the spring. Also, the press began announcing the approach of yet another “the comet of the century” which would circle the Sun around Thanksgiving. The workshops were combined with public outreach events. Teachers gain experience and confidence by staffing the learning stations during outreach events.

Crossroads at Big Creek was awarded a grant providing partial funding to offer scholarship stipends for teachers who participate in the class and workshop. Offering stipends greatly improved the recruitment of teachers. In fact, generous stipends often attract teachers with little previous training or even interest in astronomy. Reaching these teachers is, perhaps, the most important outcome of the project.

Project

Crossroads conducted a workshop pertaining to the Sun in collaboration with the Door Peninsula Astronomical Society and hosted a teacher workshop and several school field trips prior to the approach of Comet ISON. The University of Wisconsin-Green Bay offered the “Astronomy-from Standards to Lessons” class in June of 2013 with eleven teachers enrolled in the class for credit and one teacher taking the non-credit option. Crossroads provided instruction and facilities use. Each participant was given a binder containing the copies of the standards pertaining to space education. The intent was that each teacher would select a standard and prepare student-ready activities which the class would share.

The first topic discussed was the electromagnetic spectrum. To the middle school science specialists (most of whom were biology majors) the Next Generation Science Standards were nothing short of an epiphany. Comments such as “I had no idea.” ... “How can we teach this if we’ve never heard of it?” ... “I thought the spectrum was ROY G BIV”. As it turned out, the class spent the whole class on the electromagnetic spectrum, finding amazing websites and applications which would engage their students. As one teacher pointed out, “It’s everything kids care about: preparing food, television, radio, social media, and animal behavior! If this doesn’t get them interested in STEM, nothing will!”

The Comet ISON Workshop was a success, in spite of the fact that the comet broke up and disappeared while rounding the Sun, which occurred before the scheduled comet viewing session. Teachers learned a great deal by presenting hands-on activities and by interacting with amateur astronomers during public outreach events, and also improved DPAS events because they could relate to students.

The Next Generation Science Standards were not adopted by the state of Wisconsin, and it seems unlikely that the state will adopt them in the foreseeable future. Consequently, the stated goal of preparing teachers to use the Next Gen standards was not met. Apparently, now districts are responsible for creating science curricula, so introducing teachers to basic concepts was probably even more important.

Conclusions

Based on our experiences in 2013, we have concluded:

1. Offering scholarship/stipends to teachers for participation in classes and workshops greatly increases enrollments, and that continuing education classes which offer credit are more desirable to most teachers, especially those who have been teaching for some time.

2. Many “science specialists” in elementary and middle schools have not been exposed to many of the concepts upon which the Next Generation Science Standards are based.
3. When teachers present activities in public outreach settings, they are more likely to use them in their own classrooms.
4. A lot of teaching is showmanship. When teachers have access to equipment and props, they are more likely to go beyond the written word and consequently, their students are more likely to respond.

Evaluation

Unfortunately, because the class was offered in summer, Crossroads had no way of determining whether or not the participating teachers used the lessons they created once they were back in their own classrooms. We suspect and hope that the lessons have become a part of the curricula of the six districts that were represented in the class.

Acknowledgement

This project has been made possible with a grant from the Wisconsin Space Grant Consortium and with assistance from University of Wisconsin-Green Bay Education Outreach and the Door Peninsula Astronomical Society.

Driftless Dark Skies Initiative: Training Astronomy Educators¹

Jonel Kiesau
Kickapoo Valley Reserve
La Farge, WI

John Heasley
Star Stories
Lone Rock, WI

Abstract: The Driftless Dark Skies Initiative is training and supporting a cohort of a dozen astronomy educators who make use of the unique resources of the Kickapoo Valley Reserve to inspire and inform school groups and the public about the night sky and space exploration by offering nature programs and public star parties.

Background: The Kickapoo Valley Reserve is over 8,500 acres of protected property located in southwestern Wisconsin in Vernon County. KVR sees over 14,000 visitors annually for low-impact recreation including biking, hiking, horse-back riding, and birdwatching. It has proven to be an excellent environment for astronomy education. It has a thriving Education and Events Program which hosts 6000 students of all ages for hands-on nature education. The Visitor Center includes classrooms for indoor learning while its trails, woods, and prairies offer an outdoor classroom. Most importantly, KVR enjoys some of the best dark skies of Wisconsin. It is far from the light pollution which disconnects urban residents from the night sky. With the adjoining Wildcat Mountain State Park, it is a proposed Dark Sky Park. KVR has partnered with Star Stories to train astronomy educators who will connect visitors with the cosmos through star parties and classes.

Training: We recruited a cohort of 12 astronomy educators by inviting volunteer naturalists and area teachers. All were experienced in educating young people and the public. The level of astronomy knowledge varied from experienced to “willing to learn.” Training included 12 hours of instruction at four evening classes in July and August 2013. Classes were divided between indoor instruction and outdoor instruction under the stars. Additional guided practice was provided at the public star parties. The evaluation below provides an overview of the topics covered as well as the progress made. We accomplished our goal of creating astroeducators comfortable in giving public and school programs. Comments on the evaluation also made clear the desire for additional training and practice.

We have supported the work of the astroeducators by creating a presentation that can be shared indoors before going outside for stargazing. “Becoming a Stargazer” covers our place in the cosmos, how to see the night sky, and what to see. We also created a 20-page Astroeducator Guide to serve as a ready reference. In April 2014 we provided training to 20 KVR volunteer naturalist

¹ This project was made possible through the generous support of a Wisconsin Space Grant Consortium Aerospace Outreach Award. We are also grateful for the telescope support provided by the Friends of the Kickapoo Reserve, LaCrosse Area Astronomical Society, Iowa County Astronomers, Starsplitters of Wyalusing, Madison Astronomical Society, and UW Space Place.

on using the Moon and Planet activities we created.

| Astroeducator Evaluation | | | |
|--|-----------------|----------------|--------|
| On a scale of 1-5 with 1 = uncomfortable/“don't make me do this” and 5 = comfortable/“totally stoked” how prepared do you feel about doing the following with visitors to KVR? | | | |
| | Before Training | After Training | Change |
| Inspiring people with stories about the cosmos. | 2.3 | 3.9 | 1.6 |
| Explaining to people the basics of how telescopes work. | 1.7 | 3.7 | 2.0 |
| Using websites to see what sky conditions are going to be. | 2.3 | 4.3 | 2.0 |
| Using a planisphere to see what the sky will look like on given date and time. | 1.7 | 4.6 | 2.9 |
| Safely using a green laser pointer to show destinations in the sky. | 2.7 | 3.2 | 0.5 |
| Helping people to see at an eyepiece. | 2.3 | 4.2 | 1.9 |
| Setting up and using a go to telescope. | 1.1 | 3.1 | 2.0 |
| Setting up and using binoculars on a tripod. | 2.6 | 4.6 | 2.0 |
| Explaining night vision. | 2.7 | 4.4 | 1.7 |
| Discussing dark skies. | 3.4 | 4.5 | 1.1 |
| Explaining the basics about the moon. | 2.9 | 4.3 | 1.4 |
| Explaining the basics about planets. | 2.7 | 4.4 | 1.7 |
| Explaining about deep sky objects (binaries, clusters, nebulas, galaxies). | 1.6 | 3.4 | 1.8 |
| Identifying and talking about constellations and asterisms. | 1.9 | 3.6 | 1.7 |
| Talking about meteor showers and how to observe them. | 2.9 | 4.3 | 1.4 |
| Locating satellites in the sky. | 2.7 | 3.6 | 0.9 |
| Creating a public sky tour for a given date. | 1.4 | 3.0 | 1.6 |
| Using Starry Night Planetarium software to model the sky. | 1.1 | 2.6 | 1.5 |
| Giving an introductory stargazing presentation with power point. | 1.4 | 3.7 | 2.3 |
| Giving workshops for school groups. | 1.7 | 3.6 | 1.9 |

Equipment: KVR already had two dozen binoculars and two spotting scopes which could be used for astronomy. A generous donor had given an 8-inch computerized Schmidt Cassegrain telescope. The Friends of the Kickapoo Valley Reserve supported our star parties by donating an 8-inch Dobsonian telescope with Telrad.

Through the Aerospace Outreach Award, we were able to purchase additional resources. Starry Night software (elementary and middle school) gave us the ability to model astronomical events indoors and offers an excellent daytime and cloudy night option for stargazing. Three laser pointers give astroeducators the means to help visitors locate planets, stars, and constellations. Ten

planispheres with red lights offer a simple means to find astronomical destinations and to discover how the sky changes through the day and the seasons. The Friends of KVR now offer these in the gift shop. A tripod with Paragon mount allows us to hold binoculars steady for viewing and to easily adjust the height for adults and children. We also have the beginning of an astronomical library. All of these purchases have proven to be good investments in our astronomy program.

Star Parties: Star parties are public events where visitors are invited to gaze through telescopes and to learn about the night sky. We were able to offer six star parties throughout the year and were fortunate to enjoy clear skies for all but one. Astroeducators shared the dark skies of KVR with over 150 visitors. With eyes alone and then with binoculars and telescopes, stargazers were able to see stars, planets, constellations, satellites, meteors, galaxies, and nebulas. We began three of the star parties with an indoor presentation. Two of the star parties included guest speakers. Our friends from La Crosse Area Astronomical Society were generous in setting up telescopes and sharing the view at two of the star parties. Judging by the many “wows” heard at the eyepieces and the questions asked and answered, our visitors were both inspired and educated.

| Date | Attendance | Theme |
|-------------|-------------|---|
| 12 Aug 2013 | 22 | Perseids Meteor Shower |
| 13 Sep 2013 | 65 | Observing the Dark Sky LaCrosse Area Astronomical Society assisted with telescopes |
| 2 Nov 2013 | 22 | Autumn Skies/Comet ISON Guest Speaker: Dr. James Lattis, UW-Space Place LaCrosse Area Astronomical Society assisted with telescopes |
| 11 Jan 2014 | – cloudy | Kickapoo Valley Reserve Winter Festival Candlelight Hiking/Sking/Snowshoeing and Winter Astronomy at Wildcat Mountain State Park |
| 22 Mar 2014 | 18 | Falling in Love with the Night Sky Guest Speaker: Jean Napp, President Starsplitters of Wyalusing |
| 3 May 2014 | 30 | Voyage to the Planets Richland Center-Santa Teresa Sister City Project and Friends of the Kickapoo Valley Reserve Spring Fling |

Classes: We created two curriculum units and taught eight classes to over 100 students.

Moon Phases allows students to observe and describe our Moon's appearance and how it changes shape over the course of a month.. Students discover for themselves how the shape of the Moon changes from day to day using direct observation and planetarium software. Students see how the Moon is made of lighter highlands, darker seas (maria), and many craters. Students learn how different cultures and people have seen different patterns on the Moon and create their own patterns.

Planet Walk lets students visualize the size of the many worlds orbiting our Sun and the immense distances between them. Most models and charts of our Solar System show the many worlds as

very close together. This lesson lets students experience a more accurate model of our Solar System. Students experience that most of our Solar System is empty space, the planets are relatively tiny, and the distances between them is immense. By taking a thousand-yard walk, students construct a scale model of our Solar System: the Kickapoo System. They learn about the many worlds of our Solar System and how they can be grouped into zones. They come to understand that science is not a static body of facts, but an evolving process subject to constant revision as improved technology provides better data.

An evaluation completed before and after the activity shows that students are good at identifying the many worlds in our solar system but underestimate their relative sizes and distances.

We also shared an astronomy class with our neighbors at Organic Valley.

| Date | Class | Sections | Students |
|-------------|--|----------|----------|
| 30 Oct 2013 | Enjoying the Dark Skies CROPP Cooperative/Organic Valley Outreach | 1 | 10 |
| 08 Nov 2013 | Moon Magic | 2 | 19 |
| 15 Nov 2013 | Planet Walk | 2 | 24 |
| 11 Mar 2014 | Moon Magic | 3 | 50 |

Conclusions:

We were fortunate to be able to recruit astroeducators from the pool of existing nature educators and to offer them stipends for their time. Our astroeducators would benefit from additional training especially in using Starry Night Software and giving public programs on their own.

Low tech is better for public programs. Our computerized telescope is a wonderful instrument but is difficult to align and fussy to use. Binoculars and Dobsonian telescopes are much easier to use and more child friendly. They are also the type of optical equipment we recommend to parents.

Having children complete evaluations is challenging. Having parents complete and return the evaluation online lowers the response rate. Having children complete the evaluation after the class takes away from class time.

A safe solar viewing curriculum unit would give us a valuable daytime option. A constellation unit would be a valuable addition.

Our public programs and classes have been successful in inspiring and educating young people. The next step is to increase their awareness of post secondary STEM education and careers.

The Kickapoo Valley Reserve provides a wonderful and amazing environment for astronomy education and stargazing. We look forward to growing the Driftless Dark Skies Initiative in the years ahead.

Simpson Street Free Press Proceedings Paper 2014 Using Science to Bridge Achievement Gaps

James Kramer

Executive Director, Simpson Street Free Press, Madison, WI¹

Abstract

Simpson Street Free Press (SSFP) delivers high-quality academic instruction in after-school settings. Local students (ages 8-18) publish five separate youth newspapers. New academic standards emphasize writing proficiency and literacy. Productive use of out-of-school time is crucial, particularly for students from lower income backgrounds. Central to SSFP pedagogy is across the curriculum instructional practices. And science writing for publication is a central to our formula. Each of our newspapers includes several science sections, and space science is our most read and most popular content. SSFP lesson plans are expertly designed to support in-school learning. Students encounter predictable connections to the school day. Our young writers conduct research, use technology, write and read extensively. This system accomplishes multiple outcomes. Students learn transferable academic strategies. School grades and attendance are measured. SSFP students participate in civic discourse and influence their peers. Teachers use SSFP materials in local classrooms. Thousands of young readers and their families explore science through the work of SSFP student reporters. Young readers are inspired by the voices of southern Wisconsin's most effective and best-known local role models.

Organization Mission and Values

Simpson Street Free Press (SSFP) grew up in one of Dane County's most challenged neighborhoods. In those days it was 15 kids and a few sharp pencils in the back room at Broadway-Simpson Neighborhood Center. Years of steady growth demonstrate scalability. Curriculum, methods, and approach are organized within two complementary mission areas:

- **Mission #1: Organize challenging academic activities for youth – after-school and in summer.** Students develop the skills they need to do well in school and prepare for college. They learn in an authentic newsroom. Reporters conduct research, synthesize facts, and apply an organized approach to academic work. We teach across the curriculum. Students revise each assignment many times prior to publication. We use school report cards, school attendance, Common Core Standards, and “7 Traits of a Writer” to evaluate student progress.
- **Mission #2: Spark achievement, academic success, and community service among Wisconsin young people.** SSFP reporters are influential. They are leaders. Persistent achievement gaps are part of life for young people in Dane County. SSFP writers lead their peers in a different direction: drugs, alcohol, and smoking are bad; science, history, and community service are cool. Academic success is attainable for all kids. SSFP students publish five separate youth newspapers and operate a network of book clubs.

¹ Funding for Simpson Street Free Press provided in part by a generous grant from the Wisconsin Space Grant Consortium.

During the past 22 years, SSFP has honed a rigorous and richly layered after-school curriculum. Students polish their skills in an authentic workplace. The newsroom process: inquiry, close reading and research, planning and drafting, multiple rounds of revision. Students use modern technology. They have business cards, real assignments, and real deadlines. Students research and write about core subject areas (science, geography, books, history). Content area knowledge grows. Academic confidence grows quickly. School grades and attendance improve.

Project Summary

SSFP fields a menu of programs designed to promote literacy, teach writing, and foster core subject knowledge. We publish newspapers. And for 22 years, our most popular section is space science. Our reporters (and our readers) love this stuff. The source material is endless. Every new Tuesday edition of the *New York Times*, and every issue of *Discover* magazine, is full of story ideas. As they write and research, SSFP students encounter predictable connections to the school day. They learn to cite sources and explore core subject areas. They use technology. They apply an organized academic approach to every assignment. Science learning is a portal at SSFP. Students learn to write by reporting on science.

Writing about and researching space science is perfectly suited for our brand of after-school lesson plan. SSFP approach is simple, old fashion writing across the curriculum. We use apprenticeship models. Because students write for publication, this project is particularly dynamic. Once hooked, young space science reporters start to steer their own research. They get curious. They explore and take notes. Always conscious of their readers, students learn to use voice in their writing. They practice word choice and outlining. The result is excellent work. Each semester (including summer) SSFP writers produce dozens of fascinating space science features. Space science is core curriculum. As content area understanding improves, so does academic confidence. School grades and school attendance improve.



Wisconsin Idea/La Prensa

SSFP grows its own after-school instructors. We use the innovative practice of hiring program grads, now in college, as teachers and editors. Thus our organization accomplishes multiple missions. We write, teach and publish, but we are also a training ground for young professionals. Almost all SSFP editors are of color, and many are bilingual. Using a curriculum they've mastered, they work in the same schools and neighborhoods where they grew up.

Our newest publication is *La Prensa Libre de Simpson Street*. Student writers in grades 4-12 produce a bilingual youth newspaper. Again we turn to our space science lesson plans to churn out well-written articles that fascinate our young audience. The La Prensa project seeks to address

persistent achievement gaps by replicating proven after-school methods. SSFP newsroom skills are easily transferred to the classroom. Activities connect to the school day. Languages are ‘unmarked’ at La Prensa: reporters work and write collaboratively in either language or use hybrid forms (e.g., code-switching across languages). Instruction and training is preparatory. With an eye toward college-readiness, students polish the most practical of academic strategies. They write, read, and work across languages. This approach turns bilingualism into an academic advantage.

The La Prensa project, now in its pilot stage, will eventually place dozens of University of Wisconsin students in teacher/editor roles. This is the “Wisconsin Idea” element of the project. Gloria Gonzales, former SSFP student and recent UW grad, is the project coordinator. Through the La Prensa project college students, retired teachers and journalists, and local young people draw on each others’ skills and abilities. Together they create a new and valuable community asset: a bilingual newspaper.

Project Participants

All students enrolled in SSFP programs produce written work for our science sections. SSFP student writers reflect the diversity of our south Madison location. Most program participants are students of color, and most come from low-income neighborhoods. About 30% are second language learners. Dozens of academic success stories begin at SSFP, many among our most at-risk students. Thousands of Wisconsin kids read the positive messages delivered through our publications. We continue to expand the SSFP menu of programs. And we continue to dramatically expand our emphasis on science. Publishing online allows us to include more students and reach more readers. Young readers and writers love science. We engage thousands of kids, and in innovative and cost effective ways.

Like SSFP, La Prensa is an apprenticeship model. It responds to an immediate and urgent community need with award-winning curriculum and an empowering youth leadership model. La Prensa students also reflect the diversity of our home neighborhoods. About 85% of La Prensa students are of color. About 66% qualify for free or reduced lunch. The number of students enrolled in the La Prensa program will increase (25-60) by summer of 2015.



Is Pluto considered a planet? It's just one of many fascinating questions about our solar system. Scientists don't know all the answers, nor do our student reporters. But we're learning more with each new mission.

Learn more about Planet Earth, our solar system, and the universe at www.simpsonstreetfreepress.org

STEM and Literacy

Common Core or otherwise, new academic standards are coming to Wisconsin. Whatever new standards are eventually installed, they will be more rigorous. And will certainly emphasize writing proficiency and literacy. Writing about and researching science is the SSFP brand. Students learn the basics: hard work, curiosity, academic confidence, and core subject curriculum. We teach productive use of out-of-school time. SSFP methods produce solid results, particularly for students from lower income backgrounds.

At SSFP the term ‘literacy’ does not mean exclusively reading and writing. In the 21st century literacy connotes an intense knowledge of any particular field of interest. Students who learn financial literacy manage savings and plan for college. Young people who study science and math are STEM literate. SSFP develops and deploys literacy-based curriculum. Our approach is integrated, core subject curriculum deftly applied in OST settings. The National Partnership for Quality After-school Learning says, “Writing and literacy are areas where out-of-school programs can have the most impact.” The President’s Committee for the Arts and Humanities says SSFP “is pioneering new and innovative ways to apply integrated curriculum in after-school settings.” SSFP methods are based on evidence. We closely follow UW-Madison and other national research. Our students use science writing and modern media to inspire peers and thus spark achievement. SSFP science lesson plans are project-based learning that kids enjoy.

Instruction is specifically provided for science writing. Students work one-on-one with editors to read and analyze sources. Before writing, students are evaluated in their understanding of source material through comprehensive questioning. If a student fails to understand a source, additional one-on-one support is provided. Students then work with editors to plan, draft, fact-check, and finalize articles that cover science-related material. Starting with a pencil-written first draft, each student goes through multiple rounds of revision with various editors to bring every article to completion.

“The new global, high-tech marketplace demands intense creativity and thinking that goes beyond basic learning skills. With the growing importance of 21st century skills such as critical thinking and global awareness, the ability to comprehend written text is an essential building block. At its core, literacy is the use of written information to function in society, attain goals and develop knowledge. Without this tool, a student will almost inevitably struggle with other forms of learning. Literacy is an absolute necessity to further learning and development.”

—MetLife Foundation and Afterschool Alliance

Outcomes and Measurement Tools

SSFP always measures the same things. We carefully measure school grades, school attendance, research and writing assignments published, book reviews and science assignments completed. We measure hours of extra instruction time in core curriculum and literacy.

Objective #1: Students improve academic performance. Students acquire practical academic skills. Students learn to transfer these skills. **Measurement tools:** School report cards and school

attendance. Performance evaluations conducted by teachers and parents. **Outcomes:** SSFP students submit school report cards each academic quarter. We monitor school attendance. More than 80% of students improve overall core subject GPA within two semesters.

Objective #2: Students complete predetermined requirements for research/writing assignments. **Measurement Tools:** Students keep assignment logs. Editors monitor assignments. Assignments are complete once published. Slug sheets track published assignments. **Outcomes:** All (100%) students complete four research/writing assignments per semester. All (100%) complete a science writing assignment each semester, including the summer semester.

Objective #3: Students receive extra instruction in reading/language arts. Instruction is across the curriculum. **Measurement Tools:** Student timesheets and assignment logs. Slug sheets. **Outcomes:** Rough drafts, and each subsequent draft, are reviewed one-on-one with an editor. All (100%) students complete assignments in at least two of our four lesson plan categories. At least 60% of students complete assignments in three-four lesson plan categories. All (100%) students complete one science assignment, one history assignment, and one book review per semester. Students receive, on average, 4.25 hours of extra instruction time per week.

SSFP methods create obvious multipliers. We facilitate and observe things like youth leadership and civic engagement, but produce only empirical or ‘soft’ data.

Objective #4: SSFP students are engaged in the community. They acquire leadership qualities and workplace skills. **Measurement Tools:** Participation in lesson plans, interviews, and events. **Outcomes:** All (100%) students host at least two newsroom events or discussion forums. At least 75% of students participate in the Features Lesson Plan, and/or conduct interviews, speak in public, or plan and execute a Museum Series field trip. All (100%) high school students, and at least 60% of middle school students complete at least one research/writing assignment related to financial literacy and college planning.

NOTE: Student evaluations are conducted on a trimester schedule (1st, 2nd, and summer semesters). Evaluations focus on assignment completion, writing proficiency (7-Traits of a Writer) and organizational and work skills. At least 85% of program participants will achieve a 3.75 grade (on 5.0 scale) during each semester (including summer). All students will complete assignments in core subject areas (science, history, books) during each semester (including summer).

Conclusions

Based on Madison's south side, SSFP now operates satellite newsrooms at Capital Newspapers and two local schools. Current students represent seven high schools, nine middle schools, and five elementary schools. Actively engaged local kids are valuable assets in any achievement gap fight. SSFP students engage in civic discourse and influence their peers. Publishing space science content is a natural strategy for us. Every new story about a fiery comet or space probe builds our readership. We know our niche and we know young readers. Our publications encourage interest in space science. We challenge achievement gaps through science reporting and publishing. SSFP further addresses achievement gaps by helping 200 local students do well in school. Everything we do is connected to the school day. Students write across the curriculum. They focus on practical academic strategies. They learn invention strategies, drafting methods, and vocabulary. Assignments and activities grow in complexity with age and ability. We believe

learning happens, in large measure, during the revision process. Multiple rounds of editing are required during each assignment. Science research assignments fit our pedagogy perfectly. Our kids buy in and work hard. SFP students build their core subject knowledge and acquire the practical skills that result in good grades.



Promoting Women in Physics and Astronomy Through a Public Lecture Series at UW-La Crosse

S. R. Lesher

Physics Department, University of Wisconsin – La Crosse, La Crosse, WI¹

Abstract

Undergraduate women in the Physics Department at UW- La Crosse form a small percentage of majors and are spread out across years and among sub-programs. In addition, they may encounter few women scientist during their undergraduate career. As a result, they can feel isolated and uncertain about careers in their chosen fields. A women speaker was brought to UW – La Crosse to serve as a role model for undergraduate women in the physics program and to expose them to career opportunities in a space-related field. The speaker gave an interdisciplinary science seminar, a physics specific lecture, and met with students over lunch in small group discussion. Student feedback was very positive, and the visit increased the exposure to the different careers women, and all students, could have in science.

Introduction – Context and Background

The University of Wisconsin–La Crosse (UW-L) is one of the most thriving undergraduate physics programs in the nation with approximately 165 physics majors and thirteen full-time faculty members. The department offers a B.S. in physics with optional emphases in astronomy, computational physics or optics. In addition, students can pursue a B.S. in physics with a concentration in either biomedical physics or business. Finally, the department also offers a highly successful physics-engineering dual degree program in collaboration with four engineering colleges in Wisconsin and Minnesota. In 2003, the National Task Force on Undergraduate Physics Education selected the UW-L Physics Department as one of the most successful in the country and included it as one of their case studies². Later in 2003 an article in the September 2003 issue of *Physics Today* described the UW-L program as among the few “great” physics programs in the nation [1]. Each year, the American Institute of Physics (AIP) Statistical Research Center publishes a list of Bachelors-only departments averaging 10 or more physics bachelors degrees per year in its *Physics Undergraduate Enrollments and Degrees* data in the nation. This year, the UW-L Physics Department was ranked 2nd in the nation, averaging 28 graduates per year for classes in 2010 to 2012 [2]. In 2012, the AIP Division of Education visited our department in their study to learn and propagate effective practices for the preparation of physics undergraduates for Science, Technology, Engineering and Mathematics (STEM) career pathways. Our Department was chosen because of our strong record of preparing students with a bachelor degree in physics and placing them into STEM fields. Most recently, the UW-L Physics Department was awarded the 2013 American Physics Society (APS) “Award for Improving Undergraduate Physics Education” along with MIT, Colorado School of Mines and Kettering University. Many physics students have received national recognition for their achievements, and have pursued advanced physics and engineering degrees.

¹ This work was supported by the Wisconsin Space Grant Consortium and the UW-L Physics Department.

² Their report is available at <<http://www.aapt.org/Projects/ntfup.cfm>>.

Despite these strengths, the physics program has difficulty attracting women and underrepresented minorities. Of the approximately 8,500 university undergraduate students at UW-L, 45% of them are registered in the College of Science and Health where the Physics program is housed. Over half of the students in the College of Science and Health are women. However, only about 15% of the physics majors are women. The national average is about 20%. Similarly, only about 2% of the physics majors are from underrepresented minorities, against a national average of about 8% [3].

Project

In an attempt to increase the number of women physics majors and to highlight the careers of successful women in the field, the Physics Department has instituted a Public Lecture Series in Physics featuring women and other underrepresented minorities in Physics. We applied for a WSGC Special Initiatives award to support this program. The Public Lecture Series in Physics has three objectives:

- (1) to increase the recognition of women physicists in the local community,
- (2) to recognize the scientific accomplishments and contributions of women physicists, and
- (3) to have these women serve as role models for the undergraduate population at UW-L.

The speaker was M. Darby Dyer, Ph.D., Kennedy-Schelkunoff Professor of Astronomy at Mount Holyoke College. The event lasted two days and included many activities for students. On Wednesday she gave a physics seminar titled “Calibrating ChemCam: Analytical Chemistry at Arm’s Length”. Thursday Dr. Dyer met with undergraduate students for lunch in an informal, intimate setting. That evening she gave a public lecture entitled “A year in the Life of Curiosity on Mars: New Discoveries from the Red Planet” appropriate for all students and the general public.

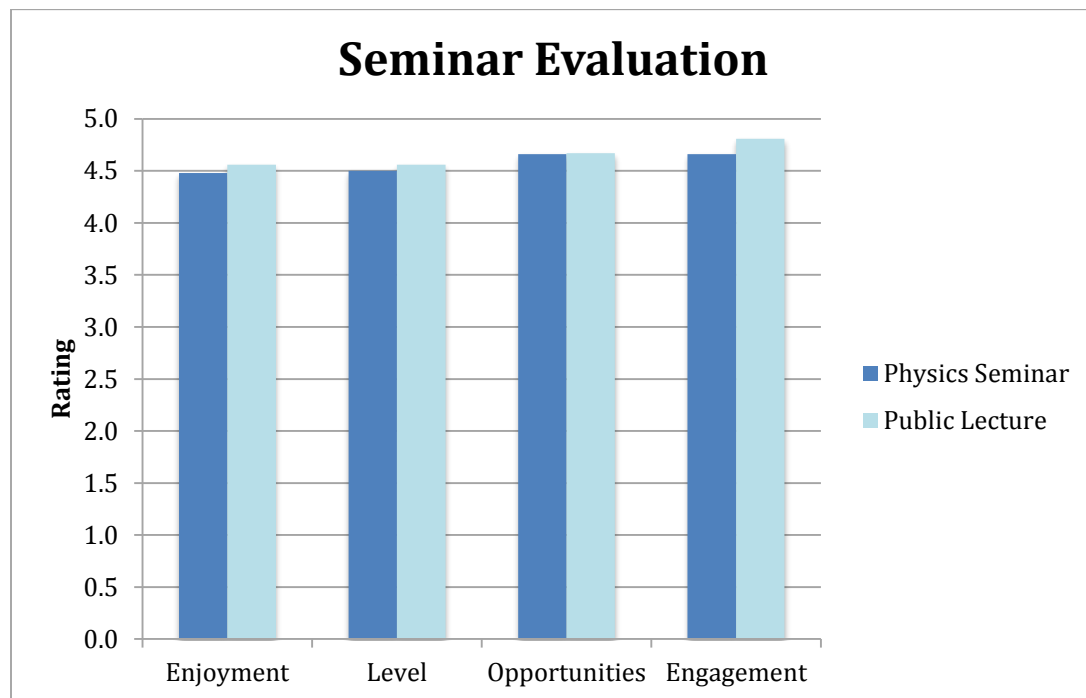
Assessment

Seminar: Dr. Dyer gave two talks during her time in the Physics Department. The Physics Seminar was during the regular Physics Seminar time-slot, with an audience composed primarily of Physics majors, but including students and faculty from other departments and at the university. Approximately 100 students, faculty, and general public were in attendance at this seminar. Approximately 200 students, faculty, and members of the general public attended the Public Lecture. The students and faculty members were part of a diverse group from various departments throughout the university. The surveys indicated both the seminar and lecture were informative to the students in attendance and are shown in the following Figure 1. The survey was taken by both physics and non-physics students (about 50/50). The respondents gave high ratings to the Seminar and Lecture on several variables: how much they enjoyed it, how appropriate the level was for the audience, how supportive they are of the opportunity for students provided by the program, and whether or not they learned something new from the experience.

Lunch: The speaker also met with interested over lunch to discuss issues facing women in physics and astronomy. This allowed the students to ask question in an informal, intimate setting. Dr. Dyer gave the “inside info” on what it is like to be a woman in the field. About 45 students attended this event. Approximately 67% of those surveyed enjoyed the informal setting, interacting

with the speaker, and believed the interaction gave them insight into women in physics and astronomy issues.

Figure 1: Average ratings of speaker from Physics Seminar (n = 44) and the Public Lecture (n = 36), 1 = strongly disagree, 5 = strongly agree with the following statements: (1) I enjoyed attending the talk. (2) The talk was given at an appropriate level for the audience. (3) I'm glad UW-L allows these opportunities to students and the community. (4) I learned something new.



Conclusion

This program directly benefited the women of UW-L Physics Department by:

- giving them the opportunity to hear and interact with a top scientist
- giving them the opportunity to talk in small groups with the speaker about being a woman in science

Finally, 82% of those surveyed agreed that the Physics Department should make this Lecture Series an annual event featuring a woman speaker. The survey indicate that the students appreciate the opportunity to meet more women scientists, hear about their research, and discuss issues relating to a career in science. It has helped these young women envision both the challenges and rewards of becoming the next generation of experts in Physics / Engineering fields, including the possibility of pursuing space- or aerospace-related science, design, or technology. Taylor Bailey, a junior physics major, sums it up, “Dr. Darby Dyar’s visit to UW-L last spring gave me a chance to not only learn about the incredible advances in the field of spectroscopy applied to the most recent Mars rover expedition, but also talk with her about being a woman in science and the struggles she and other women face everyday. This scientist is working for an organization I can only dream about getting a chance to apply to and her interesting background in chemistry,

geology, and physics shows me that as long as I continue to be passionate about what I'm doing, I will find work that is fulfilling and enjoyable and that women in the sciences can, in fact, do it all."

References

- [1] Hilborn & Howes, *Physics Today*, September (2009) pg. 38.
- [2] American Institute of Physics. Web. 2014
<<http://www.aip.org/statistics/trends/highlite/edphysund/table4e.htm>>.
- [3] "APS Bridge Program." American Physical Society. Web. 09 Jan. 2013.
<<https://www.uwgb.edu/WSGC/k12/requirements/si.aspx>>.

Rocket Science for Educators Workshop for Science Technology Engineering and Mathematics

Todd H. Treichel¹

*American Institute of Aeronautics and Astronautics (AIAA) – Wisconsin
& Orbital Technologies Corporation, Madison, Wisconsin 53717*

Daniel W. Bateman²

Spaceport Sheboygan, Sheboygan, Wisconsin 53081

Abstract

The Wisconsin AIAA chapter has leveraged the talent of its members to provide a variety of outreach opportunities for precollege aged students. Hands-on demonstrations, visual aids, and real-life space flight examples provide a foundation for bringing precollege aged students face-to-face with space-related science, designed hardware, technology, and potential benefits; increased interest in aerospace and space related fields that lead to study at the university level followed by career. The Rocket Science for Educators program consists of a workshop used to assist schools in implementing rocket science into respective math or science curriculums. Grant assistance provided by the Wisconsin Space Grant Consortium (WSGC) makes this workshop possible. In 2014 Spaceport Sheboygan teamed with AIAA for a training event where participating educators attended a weekend workshop and received design software training and associated set of rocket science materials that they may take back to their respective schools.

Nomenclature

| | | |
|----------------|---|---|
| <i>AIAA</i> | = | American Institute for Aeronautics and Astronautics |
| <i>CG</i> | = | Center of gravity |
| <i>CM</i> | = | Center of mass |
| <i>G</i> | = | Acceleration force due to gravity |
| <i>V</i> | = | Velocity |
| <i>MSOE</i> | = | Milwaukee School of Engineering |
| <i>NASA</i> | = | National Aeronautics and Space Administration |
| <i>ORBITEC</i> | = | Orbital Technologies Corporation |
| <i>STEM</i> | = | Science Technology Engineering and Mathematics |
| <i>WSGC</i> | = | Wisconsin Space Grant Consortium |

¹ Senior Systems Engineer, Space Center, 1212 Fourier Drive, Madison, Wisconsin, USA

² Executive Director at Spaceport Sheboygan, 802 Blue Harbor Dr, Sheboygan, Wisconsin, USA

The authors acknowledge Wisconsin Space Grant Consortium for making this STEM project possible.

I. Introduction

The Wisconsin section of AIAA is based in Madison, Wisconsin and has a current membership of approximately 95 members and has recently won the 2013 *Harry Staubs Pre-College Outreach Award*. The award is presented annually to sections that have developed and implemented an outstanding precollege (K–12) outreach program that provides quality educational resources for teachers in science, technology, engineering, and mathematics (STEM) subject areas. In 2010, 2011, 2012, and 2013 AIAA-Wisconsin was awarded a WSGC outreach grant and utilized the 2013 grant to successfully administer a *Rocket Science for Educators* workshop for K-12 educators at Spaceport Sheboygan. The AIAA and Spaceport Sheboygan joined forces to provide advanced teaching with special emphasis placed on software design and simulation for high powered rockets.

II. Goals and Value of Project

A decline in both the quantity and quality of students pursuing careers in STEM is widely noted in policy reports, the press, education, and government. Fears of increasing global competition compound the perception that there has been a drop in the supply of high-quality students moving up through the STEM pipeline in the United States. A recent article published on February 12, 2010, by the Milwaukee Journal Sentinel, reveals the following (Miller, 2010):

Grade school science teachers aren't doing the best job of informing their students about careers in science and engineering, according to a new survey of students from the American Society for Quality (ASQ). The survey of more than 1,110 students, which was done in December 2009, tried to discover how well teachers translate their knowledge and passion for science to getting children excited about engineering and science careers. It found that 63% of students think their teachers are not doing a good job of talking to them about engineering careers, and 42% said their teachers aren't good at showing them how science can be used in a career.

Among the survey's findings:

- *85% of students said their teachers deserve at least a "B" grade when it comes to knowledge about science topics, and 55% gave them an "A."*
- *Nearly one third of students give their teachers a "C" or lower for making science more exciting and fun to learn and assigning fun hands-on projects in the classroom.*
- *Students in grades 3-6 rate their science teachers higher for making science exciting and hands-on than students in grades 7-12 rate their science teachers.*
- *72% of students in 3-12 grades think a person needs to do well in science and math to get a good paying job in the future.*
- *As students get older (7-12 grades) however, they are less likely to believe that science and math are necessary to getting a good paying job.*

The Wisconsin AIAA chapter has leveraged the talent of its members to provide a variety of outreach opportunities for precollege aged students. Hands-on demonstrations, visual aids, and real-life space flight examples provide a foundation for bringing precollege aged students face-to-face with space-related science, designed hardware, technology, and the potential benefits; increased interest in aerospace and space related fields that lead to study at the university level followed by career. Section officers discussed and reviewed a compilation of various outreach

projects summarizing a three year period covering 2006 – 2008. A survey form was constructed in an attempt to measure effectiveness of outreach efforts.

In 2009 the Wisconsin AIAA conducted a series of workshops on Physics of Propulsion and Space Flight. To test the effectiveness of these workshops, participants were asked to participate in a pre and post workshop survey. Survey results are summarized in Figure 1 where students sampled, grades six through eight, considered math and science important but only 60% were interested in STEM subjects. At the conclusion of the workshop series, students again were surveyed where a 35% increase in STEM interest resulted. Over the last century, America’s economy has shifted from an agricultural and industrial focus to one that requires greater scientific and mathematical knowledge as well as technological expertise. According to the Bureau of Labor Statistics, of the thirty fastest growing occupations projected for 2016, twenty-two of them are in STEM related fields. AIAA Wisconsin members and involved teachers were intrigued by these measureable results. Thus, causing the development of an educational outreach program that reaches out to K-12 teachers.

WI AIAA 2009 Outreach Survey Results
(35 Students , 6th – 8th Grade)

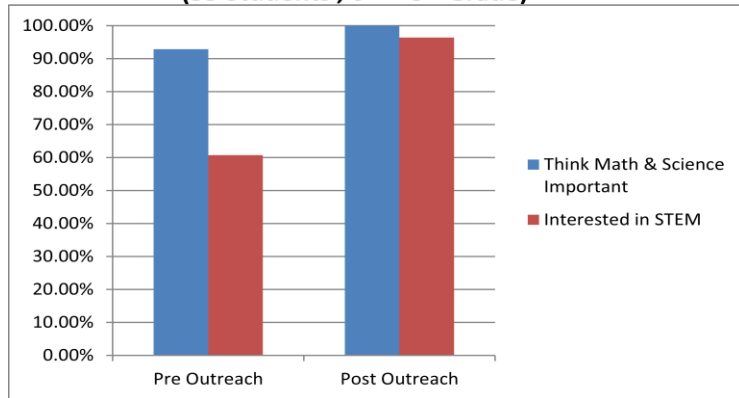


Figure 1. 2009 outreach survey summary.

The goal of the *Rocket Science for Educators* workshop is to assist schools in implementing rocket science into respective math or science curriculums. A proposal was submitted to the Wisconsin Space Grant Consortium (WSGC) to assist with funding the newly designed program. The *Rocket Science for Educators* workshop was designed specifically for educators from public and private institutions and those educators experienced with teaching math or science subjects. Participating educators attend a weekend workshop and receive a set of rocket science materials that they may take back to their respective schools for use and implementation. A workshop taught by aerospace professionals provides a unique opportunity for teachers to provide meaningful activities in their classrooms and improve student performance in the fields of science, technology, engineering, and mathematics.

III. Rocket Science for Educators Workshop

The WSGC grant funded Rocket Science for Educators workshops contained between twelve and fourteen educators who were recruited to attend a rocket science workshop at no charge. Workshop attendees consisted of math, science, art, and special needs teachers from K-12 institutions, where the origins of various participants are illustrated in Error! Reference source not found.. The first workshop was conducted at Orbital Technologies Corporation (ORBITEC), located in Madison, the second workshop at East DePere High School located in DePere, and the third workshop was held at Milwaukee School of Engineering (MSO) in Milwaukee, and the fourth was an advanced workshop hosted at Spaceport Sheboygan, Sheboygan, Wisconsin. The workshops utilized aerospace topics to provide STEM education to educators for preparing today’s students for tomorrow’s jobs allowing them to be competitive in an increasingly global economy.

Table 1 illustrates workshop topics and how each topic relates to an educational discipline. Lectures and hands on activities were conducted including design, construction, planned experimentation, altitude analysis and differential pressure, static rocket engine firing, and the launching of a payload capable rocket. Key airframe and propulsion topics were discussed describing center of mass (CM), center of gravity (CG), velocity (V), and g-force (G) considerations for flight stability. At the close of the workshop, instructors provided constructive feedback accompanied by a short competency quiz to demonstrate participants' mastery of course subject matter. Educators were issued an achievement plaque and a set of materials that can be used for implementation into their respective math or science curriculums. Curriculum adaptable aerospace reference material, rocket design and simulation software license, and rocket construction material (see Figure) were provided to each participant completing the workshop. Highlights of the workshop consisted of a series of lectures which included demonstration (static) firing of an oxygen and propane fueled reaction control system (RCS) thruster built by ORBITEC (Madison, Wisconsin) (see Error! Reference source not found.).



Figure 2. Rocket design simulation software and reference materials.

Safety rules for storage and handling of propellant materials was discussed and making a science project out of home-made rocket engines was discouraged for reasons of safety. Extensive time was spent using RockSim design software to demonstrate rocket design techniques, 3D imaging, and flight simulation followed by construction and flight of a payload capable rocket. RockSim is a computer program that allows you to design any size rocket, and then simulate its flight to see how high, and how fast it will fly. Prior to teachers building their payload capable rockets, an analysis of various payload weights were conducted with different engine thrust parameters to determine if the actual flight would be stable and safe to launch. The purpose of lectures, demonstrations, and take-home materials was to provide educators with educational tools that:

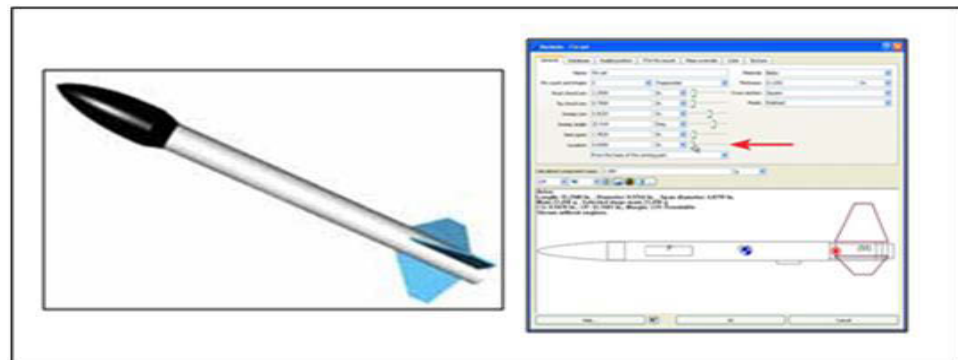


Figure 3. RockSim software design and simulation.

Extensive time was spent using RockSim design software to demonstrate rocket design techniques, 3D imaging, and flight simulation followed by construction and flight of a payload capable rocket. RockSim is a computer program that allows you to design any size rocket, and then simulate its flight to see how high, and how fast it will fly. Prior to teachers building their payload capable rockets, an analysis of various payload weights were conducted with different engine thrust parameters to determine if the actual flight would be stable and safe to launch. The purpose of lectures, demonstrations, and take-home materials was to provide educators with educational tools that:

1. Provide basic knowledge of aerospace engineering and rockets.
2. Provide rocket design and simulation software training and user license.
3. Ability to conduct flight experiments using an electronic altimeter.
4. Allows educator to have access to reference material for rocket propulsion.
5. Provide knowledge of how to build an electric powered launch pad.
6. Assure safety and enable educator with skills to properly conduct a rocket launch for educational groups.
7. Build interest and excitement about STEM.
8. Provide an opportunity for hands-on experiences with STEM subjects by designing, building, launching, and recovering payload capable rocket.
9. Raise student educational aspirations, knowledge of STEM, and interest in pursuing a career in aerospace.
10. Improve teaching of STEM subjects by collaborating with teacher preparation and professional development activities.

Table 1. Rocket science for educator’s workshop curriculum.

| Education Module | Aerodynamics & Physics | Chemistry of Propulsion | Geometry & Measurement | Computer Aided Design | Design Simulation | Modeling | Electronics & Circuitry | Scientific Inquiry | Problem Solving | Communication | Graphic Design & Development |
|-----------------------------|------------------------|-------------------------|------------------------|-----------------------|-------------------|----------|-------------------------|--------------------|-----------------|---------------|------------------------------|
| Newton’s Laws | X | | X | | | | | | X | | |
| Principles of Flight | X | | X | X | X | | | | | | |
| Rocket Engines | X | X | X | X | X | X | X | | | | |
| Rocket Stability | X | X | X | X | X | X | | | | | |
| Techniques of Rocket Design | X | X | X | X | X | X | | X | X | X | |
| Payload Science | X | X | X | X | X | X | X | X | X | X | X |
| Recovery | X | | X | X | X | X | | X | X | X | X |
| Planned Experimentation | X | X | X | X | X | X | | X | X | X | |
| Rocket Construction | | | X | X | X | X | X | | X | X | X |
| Engineering Change Mgt. | | | X | X | X | X | X | | X | X | X |
| Safety Procedures | | X | | | | | X | | | X | |
| Weather | X | | | | X | | | X | X | X | |
| Launch Pad & Controls | X | | X | | | | X | | | X | |
| Analysis | | | | | | | | X | X | X | X |

The purpose of workshop presentations was to give teachers a strong foundation in rocketry, understand the physics and science behind rocket propulsion, and bring a motivating set of materials and subject matter back to their classrooms. A particular emphasis on rocket propulsion and rocket stability was contained in take-home binder to accompany rocket propulsion discussions, talks about the physics, how rockets produce thrust, the types of propellants used in rockets, characteristics of high and low thrust motors, the nomenclature for rocket motors, the thrust curve, and how to select the best type of engine for a rocket and desired mission.

At the conclusion of launching the various payloads a post-launch review was conducted to discuss lessons learned and the process of corrective actions for improvement and future experimentation. Prior to adjournment of each workshop, a survey was administered to test workshop effectiveness where each educator was asked to score the workshop for relevance and fit-for-use within their respective curriculums. The scoring scale was 1 – 10, where 1 indicates that they should have stayed home and 10 indicating that the workshop exceeded expectations). Workshop survey results are illustrated in Figure 4, 5, and 6 respectively. An average score between 8.9 and 9.4 over the three separate workshops revealed a worthwhile effort and a desire among AIAA Wisconsin section members to pursue this type of outreach effort in the future.

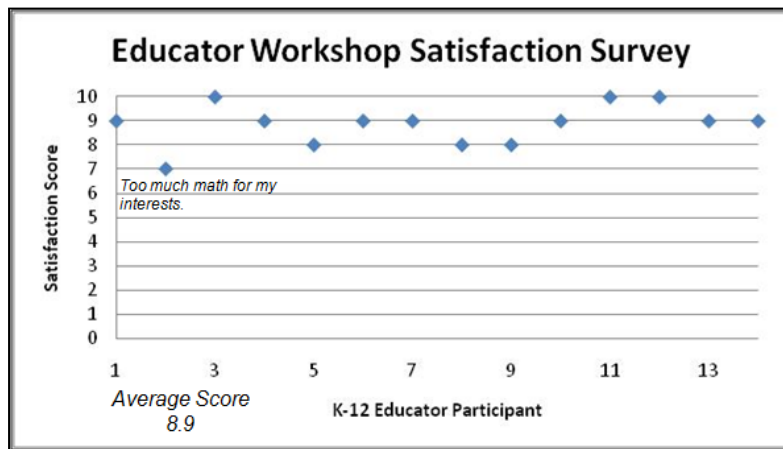


Figure 4. 2010 Rocket Science for Educators workshop survey results.

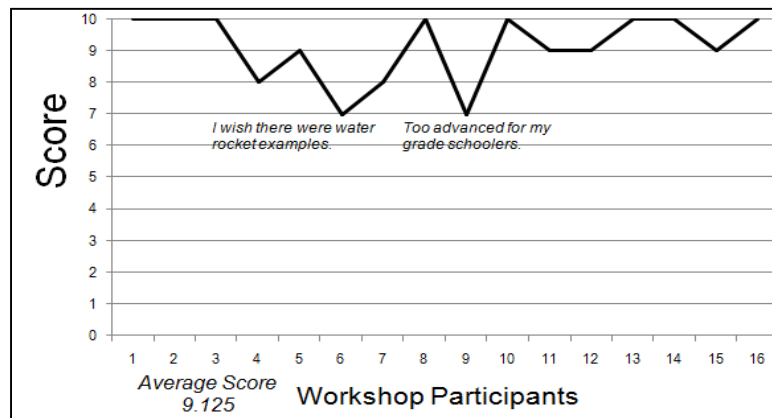


Figure 5. 2011 Rocket Science for Educators workshop survey results.

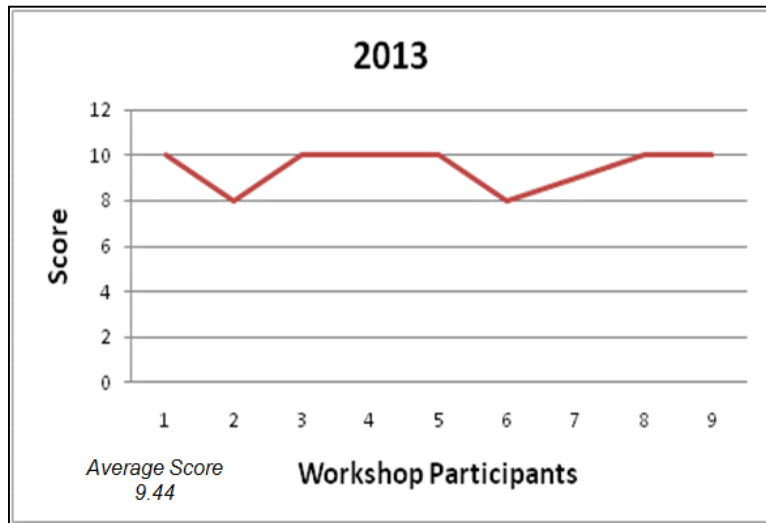


Figure 6. 2012 Rocket Science for Educators workshop survey results.

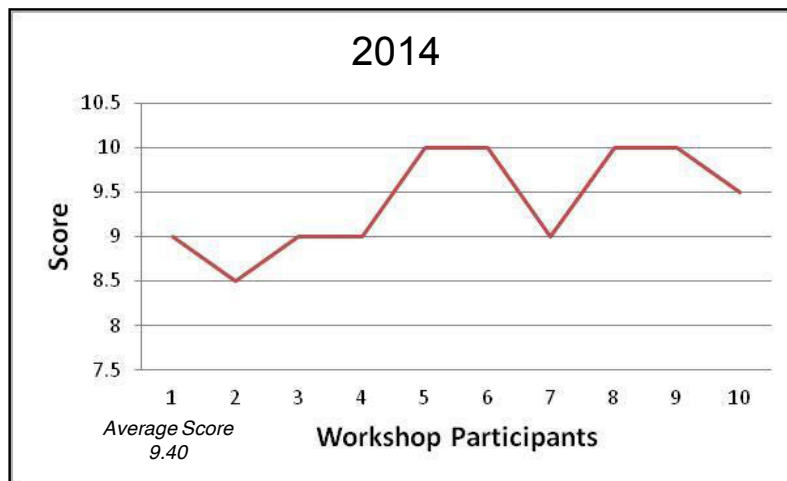


Figure 7. 2013 Rocket Science for Educators workshop survey results.

As a part of the 2013 grant participants were given, RockSim Software, training on the software, lunch, and a travel stipend to attend. Also in attendance were three high powered rocket certified instructors from Tripoli and NAR. The instructors guided the participants through the installation of the software. The teachers then had to do real problems using the software to solve the issues. This included building a rocket in the software that fit within guidelines but still achieved a certain goal. The participants were also given information on Wisconsin Space Grant Consortium programs for students beyond high school. Workshop feedback from participants stated that his information was deemed very useful.



Figure 8. Rocket Science for Educators workshop at Spaceport Sheboygan.

IV. Conclusion

In June 2011 the 14 educator workshop participants were contacted and asked to respond to five questions about their use of workshop materials and most importantly if respective activities improved student interest in STEM. Out of the 14 educators 11 responded to the survey and *yes* answers were recorded and are illustrated in Figure .

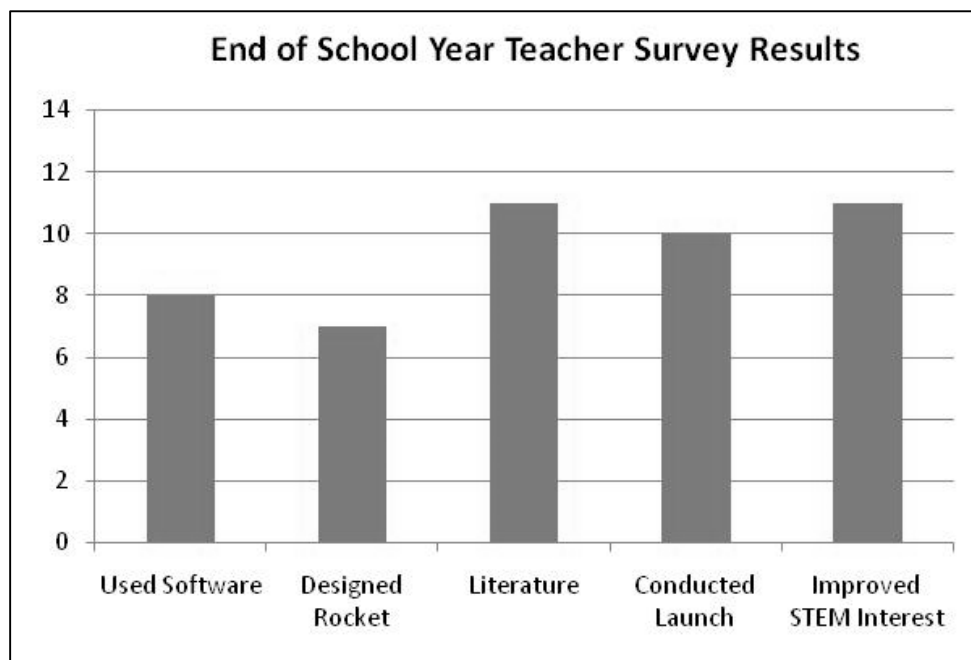


Figure 9. End of school year survey results from educators.

The following are three examples cited from workshop participants when soliciting end-of-school year feedback about how Rocket Science tools taught showed positive impacts:

2010: I used the book and materials we were given to help me gain more confidence before I had my students assemble rockets for launching. I had never done this at

school and had wanted to for a long time. The experience with the rockets during the workshop really made me have enough knowledge to give it a try with my students.

I used the RockSim software with several classes. My advanced reading group read "Rocket Boys" (grade 7/8) and then launched rockets. We used RockSim to look at what would happen to the Rockets during flight. In both of my Earth Science classes (grade 7) we launched rockets in the spring, and again used RockSim to predict what would happen. It predicted that one of the rockets would launch and then crash to the ground nosecone first. That is what actually happened. Also several of my advanced science students spent time using the software on their own, it was very exciting for them and encouraged them to work on some rockets at home.

Building and launching rockets is always exciting for my students. This is a great science experience because we have successes and failures just like in all science experimentation! The students feel so empowered when they get a chance to make scientific decisions and then test what they build. We have great discussion about how scientists make building and experimentation decisions. Anytime students are actively building and experimenting they are inspired and ready to learn. Students that don't always show interest in science are active participants with hands-on activities like rocket building and launching.

2012: I'm noticing as the years go by, fewer kids build things. They use their hands for video games, but to actually build a rocket and understand why it does what it does is so valuable. So I just wanted to say thanks again for the AIAA rocket construction and launch. It makes such a difference in getting kids to see math and science outside of a textbook and to put a real world interest at work with my students goes along way with inspiring them with math and science topics.

2014: As a result of this excellent workshop one of my students who represents both minority and female demographic, was teacher nominated and used the AIAA/WSGC sponsored rocket science project as part of her nomination application and was accepted to the 2013 Camp Badger program at University of Wisconsin – Madison. Camp Badger is a one-week, residential program for Wisconsin teenagers entering eighth grade in the fall where they have demonstrated exceptional math and science skills and given the opportunity to explore technology and engineering through advanced learning.

The International Journal of Science Education published a study researching students' attitudes about scientific professions. Researchers asked high school students to rate their attitudes toward scientific professions and describe why or why they would not consider a STEM related career. The study revealed that participants, across both sexes, considered scientific professions to be less creative and less people-oriented than other more popular career choices. The Hofstra University study concluded that students may be led away from STEM careers by common misperceptions that science is difficult, uncreative, and socially isolating. Researchers stated that finding ways to encourage students to seek STEM careers continues to challenge teachers, career counselors, and

mentors (Masnick, Valenti, Cox, & Osman, 2010). Let's face it, astronauts make science cool. They are the NFL football players of science. This high powered rocket project demonstrates the *coolness* of science by connecting student eyes, ears, and fingers to a real rocket flight vehicle and experiences that will inspire future interests.

A simple, compelling philosophy drives AIAA Wisconsin's commitment to math, science, and technology education. Make it exciting, make it empowering, and make it fun. The Rocket Science for Educators workshop is a far-reaching program that targets precollege students, and the educators who inspire them. Learning starts with a teacher, a curious student, and fun in the classroom. The AIAA sponsored *Rocket Science for Educators* workshop provide educators with first-hand experience and training from real aerospace professionals that will spark students' excitement about machines ... space ... aviation ... how things work.... flying ... and why things happen. In short, all the facets of math and science. Please feel free to contact the author if you are interested in learning more about this STEM workshop.

References

1. Chiaverini, M. J., Kuo, K. K. (2007). *Fundamentals of hybrid rocket combustion and propulsion*. Reston, VA: AIAA Press.
2. Fortescue, P., Stark, J., Swinerd, G. (2003). *Spacecraft systems engineering* (4th ed.). West Sussex, England: John Wiley and Sons Ltd.
3. Masnick, A. M., Valenti, S. S., Cox, B. D., & Osman, C. J. (2010, March). A multidimensional scaling analysis of student attitudes about science careers. *International Journal of Science Education*, 32 (5), 653-667.
4. Miller, S. A. (2010, February 14). Engineers step up for STEM next week. *Milwaukee Journal Sentinel*, pp. A37.
5. RockSim software. *Model rocket design and simulation software* (Ver. 9.0). Purchased from: www.apogeerockets.com. Colorado Springs, CO: Apogee Components.
6. Van Milligan, T. S. (1995). *Developing Creativity Using Model Rockets to Teach the Techniques of Problem Solving*. Colorado Springs, CO: Apogee Components.
7. Van Milligan, T. S. (2008). *Model rocket design and construction* (3rd ed.). Oregon, IL: Quality Books, Inc.

24th Annual Wisconsin Space Conference

PART SIX

Conference Program

24th Annual Wisconsin Space Conference

Commercial Space Flight

August 15, 2014

BioPharmaceutical Technology Center
Promega Corporation Campus
Fitchburg, Wisconsin

Presented by:

**Wisconsin Space Grant Consortium
BioPharmaceutical Technology Center Institute
Orbital Technologies Corporation**

CONFERENCE PROGRAM

7:30-8:15am **Registration & Continental Breakfast**
Poster Drop Off (formal poster session at 12:00-1:30pm)
Bring posters to registration and staff will set them up.

***** Plenary Session *****

8:15-8:30am **Welcome and Introduction**
Kevin Crosby, Director of WSGC; Chair, Natural Science Division, Professor of Physics, Astronomy and Computer Science, Carthage College

8:30-9:15am **Session 1: Keynote Address**
Introduction: Michael LeDocq, Chair, WSGC Advisory Council; Instructor, Department of Natural Science, Western Technical College

Keynote Speaker: Jeff Johnson, Environmental Control & Life Support Systems (ECLSS) Program Manager for SNC Dream Chaser

***** Plenary Session *****

9:15-10:00am **Session 2: Team Projects**
Moderator: William Farrow, WSGC Associate Director for Student Satellite Initiatives; Assistant Professor, Milwaukee School of Engineering

Simpson Street Free Press, *After-school Academic Newspaper*, **McKenna Kohlenberg**, Assistant Editor; **Taylor Kilgore**, Assistant Editor; **Ali Khan**, Teen Editor; **Lucy Ji**, Teen Editor

Balloon Payload Team, *The Elijah Project - 2014 High Altitude Balloon Payload*

Madeline Lambert, University of Wisconsin-La Crosse

Jadee Kellogg, Ripon College

Daniel Ochoa, Milwaukee School of Engineering

Evan Schilling, Milwaukee School of Engineering

Michael Stefik, University of Wisconsin-Milwaukee

Michael Wiznitzer, Milwaukee School of Engineering

Balloon Launch Team, *2014 Elijah High Altitude Balloon Launch Team Flight Results*

Rachel Beyer, Marquette University

Amber Koeune, Milwaukee School of Engineering

Jordan Petrie, Milwaukee School of Engineering

Leeta Russell, Milwaukee School of Engineering

Michael Stefik, University of Wisconsin-Milwaukee

Alana Tirimacco, Milwaukee School of Engineering

10:00-10:15am **Morning Break**

***** Concurrent Sessions -- Research Stream *****

- 10:15-11:45am **Session 3R: Physical Sciences (Auditorium)**
Moderator: Leah Simon, Assistant Professor of Physics, Ripon College
- Madeline Wade**, *Searching for Gravitational Waves from Sub-Solar Mass Black Holes*, Graduate Student, Department of Physics, University of Wisconsin-Milwaukee
- Sydney Chamberlin**, *Black Holes, Lasers, and Data Analysis: Contributions to Gravitational Wave Searches with the Excess Power Pipeline*, Research Graduate Assistant, Department of Physics, University of Wisconsin-Milwaukee
- Colin Egerer**, *Clarifying the Role of Thermodynamics in Self-gravitating Dark Matter Systems*, Undergraduate Student, Department of Physics, University of Wisconsin-La Crosse
- Sean DuBois**, *Assessment of Ecosystem Photosynthetic Parameters Along Two California Climate Gradients*, Graduate Student, Nelson Institute for Environmental Studies, University of Wisconsin-Madison
- David Helminiak**, *Simulations of Granular Material Motion*, Undergraduate Student, Department of Computer Engineering, Marquette University
- Nathaniel Helminiak**, *Experiments with Granular Material Motion*, Undergraduate Student, Department of Mechanical Engineering, Marquette University

***** Concurrent Sessions -- Education Stream *****

- 10:15-11:45am **Session 3E: K-12 Education and General Public Outreach (Room 122)**
Moderator: Carol Lutz, Co-chair for Rockets for Schools, Sheboygan, WI
- Todd H. Treichel**, *Rocket Science for Educators Using Rocket Design and Simulation Software*, Senior Systems Engineer, Orbital Technologies Corporation; American Institute of Aeronautics and Astronautics (WI)
- Barbara Bielec**, *Science Outreach at the BTC Institute - Aerospace Outreach Program & Special Initiatives Program*, K-12 Program Director, BTC Institute
- Daniel Bateman**, *Teacher Workshop on Rocksim*, Executive Director, Spaceport Sheboygan
- John Heasley**, *Driftless Dark Skies Initiative: Training Astronomy Educators*, Space Science Educator, Star Stories
- Coggin Heeringa**, *Teaching Teachers*, Director, Crossroads at Big Creek
- Shelly Leshner**, *Promoting Women in Physics and Astronomy through a Distinguished Lecture Series*, Assistant Professor, Department of Physics, University of Wisconsin- La Crosse
- 11:45-1:15pm **Lunch and Poster Session**

***** Poster Session *****

Facilitator: Mike LeDocq, Chair, WSGC Advisory Council; Instructor, Department of Natural Science, Western Technical College

Brian Harvey, *Burn me Twice, Shame on Who? Testing for Wildfire Feedbacks in Forests of the US Northern Rocky Mountains*, Graduate Student, Department of Zoology, University of Wisconsin-Madison

Michael Brusich, *CAERENet*, Undergraduate Student, Department of Physics, Carthage College

Justin Collins, *Engineering Sustainable Space Nutrition Modules for Classroom Spiral Insertion*, Undergraduate Student, Department of Mechanical Engineering, Milwaukee School of Engineering and Sweet Water Foundation

David Helminiak, *Simulations of Granular Material Motion*, Undergraduate Student, Department of Computer Engineering, Marquette University

Nathaniel Helminiak, *Experiments with Granular Material Motion*, Undergraduate Student, Department of Mechanical Engineering, Marquette University

Tyler Laszczkowski, *Expanding Our Knowledge of Interstellar Neutral Hydrogen Shells*, Undergraduate Student, Department of Physics, University of Wisconsin-La Crosse

Brendan Krull, Tessa Rundle, Kevin LeCaptain, Amelia Gear, *The Onset of Normal Field Instability in a Ferrofluid in a Reduced Gravity Environment*, Undergraduate Students, Department of Physics, Carthage College

Jon Woods and Luke Goetsch, *Spatial ID Environmental Reader (SPIDER)*, Undergraduate Students, Software and Hardware Engineering, East Troy High School

Balloon Payload Team, *The Elijah Project - 2014 High Altitude Balloon Payload*

Rachel Beyer, Marquette University

Amber Koeune, Milwaukee School of Engineering

Jordan Petrie, Milwaukee School of Engineering

Leeta Russell, Milwaukee School of Engineering

Michael Stefik, University of Wisconsin-Milwaukee

Alana Tirimacco, Milwaukee School of Engineering

1:15-1:30pm

Group Photograph (Atrium)

***** Research Stream *****

1:30-2:45pm

Session 4R: Space Systems Engineering (Auditorium)

Moderator: Kevin Crosby, Chair of Natural Science, Professor of Physics and Computer Science, Carthage College

Aaron Olson, *Implantation and Extraction of Helium from Lunar Regolith Simulant*, Graduate Student, Department of Engineering Physics, University of Wisconsin- Madison

Jalal Nawash, *Efficiency of Select Solar Cells at High Altitudes Using a Weather Balloon*, Assistant Professor, Department of Physics, University of Wisconsin- Whitewater

Todd Treichel, *Design and Development of LED Lighting System for Human Spacecraft*, Senior Systems Engineer, Orbital Technologies Corporation; American Institute of Aeronautics and Astronautics (WI)

Jeff Clark, *Remote Sensing of Physical Models in the Laboratory*, Professor, Department of Geology, Lawrence University

Trent Cybela, *Fire in Orbit: Equipping Commercial Spaceflight for Fighting Fires beyond Earth*, Undergraduate Student, ECLSS (Environmental Control and Life-Support Systems), Orbital Technologies Corporation & University of Wisconsin-Platteville

2:45-3:00pm **Afternoon Break**

***** Plenary Session *****

3:00-4:00pm **Session 5: Rocket Teams**

Moderator: William Farrow, WSGC Associate Director for Student Satellite Initiatives; Assistant Professor, Milwaukee School of Engineering

Rocket Team: First Place – Non-Engineering Division - Team Night Skies

The Flight of Wombat I, **Christine Sutherland, Aaron Jarosh and Grace Zeit**, Undergraduate Students, University of Wisconsin-Sheboygan

Rocket Team: Third Place – Engineering Division – Team Rocket

Alex Folz, Collin Matthews and Justin Collins, Undergraduate Students, Department of Mechanical Engineering, Milwaukee School of Engineering (non-presenting team members: Garrett Sauber and Roberto Fernandez)

Rocket Team: Second Place – Engineering Division – Woosh Generator

Eric Johnson, Stephan Skibinski and Leeta Russell, Undergraduate Students, Milwaukee School of Engineering, Department, Non-Presenting team members: James Ihrcke, Kathryn Baisley, Kirsti Pajunen

Rocket Team: First Place – Engineering Division - Pioneer Rocketry

Trent Cybela, Luke Sackash, Andrew Heindl, Jacob Ellenberger and Maria Smiles, *High Aspirations: Rocketry at the University of Wisconsin–Platteville*, Undergraduate Students, Multiple-Discipline Engineering (Mechanical, EP, Software, Electrical)

4:00-4:30pm **Awards Ceremony and Closing Remarks**

4:30-5:30pm **Reception**